OPTICAL ABSORPTION AND PHOTOCONDUCTIVITY IN SIMPLE CHALCOGENIDE GLASSES

BY

JÓN PÉTURSSON

A THESIS SUBMITTED FOR THE DEGREE OF DOCTOR OF PHILOSOPHY
AT THE UNIVERSITY OF EDINBURGH
IN
SEPTEMBER 1975

PREFACE

This thesis has been composed by myself and is the result of my own work except when otherwise indicated.

I am indebted to Dr A E Owen, for his guidance and encouragement throughout the course of this work. I would also like to express my thanks to colleagues in the Department and in particular, Dr Joseph M Marshall, for many critical discussions. The assistance of the technical staff of the Department of Electrical Engineering is gratefully acknowledged.

I am grateful for financial assistance from the British Post Office Research Establishment, the Science Fund of Iceland, the Icelandic Students Loans Fund and the University of Edinburgh as well as from relatives.

I wish to thank Miss Linda Murray for her excellent typing of the text.

Most of all, I wish to thank my wife, Anna and my children, Halldóra and Dofri, for enduring my absence during the writing of this work.

ABSTRACT

The interband optical absorption has been studied as a function of composition, photon energy and temperature in the As-Se system. Thin films with bulk-like properties were prepared by a glass-blowing technique. The power-law dependence of absorption on photon energy was examined. Films with 1 - 50% As are characterized by the well-known quadratic energy relationship while pure Se follows a linear relationship which is also detectable in Se doped with 0.1% As. A close correlation is found between the changes in the 'optical gap' and the slope of the absorption curve, with temperature and preparation although these parameters vary differently with composition.

The smallest optical gap occurs near the composition $As_{43}Se_{57}$ and a local maximum is postulated at $As_{57}Se_{43}$. A simple relationship is found between the inverse of the slope of the absorption curve vs composition which may be valid over the whole range from pure Se to pure As. This parameter shows no extrema near the stoichiometric composition. The results are compared in detail with other properties of As-Se glasses reported in the literature. It is concluded that the compositional behaviour is not the result of disorder induced localization of states near the band edges. A model is proposed in which the band width is related to the atomic density as a result of interaction between orbitals which do not form a common covalent bond.

Some preliminary measurements of the absorption and the photoelectric properties of films doped with up to 1% Cu (atomic) reveal an annealing effect at ~340 K and a photomobility which is higher than in the undoped glasses. The conductivity in samples doped with Cu is

not due to extended state conduction. Comparison with the literature on glasses doped with Ag suggests that ionic conduction is important in these glasses and some suggestions are put forward to explain these and other observations, such as photodoping, in terms of photo-enhanced ionic conductivity.

TABLE OF CONTENTS

CHAPTER 1 INTRODUCTION

1.1 AMORPHOUS SOLIDS AND GLASSES

Condensed matter can be categorized into liquids, crystalline solids and non-crystalline or amorphous solids. The structure and properties of crystalline solids have been studied intensively and interpreted with the aid of quantum mechanics for nearly half a century, and a fairly complete understanding has been gained of some crystalline materials.

A crystal may be defined as a substance consisting of atoms arranged in a pattern that repeats periodically in three dimensions[1].

In the idealized mathematical description of a crystal each pattern unit is associated with a lattice point and a unit cell. A given lattice point is in exactly the same environment as any other lattice point, and the contents of every unit cell, called *the basis*, is exactly identical to that of every other unit cell. A lattice can be completely characterized by the possible symmetry operations that leave it unaltered. These symmetry operations consist of rotations, inversions and reflections in addition to translations which are always possible by definition. The basis may also have some symmetry and when this is taken into account, the symmetry operations of the whole crystal lattice (as opposed to the space lattice) may include screw axes and glide-reflection planes. All these operations form the *space group* of the crystal, which gives a complete description of the crystal lattice and characterizes the *long-range order* (LRO) in the crystal.

The electronic structure of the constituent atoms determines the kind of chemical bonds that form between them. The nature of these bonds, ie, their strength, number and directionality, together with the prevailing thermodynamic conditions, governs the resulting crystal structure (if any), and many properties of the crystal. Other properties, eg, the possible directions of reflected X-rays, are determined solely by the space group. The immediate surroundings of a given atom, such as the number of nearest and next nearest neighbours and their distance, are identical to those of any corresponding atom in any other unit cell. This is called the *short range order* (SRO).

In reality all crystals contain imperfections such as broken bonds, lattice vibrations, dislocations, impurity atoms, etc. These can normally be treated as perturbations to the periodic potential of the crystal. This may however mean that the LRO only persists, undisturbed, for a few tens of atoms. Nevertheless, the ideal crystal lattice is still a good starting point when considering or calculating the properties of imperfect crystals.

In liquids (other than liquid crystals) and non-crystalline or amorphous solids, there is no long range order. There is no periodicity and no way of defining an extended regular lattice as a realistic description of the structure. Nevertheless, the same chemical properties of the individual atoms still control the local interactions and environment, and most of the chemical bonds will still be satisfied. This forces some similarity with the crystalline phase, in-so-far as it is compatible with the loss of long range order. Thus, there remains a short range order which extends

only to a distance of 10 - 20 Å.

A material which has ordered regions which are more than 20 Å across can be distinguished by X-ray or electron diffraction. The diffraction pattern of a single crystal consists of isolated points, that of a polycrystal is a series of concentric but sharp rings. As the crystallites become smaller the rings broaden into diffuse haloes with no distinguishible changes below about 20 Å. *A truly amorphous material may be conveniently defined as one without LRO, meaning order beyond ~20 Å.*

It is at present extremely difficult to obtain unambiguous information from experiments on the SRO beyond the second nearest neighbours. The most useful methods are dark field microscopy and extended X-ray absorption fine structure (EXAFS) but even here the interpretation of results is controversial.

Three different approaches have been used hitherto to describe the SRO of non-crystalline materials.

- *The perturbed crystal approach :* A high density of conventional structural defects are supposed to be frozen into an otherwise ideal crystal[2].

- *The microcrystal approach :* It is assumed that perfect order exists over a small distance, at least out to the third or fourth neighbours, after which there is an abrupt change in the orientation of the next ordered domain, the intervening space being filled by a CRN[3,4].

- *The continuous random network approach (CRN) :* It is supposed that the atoms form a continuously interconnected three-dimensional array without any discontinuities. In an ideal CRN all bonds are satisfied, even for impurity atoms. This is achieved by fluctuations in bond lengths, bond angles and dihedral angles. This model was originally put forward by Zachariasen[5] in 1932.

Information on the nearest and next nearest neighbours of a given type of atoms can be obtained from diffraction experiments in terms of the radial distribution function (RDF) which gives the electron density in concentric shells around a reference atom (or nuclear densities in the case of neutron diffraction), as a function of radial distance. Positions of peaks in the RDF correspond to distances to neighbouring atoms and their area to number of atoms in the corresponding coordination shell. Beyond the second peak, however, the RDF is usually smeared out but still gives useful information.

Before comparing the various structural models it should be emphasized that *amorphous solids are not in thermal equilibrium*, ie, they are metastable and their free energy is not the lowest possible for that temperature. In some cases, such as non-stoichiometric materials and polymeric molecules with a low level of structural symmetry, there may be no crystalline counterpart and the amorphous structure forms itself naturally as the low temperature state.

The liquid state is amorphous insofar as it possesses SRO and not LRO. A liquid, however, is in a dynamic thermal equilibrium ,

its free energy is minimized and its molecules are in constant Brownian movement. When a liquid is cooled the molecular movements become sluggish and below the melting point crystallization will occur under the right conditions, ie, if there is a crystalline form and if there is sufficient time for nucleation and crystal growth to take place. If crystallization cannot proceed, however, the material is in a supercooled liquid state in which molecular motion takes place but not crystallization. Upon further cooling a point will be reached when the molecules cannot rearrange themselves in response to the decreasing temperature and the structure freezes in. The temperature at which this occurs, ie, when the cooling rate equals the relaxation rate, is called the *glass transition temperature* or simply glass temperature (Tg). At Tg there is an abrupt change in second order thermodynamic quantities such as the specific heat Cp, the expansion coefficient α and the compressibility K. As a result there is a change in slope at Tg of the first order extensive variables such as volume V, entropy S and enthalpy H. This is illustrated in Figure 1.1 and has been discussed by Owen[6]. The parameter Tg depends on cooling rate and is often taken as the temperature at which the second order variables are midway between their liquid value and the low temperature value. The reduction in Cp is easily understood in terms of the reduction in the number of degrees of freedom when molecular movement ceases below Tg. Amorphous solids formed in this way are called 'glasses', 'glassy solids' or 'vitreous solids'. There are, however, other methods of preparing amorphous solids and in fact many materials do not have a glassy form, ie, they always crystallize when cooled from the melt. The method of preparation,

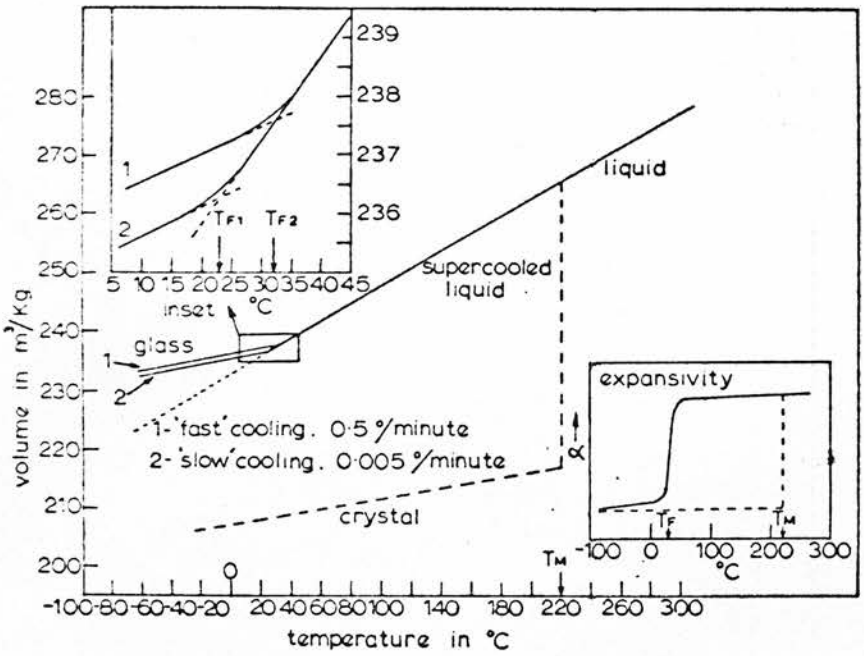

FIGURE 1.1

A typical volume-temperature diagram showing the glass transition and the effect of different cooling rates (Ref 8).

and especially the rate of cooling and the amount of cooling greatly affect the structure and other properties of solids, and have to be considered when evaluating which structural model is most appropriate. As an example, it is possible to 'amorphize' crystals by excessive doses of high energy radiation or by mechanical stress and it is obviously tempting to relate this type of amorphous solid to the original crystal structure, ie, to adopt the perturbed crystal approach. Similarly, when fast cooling from the melt is required to prevent nucleation and crystallization, the microcrystalline approach may be most appropriate but a material which only crystallizes with great difficulty is perhaps most likely to relate to the CRN approach.

The principal methods of preparation of amorphous solids are

(a) Glass formation by cooling a liquid : This requires the prevention of nucleation and crystal growth. The rates of these processes go through maxima as the temperature is lowered below the melting point[7]. Thus, if the temperature can be lowered below these maxima quickly enough, nucleation and crystal growth will be insignificant. The actual quenching rates used may vary from about one deg/day in the case of oxide glasses used in optical equipment and up to 10^7 deg/sec when 'splat cooling'[8] is used. Below Tg the structure of the (supercooled) liquid is'frozen in'. Some materials, such as Si and Ge undergo drastic changes in bonding when they melt and their melts cannot be cooled into glasses.

(b) Thermal evaporation : This is the most widely used method for the production of amorphous thin-films. The source material is heated in a vacuum of 1 μm or better, until it evaporates. The condensed vapor is collected on a suitable substrate as a thin-film. Normally

the substrate temperature is held below Tg (if known). This means that the effective 'cooling rate' is extremely high and very little rearrangement can take place after the vapor molecules have been deposited. The structure of evaporated films may thus differ greatly from that of the same material cooled from the melt[9]. Generally, thermally evaporated films may be expected to contain more broken bonds and be more disordered than glasses. If the substrate is held near or just above the glass transition temperature *annealing* will take place and this often results in a structure very similar to that of the glass. Nucleation and crystal growth may also take place if the substrate temperature is high enough. A major problem with evaporation of compounds is that the composition of the deposited film is often different from that of the starting material.

(c) Sputtering :This is now a widely used method for producing amorphous films which are usually closer to the glassy form in their properties than thermally evaporated films[9,10]. Ions (usually argon) are accelerated by a dc or rf field onto a target of the material to be sputtered. Atoms or groups of atoms are thus 'knocked-out' of the target and collected on a substrate. Compositional changes are more controllable than in the thermal evaporation process. There is, however, some contamination of the deposited film by the sputtering gas.

(d) Irradiation or ion bombardment : Heavy dosages of fast neutrons, gamma rays or ions can transform crystals of some materials into an amorphous form. These amorphized crystals often have high densities of broken bonds and other defects. Upon annealing they either crystallize or become more glass-like[8].

(e) Deposition from solution : This can be achieved either by chemical reaction and precipitation or by electrolytic deposition. The results are often more reproducible than in the case of evaporation[11].

There are many other methods, such as glow-discharge decomposition, vapor phase hydrolysis, shock-wave transformation and oxidation. The first of these has been used with great success by Spear et al[12] to deposit a-Si from silane gas ($Si H_4$).

It should be clear from the above discussion that the properties of an amorphous material depend on its history as well as its environment at the time of measurement.

1.2 TYPES OF AMORPHOUS SEMICONDUCTORS

Amorphous semiconductors may be classified or grouped according to the types of chemical bonds and their strength. Examples of each are given below.

(a) Tedrahedrally bonded amorphous semiconductors : These can only be prepared by vapor deposition or electrolytic deposition because their melts are metallic and characterized by higher coordination numbers. Examples are Si and Ge which have been widely studied because of their well understood crystalline forms. Si C and the III-V compounds have also been studied in the amorphous form. All of these materials show properties not shared by other amorphous semiconductors. Among these are large electron spin resonance (ESR), corresponding to approximately 10^{20} spins/cm^3 [13] and a highly structure sensitive electrical conductivity[12].

(b) Chalcogenide or lone pair semiconductors : Generally these consist of one or more of the elements S, Se or Te from group VI alloyed with elements from groups IV and V such as Si, Ge, Sn, P, As, Sb or Bi. They can be either elements (S, Se, Te) stoichiometric compounds (As_2S_3, As_2Te_3, As_2Se_3, Sb_2S_3, etc) or cross-linked networks (As-Se, Ge-As-Se, Si-Ge-As-Te, etc). Many chalcogenides can easily be prepared in glassy form and some, like As_2S_3 , are very difficult to prepare as crystals. On the other hand liquid As_2Te_3 is a degenerate semiconductor with different coordination from As_2S_3 and As_2Se_3 and is not easily quenched from the melt. According to Kastner[14] some of the valence band states in S, Se and Te originate from non-bonding lone pair (LP) states. The LP states may be responsible for the switching action observed in many multicomponent amorphous chalcogenides[15]. ESR measurements on these materials reveal no observable signal, indicating less than 10^{14} singly occupied states per cm^3. This is many orders of magnitude less than the number of localized states estimated from measurements of photoemission, ac conductivity and glow curves. The chalcogenide glasses are usually insensitive to impurities in their amorphous or glassy forms but there are exceptions to this. Thus 50 ppm of oxygen in a-Se increase the conductivity by six orders of magnitude[16]. Addition of less than 1% of silver or copper to As-S or As-Se glasses changes their electrical and optical properties very drastically[17,18].

(c) Transition-metal oxide glasses : The transition-metal oxide glasses are easily prepared from the melt. They contain transition metal ions in different valence states, and conduction is by charge

transfer process (hopping) between these ions. For instance, in V_2O_5-P_2O_5 glasses the vanadium ions are either tetra-or penta-valent (V^{4+} or V^{5+}). The 3d states form a band of localized states in which the hopping conduction occurs. The charges distort the surrounding lattice, ie, they form *polarons*[43].

(d) Miscellaneous types : In addition to groups (a) and (b) above there are other types of covalently bonded amorphous semi-conductors, such as the elements B and As and the tetrahedral glasses, $A^{II}\ B^{IV}\ C_2^{V}$, eg, Cd Ge As_2, Sn Si P_2. The tetrahedral glasses can be quenched from the melt. Some are n-type and some p-type and Cd Ge As_2 shows ambipolar conduction.

This list is by no means exhaustive and it does not include glassy or amorphous dielectrics like Si O_2 and Al_2O_3, organic semiconductors and insulators, nor amorphous metals and alloys which can only be prepared by extremely rapid cooling, if at all.

The present work is concerned with the arsenic chalcogenides and the following sections consider their atoms and electronic structure in more detail.

1.3 THE STRUCTURE OF CHALCOGENIDE GLASSES - AN INTRODUCTION

When isolated atoms, with discrete energy levels are brought together, electrons in the outermost energy levels begin to interact and mixing of the atomic wave functions gives rise to new wave functions which can be either symmetric or antisymmetric. Each atom has a tendancy to complete its valence shell; thus, if atoms from groups I and VII of the periodic table are brought

together one electron outside the closed shell of the group I atom is transferred almost completely to the group VII atom to fill its valence shell. This results in ionic bonding. In II-VI compounds the transfer of electrons is less complete. When atoms from intermediate groups are brought together the outermost electrons are shared by the atoms, resulting in covalent bonds which are related to the orbitals of the free atoms and thus tend to be highly directional. In both cases the electrons with symmetric wave functions have lower energy than those with anti-symmetric wave functions. A condition for a stable condensed state is that its free energy be less than in the gaseous state (ie, when the atoms are separated). This is the case for the symmetric wave functions which are therefore called bonding states, whereas the higher energy antisymmetric states are called antibonding states. The potential minima in the bonding states, as a function of interatomic separation, determine the equilibrium interatomic distance. Both the bonding and anti-bonding states are spread out into bands and an example is shown in Figure 1.2. The rise in energy at very short interatomic distances is due to interaction with closed shells. The Pauli exclusion pinciple prevents valence electrons from occupying the same space as core electrons. Electrons cannot propagate in energy states outside the bands because of quantum mechanical conditions, ie, their wave vector becomes imaginary and so the wave function decays exponentially with distance. Electrons in a band can either be localized, ie, bound to a certain site or atom, or extended with a wave function which extends throughout the material. The bonding band is called the valence band. The antibonding band

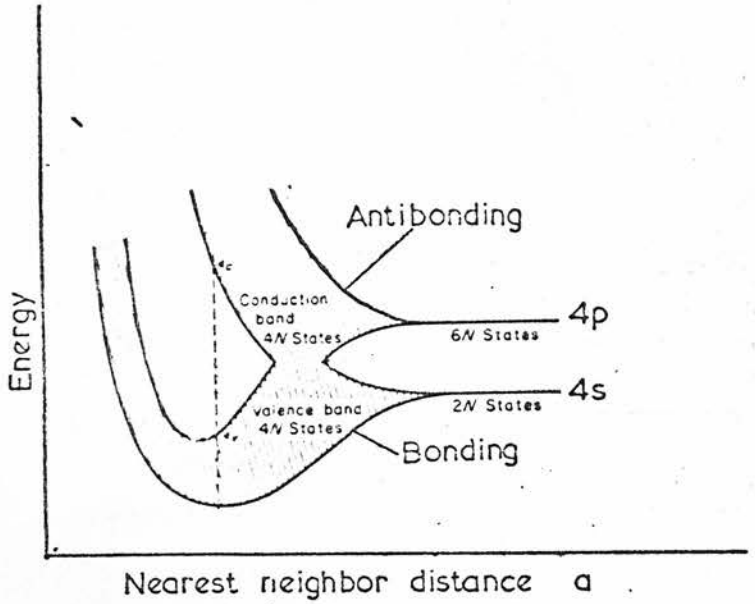

FIGURE 1.2(a)

Bonding and antibonding bands in solid Ge, arising from the hyridized 4s and 4p atomic orbitals.

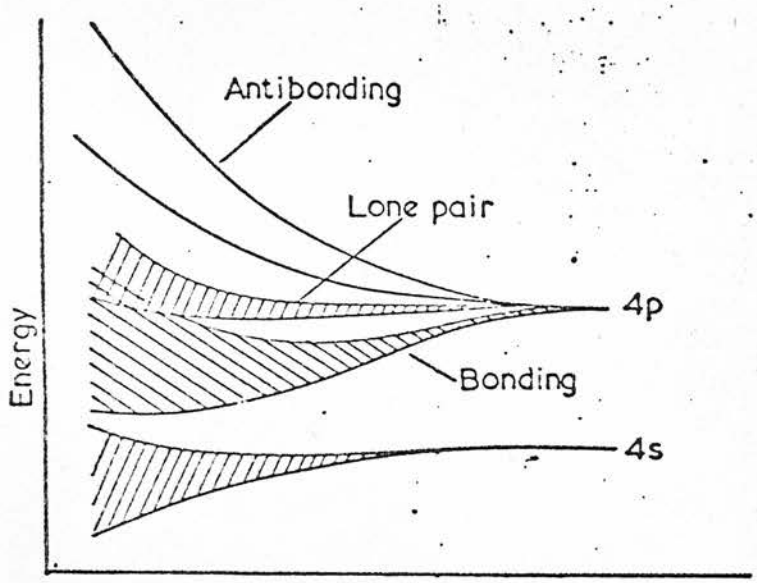

FIGURE 1.2(b)

Similar diagram for Se assuming no hybridazation. Two electrons per atom form a non-bonding pair(Ref 14).

forms the (first) conduction band in semiconductors and insulators. Some materials contain lone-pair (LP) states, ie, two electrons per atom which do not share in the binding process but may actually form bands which are between the bonding and the antibonding bands. In this case the LP band forms the valence band as shown in Figure 1.2(b). Lone-pair states are important in the materials studied in this work but there is some controversy as to whether they form a separate band or are mixed with the bonding states.

The study of amorphous materials is still in its infancy. Systematic work was begun by the Leningrad school[19,20] nearly two decades ago but only in the last ten years or so has the interest been widespread. There are great difficulties because the theoretical problem of interpreting amorphous materials is inherently much more complicated than for crystals. When trying to predict the properties of an amorphous semiconductor the empirical rule of Ioffe and Regel[21] is useful. It states that a molten or amorphous semiconductor retains its semiconducting properties in spite of the breakdown of the LRO if the non-crystalline phase conserves the SRO present in the related crystal. Ioffe and Regel characterized the SRO by the number of atoms in, and the radius of, the first coordination sphere. On the other hand, the second to fourth neighbours are also important and this again raises the question of which structural model is most appropriate. Rudee's[4] dark-field electron microscopy observations indicate ordered domains of about 14 - 20 Å diameter in vapor-deposited films of Ge and Si. Similarly, offset bright-field microscopy[3] produces fringes indicating similar ordered domains or micro-

crystals. According to some observers, however, these effects may be instrumental[22]. Randomly oriented microcrystals of this size require that about half of the atoms be in the intermediate CRN regions which are supposed to separate the 'crystallites'. It is possible to test this approach by building models and comparing the density, RDF and other properties calculated from these models with experimental results. Acceptable agreement between model and experiment can however, only be achieved by assuming, without thermodynamic justification, that the crystallites, are heavily distorted, or by giving them peculiar shapes, or by admitting the presence of crystallites or atomic clusters in symmetries or morphologies not otherwise observed. Results of ESR measurements show that even in a-Si and a-Ge less than one bond in a thousand is broken. The evidence is that these broken bonds are on the inside of voids[13].

It seems therefore that a-Si and a-Ge consist of either small (wurtzite) microcrystals, 10 - 20 Å in size, which are connected by a CRN structure, or that they are wholly CRN structures. The presence of a nucleation barrier in many glassy or amorphous materials also argues against the microcrystalline model. There is even less evidence for microcrystals in amorphous chalcogenides. The perturbed crystal approach is not consistent with the low density of localized states in glasses. It therefore appears that the CRN model is the most appropriate, at least for the chalcogenide glasses.

A related question is whether amorphous materials have a molecular or polymeric nature. Tedrahedrally bound amorphous

solids, such as Si, Ge and GaAs, it is generally agreed, do not contain molecular units. On the other hand it has been suggested that amorphous chalcogenides may be molecular especially when prepared as evaporated films and when the composition has a molecular crystalline counterpart, eg, As_4Se_4. Amorphous Se is thought to contain a mixture of Se_8 molecular rings and polymeric chains. Tobolsky, Eisenberg[23] and others have shown that group VI materials like Se and S possess a characteristic polymerization temperature, below which the material is molecular or monomeric. Above this transition temperature there is partial polymerization, with the remaining molecular material acting as a plasticiser. In S at atmospheric pressure the polymerization temperature is 160°C which is 45° above the melting point of crystalline sulfur and in this temperature range the liquid consists of S_8 rings. The rings can re-arrange themselves fairly easily into a crystal (orthorhombic below 96°C, monoclinic above). The glass transition temperature is about -20°C. In the case of selenium, on the other hand, the polymeric transformation temperature is 135° below the melting temperature, and only about 40° above the glass transition temperature[24,25]. This means that the depolymerization which should take place when Se is cooled will proceed very slowly and normally the polymeric nature of the melt will be largely retained in the glass. A slowly cooled sample of Se contains a higher proportion of Se_8 rings than a rapidly cooled sample. The addition of arsenic to Se or S causes a breaking of the rings and branching of chains. This increases the glass transition temperature until it becomes higher than the polymerization temperature. Below the glass transition temperature re-arrangement of molecules or

molecular sub-units becomes, by definition, impossible on the time-scale of the measurement. Therefore, a material which is polymeric at the glass transition temperature, will remain so at lower temperatures, whatever the cooling rate. The degree of polymerization at equilibrium, at least in Se and S where it can be easily defined, is maximum a few degrees above the polymerization temperature and then decreases again with increasing temperature. This means that a material cooled rapidly from a high temperature to below the glass transition temperature will not have time to polymerize. An extreme example of this occurs when an amorphous material is prepared by thermal evaporation onto a cold substrate - a process which is expected to produce highly molecular films[26]. Depending on the relative values of the starting temperature, cooling rate and polymerization and glass transformation temperatures, it is thus possible to obtain amorphous samples which are *either more or less polymerized than at equilibrium*. This has important consequences since it is possible to influence the polymeric structure, even below Tg, by radiation; eg, the photopolymerization proposed by De Neufville et al[26]. Another important point is that tetrahedral solids can only change their dimensions, under the action of pressure or temperature changes, by changes in bond lengths, whereas materials with lower co-ordination, even if they possess a continuous extended network, can do so by adjustment of bond angles or rotation about bonds. Thus, the diagrams in Figure 1.2 do not tell the whole story, and, in fact, the width of the bands depends partly on the Van der Waals interaction between electrons which do not form a common bond, ie, closed shell electrons and LP electrons[27]. This explains the large negative

pressure coefficient of the optical gap ($\frac{dE}{dP}$) in 'low-coordination' materials like, S, Se, As-S, As-Se, etc.

The question of the macrostructure of amorphous materials is also important. The following are the most important sources of heterogeneities :

(a) Density fluctuations : Density fluctuations in a liquid can be 'frozen' in when a glass is formed. Evaporated samples may contain dense clusters connected by less dense regions (or, in the extreme case, voids). This may affect the optical properties and charge transport[7]. In organic polymers dense regions corresponding to single macromolecules can often be observed directly by electron microscopy.

(b) Crystallization : Nucleation and crystal growth can take place during preparation or as a result of annealing. In some materials photo-induced or photo-enhanced crystallization has been reported[29]. There have been many reports of photodecomposition and crystallization in arsenic chalcogenides[30,31,32,33]. It appears that these phenomena are closely related to the processes of photoinduced polymerization[26] and depolymerization, as will be discussed later.

(c) Phase separation : Phase separation is the unmixing of an initially homogeneous multicomponent material into two or more amorphous or crystalline phases. This tends to occur when the free energy is lower in the two-phase state because of a double minimum in the free energy vs composition curve. The temperature and composition range in which the two phases coexist is called the *immiscibility gap*. Near its boundaries only large composition fluctuations are thermodynamically stable but in the so-called

spinodal decomposition region all fluctuations are stable and tend to grow. In this region there is no activation barrier and the process is diffusion limited. If there is an immiscibility gap below Tg only, then unmixing may be prevented unless aided by prolonged annealing, or, in some cases, radiation (photodecomposition). Myers and Felty[25] have measured the liquidus and glass transition temperatures in the systems As-S, As-Se and As-S-Se. Below 43% As the first system forms a stable homogeneous phase but As_4S_4 molecular crystal phase tends to separate out from As-rich compositions. On the other hand , the As-Se system in the range 40 - 55% As, has a tendency to separate into As_2Se_3 crystal and an As-rich liquid at temperatures below 264^{o}C. There are also indications of a subliquidus in the 10 - 20 % As range which Myers and Felty suggest is related to a tendency to separate into a Se_8 molecular phase and a branched As-Se network. Bagley et al[34] observed an increase of ~30 deg in Tg with annealing at 297^{o}K in $As_{7.7}Se_{92.3}$ and $As_{10}Se_{90}$. They found no trace of a double glass transition however, as would be expected in a phase separated glass.

Inhomogeneities have been detected in many chalcogenide glasses by electron microscopy and infra-red microscopy[35]. It is expected that the simple systems, Se to $As_{55}Se_{45}$ and $As_2Se_3Cu_x$ where x is small, will be relatively homogeneous when quenched in air or water, although annealing (even at room temperature for Se-rich glasses) or photoeffects may tend to make them less so. Figure 1.3 shows the RDF's for a-Se and a-As_2Se_3. Selenium is twofold coordinated and As threefold coordinated. Many different experiments show that with the increase of As up to ~43% atomic the degree of interconnection increases.[25,36,37,38,39] Beyond 43%

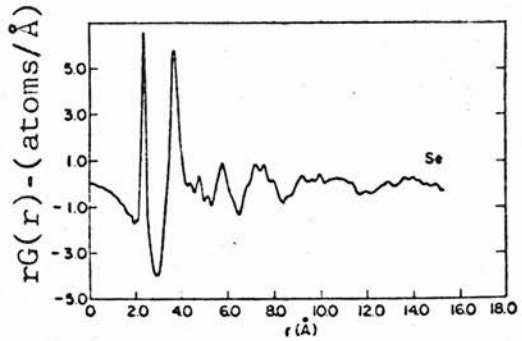

FIGURE 1.3(a)

Reduced radial distribution function for amorphous selenium (Ref 44).

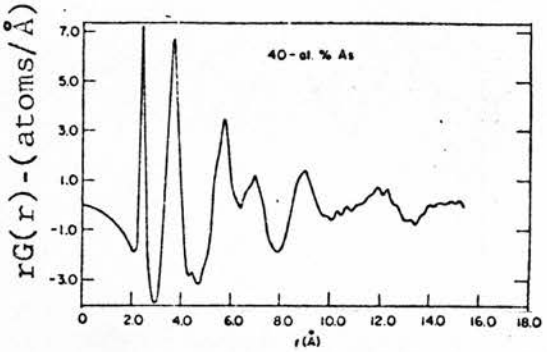

FIGURE 1.3(b)

Reduced radial distribution function for a-As_2Se_3 (Ref 44).

As it decreases again.

1.4 ELECTRONIC STRUCTURE OF AMORPHOUS SOLIDS

In a perfect crystal each electron moves in a periodic potential with wave function

$$\psi(\underline{k}) = u(\underline{r}) \exp(i\, \underline{k} \cdot \underline{r}) \qquad 1.1$$

where $u(\underline{r})$ has the periodicity of the lattice. The wave vector $\underline{k}$ is a quantum number for the electron. Each wave vector has a corresponding eigenvalue of energy. This leads to the familiar E - $\underline{k}$ relationships. Some values of E correspond to imaginary wave vectors and the probability of finding an electron in such a state vanishes. Every crystal has imperfections such as phonons, excited electrons or holes, vacancies, interstitial or impurity atoms or broken bonds. These imperfections lead to the scattering of electrons. Thus the electrons (and holes and phonons) have a finite mean free path L, which depends on the density of imperfections. If the density of imperfections becomes so high that the periodicity or LRO is lost equation 1.1 is no longer valid. Then $kL \sim 1$ or $\Delta k \sim k$. Another rule due to Ioffe and Regel[40] states that $kL < 1$ is not possible since it would correspond to a mean free path shorter than the electron wavelength. It is expected that when the interaction of the carriers with irregular potentials is sufficiently strong they will become localized. Thus an impurity or interstitial atom in a crystal may give rise to a localized state in the band gap. Increasing the density of imperfections will eventually cause the localized wave functions to overlap. Mott and Twose[41] adopted concepts

on spin diffusion from a paper by Anderson to show that below a certain critical density of states all states are effectively localized. Since the density of states varies with energy this means that at a given energy E_c a transition occurs from localized to extended states. This is called *Anderson localization* and E_c is called a *mobility edge* since the mobility of electrons in extended states is orders of magnitude greater than that of localized electrons. The critical density, and hence E_c, depend on the range of random potential fluctuations. A related phenomenon, called the Anderson transition, occurs when the Fermi level becomes greater than E_c, ie, an insulator-metal transition takes place.

In the range of localized states all carriers will have zero mobility at absolute zero temperature, even though their wave functions overlap with those from neighbouring states. At finite temperatures, carriers trapped in localized states (traps) can contribute to conduction by thermally assisted hopping or by thermal activation into the extended states. Hopping can take place both in band edge localized states or in states near the middle of the gap. Extended-state conduction will take place if there are any carriers in the extended states. Which process dominates depends on the densities of states, mobilities and temperature. Figure 1.4 shows an example of a density of states curve, a mobility curve and the resulting contributions of the different types of conduction. The figure illustrates the situation for electrons but with obvious changes, a similar diagram could be drawn for holes.

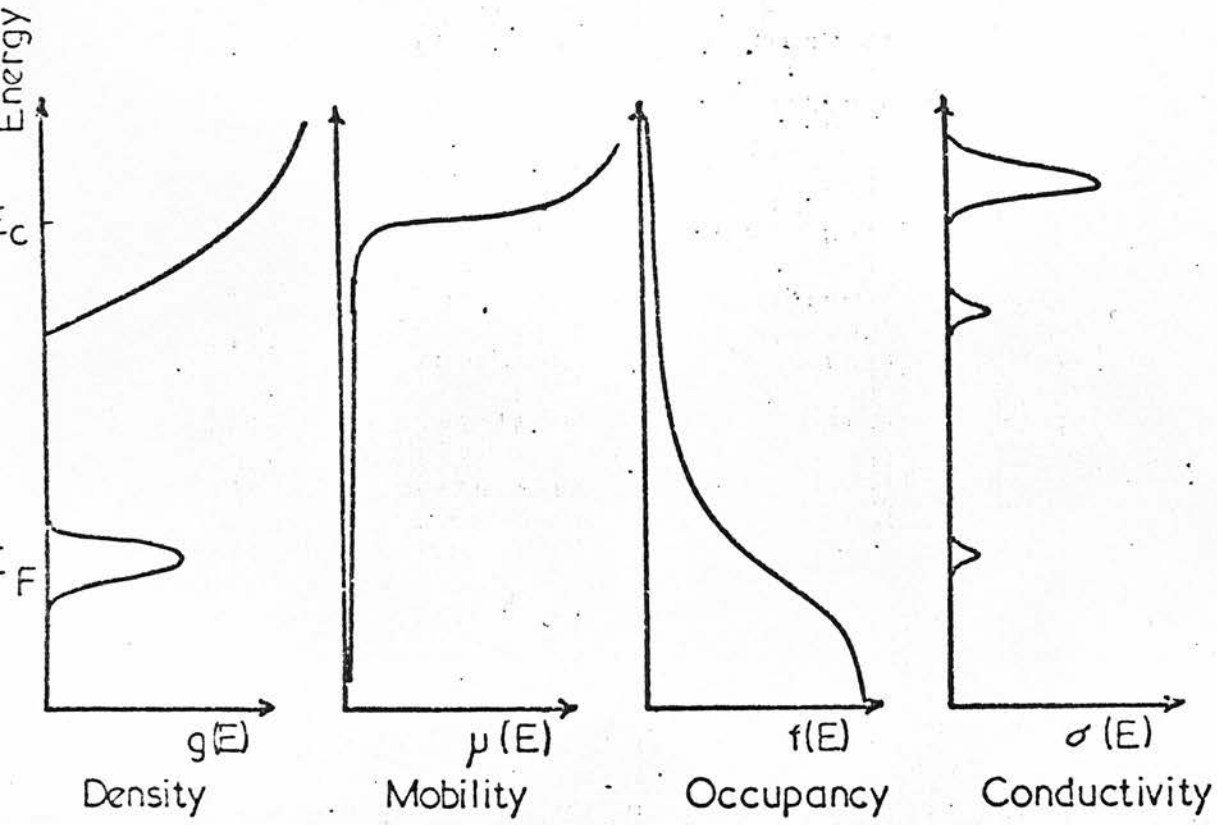

FIGURE 1.4

The density of states, the mobility and the Fermi occupancy function of a typical amorphous semiconductor. The product of these functions is proportional to the conductivity.

1.5 OPTICAL ABSORPTION IN AMORPHOUS SEMICONDUCTORS

Ideally the electron states represented by any two different wave vectors are orthogonal and do not mix. An imperfection in the periodic potential causes a perturbation which can induce scattering or a transition (inelastic scattering). The probability of the transition actually taking place is proportional to the square of the matrix element of the perturbing potential between the initial and final states

$$H_{ij} = \langle \underline{k}_i \mid H \mid \underline{k}_j \rangle \qquad 1.2$$

When the perturbing potential arises from optical radiation the Hamiltonian H can be expressed as $H = \underline{j} \cdot \underline{A}$ where $\underline{j}(= \frac{e}{m} \underline{p})$ is the current operator and $\underline{A}$ is the vector potential of the electromagnetic field. In the case of phonon-assisted transitions (involving an electron, a photon and a phonon) other matrix elements which arise from the perturbation Hamiltonian of the lattice vibrations are also involved. In the dipole approximation all matrix elements vanish unless both wave vector and energy are conserved. This gives rise to the k-selection rule. Transitions which are forbidden according to this rule can still take place with a much reduced probability. For example, the magnetic field of the radiation will interact with the magnetic dipoles of the system with a probability which is typically 10^{-4} times the probability of the electric dipole interaction.

Thus in crystals, transitions between states are only allowed if both energy and the quantum number $\underline{k}$ are conserved. Photons which

have energy of the same order as the band gap have wavelengths in the range 10^3 - 10^5 Å which means that their wave vector is negligible compared to $\underline{k}$ and the initial and final electron wave vectors must be identical

$$\underline{k}_i = \underline{k}_f \qquad 1.3$$

and

$$E_i \pm h\nu = E_f \qquad 1.4$$

These are termed direct or vertical transitions. If phonons with wave vector $\underline{q}$ and energy $\hbar\omega_{\underline{q}}$ take part then

$$\underline{k}_i \pm \underline{q} = \underline{k}_f \qquad 1.5$$

and

$$E_i \pm h\nu \pm \hbar\omega_q = E_f \qquad 1.6$$

Phonon-assisted transitions are called indirect transitions.

The concept of functional E - $\underline{k}$ relationships breaks down when Δk becomes comparable to $\underline{k}$. In amorphous materials, equations 1.3 and 1.5 are no longer thought to apply, at least not near the band edges, because $\underline{k}$ is not a good quantum number. This means that an electron can make a transition between any two states as long as the energy is conserved. The term non-direct transitions is frequently used for these transitions. Since the one-electron Schrödinger equation remains to be solved for amorphous materials it is not possible to calculate matrix elements for non-direct transitions. In presenting optical absorption data it is generally assumed that the matrix element is nearly independent of photon energy immediately

above the onset of interband transitions between extended states. Davis and Mott[42] have argued that transitions where either the initial or the final state is localized and the other is extended should have similar matrix elements as those between two extended states. Both these assumptions will be used and discussed in this work.

1.6 AIMS OF THE PRESENT WORK

The present project is a part of a more general programme in these laboratories to study the electrical and optical properties of vitreous semiconductors. This includes transit-time drift mobility measurements in a-Se and As-Se glasses, photomobility measurements in As_2Te_3, As-Se, As_2Se_3-As_2Te_3 and in multicomponent glasses, photoconductivity in As_2Te_3, As_2Se_3 and multicomponent glasses, Raman studies of As-S and As-Se glasses and measurements of ac and dc electrical conductivity.

The major part of the present work is concerned with optical absorption in As-Se glasses. This was originally intended to supplement photoconductivity experiments but soon became a detailed study, in its own right, of interband absorption as a function of photon energy, temperature, composition and preparation. The reasons for choosing these materials are that a-Se and a-As_2Se_3 have been investigated more fully than any other chalcogenide glasses, the latter often being regarded as a prototype of the more insulating chalcogenide glasses. Research into the non-stoichiometric compositions has, however, been much more limited. It is thought that a systematic study of the change in properties with composition

will be of great value in understanding the physics of disordered materials in general. Considerable work has been done in the USSR, Japan and elsewhere on the macroscopic physico-chemical properties in the As-Se system and other related systems like As-S. These will be compared to the optical measurements reported here. Sample preparation and photostructural effects will also be considered, using the ideas on different degrees of polymerization that were discussed in section 3 of this chapter.

The second and minor part of this work is concerned with the effects of impurities like Ag and Cu on arsenic chalcogenides. According to the CRN theory all bonds should be satisfied in a glass, even for impurity atoms. The effect of small amounts of impurities can therefore be expected to be small in glasses, in contrast to crystals where an impurity concentration as low as 10^{13} cm^{-3} or less can drastically alter the electrical and optical properties. This is indeed usually the case, but Ag, and Cu in As-Se or As-S glasses are notable exceptions. The conductivity has been shown to increase by many orders of magnitude with the addition of 1% or less of Ag or Cu. The optical gap is also reduced. It was hoped that measurements of optical and electric properties of a-As_2Se_3-Cu especially photomobility, would throw some light on why small additions of these metals have such a drastic effect. It was quickly discovered, however, that electrical measurements were invariably plagued by erratic variations when the Cu-doped samples were raised to the relatively low temperature of about $340^{o}K$. These variations disappeared on cooling but it was noticed that some permanent changes in the low temperature properties had taken place. All electrical measurements reported in the literature are

for samples that have been heated well above the temperature quoted above which is much lower than the glass transition temperature of a-As_2Se_3-Cu. It was decided to investigate this effect further.

1.7 REFERENCES

1. Barret, C S, Structure of Metals : McGraw Hill Book Company, New York, 1952, p 1.
2. Eckstein, B, Mater Res Bull, 3, p 199, 1968.
3. Rudee, M L and Howie, A, Phil Mag 25, p 1001, 1972.
4. Rudee, M L, Thin Solid Films, 12 , p 207, 1972.
5. Zachariasen, W H, J Am Chem Soc 54, p 3841, 1932.
6. Owen, A E, Contemp Phys 11, p 227, 1970.
7. Bagley, B G, Amorphous and Liquid Semiconductors (J Tauc editor), Plenum Press, London and New York, 1974, p 5.
8. Owen, A E, Electronic and Structural Properties of Amorphous Semiconductors (P G LeComber and J Mort, editors), Academic Press, London and New York, 1973, p 170.
9. Ast, D G, J Vac Sci Technol 10, p 748, 1973.
10. Fritzsche, H, Electronic and Structural Properties of Amorphous Semiconductors (P G LeComber and J Mort, editors), Academic Press, London and New York, 1973, p 579.
11. Knights, J C, Solid State Comm 16, p 515, 1975.
12. LeComber, P G, Madan, A and Spear, W E, Electronic and Structural Properties of Amorphous Semiconductors (P G LeComber and J S Mort, editors), Academic Press, London and New York, 1973, p 373.
13. Agarwal, S C, Phys Rev B 7, p 685, 1973.
14. Kastner, M, Physics Rev Lett 28, p 355, 1972.
15. Ovshinsky, S R and Sapru, K, Proc on the 5th International Conference on Amorphous and Liquid Semiconductors, Garmisch-Partenkirchen, Germany (J Stuke and W Brenig, editors), Taylor and Francis, London, 1974, p 447.
16. Mott, N F and Davis, E A, Electronic Processes in Non-crystalline Materials, Oxford, 1971.

17. Danilov, A V and El Mosli, M, Fiz Tverd Tela 5, p 2015, 1963.

18. Owen, A E, Glass Ind 48, p 637, 1967.

19. Kolomiets, B T, Phys Stat Sol 7, p 359, 1964.

20. Kolomiets, B T, Phys Stat Sol 7, p 713, 1964.

21. Grigorovici, R, Amorphous and Liquid Semiconductors (J Tauc, editor), Plenum Press, London and New York, 1974, p 69.

22. McFarlane, S C and Cochran, W, J Phys C 8, p 1311, 1975.

23. Tobolsky, A V and Eisenberg, A, J Colliod Sci 17, p 49, 1962.

24. Eisenberg, A and Tobolsky, A V, J Polym Sci 46, p 19, 1960.

25. Myers, M B and Felty, E J, Mat Res Bull, 2, p 535, 1967.

26. De Neufville, J P et al, J Non-cryst Sol 13, p 191, 1974.

27. Kastner, M, Phys Rev B 7, p 5237, 1973.

28. Haward, R N, Molecular Behaviour and the Development of Polymeric Materials (A Ledwith and A M North, editors), Chapman and Hall, London, 1974, p 446.

29. Dresner, J and Stringfellow, G B, J Phys Chem Sol 29, p 303, 1968.

30. Berkes, J S et al, J Appl Phys 42, p 4908, 1971.

31. Tokuda, W et al, J Appl Phys 45, p 5098, 1974.

32. Asahara, Y and Izumitani, T, J Non-cryst Sol 16, p 407, 1974.

33. Apling, A J et al, Thin Solid Films 27, p L11, 1975.

34. Bagley, B G et al, Proc on the 5th International Conference on Amorphous and Liquid Semiconductors, Garmisch-Partenkirchen, Germany (J Stuke and W Brenig, editors), Taylor and Francis, London, 1974, p 1169.

35. Vasko, A, Mat Res Bull 3, p 209, 1968.

36. Tobolsky, A V et al, J Coll Sci 17, p 717, 1962.

37. Renninger, A L et al, J Non-cryst Sol 16, p 1, 1974.

38. Kunugi, M et al, Zairyo 18, p 807, 1969.

39. Fischer, M and Krebs, H, Glastechn Ber 47, p 42, 1973.

40. Ioffe, A F and Regel, A R, Progr Semic 4, p 237, 1960.

41. Mott, N F and Twose, W D, Adv in Phys 10, p 107, 1961.

42. Davis, E A and Mott, N F, Phil Mag 22, p 903, 1970.

43. Austin, I G and Garbett, E S, Electronic and Structural Properties of Amorphous Semiconductors (P G LeComber and J Mort, editors), Academic Press, London and New York, 1973, p 393.

44. Renninger, A L and Averbach, B L, Phys Rev B 8, p 1507, 1973.

CHAPTER 2 OPTICAL PROPERTIES OF AMORPHOUS SEMICONDUCTORS

2.1 INTRODUCTION

This chapter is concerned with the interaction of electromagnetic radiation with semiconductors in general and amorphous semiconductors in particular.

A plane electromagnetic wave travelling in an absorbing medium can be represented by the equations for the electric and magnetic field, respectively

$$\underline{\mathcal{E}} = \underline{\mathcal{E}}_o \exp\ [i(2\pi\nu t - \underline{K} . \underline{r}\ )\ ] \qquad 2.1$$

and

$$\underline{H} = \underline{H}_o \exp\ [i(2\pi\nu t - \underline{K} . \underline{r}\ )\ ] \qquad 2.2$$

where $\underline{K}$ is the complex wave vector

$$\underline{K} = \underline{K}_1 + i\underline{K}_2 \qquad 2.3$$

Equations 2.1 and 2.2 are a solution of Maxwell's equations for the propagation of an electromagnetic field in a medium provided that the magnetic permeability $\mu = 1$ and

$$K^2 = 4\pi^2 \nu^2 \varepsilon/c^2 = 4\pi^2 N^2/c^2 \qquad 2.4$$

where c is the speed of light in vacuum.

The complex dielectric constant ε and the complex refractive index N are defined by the following relations

$$\varepsilon = \varepsilon_1 - i\varepsilon_2 = \varepsilon_1 - 2\, i\sigma/\nu \qquad 2.5$$

$$N = n - ik = \varepsilon^{\frac{1}{2}} \qquad 2.6$$

Here σ is the frequency dependent conductivity, n the real refractive index of the medium and k (not to be confused with $\underline{k}$, the wave vector for electrons) is the extinction coefficient or absorption index of the medium. All parameters in equations 2.5 and 2.6 depend on frequency ω. It follows from equations 2.5 and 2.6 that

$$\varepsilon_1 = n^2 - k^2 \qquad 2.7$$

and

$$\varepsilon_2 = 2nk \qquad 2.8$$

For homogeneous plane wave ($\underline{K}_1$ and $\underline{K}_2$ parallel) this gives for the x-component of $\underline{\mathcal{E}}$

$$\mathcal{E}_x = \mathcal{E}_{xo} \exp\,[\,i2\pi\nu(t - xn/c)\,]\, \exp\,[\,-2\pi kx/\lambda\,] \qquad 2.9$$

This represents a wave travelling in the x-direction with velocity c/n. The wave amplitude is attenuated by $\exp\,[\,-2\pi kx/\lambda\,]$.

The attenuation of the energy density, or light intensity, is given by the square of the amplitude, ie,

$$F/F_o = \exp\,[\,-4\pi kx/\lambda\,] = \exp\,[\,-\alpha x\,] \qquad 2.10$$

where F is the intensity and α is the absorption coefficient. Thus

$$\alpha = 2\omega k/c = 4\pi k/\lambda \qquad 2.11$$

where λ is the wavelength.

When the wave is incident upon an interface between two media with different refractive indices n_1 and n_2, one of which is absorbing, some of the light will be refracted. This follows from the necessary boundary conditions that the tangential components of $\underline{\mathcal{E}}$ and $\underline{H}$ must be continuous across the interface. At normal incidence the fraction of reflected intensity is given by the reflection coefficient

$$R = \frac{(n_1-n_2)^2 + k^2}{(n_1+n_2)^2 + k^2} \qquad 2.12$$

For vacuum $\varepsilon = N^2 = 1$ which simplifies equation 2.12.

Equation 2.12 allows the determination of the real refractive index if the absorption is low. Both n and k (or α) can in theory be determined from measurements of the reflected and transmitted intensities. The value at a given wavelength of any one complex parameter N or ε , is sufficient to determine all the parameters in the above equations. It is, however, necessary to know only one real or imaginary part over a wide frequency range. All other parameters may then be obtained through use of the Kramers-Kronig dispersion relations. For example, $\varepsilon_1(\omega)$ and $\varepsilon_2(\omega)$ are related by

$$\varepsilon_1(\nu) = 1 + \frac{2}{\pi}\int_0^\infty \frac{\nu'\,\varepsilon_2(\nu')\,d\nu'}{(\nu')^2-\nu^2} \qquad 2.13(a)$$

and

$$\varepsilon_2(\nu) = -\frac{2\nu}{\pi}\int_0^\infty \frac{\varepsilon_1(\nu')\,d\nu'}{(\nu')^2-\nu^2} \qquad 2.13(b)$$

If $\varepsilon_2(\nu)$ is assumed to be zero for all ν it follows from equation 2.13(a) that $\varepsilon_1(\nu) = 1$ for all ν , ie, there is no dispersion without attenuation somewhere in the spectrum. At low frequencies equation 2.13(a) simplifies to

$$\varepsilon_1(0) = n_0^2 = 1 + \frac{2}{\pi}\int_0^\infty \frac{\varepsilon_2(\nu')\,d\nu'}{\nu'} \qquad 2.14$$

This is called a sum rule and is useful for comparing the reflection and absorption data with the low frequency dielectric constant. Another sum rule is obtained for high frequencies

$$\varepsilon_1(\nu) = 1 - \frac{2}{\pi\nu^2}\int_0^\nu \nu'\varepsilon_2(\nu')\,d\nu' \qquad 2.15$$

provided that ν is well separated from the nearest absorption band so that $\varepsilon_2(\nu') = 0$ when $\nu' \sim \nu$.

The first order perturbation operator describing the interaction between the radiation and electrons is

$$H(\underline{r},t) = \frac{e}{m}\,\underline{A} \cdot \underline{p} \qquad 2.16$$

where e is the electron charge, m the free electron mass, $\underline{p}$ the momentum of the electron and $\underline{A}$ the vector potential of the electromagnetic radiation.

$$\underline{A} = \frac{\mathcal{E}_0}{i2\pi\nu} \exp\,[\, -i(2\pi\nu t - \underline{K} \cdot \underline{r}\,] + \text{c.c.} \qquad 2.17$$

where c.c. denotes the complex conjugate term which will be neglected here as it corresponds to stimulated emission whereas absorption is the feature of interest here. The problem is easily solved in the case of periodic wavefunctions by using time dependent perturbation theory. The transition probability for an electron going from an occupied valence band state $E_v(\underline{k}_v)$ to an empty conduction band state $E_c(\underline{k}_c)$ is then

$$w(\nu,\ t,\ \underline{k}_v,\ \underline{k}_c) =$$

$$\frac{e^2}{m^2\hbar^2} \left| \int_0^t dt' \int_v \underline{dr}\ \Psi_c^{*}\,(\underline{k}_c,\ \underline{r},\ t')\ \underline{A} \cdot \underline{p}\ \ \Psi(\underline{k}_v,\ r,\ t') \right|^2 \qquad 2.18$$

where $E_c(\underline{k}_c)$ is empty at t = 0. The time dependent wave functions can be written as

$$\Psi_v(k_v,\ \underline{r},\ t) = \exp\ [-\frac{i}{\hbar} E_v(\underline{k}_v)\ t\ ]\ \exp\,[\ i\underline{k}_v \cdot \underline{r}\ ]\ u_v(\underline{k}_v,\ \underline{r}) \qquad 2.19$$

and similarly for Ψ_c. The terms u_v and u_c contain the periodicity of the lattice. The time dependent part can be integrated seperately from the spatial part. Both terms contain exponentials with imaginary arguments so that the integrals vanish unless the arguments are zero. That is

$$E_c - E_v - h\nu = 0 \qquad 2.20$$

which is the same as equation 1.4. Also

$$\underline{K} - \underline{k}_c + \underline{k}_v = 0 \qquad 2.21(a)$$

Since the momentum of photons in the wavelength range of interest here is very small this simplifies to

$$-\underline{k}_c + \underline{k}_v = 0 \qquad 2.21(b)$$

which is the same as equation 1.3.

It is also necessary to sum over all states $\underline{k}$ in both bands. Thus

$$\varepsilon_2(\nu) = \frac{\hbar^2 e^2}{\pi^3 m^2 \nu^2} \sum_{ij} | H_{ij} |^2 \delta(E_i - E_j - h\nu) \qquad 2.22$$

where the conservation of energy is expressed as a delta function and where H_{ij} is the *matrix element* for transitions between states i and j;

$$H_{ij} = \int_V \underline{dr} \ \exp\ [-i(\underline{k}_j - \underline{K}) \ . \ r\ ] u_j^* \ \frac{\underline{\mathcal{E}}_o}{\mathcal{E}_o} \ . \ \nabla \exp(i\underline{k}_i \ . \ \underline{r}) \ u_i \quad 2.23$$

In semiconductor crystals the densities of states increase approximately parabolically with energy from the band edges into the bands. With conservation of energy and wave vector this means that the absorption will increase as the square root of excess photon energy, ie,

$$\varepsilon_2(\nu) \propto \frac{(h\nu - E_g)^{\frac{1}{2}}}{(h\nu)^2} \qquad 2.24(a)$$

where E_g is the smallest direct band gap. These are called direct transitions. There may be a smaller band gap for which equation 2.21(b) is not satisfied. At finite temperatures transitions can still take place, between states that do not satisfy this condition, but with the assistance of phonons. This can be considered as a two stage process: (a) a direct transition to a state for which $\underline{k}_i = \underline{k}_f$; and (b) a phonon assisted transition. Energy and quantum numbers must be conserved for the whole process but not for the individual stages. This gives rise to equations 1.5 and 1.6. Equation 2.22 must also be modified to include the square of the matrix element for the electron-phonon interaction and the density of phonons. The final expression is

$$\varepsilon_2(\nu) = \frac{\nu^{-2} C(h\nu + h\nu_q - E_g)^2}{\exp(h\nu_q/kT) - 1} + \frac{\nu^{-2} C(h\nu - h\nu_q - E_g)^2}{1 - \exp(h\nu_q/kT)} \qquad 2.24(b)$$

where E_g is the smallest indirect gap, $\hbar\omega_q$ the phonon energy and C includes the matrix elements. This describes an indirect transition. Even if energy and quantum numbers are conserved the matrix elements may vanish in the first approximation because of the symmetry of the Bloch functions $u_v(\underline{k}_v)$ and $u_c(\underline{k}_c)$. In that case the transitions are said to be 'forbidden' but can still take place with a greatly reduced probability, giving a three-halves and cube power laws for forbidden direct and forbidden indirect transitions respectively.

The above discussion applies when both the initial and the final states are extended throughout the sample and have well-defined wave vectors. One or both of these conditions may be violated for localized states in crystals and amorphous materials. As was discussed in Chapter 1, $\Delta k \doteq k$ near the band edges in amorphous materials, which implies that k is no longer conserved in transitions. The energy however, must still be conserved. This gives rise to *non-direct* transitions and new power laws which will be discussed in the next section.

Considering localized states, whether in crystalline or amorphous material it is clear that transitions between two such states are unlikely unless their spatial seperation is small. The matrix element H_{ij} will be proportional to the overlap of the two exponentially decaying wave functions. There is, however, a much greater probability of transitions when only one of the two states is localized. Davis and Mott[1] have argued that in amorphous materials the matrix element is similar when one state only is extended as when both are extended.

2.2 INTERBAND ABSORPTION IN AMORPHOUS MATERIALS

2.2.1 POWER LAWS

Under the assumptions of relaxed selection rules and an energy independent matrix elements, the absorption can be obtained by integrating over all transitions that satisfy the energy conservation conditions. Thus

$$\alpha = \frac{2\pi\nu}{nc}\,\varepsilon_2(\nu)$$

$$= \frac{h^3e^2M^2}{2\pi^4m^2nc}\,\frac{1}{h\nu}\int_{E_c-h\nu}^{E_v} N_c(E + h\nu)\,N_v(E)\,dE \qquad 2.25$$

where E_v and E_c are the edges of the valence and conduction bands respectively. Assume that the densities of states $N_c(E)$ and $N_v(E)$ vary as some powers p and s, ie,

$$N_c(E) = N_c \times (E - E_c)^p \qquad 2.26$$

and similarly for the valence band. Equation 2.25 can now be integrated by substituting

$$y = \frac{E_v - E}{h\nu - (E_c - E_v)} \qquad 2.27$$

This gives

$$\alpha h\nu = \frac{h^3e^2M^2N_vN_c}{2\pi^4m^2nc}\,(h\nu - E_g)^{p+s+1}\int_0^1 (1 - y)^p y^s dy \qquad 2.28$$

where $E_g = E_c - E_v$.

The integral in equation 2.28 can easily be evaluated by the use of gamma functions and gives a numerical factor $\sim\frac{1}{2}$.

In amorphous semiconductors the observed behaviour of absorption as a function of energy is of this form at energies corresponding to $\alpha \geqslant 10^4$ cm^{-1}. Thus the absorption in a-Se is linear with photon energy^2 in the range 2.1 eV < hν < 3.1 eV

$$\alpha h\nu = \frac{2\pi}{nch}\ \varepsilon_2(\nu)\ (h\nu)^2 = C_1(h\nu - E_{01}) \qquad 2.29$$

This seems to be an exceptional case, however, and the most commonly observed form is a square relation:

$$\alpha h\nu = C_2(h\nu - E_{02})^2 \qquad 2.30$$

which gives good agreement with the data for example, amorphous As_2Te_3 [3,4], As_2Se_3 [5,6], As_2S_3 [5,7], As [8], tedrahedrally bonded amorphous materials for example, a-Si [9] and also many multicomponent glasses (eg, $Ge_{10}As_{40}Se_{50}$ [10], and $Si_{12}Te_{48}As_{30}Ge_{10}$ [11]). Other multicomponent glasses (eg, $Ge_{15}Te_{81}Sb_2S_2$ [12]) have an absorption coefficient that obeys a cubic relation

$$\alpha h\nu = C_3(h\nu - E_{03})^3 \qquad 2.31$$

There are two different interpretations of these observations. Figure 2.1 outlines the density of states, diagrams proposed by Tauc[13], and by Davis and Mott[1] to account for equation 2.30. In both cases

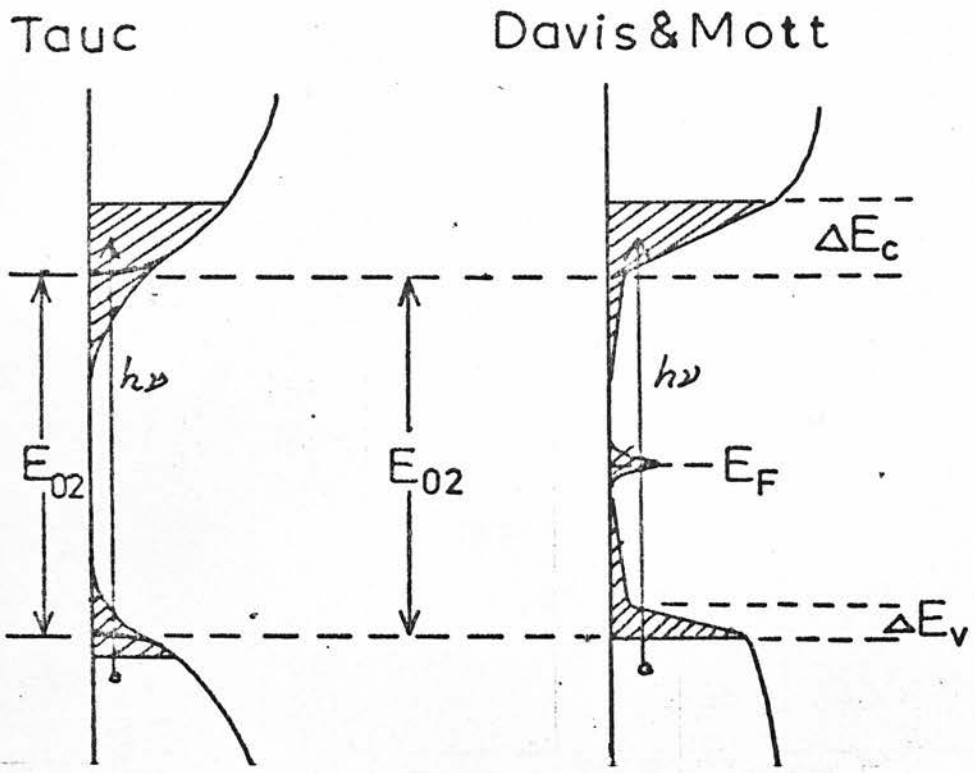

FIGURE 2.1

Different interpretations of the extrapolated optical gap E_{o2} (Ref 1,13).

the matrix elements are assumed to be the same for transitions between two extended states as between one localized and one extended state. Tauc assumes parabolic band edges similar to those in crystals. Thus,

$$N_v = \left(\frac{4\pi}{h^3}\right)(2m_h^*)^{3/2} \qquad 2.32(a)$$

and

$$N_c = \left(\frac{4\pi}{h^3}\right)(2m_e^*)^{3/2} \qquad 2.32(b)$$

where m_h^* and m_e^* are the density of states effective masses of holes and electrons respectively. According to this model $p = s = \frac{1}{2}$. The gap that appears in equation 2.30 is not the true gap, but that obtained by extrapolating the parabolic densities of states to zero density. It follows that if the mobility edges do not coincide with the extrapolated edges, then there will be a deviation from equation 2.30 as $h\nu$ approaches E_{02} from above.

This is because the limits of integration in equation 2.25 do not correspond to the extrapolated band edges but rather to the onset of extended-to-localized transitions and hence a correction factor should be applied. This correction factor is shown in Figure 2.2 - as a function of $h\nu$ for the case of mobility edges lying outside the band edges. The assumption was made that the matrix element for localized-to-localized transitions is negligible. The quantity ΔE is the difference between the mobility edge E_c (or E_v) and the extrapolated optical edge E_c^o (or E_v^o). As Figure 2.2 shows, when $h\nu \leq E_{02} + \Delta E$, no transitions involving extended states are possible. The square law (equation 2.30) should, according to Figure 2.2, hold for

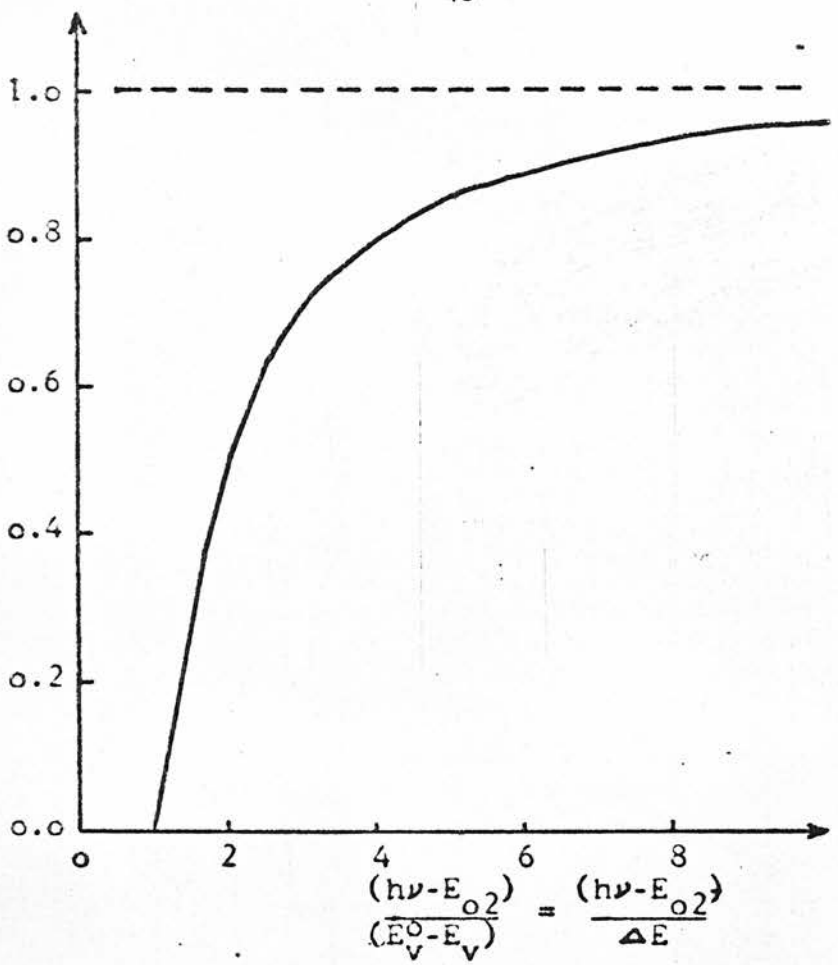

FIGURE 2.2

A correction factor to the parabolic absorption function. ΔE is the difference between the mobility edge E_c (or E_v) and the extrapolated optical edge E_c^o (or E_v^o). It is assumed that the mobility gap is larger than the extrapolated optical gap (as shown in FIGURE 2.1(a)).

$$h\nu \geq E_{02} + 4\Delta E \qquad 2.33$$

This can be used to place an upper limit on ΔE, for whichever band it is smaller.

In the Davis and Mott interpretation on the other hand, transitions between a linear tail of localized states in one band and extended states in the other band are assumed to dominate, the density of the latter varying slowly enough with energy to be taken as constant above the mobility edge. Thus p = 1, s = 0, or vice versa. The density of states in the linear tails can be expressed as

$$N_c(E) = \frac{N_c' \cdot (E - E_A)}{\Delta E_c} \qquad 2.34(a)$$

and

$$N_v(E) = \frac{N_v' \cdot (E_B - E)}{\Delta E_v} \qquad 2.34(b)$$

where $\Delta E_c = E_c - E_A$ and $\Delta E_v = E_B - E_v$. The gap E_{02} in this case is $E_c - E_B$ or $E_A - E_v$, whichever is smaller.

The two different expressions for C_2 in the two interpretations are then,

Tauc : $$C_2 = \frac{\pi}{8} \frac{N_c N_v M^2}{n} D \qquad 2.35$$

Davis and Mott : $$C_2 = \frac{1}{2} \frac{N_c' N_v' M^2}{\Delta E n} D \qquad 2.36$$

where D is a constant, n is the refractive index, the numerical factors account for the integral in equation 2.28 and ΔE is the depth of the deeper of the two tails. The linear tails, in the Davis and Mott interpretation are due to disorder and are expected to be 0.1 - 0.2 eV in simple chalcogenide glasses like As_2Se_3 [14].

A major objection to the Davis and Mott interpretation, as they point out themselves[14], is that it is inconsistent with the relatively wide energy range over which equation 2.30 is observed to hold, eg, 1.5 eV in a-As_2Se_3 [6]. Both interpretations give estimates of C_2 in reasonable agreement with experiment.

To account for equation 2.29 it is necessary to assume energy independent densities of states in both bands (p = s =0) or that the matrix element is energy dependent, as Maschke and Thomas[15] did. Using the convoluted density of states appropriate to trigonal Se and relaxing the k-conservation rule these authors have calculated a spectrum in agreement with the ε_2 curve. They find that M^2 decreases sharply in the range 2 - 3 eV.

In the case of equation 2.31 linear densities of states (p = s = 1) are assumed. Localized-to-localized transition may give a significant contribution to the absorption described by this equation and may also be responsible for the absorption that is observed below the 'optical gaps' E_{01} and E_{02}. This will be discussed in the next section.

2.2.2 VARIATION OF THE GAP WITH TEMPERATURE

It is a common practice when considering the variation of the band gap in amorphous semiconductors with temperature, pressure, preparation or composition, to arbitrarily define an optical gap as the photon energy corresponding some fixed value of absorption. This can often give quite useful information. It should be realized, however, that in general, the shift in such an arbitrary gap is not the same as that of the 'true' band, whatever that may be. Indeed, it depends on the actual value of absorption chosen. This has been clearly demonstrated for the case of a-As_2S_3 by Street et al[14]. They find that for $\alpha \geqslant 10^4$ cm^{-1} equation 2.30 applies, with *both* E_{02} and C_2 decreasing with increasing temperature. Reduction in E_{02} tends to increase the absorption at a given wavelength, whereas a reduction in C_2 has the opposite effect. Some of their results are shown in Figure 2.3. For $\alpha < 10^4$ cm, they find the widely observed exponential form of absorption which will be discussed in the next section. Here, the temperature shift is greater for lower levels of absorption because of thermal broadening of the exponential absorption edge. The shift in E_{02} is 0.12 eV between 10 K and 295 K, which corresponds to a shift of the absorption curve with $h\nu$ at a point where α is in the range 10^3 cm^{-1} to 10^4 cm^{-1}. This supports the validity of approximating E_{02} by the energy at which $\alpha = 10^4$ cm^{-1}.

Treating the gap as a thermodynamic variable one can write

$$\left(\frac{\partial E_g}{\partial T}\right)_P = \left(\frac{\partial E_g}{\partial T}\right)_V - \frac{\alpha_V}{K}\left(\frac{\partial E_g}{\partial P}\right)_T \qquad 2.37$$

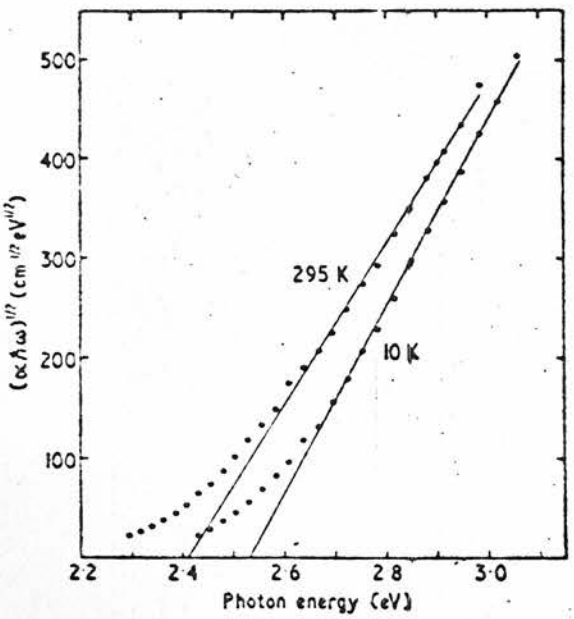

FIGURE 2.3(a)

Absorption data for a-As_2S_3 plotted according to equation 2.3o (Ref 16).

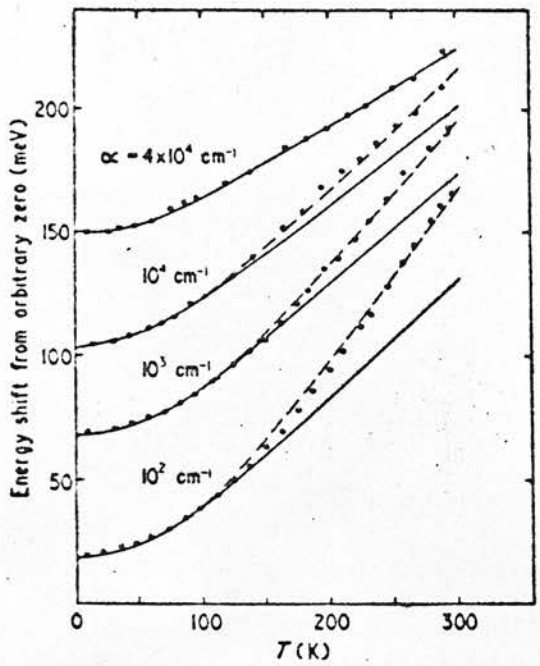

FIGURE 2.3(b)

Temperature shift of the edge at various values of the absorption coefficient, the shift is larger for low values of absorption (Ref 16).

where E_g is the optical gap, however it is defined, α_v is the volume expansion coefficient.

$$\alpha_v = \frac{1}{V}\left(\frac{\partial V}{\partial T}\right)_P \qquad 2.38$$

and K the compressibility

$$K = -\frac{1}{V}\left(\frac{\partial V}{\partial P}\right)_T \qquad 2.39$$

The second term on the right of equation 2.37 represents the effect of lattice dilation but is normally less than a quarter of the observed temperature shift in both the crystalline and amorphous forms of tetrahedral materials and arsenic-chalcogenides, and frequently has the wrong sign as well[16,17]. The constant volume term is usually interpreted as being due to non-linear terms, principally quadratic, in the electron-phonon interaction. No adequate treatment of this phenomenon exists. Thus Harbeke[18] states that 'the positive contribution of the electron-phonon interaction is not understood in terms of present-day theory'. Street et al[16] have adopted a semi-empirical approach based on the shifts of the zero-phonon transitions of colour centres, in which the energy shift is proportional to the change in internal thermal energy. To test whether this is true for interband transitions they compared published data on energy gaps in crystalline Ge and Si with specific heat data and found that the expected proportionality does indeed hold. Thus

$$E_g(0) - E_g(T) = E_g(0) \times \phi(T) \propto \int_0^T C_v(T)\, dT \qquad 2.40$$

for these materials, where E_g can be either the direct or indirect gap, and $\phi(T)$ is the fractional shift of $E_g(T)$ relative to $E_g(0)$. At room temperature $\phi(T)$ is approximately linear. Street et al explain their results for a-As_2S_3 on the assumption that equation 2.40 applies to this material also, although they do not actually prove that it does. The heat capacity of a-As_2S_3 has been measured in the temperature range 53-305 K by Tarasov and Zhdanov[19]. Figure 2.4 compares the change in internal energy calculated from their work with the results of Street et al[16] for the temperature shift of the energy at which $\alpha = 10^4 cm^{-1}$. The fit is quite reasonable. It should be pointed out, however, that over most of the temperature range both quantities vary approximately linearly with T, so the fit could be fortuituous. It is also difficult to see why different modes of lattice vibration should contribute to the band gap shift in proportion to their energy.

For the lack of any better working hypotheses however, and with the above qualifications in mind, it will be assumed in this work that the proportionality 2.40 holds, and therefore that

$$\beta = \left(\frac{\partial E_g}{\partial T} \right)_V = a\, C_v(T) \qquad 2.41$$

where a is a material constant and $C_v(T)$ is the specific heat at constant volume.

There is an indication from the work of Edmonds[20] that the same equation may apply above T_g as well. For the photon energy corresponding to $\alpha = 100\ cm^{-1}$ he observed a temperature shift of $\sim 7 \times 10^{-4}$ eV/K below, and $\sim 1.4 \times 10^{-3}$ eV/K above T_g. According to

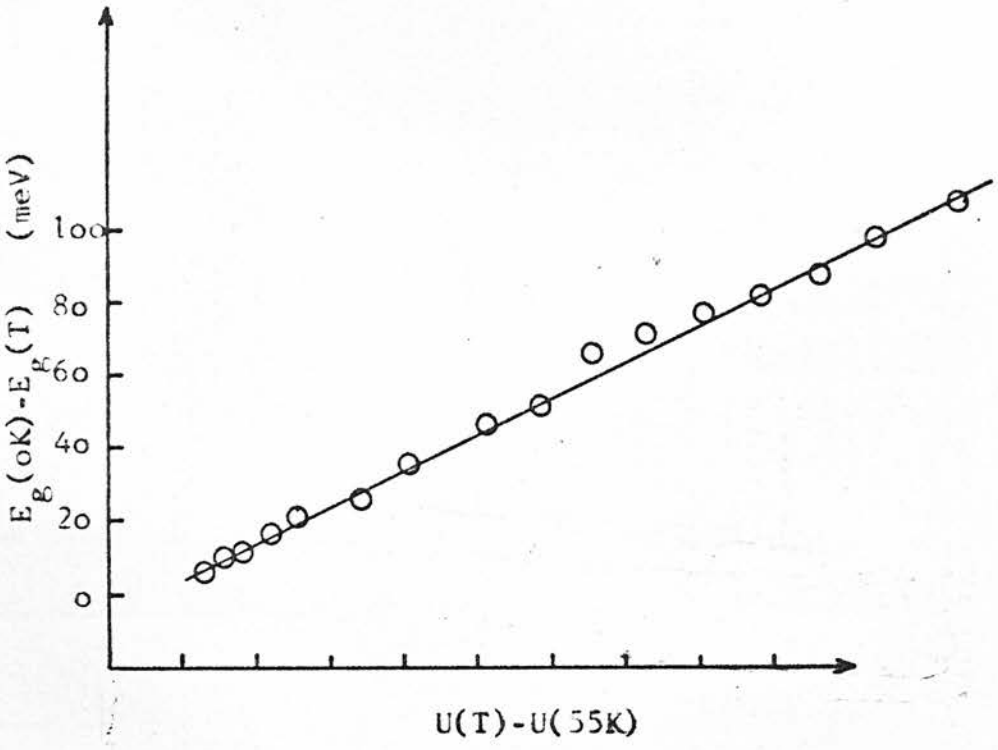

FIGURE 2.4

Change in the optical gap of a-As_2S_3 vs the change in the internal thermal energy. E_g is the photon energy at which $\alpha = 10^4 cm^{-1}$ (Ref 16). U(T) was calculated from the specific heat (Ref 19).

Schnaus et al[21] C_p - the specific heat at constant pressure - increases by about 70% at T_g. Some of the increase in the temperature coefficient as measured by Edmonds is undoubtedly due to the decrease in the exponential slope with T but probably not all. Hurst and Davis[22] found that the measured activation energy E_σ for conductivity increased from 0.90 eV in the glass to 1.02 eV in the liquid. E_σ is thought to correspond to the 'true' activation energy extrapolated linearly to 0 K, so this can be taken as a further evidence for an increased temperature coefficient of the band gap above T_g. An obvious next step is to ask whether other forms of internal energy might affect the gap in the same way, eg, can the different gaps observed in differently prepared amorphous samples be accounted for by the difference in the structural part of the internal energy? This question will be discussed further in a later section.

2.2.3 VARIATION OF THE GAP WITH PRESSURE

The variation of the absorption edge with pressure in several amorphous materials has been discussed in detail by Kastner[17]. He found that in general the gap in amorphous chalcogenides has a large negative pressure coefficient, $-\left(\frac{\partial E_o}{\partial P}\right)_T \gtrsim 10^5$ eV/bar. In amorphous tetrahedral materials on the other hand the pressure coefficient is positive and much smaller, this in spite of the fact that tetrahedral crystals can have a pressure coefficient of either sign. The little data there is on effects of pressure in crystalline chalcogenides[21] indicates that it is much the same as in their amorphous counterparts.

Referring to Figure 1.2, it is clear that a reduction in the interatomic distance by applied pressure should cause an increase in the gap, this is in agreement with observation in the case of tetrahedrally bonded amorphous solids. Kastner argues that in solids of lower coordination, like Se or As_2Se_3, the atoms can move closer together without change in bond lengths. Thus in Se the distance between chains or Se_8 molecules is reduced with increasing pressure while the covalent bond lengths are relatively unaffected. Kastner relates the ability to compress materials in this way with the average bond-free solid angle (BFSA), ie, the solid angle of an atom that does not contain bonding orbitals. This also explains the large compressibility of these materials. Interaction between the non-bonding lone-pair orbitals, as well as closed shell interactions, is then responsible for the observed pressure coefficients of both the gap and the volume. In molecular solids, in the case of molecules without charge or dipole moment, the closed shell interaction gives rise to an attractive interaction between induced dipoles.

$$U_d = - \sum_{ij}' \frac{| I_{ij} |^2}{(E_i - E_j)} \qquad 2.42$$

where $| I_{ij} |^2$ is a matrix element and varies with distance like r^{-6}. The sum is taken over all empty states i and filled states j of the isolated molecule.

This term is balanced by a repulsive exchange term

$$U_e \propto \frac{s^2}{r} \qquad 2.43$$

where s is the orbital overlap and r the intermolecular separation.

It is likely that in low coordination materials the first term is responsible for the reduction in band gap by causing pressure broadening of the bands.

Thus a diagram similar to Figure 1.2(b) could be drawn for a LP semiconductor under pressure by broadening the bands without actually changing the position of the bonding band minimum. The exchange term may be overshadowed in partially cross-linked materials by the forces associated with the bending of covalent bonds.

For the general case Kastner writes

$$\left(\frac{\partial E_g}{\partial P}\right)_T = \left(\frac{\partial E_o}{\partial P}\right)_T - \left(\frac{\partial J}{\partial P}\right)_T \qquad 2.44$$

where the first term on the right hand side represents the average separation of the valence and conduction bands or the average bond strength and can be related to the dielectric constant ε_1 in tetrahedral semiconductors. This term dominates in tetrahedral semiconductors whereas the second term, which is the band broadening term, dominates in molecular and low coordination materials.

Kastner also discusses the results of Nunoshita and Arai[23] who found that for 25 glasses in the Si-As-Te system

$$\Delta E = E_1 - \rho\delta \qquad 2.45$$

where ΔE is twice the activation energy of the dc conductivity, E_1 and δ are constants and ρ is the density. Furthermore, their results also indicate[24] a proportionality between ΔE and the optical gap, defined either as the photon energy at which $\alpha = 10\ cm^{-1}$ or by equation 2.30. Kastner shows that changes in density arising from differences in composition and from compression have similar effects on the optical gap. This is all the more surprising when one considers the widely different atomic masses of the constituent atoms which are 28 : 75 : 128 for Si : As : Te respectively. All the compositions contain at least 30% Te (atomic), and the As content has very little effect on either ρ or ΔE. This shows that the Si : Te ratio controls both parameters. It is perhaps relevant in this connection that the approximate mass ratios and bond numbers for Si : As : Te are 1 : 3 : 5 and 4 : 3 : 2 respectively, thus two As atoms have the same mass and same number of bonds as one Si atom plus one Te atom. If a constant fraction of Ge atoms is included, equation 2.45 still applies but the value of E_1 is increased. It seems difficult to explain the results for this system (Si-As-Te) with Kastners BFSA and Van der Waals interactions, considering that average bond energies must depend on the Si : Te ratio, ie, it is expected that most of the increase in E_g with increased consentration of Si is due to increase in E_o in equation 2.44 rather than to a decrease in J. On the other hand, according to Kastner, the main affect of pressure in these materials is on J.

2.2.4 THE PREFACTORS C_1 AND C_2

Consider equations 2.35 and 2.36 and a similar equation for the linear absorption case 2.29, ie

$$C_1 = \frac{N_c N_v M^2}{n} D \qquad 2.46$$

where N_c and N_v now denote the approximately constant densities of states in the conduction and valence bands respectively.

It is clear that any changes in C_1 and C_2 must be accounted for by changes in the densities of states, refractive index, matrix element or, in the case of equation 2.36, changes in the linear tail depth ΔE. Four cases need to be considered, ie, the variation with pressure, temperature, preparation and composition. For the first of these, the only experimental data known to the present author are Kastner's measurements of absorption in a-$Ge_{16}As_{35}Te_{28}S_{21}$ at 0 and 2 kbar at room temperature.

He found that the whole absorption curve shifted without a change in shape and inferred that only the gap width is pressure dependent. This is not conclusive however, since Kastner does not plot his high absorption data as $(\alpha h\nu)^{\frac{1}{2}}$ vs $h\nu$. Kastner's analysis also shows that the refractive index, at least at longer wavelengths, changes only by a small amount with pressure or temperature - of the order of 1% for a pressure of 1 kbar or a temperature change of 300 K.

Cornet and Rossier[4] state that $C_2 = 5.2 \times 10^5$ cm^{-1} eV^{-1}, independent of temperature and composition in the As-Te system, for

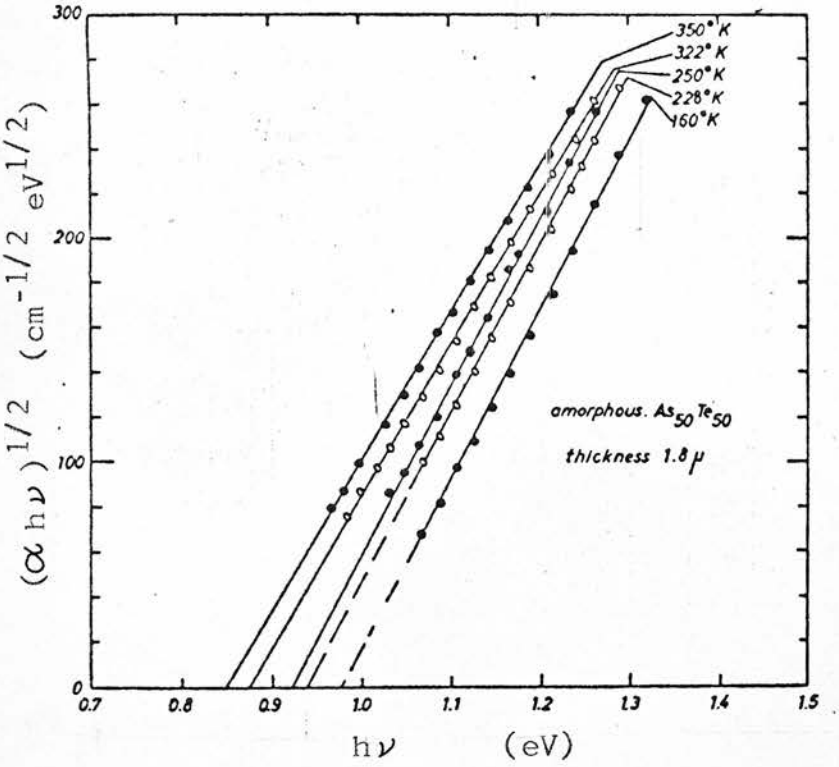

FIGURE 2.5

A square low plot for a-AsTe. The lines are closer together at high absorption, indicating that C_2 decreases with increasing temperature. (Ref 4).

25 - 60% As, atomic. They show some results on absorption in a-AsTe as a function of photon energy at different temperatures. This is reproduced in Figure 2.5 and it *does* show a progressive decrease in C_2 with increasing temperature, contrary to the author's statement. Weiser and Brodsky[25] find a similar change for a-As_2Te_3. Figure 2.3 illustrates results on a-As_2S_3 obtained by Street et al[16], who find a much larger shift in the same direction. These, and some other results are collected in Table 2.1, which includes all cases known to the present author, where C_2 has been determined at different temperatures.

It is clear that for the simple amorphous chalcogenides at any rate $\frac{dC_2}{dT} < 0$, the only exception being a-GeTe. It is interesting that the results of Kosek and Tauc[7] indicate a much larger shift for the case of a-As_2S_5 than for a-As_2S_3.

Also listed in Table 2.1 are the room temperature values of E_{02}. Comparison of the values of E_{02} and C_2 for each composition reveals a possible correlation, ie, that C_2 increases with increasing E_{02}. This is strongly supported by the results collected in Table 2.2, which show a large positive correlation between these two parameters as a function of preparation and treatment. Since the density also depends on preparation and treatment it might be expected that changes in C_2 and E_{02} are related to changes in density and, extending Kastner's arguments, that C_2 should depend on pressure in the same way as E_{02}. Table 2.1 shows clearly that the correlation between C_2 and E_{02} does not extend to different compositions. Thus C_2 is not much different in As_2Te_3 and As_2S_3 although E_{02} is four times larger in the latter. This is to be expected since C_2 depends only

	10^{-5}x C_2(300 K)	10^{-5}x $C_2(T_L)$	T_L	E_{02}(300 K)	Ref.
As	5.2 eV^{-1} cm^{-1}			1.2 eV	8
As_2S_3	5.1	5.3 eV^{-1} cm^{-1}	80 K	2.34*	7
"	6.6	8.6	10 K	2.41	16
"	7.4			2.32	5
"	6.1			2.4	26
"				2.36*	27
As_2S_5	6.2	10.6	80 K	2.45*	7
As_2Se_3	5.4			1.70	10
"	5.7			1.69	28
"	8.3			1.76	5
"	13	14	104 K	1.86	29
"				1.75*	27
As_2Te_3	4.7	5.6	77 K	0.83	25
"	5.2				4
"	5.4			0.82	3
"	8.6	8.6	99 K	0.90	29
AsTe	5.2	5.9	160 K	0.91	4
$As_{16}S_{80}Te_4$	15.6			2.30	30
$As_{16}S_{80}Te_4Ag_x$	4.0			1.25	30
$Ge_{10}As_{40}Se_{50}$	3.3			1.70	10
Si	5.2			1.26	9
GeTe	2.1	1.9	77 K	0.70	31

* corrected by adding 0.02 eV to the author's values, who plotted $\alpha^{\frac{1}{2}}$ vs $h\nu$ rather than $(\alpha h\nu)^{\frac{1}{2}}$.

TABLE 2.1

	10^{-5} C_2	Treatment	E_{02}	Ref.
As_2S_3	6.2 eV^{-1} cm^{-1}	Annealed at 443 K	2.39 eV	32
"	5.9	Same and illumination at 290 K	2.35	32
"	4.6	Same and illumination at 77 K	2.22	32
Ge*	4.2	Annealed at 293 K	0.78	33
"*	2.0	Annealed at 80 K	0.40	33
SiC	1.6	Sputtered, virgin	1.6	34
"	1.7	Annealed at 900 K	2.1	34

* Deposited and measured at 8 K

TABLE 2.2

on the matrix element and the shape of the band edges, whereas E_{02} depends on the relative positions of the valence and conduction bands, as well as the bandwidths.

It is therefore concluded that changes in the nature and distribution of the states at the band edges are responsible for changes in both E_{02} and C_2 and that the changes in these two parameters will therefore be related. Such changes can also be expected to influence other properties such as the electric conductivity.

2.2.5 THE BAND EDGES

Figure 2.7 illustrates the broadening of parabolic bands such as might be caused by increased van der Waals interaction (equations 2.42 and 2.44) with closed shells and/or LP states. It is clear from Figure 2.7 that E_{02}, N_v and N_c would all decrease with increased band broadening. The mobility gap need not, however, change in the same direction as the optical gap.

Figure 2.8 shows how linear tails of states might be affected by increasing disorder. In case (a) only the mobility edges move and

$$C_2 \propto \frac{N_c' \, N_v'}{\Delta E_c} = ab(\Delta E_v) \qquad 2.47$$

where a and b are constants. Thus, both C_2 and E_{02} should increase linearly with ΔE_v, while the mobility gap increases with ΔE_v and ΔE_c.

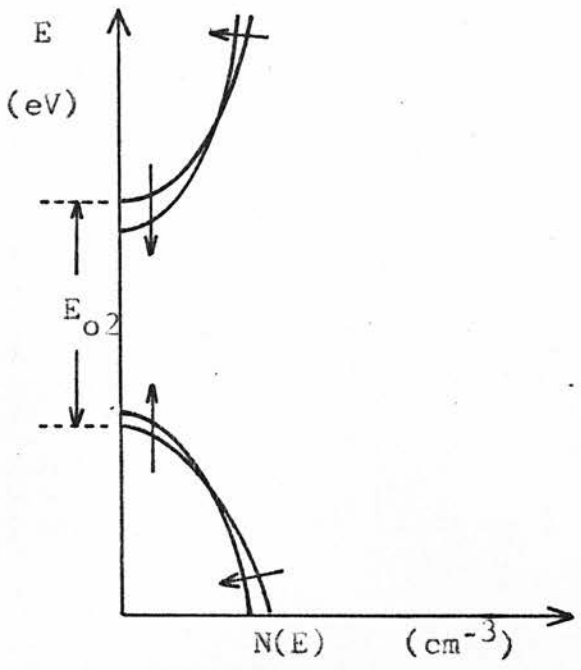

FIGURE 2.7

A parabolic density-of-states model for amorphous chalcogenides, the arrows indicate the effect of increasing non-covalent interactions with an increase in pressure or density (Ref 17).

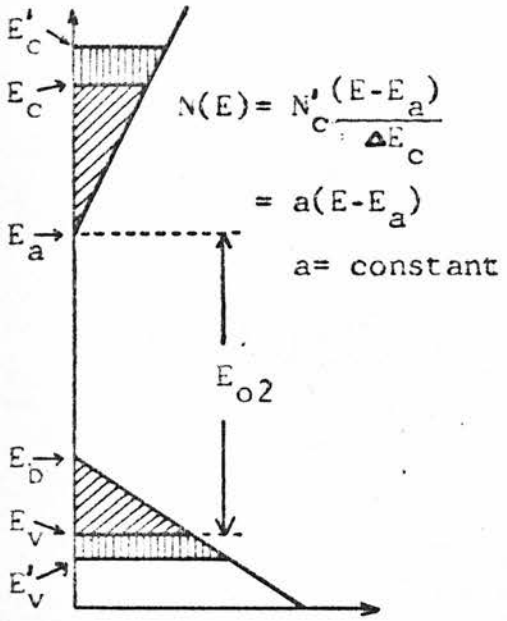

FIGURE 2.8(a)
The mobility edges move into the bands with increasing disorder.

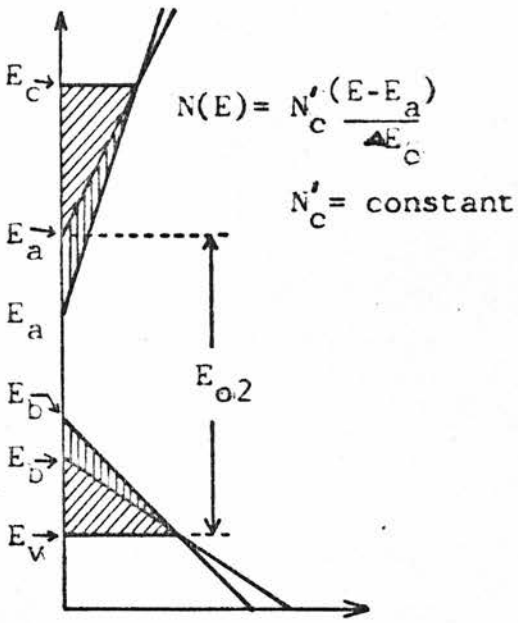

FIGURE 2.8(b)
The tails of localized states extend further into the gap with increasing disorder.

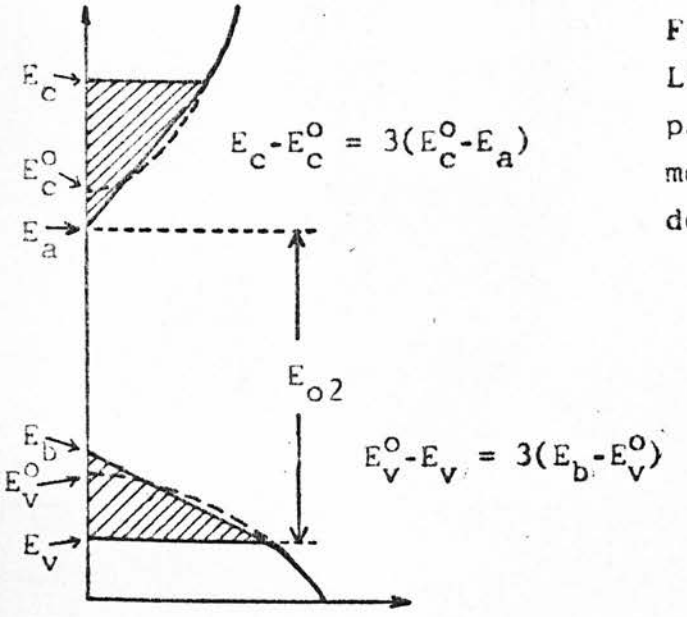

FIGURE 2.8(c)
Linear tails merging into parabolic bands at the mobility edges. The total density of states is conserved

In case (b) the mobility edges do not move but the linear tails extend further into the gap with increased disorder, keeping the density at E_c and E_v unaltered. Thus N_c' and N_v' are constant and

$$C_2 \propto 1/\Delta E_c \qquad 2.48$$

and

$$\Delta E_c + E_{02} = E_c - E_v = \text{constant} \qquad 2.49$$

A third and possibly more realistic case is shown in Figure 2.8(c). Here, the linear tails merge into the parabolic bands at the mobility edges. Variations in band-tailing are allowed subject to the constraints that there be no discontinuity in N(E) at the mobility edges and that the total number of states remains constant. These conditions can be used to relate N_c' to N_c and N_v' to N_v. The result is that

$$C_2 \propto \frac{N_c' \, N_v'}{\Delta E_c} = N_c \, N_v \, \frac{3}{4} \left(\frac{\Delta E_v}{\Delta E_c} \right)^{\frac{1}{2}} \qquad 2.50$$

and

$$E_{02} = E_p + \frac{1}{4} (3\Delta E_v - \Delta E_c) \qquad 2.51(a)$$

$$E_c - E_v = E_p + \frac{3}{4} (\Delta E_v + \Delta E_c) \qquad 2.51(b)$$

where E_p is the extrapolated parabolic gap $E_c^{\,o} - E_v^{\,o}$. Thus an increase in ΔE_c will cause a decrease in C_2 and E_{02} and an increase in the mobility gap. The results for these three cases are collected

in Table 2.3 in which constant factors are omitted for clarity.

	C_2	E_{02}	$E_c - E_v$
Fig 2.8(a)	$\propto \Delta E_v$	$= \text{const} + \Delta E_v$	$= \text{const} + \Delta E_v + \Delta E_c$
Fig 2.8(b)	$\propto 1/\Delta E_c$	$= \text{const} - \Delta E_c$	$= \text{const}$
Fig 2.8(c)	$\propto(\Delta E_v/\Delta E_c)^{\frac{1}{2}}$	$= \text{const} + \frac{1}{4}(3\Delta E_v - \Delta E_c)$	$= \text{const} + \frac{3}{4}(\Delta E_v + \Delta E_c)$

TABLE 2.3

The roles of the conduction band and the valence band could of course be interchanged in Figure 2.8. This corresponds to interchanging the subscripts in Table 2.3.

The experimental correlation between changes in C_2 and E_{02} follows directly from the parabolic band model and from cases (a) and (b) of the linear tail model. It is not inconsistent with case (c) if ΔE_v either changes much less than ΔE_c or changes in the opposite direction.

2.2.6 REFRACTIVE INDEX

The square of the refractive index at photon energies below the absorption edge equals the real part ε_1 of the dielectric constant and can be found from equation 2.13(a) or 2.14 if suitable assumptions are made as to the energy distribution of $\varepsilon_2(\nu)$ in the high absorption region. In classical dispersion theory, it is assumed that the solid is an assembly of oscillators with natural frequency ν_0, which are set into forced vibration by the radiation.

This leads to

$$n^2(\nu) = \varepsilon_1(\nu) = 1 + \frac{Ne^2}{\pi m} \frac{1}{(\nu_o^2 - \nu^2)} \qquad 2.52$$

where N is the electron density and m the electron mass. Most materials have dispersion curves that follow this law very closely, ie, a plot of $(n^2(\nu) - 1)^{-1}$ vs ν^2 gives a straight line over a considerable range in ν. It is customary to replace m by some average effective mass m* of the valence band electrons and write for $\nu << \nu_o$

$$\varepsilon_1 - 1 = \left(\frac{h\nu_p}{E_o} \right)^2 \qquad 2.53$$

where $E_o = h\nu_o$ and $\nu_p = (Ne^2/\pi m^*)^{\frac{1}{2}}$ is called the plasma frequency. This is a special case of the Drude relation;

$$\varepsilon_1 - 1 = 4\pi N_A \alpha_p \qquad 2.54$$

where α_p is the polarizability per atom and N_A the atomic density. The Drude relation only applies in the nearly-free-electron limit, when the charge distribution is spatially uniform and the local field equals the macroscopic field.

As discussed by Kastner[17,35], equation 2.54 can explain satisfactorily the pressure dependence of the refractive index in silicon and diamond where E_o is related to the average bonding-antibonding separation, which changes with the bond lengths under pressure. Equation 2.54 fails however, to explain the large positive pressure coefficient of the refractive index in amorphous

LP semiconductors. Kastner argues that this is because of their large bond-free-solid-angle and low coordination, ie, that these materials can be compressed without a change in bond lengths as was explained before. In this case the Lorenz-Lorentz (LL) relation, which includes local field corrections, gives a much better agreement

$$\frac{\varepsilon_1 - 1}{\varepsilon_2 + 2} = \frac{4\pi}{3} N_A \alpha_p \qquad 2.55$$

where α_p as calculated from this equation should be independent of density if the chemical bonding does not change much.

It has been argued recently[36] that polarization as described by α_p in equation 2.54 and 2.55 is not a physically correct description, at least in ionic solids. Wemple and DiDomenico[37,38,39] have developed a phenomenological model for dispersion. They write equation 2.52 as

$$n^2(\nu) - 1 = \frac{E_d E_o}{E_o^2 - (h\nu)^2} \qquad 2.56$$

where E_d is called the dispersion energy and measures the oscillator strength. They showed that E_d can be written as

$$E_d = N_{cat} Z_a N_e \beta \qquad 2.57$$

where N_{cat} is the coordination number of cations, Z_a the valency of anions, N_e the effective number of valence electrons and β is a constant which is 0.26 $\pm$ 0.04 eV for ionic materials and 0.37 $\pm$ 0.05 eV for

covalent materials. Applying these equations to chalcogenides, assuming $\beta \triangleq 0.37$ eV, they find that N_{cat} is greatly enhanced over the values expected from bond number, ie, interchain-or interlayer neighbours are important. This effect is especially pronounced in crystalline chalcogenides and they explain the reduction in the low energy peak of the $\varepsilon_2(\nu)$ spectrum of a-Se, as compared to that of the crystal, by assuming that N_{cat} is smaller in the amorphous form.

These observations seem to be qualitatively consistent with Kastner's BFSA concept. Thus the positive pressure coefficient of the refractive index in chalcogenides should be due to the increased interaction between electrons that do not form a (common) bond. This in turn should increase N_{cat} and thus E_d. The effects of increased pressure on E_o, caused by compression of bonds, should be much smaller in these materials. This is supported by the results of Galkiewic and Tauc[40] on a-As_2S_3. They found that equation 2.56 holds for 0.4 eV < $h\nu$ < 2 eV with $E_o = 4.7$ eV, $E_d = 22.8$ eV, $\left(\frac{\partial \ln E_o}{\partial P}\right)_T = 0.04 \times 10^{-5}$ bar^{-1} and $\left(\frac{\partial \ln E_d}{\partial P}\right)_T = 1.7 \times 10^{-5}$ bar^{-1}. It is interesting to note that E_o actually increases with pressure even though the band gap decreases, $\left(\frac{\partial E_g}{\partial P}\right)_T = -1.0 \times 10^{-5}$ eV bar^{-1}.[17] This is of course entirely consistent with Kastner's BFSA concept; it means that the bands are broadened by the application of pressure and (from the increase in E_d) that the probability of interband transitions is enhanced. The increase in effective N_{cat} may be interpreted as an increase in the matrix element for interband transitions, ie, C_2 will tend to increase as a result. This will be balanced however, by the reduction in N_c and N_v caused by the band broadening. Since E_o, E_d and E_g are all measurable quantities which contain information about average bond energies and the shape of the joint density of states

it is tempting to try to express the parameters C_1 and C_2 in terms of these quantities. Furthermore, E_o often coincides with the first peak in the $\varepsilon_2(\nu)$ spectrum. From equations 2.25 and 2.30

$$\varepsilon_2(\nu) = \frac{hcn}{2\pi} \frac{C_2}{(h\nu)^2} (h\nu - E_{02})^2 \qquad 2.58$$

where c is the speed of light. A first approximation would be to assume that

$$\varepsilon_2(E_o) \propto E_d \qquad 2.59$$

and use equation 2.58 or a corresponding linear law to evaluate $\varepsilon_2(E_o)$. This might be expected to be a good approximation when equation 2.58 holds up to $h\nu \sim E_o$. For instance, in a-As_2Se_3 E_o = 3.7 - 4.0 eV depending on preparation while E_d is nearly constant[41] and there is no deviation from equation 2.58 at $h\nu$ = 3.5 eV [6]. Thus, as indeed must be the case if E_o corresponds to a peak in ε_2 and C_2 (or C_1) to the steepness of the ε_2 curve between the band edge and the peak, C_2 should be proportional to E_d and depend inversely on the E_o/E_{02} ratio. A closer inspection of the results of De Neufville et al[41] reveals however that, at least in a-As_2S_3 and a-As_2Se_3, annealing of evaporated films reduces E_o much more than E_{02} (as a result of polymerization) while E_d changes only slightly. If equation 2.59 is based on valid assumptions this should lead to a steeper absorption curve, ie, an increase in C_2. Exactly the reverse is true as was discussed before and shown in tables 2.1 and 2.2 where it was established that the reduction in E_{02} was always accompanied by a reduction in C_2. It must be concluded that E_o

is *not* directly related to the position of a peak in the ε_2 spectrum. It can be shown[37,38] that E_o and E_d are related to weighted integrals over the whole ε_2 spectrum so the above conclusion is not very surprising. This does not necessarily mean that the absorption and dispersion parameters cannot be related in a more complex way. Equation 2.59 may still be valid for amorphous materials having only a single peak in their ε_2 spectrum.

2.2.7 OPTICAL PARAMETERS IN RELATION TO STRUCTURE

It is well known that the structure of chalcogenide glasses is dependent on previous thermal history and can also be affected by illumination. Many suggestions, sometimes conflicting, have been proposed to account for these effects. Most reports deal with evaporated films which can be irreversibly changed by either annealing or illumination with high density of bandgap radiation. This changes both the optical absorption and the structure. Many compositions can also be reversibly cycled between an 'annealed state' and an 'exposed state' which have different absorption coefficients. The annealed state is usually similar to bulk or sputtered samples.

Berkes et al[42] observed an increase in absorption in evaporated a-As_2Se_3 and a-As_2S_3. There was also a growth of cubic As_2O_3 crystals on the film surface if O_2 or H_2O was present. They proposed an explanation in terms of photo-decomposition into elemental As and a Se rich matrix, or, in the case of As_2S_3 into elemental As and S. No As crystals were detected and they

attributed the increase in α to arsenic clusters with a small band gap. The reversibility was explained by a metastable solubility limit for the arsenic clusters. It is interesting that Tanaka and Kikuchi[43] explain a *decrease* in absorption in flash evaporated As_2S_3 by the same mechanism, arguing that the increase in absorption due to the clusters of arsenic is more than compensated from by the larger band gap of sulfur rich compositions. Later investigations[10,44] have shown that photo-decomposition does not take place in these compounds although it may well do so in compositions that are rich in As.

De Neufville et al[41,44] conclude from their investigation of absorption, refractive index and X-ray diffraction that as-evaporated films of As_2S_3, As_2Se_3, AsSe and $Ge_{10}As_{40}Se_{50}$ contain a high proportion of As_4Se_6, As_4Se_4 or similar hard sphere molecules and that either annealing or illumination will cause these to polymerize into an extended network, thus explaining both structural and optical changes. This is supported by the observation[45] that unexposed evaporated As_2S_3 etches faster in a NaOH solution than As_2S_3 exposed to illumination. This property was used to make diffraction gratings. The compositions AsSe and $Ge_{10}As_{40}Se_{50}$ retain some of their molecular structure. The refractive index is increased as a result of the polymerization, mostly due to a reduction in E_o which is 0.4 eV lower in annealed As_2S_3 than in a freshly evaporated sample although E_g (at $\alpha = 10^4 cm^{-1}$) is reduced by only 0.04 eV. As discussed before this would mean, if the peak in the ε_2 spectrum occurred at E_o, that C_2 should increase as E_g or E_{02}decreased. In As_2Se_3 the reductions in E_o and E_g are 0.14 eV and 0.05 eV respectively.

De Neufville et al do not observe structural changes when the films are cycled between the 'exposed' and 'annealed' states and the changes in E_o are small for As_2S_3 and As_2Se_3 but quite large for the 'partly molecular' films, AsSe and $Ge_{10}As_{40}Se_{50}$. E_o changes by 0.30 - 0.35 eV in the latter.

Other work[10] shows that E_{02} changes by 0.2 eV in $Ge_{10}As_{40}Se_{50}$ during the reversible transformation; it is stated that the band edge shifts without changing its shape and C_2 is unchanged. References 10 and 41 both suggest that trapped carriers excited by the illumination are responsible for the reversible effect.

Recent work by Tanaka[32,45] on a-As_2S_3 strongly suggests on the other hand that even the reversible effects are caused by structural changes. Figure 2.9(a) and (b) show his results on absorption and X-ray diffraction measurements. All measurements were performed at room temperature. Both the gap and C_2 are reduced by exposure to band gap radiation; the values derived from Figure 2.9(a) were given in Table 2.2. The change in the angle 2θ at which the maximum occurs in Figure 2.9(b) is caused by a reduction in the average *intermolecular* distance. The lowering of the peak and filling-in of the minimum are caused by some re-arrangement of the short-range order in De Neufville's[44] interpretation of the irreversible effect, and a similar change in the X-ray pattern is caused by polymerization. The obvious interpretation of Tanaka's results seems to the present author to be that the reversible changes are caused by the same mechanism as the irreversible ones, and that the degree of polymerization is even higher after illumination than annealing. This also explains the higher density of the

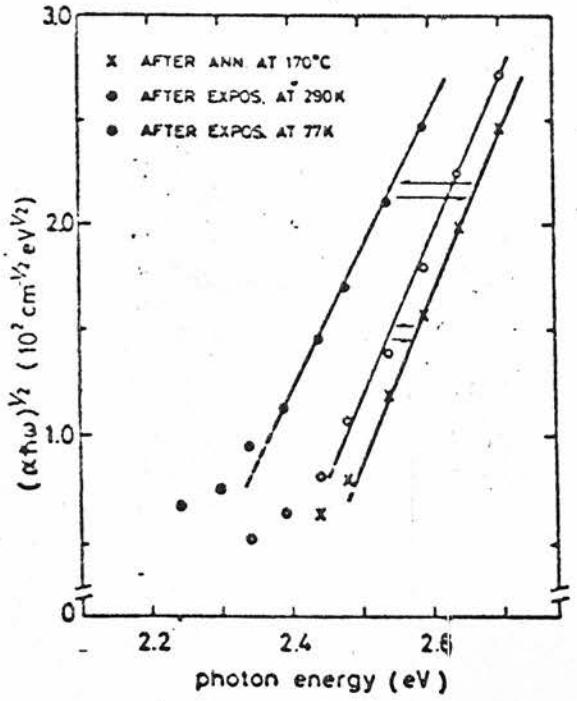

FIGURE 2.9(a)
Reversible changes in the optical absorption edge of As_2S_3 film by succsessive cycles of annealing and illumination both at 29oK and 77K (Ref 32)..

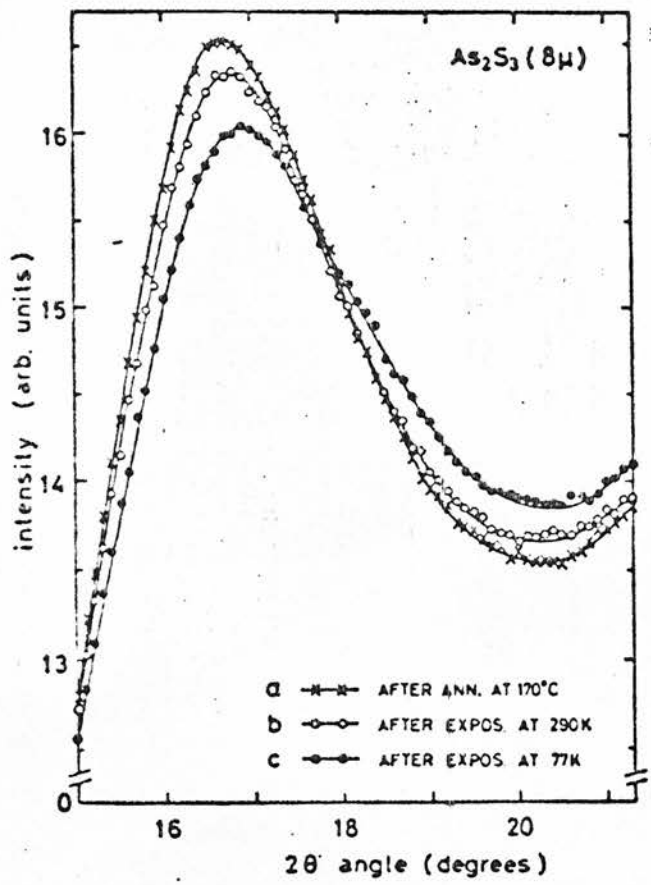

FIGURE 2.9(b)
X-ray intensity curves after annealing and illumination at 29oK and 77K. The changes are reversible (Ref 32).

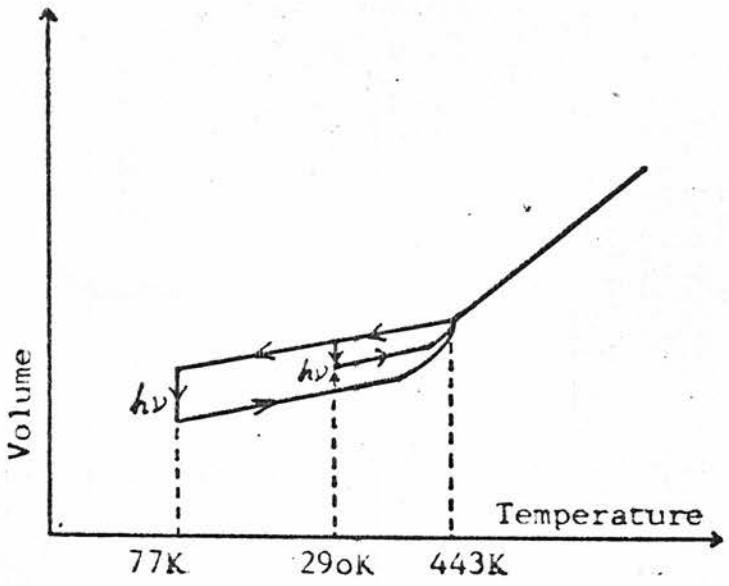

FIGURE 2.1o

Schematic representation of the volume changes of As_2S_3 films due to illumination and annealing.

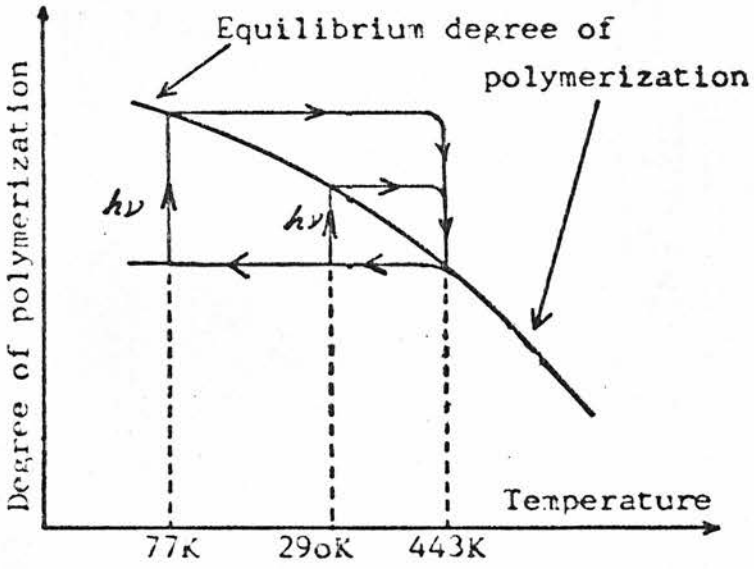

FIGURE 2.11

Illumination causes the glass to approach the equilibrium polymerization state.

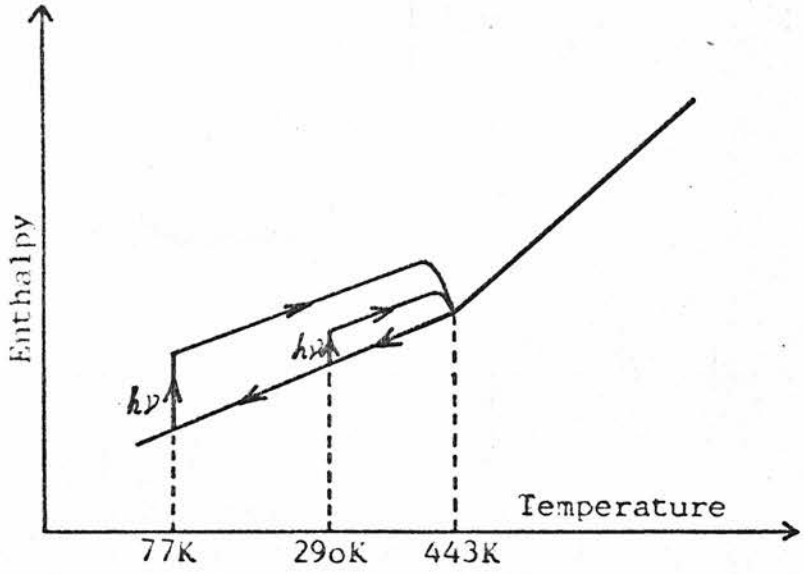

FIGURE 2.12
Changes in the enthalpy of As_2S_3 associated with the changes in volume and polymerization (FIGURES 2.1o & 2.11). Polymerization increases the internal energy.

illuminated films (as shown by the changed position of the X-ray peak). Figure 2.10 shows a representation of Tanaka's results in terms of a V-T diagram. The implication is that to each temperature there corresponds a certain degree of polymerization and volume. Such a state is of course metastable with respect to the crystal and cannot be achieved thermally at temperatures below T_g, but can be approached at any temperature with the aid of illumination of band gap energies. Thus illumination is simply helping the glass to approach a more stable state at the prevailing temperature. This is further illustrated in Figure 2.11 where the vertical axis represents the degree of polymerization. Evaporation corresponds to a state of polymerization at a very high temperature which is retained in the film because of the rapid cooling. This can also explain the results on AsSe and $Ge_{10}As_{40}Se_{50}$ but there the equilibrium degree of polymerization near T_g is much lower.

How does this account for changes in optical absorption? There are two possible interpretations. One follows from Tanaka's[32] observation that the reduction in E_{02}, and increase in density, scale approximately with the expected changes in these properties from the application of pressure[17], that is equation 2.45 seems to apply. Another possibility is that the changes in E_{02} are related to changes in the internal energy, an idea that was discussed in subsection 2 of this section. Tobolsky and Eisenberg and others[46,47,48] have shown that the enthalpy of polymerization of S, Se and S-Se-As is positive. This will be discussed further in Chapter 4 but it means that an enthalpy-temperature diagram, corresponding to the V-T diagram in Figure 2.11, can be drawn. This is shown in Figure 2.12. The increase in energy is possible because the entropy

is increased as well.

If this model is correct, then one must also account for the apparent connection between density and the gap. The density, of course, increases with polymerization as a result of the increase in connectivity. If the compressibility is linear with pressure however, then the change in internal energy upon the application of pressure is

$$\Delta U = \kappa P^2 \qquad 2.60$$

ie, if $\Delta E_g \propto \Delta U$ for the application of pressure then $\left(\frac{\partial E_g}{\partial P}\right)_T \propto P$ rather than a constant. Thus it appears that the above model cannot be used to explain the pressure coefficient, which according to Kastner is linear up to $P \sim 6 \times 10^4$ bars in selenium.

In summary then, the 'density model' can account for

(a) the pressure coefficient of the gap (qualitatively);

(b) the effect of structural changes on the gap (semi-qualitatively);

but not for (c) the temperature coefficient. The 'internal energy model' on the other hand can explain (c) quantitatively, (b) qualitatively and (a) not at all.

It is therefore clear than the two models are not equivalent although density and internal energy are obviously related. The physical basis for the internal energy model is of course that, apart from excitation of electrons into the conduction band, an increase of internal energy can be thought of as an upward shift of the mean energy of the valence band, the assumption here being that the shift of the valence band edge is linearly related to the shift

of the mean energy of the whole band.

Both models will be discussed further in later chapters.

2.3 THE EXPONENTIAL ABSORPTION TAIL

2.3.1 THE URBACH RULE

At photon energies below the extrapolated gaps E_{01} or E_{02}, most amorphous materials have an absorption constant which increases exponentially with photon energy. This behaviour normally covers a range of 0.5 eV or less in photon energy and a range from $\alpha \sim 1\ cm^{-1}$ to $\alpha \sim 10^3 cm^{-1}$ in absorption coefficient. Exponential absorption edges were first discovered in alkali-halide crystals by Urbach[49] and subsequently in many other crystals. In ionic crystals the exponential region may extend over nearly 1 eV and is usually expressed as

$$\alpha = \alpha_o \exp\left[\frac{h\nu - E_g(T)}{\sigma(T)} \right] \qquad 2.61$$

This is referred to as the Urbach rule; α_o is a constant and $E_g(T)$ is some temperature dependent gap. It is generally agreed that in ionic crystals the exponential edge is caused by optical phonons. If it is assumed that the broadening of the edge is proportional to the mean square displacement of ions $\langle U^2 \rangle$ which in turn is proportional to their total energy then

$$\langle U^2 \rangle \propto kT^* = \theta\left(\frac{1}{\exp(\theta/kT) - 1} + \tfrac{1}{2} \right) \qquad 2.62$$

where θ is a characteristic phonon energy and T* is an effective temperature. It follows from this that

$$\sigma(T) = \frac{2\sigma_p \, kT^*}{\theta} = \sigma_p \coth (\theta/2kT) \qquad 2.63$$

where σ_p is a constant independent of T. At low temperatures the slope is determined by the zero point vibrations but at higher temperatures the contribution of thermal vibrations is more important. For $2kT > \theta$ it follows from equation 2.62 that $T^* = T$. Neglecting the temperature dependence of the gap, absorption curves measured at different temperatures should extrapolate to a common focal point at $h\nu \triangleq E_g$.

2.3.2 OTHER FORMS OF EXPONENTIAL TAILS

Various forms of exponential tails are observed in covalent solids and liquids and in ferroelectrics. The temperature dependence of σ may be different but the actual value is surprisingly similar in all cases.

Dow and Redfield[50] have argued that the exponential rule is so universally observed that it must be caused by a single mechanism and that this mechanism involves electrostatic interactions between the excited state electron-hole pair and random electric microfields. The microfields in turn are caused by LP phonons in ionic crystals, domains in ferroelectrics and impurities, defects or disorder in covalent materials. In their model it is assumed that an electron in the coulombic potential well of a hole (ie, an exciton) is likely to find a potential well nearby caused by the microfields. It can

then tunnel out of the coulombic well with an exponentially small tunnelling probability. Thus, the exciton peak is broadened into an exponential tail. Figure 2.13 shows a plot (after Dow and Redfield) of the potential energy of the electron as a function of position, in two dimensions, and illustrates how it can tunnel out of the coulombic well.

Many other mechanisms have been proposed. Tauc[13], for example, suggested that electrically deformed band edges, should make transitions possible at $h\nu < E_g$, between spatially separated states in the bands as shown in Figure 2.14. Since the band edge states are localized this involves a tunnelling factor which depends exponentially on distance. The tunnelling distance depends on photon energy.

2.3.3 THE EXPONENTIAL TAIL IN AMORPHOUS SEMICONDUCTORS

In amorphous semiconductors the slope of the exponential edge usually changes less below room temperature than the Urbach rule dictates. This is to be expected because the random internal fields caused by structural disorder are temperature independent. Street et al[16] argue that in all the random field models σ depends on the total internal field and it is therefore plausible to write

$$\sigma(T) = \sigma_s + \sigma_p \coth(\theta/2kT) \qquad 2.64$$

where σ_s is a temperature-independent structural term and σ_p a LO phonon term. They also cite evidence from ferroelectric crystals

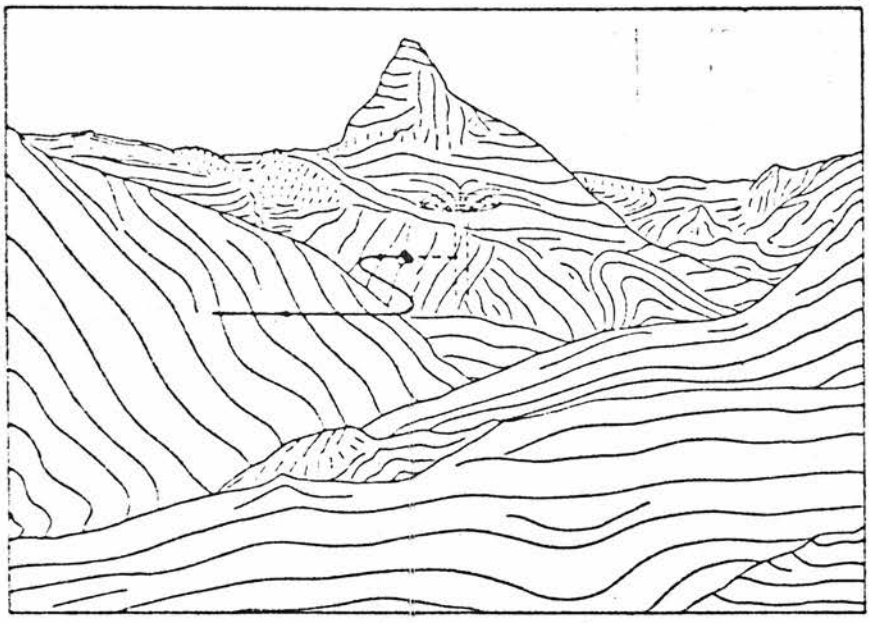

FIGURE 2.13

Dow and Redfield model. Random internal electric fields of various origins make the potential seen by an electron spatially nonuniform. Electron-hole pairs dissociate by tunnelling.

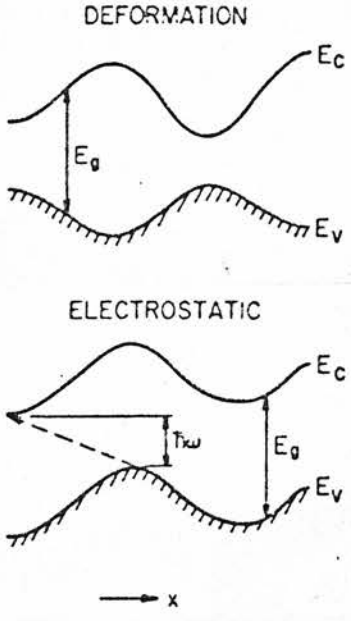

FIGURE 2.14

In electrostatically deformed bands absorption can take place at energies less than the 'direct' band gap. If the wave functions are localized the matrix element depends exponentially on photon energy (Ref 13).

that different σ terms can be added in this way. σ_s dominates at low temperatures and is expected to depend on preparation. This explains the differences in σ as observed by different authors or on different samples.

The LO phonon term does however contribute significantly to the temperature dependence of α as Figure 2.3(b) clearly showed. Equation 2.61 can be re-arranged as follows

$$h\nu = E_g(T) + \sigma(T)\ \ln(\alpha/\alpha_o) \qquad 2.65$$

If an arbitrary energy 'gap' is defined as the photon energy $E = h\nu$ at which α has some constant value, α_c say, then

$$\left(\frac{\partial E}{\partial T}\right)_P = \left(\frac{\partial E_g(T)}{\partial T}\right)_P + \ln(\alpha_c/\alpha_o)\left(\frac{\partial \sigma(T)}{\partial T}\right)_P \qquad 2.66$$

Since $E_g(T)$ decreases and $\sigma(T)$ increases with increased temperature and $\alpha_c < \alpha_o$ the shift in E is larger than in E_g and depends on α_c. The smaller α_c is chosen to be the larger is the shift in E. Street et al[16] used this to show that $\sigma_p \sim 1.5 \times 10^{-2}$ eV/K and $\sigma_s \sim 4.8 \times 10^{-2}$ eV/K in a-As_2S_3, so that the structural contribution is about three times larger than the zero point phonon contribution.

2.3.4 THE EXPONENTIAL TAIL IN THE ARSENIC CHALCOGENIDES

The parameter $\sigma(T)$ usually lies in the range 0.04 - 0.08 eV at room temperature in arsenic chalcogenides. Nunoshita and Arai[24] find that in the Si-As-Te system σ increases as the edge moves to higher energies, ie, with increased Si:Te ratio. Cornet and Rossier[4]

found that σ depends very little on composition in the As-Te system for 25-60% As (atomic) but above 200 K it does depend on temperature as their results shown in Figure 2.15 clearly indicate.

Kosek and Tauc[7] measured optical absorption in the As-S system. They found that both the gap and $\sigma(T)$ increase with sulfur content in the composition range As_2S_3 to As_2S_5. Thus at 293 K σ = 0.054 eV in As_2S_3 and 0.065 eV in As_2S_5. At 80 K σ is 20% lower in both compositions. Street et al[16] in the measurements discussed earlier found σ = 0.069 eV and 0.062 eV at 295 K and 10 K respectively, in a-As_2S_3. Thus if their interpretation is correct, the term σ_s in equation 2.64 must be smaller in the samples used by Kosek and Tauc.

Edmonds[20] found no signs of compositional dependence in the a-$(As_2Se_3)_x(As_2Te_3)_{1-x}$ system. He found that σ is strongly temperature dependent in liquid As_2Se_3, as expected from the thermal disorder characteristic of liquids. Thus $\sigma \sim 0.05$ eV at room temperature and ~0.11 eV at 659 K. The temperature coefficient of an arbitrary gap corresponding to $\alpha = 10^2$ cm^{-1} is twice as high in the liquid. This is partly due to the increased temperature dependence of $\sigma(T)$, but the change in the activation energy of the conductivity indicates that the temperature coefficient of the band gap is also increased.

Kolomiets[51] finds that substitution of Te for the Se in a-As_2Se_3 increases σ from 0.050 eV for As_2Se_3 to 0.082 eV for $(As_2Se_3)_9(As_2Te_3)_1$. This contradicts Edmonds' results. Doping with Ag also increases σ. In a-Se σ seems to be more temperature dependent than in most other amorphous semiconductors. Thus Chopra and Bahl[54] found $\sigma \propto T$ at room temperature in a-Se and Se doped with up to 5% As. They found

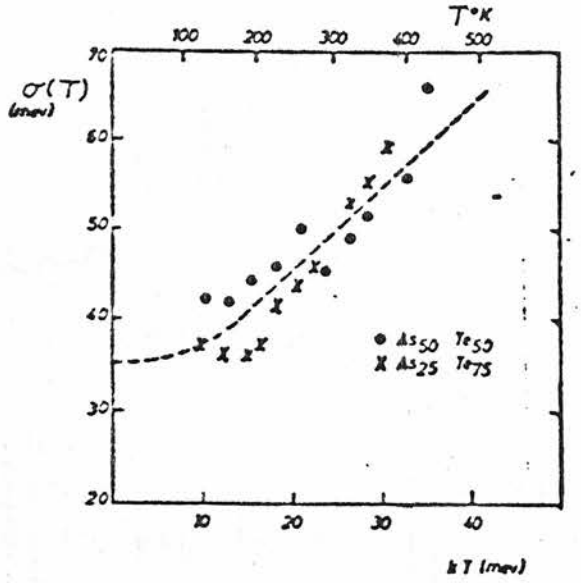

FIGURE 2.15
Temperature dependence of the inverse of the slope of the exponential absorption tail for As-Te films. (Ref 4).

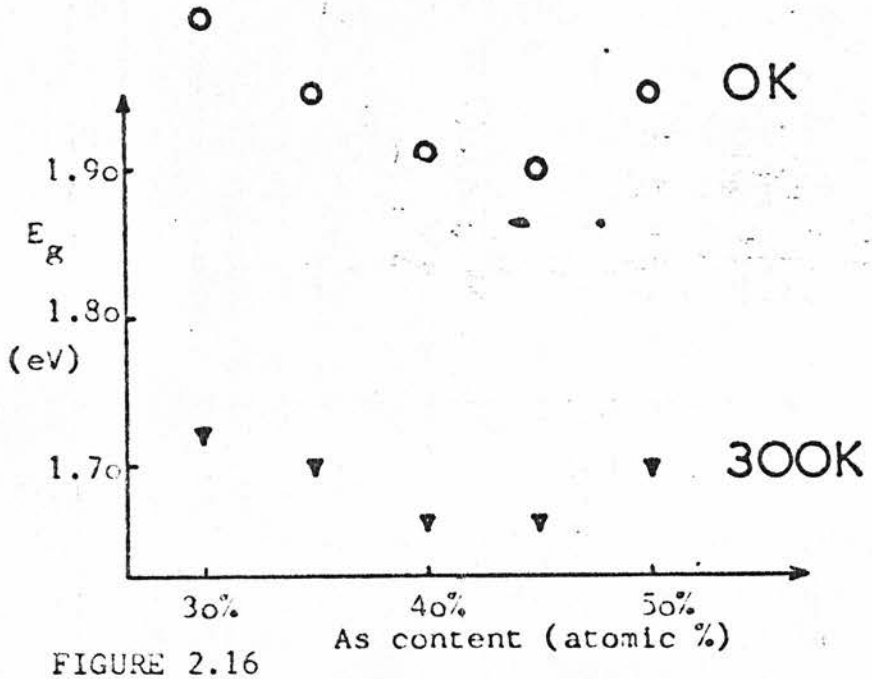

FIGURE 2.16
E_g vs composition in the As-Se system at room temperature and extrapolated to oK. E_g is the photon energy at which $\alpha = 5oocm^{-1}$ (Ref 53).

σ = 0.052 eV at room temperature in these compositions. For a-As_2Se_3 their value is 0.075 eV and independent of T. Both monoclinic and trigonal selenium have exponential edges which are related to exciton bands. The slope and position of the edge is very similar in the amorphous and trigonal forms[52] but there is no exciton peak in a-Se.

Hurst[53] has measured absorption in the exponential region for As-Se glasses. Table 2.4 gives his results for σ(T) at two temperatures.

% As	30	35	40	45	50
300 K	0.061	0.056	0.059	0.054	0.058
80 K	0.048	0.043	0.043	0.037	0.041

TABLE 2.4

The values are too scattered to show any composition dependence but σ is clearly a function of temperature, contrary to the findings of Chopra and Bahl[54]. In addition, the latter authors' value of 0.075 eV is higher than found by Hurst, thus indicating a larger temperature independent structural contribution.

Figure 2.16 shows the compositional dependence of a gap arbitrarily defined by α = 500 cm^{-1}, as determined by Hurst. There is a minimum near the stoichiometric composition As_2Se_3, probably slightly on the arsenic-rich side. This behaviour is mirrored by the behaviour of many physical properties of this system which tend to show extrema near this composition. This will be discussed later.

Sussman et al[55] have measured absorption and electro-absorption in the As-Se system. Some of their results are shown in Figure 2.19 and indicate 0.060 eV in a-Se, decreasing steadily with increasing As content. At 40% As $\sigma \triangleq 0.050$ eV. Knights[56] found $\sigma \triangleq 0.06$ eV in a-As.

2.4 OTHER OPTICAL EFFECTS

2.4.1 PHOTOLUMINESCENCE

Radiative recombination in arsenic-chalcogenides was first measured by Kolomiets et al[57,58] and has since been extensively studied by several workers. The main features are as follows.

The photoluminescence (PL) spectrum consists of a broad peak with its maximum energy close to half the band gap energy, the width of the PL spectrum being 25-50% of the energy of the maximum. The excitation spectrum, when normalized to the incident number of photons has a maximum near the band gap, usually at $\alpha \triangleq 100\ cm^{-1}$. When normalized to the number of absorbed photons the exitation spectrum is constant below the band gap but falls off at higher energies.

The PL and excitation spectra are roughly similar in arsenic glasses and $As_2Se_{3-x}S_x$ crystals apart from the effect of a larger band gap in the crystals and no fall-off in the excitation spectra at high energies.

The PL intensity is proportional to the excitation intensity, indicating monomolecular recombination kinetics. This is also supported by the fact that the life-time and quantum efficiency

are intensity independent. Both life-time and intensity are strongly temperature dependent and subsequently most measurements of photoluminescence have been performed at cryogenic temperatures. This makes comparison with other experiments such as photo-conductivity difficult. It is clear from the similarity between results on crystals and glasses that some kind of defect levels in the gap must act as recombination centres. Street et al[59] have shown that surface recombination is not responsible for the excitation spectra, and that instead a bulk energy-dependent quantum efficiency is indicated. They proposed that luminescence only occurred if the photogenerated electron-hole pair is generated very close to a recombination centre. Figure 2.17 is taken from Street et al[60], and shows the PL spectra, excitation spectra and absorption spectra in a-As_2Se_3, As_5Se_{95} and a-Se. The PL peak in a-Se is very weak and occurs at a lower energy than in a-As_2Se_3 although the band gap in Se is larger. Figure 2.18 shows that the PL intensity increases linearly with As content. Street et al[60] also showed that the position of the peak in arsenic-chalcogenide glasses scales with the band gap.

To explain these and other results Street et al[61,62] proposed a model for PL recombination in crystalline and amorphous arsenic chalcogenides in which the hole forms a polaron which is trapped at an acceptor-like As broken bond and the radiative transition occurs between this hole and an electron close to, or in, the conduction band. The density of broken As bonds is expected to be proportional to the As content and of the order 10^{17} - 10^{18} cm^{-3} in As_2Se_3 or As_2S_3.

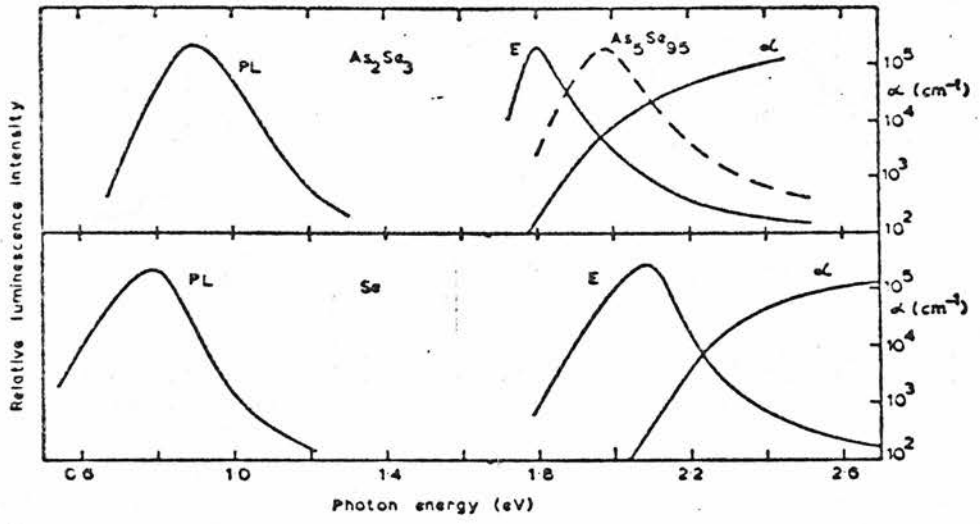

The photoluminescence spectra (PL), excitation spectra (E) and optical absorption (α) of amorphous As_2Se_3 and Se at 10 K. The dashed curve gives the excitation spectrum of As_5Se_{95}.

FIGURE 2.17

(Ref 6o).

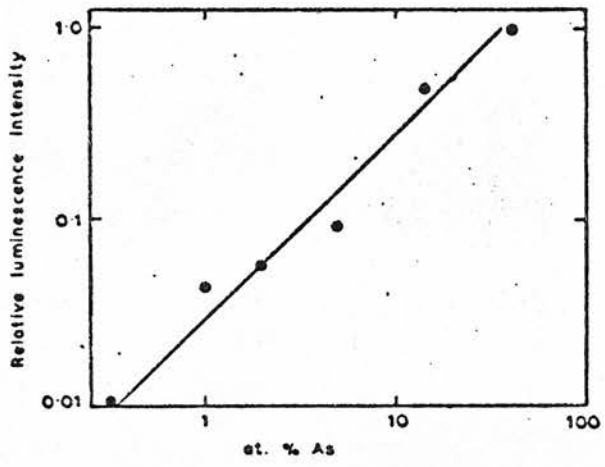

The dependence of the PL intensity on As concentration at 10 K.

FIGURE 2.18

(Ref 6o).

Bishop and Guenzer[63] have observed that the PL spectra in a-As_2Se_3 and $As_2Se_{1.5}Te_{1.5}$ can be quenched or enhanced by IR radiation and argue that these results provide evidence for the existence of a band of localized states in the band gap which are attributable to defects specific to As_2Se_3. Bishop et al[64] found that IR radiation could induce absorption and that radiation corresponding to the photoluminescence spectra of a-arsenic chalcogenides induced paramagnetic states. From this they estimated the density of defects as 10^{16} - 10^{18} cm^{-3} in As_2Se_3 and 10^{17} cm^{-3} in As_2S_3 and Se. This is in good agreement with the estimates by Street et al[62].

2.4.2 ELECTROABSORPTION

When a modulated electric field is applied across a sample of a wide band-gap material along the direction of light propagation the result is a modulated absorption.

Electroabsorption as a function of field and photon energy can give valuable information about various absorption processes. The effect is expected to be smaller in amorphous semiconductors as a result of larger effective masses.

Kolomiets et al[65] found that the absorption curve for a-As_2Se_3 was shifted towards lower energies by a constant amount, below the optical gap (~ 1.8 eV at 300 K), but above that energy the shift decreased with increasing energy. The shift at any energy is proportional to the square of the applied field and increases with increasing temperature.

Street et al[16] obtained substantially similar results for a-As_2S_3. They found that $\Delta\alpha/\alpha \doteq$ constant below 2.25 eV and tends asymtotically to zero at higher photon energies.

Usually these and similar observations have been interpreted in terms of (a) the Franz-Keldysh effect, (b) the Stark effect of excitonic or localized states, (c) perturbation of the Dow and Redfield field broadened exciton model for exponential edges.

Recent work by Sussman et al[55] indicates however that none of these interpretations is adequate. They studied the As-Se system and found important differences from earlier results, notably that the $\Delta\alpha/\alpha\mathcal{E}^2$ spectrum has a maximum at or below the band gap and does not level off at low photon energies. This means that σ decreases with field. Some results from Sussman et al are shown in Figures 2.19 and 2.20. They express the change in absorption as

$$\Delta\alpha = (\Delta\alpha)_o \exp\left[\frac{h\nu - E_g}{\sigma_{\Delta\alpha}}\right] \qquad 2.67$$

and find that in a-As_2Se_3 $\Delta\alpha/\alpha$ decreases on cooling in agreement with Kolomiets et al[65]. In Se however, the trend is in the opposite direction as shown in Figure 2.20. There is some evidence of a double peak in the results for Se with maxima at 1.95 and 2.05 eV at 300 K. Sussman et al propose a model in which there are two different absorption mechanisms, one of which is unsensitive to the field. This is supposed to arise from the anisotropic bonding, ie, although glasses are isotropic on a macroscopic scale there is still local anisotropy due to chains

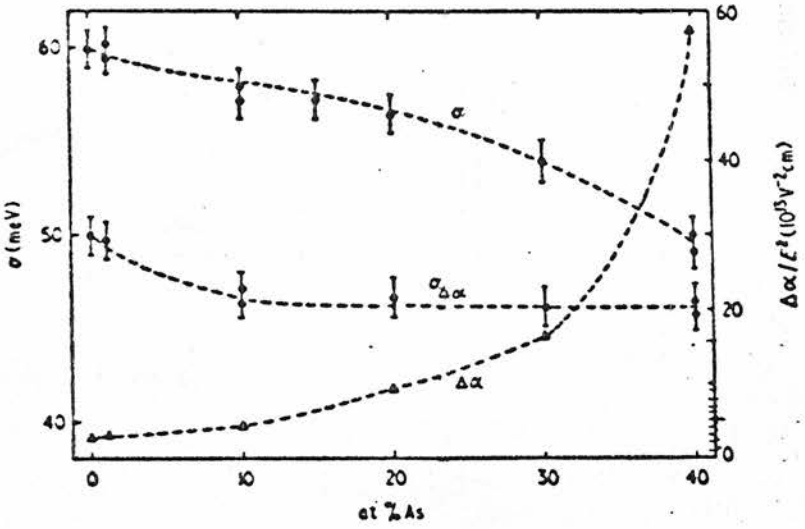

FIGURE 2.19

Variation of σ, $\sigma_{\Delta\alpha}$ and $\Delta\alpha$ (at $\alpha = 20 cm^{-1}$) in As-Se alloys at 300K. (Ref 55).

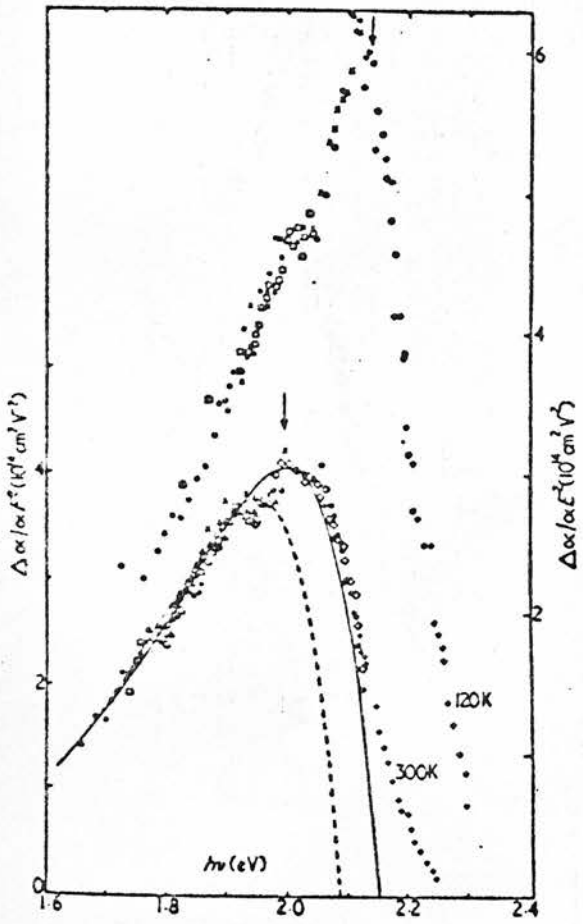

FIGURE 2.20

Electroabsorption spectra of amorphous Se at 120K (right vertical scale) and 300K (left vertical scale). The full and broken curves are theoretical fits (Ref 55).

and layers. This explanation is supported by the large anisotropy in electro-reflectance in trigonal selenium[66] and of photoelasticity[67] in a-Se.

2.5 REFERENCES

1. Davis, E A and Mott, N F, Phil Mag 22 , p 903, 1970.
2. Davis, E A, J Non-Cryst Sol 4, p 107, 1970.
3. Rockstad, H K, J Non-Cryst Sol 2, p 192, 1970.
4. Cornet, J and Rossier, D, Phil Mag 27, p 1335, 1973.
5. Felty, E J and Myers, M B, cited in ref 14, p 250.
6. Weiser, K, 1970, cited by Owen, A E, Cont Phys 11, p 257, 1970.
7. Kosek, F and Tauc, J, Czech J Phys B 20, p 94, 1970.
8. Greaves, G N, Knights, J C and Davis, E A, Proc on the 5th International Conference on Amorphous and Liquid Semiconductors, Garmisch-Partenkirchen, Germany (J Stuke and W Brenig, editors), Taylor and Francis, London 1974, p 369.
9. Brodsky, M H et al, Phys Rev B 1, p 2632, 1970.
10. Technical Publication No 67, The Electrical Communication Laboratories, Nippon Telegraph and Telephone Public Corporation, 1972.
11. Marshall, J M, private communication.
12. Fagen, E A, cited in ref 14, p 252.
13. Tauc, J,'Amorphous and Liquid Semiconductor', (J Tauc, editor), Plenum Press, London and New York, 1974.
14. Mott, N F and Davis, E A, Electronic Processes in Non-crystalline Materials, Oxford, 1971, p 251.
15. Maschke, K and Thomas, P, Phys Stat Sol 41, p 743, 1970.
16. Street, R A et al, J Phys C 7, p 1582, 1974.
17. Kastner, M, Phys Rev B 7, p 5237, 1973.
18. Harbeke, G, 'Optical Properties of Solids' (F Abeles, editor), N-Holl Publ Co, Amsterdam-London, 1972, p 54.
19. Tarasov, V V and Zhdanov, V M, Russ J Phys Chem 44, p 1349, 1970.

20. Edmonds, J T, Brit J Appl Phys 17, p 979, 1966.

21. Schnaus, U E et al, Phys and Chem Glasses 11, p 213, 1970.

22. Hurst, C H and Davis, E A, J Non-Cryst Sol 16, p 343 and p 355, 1974.

23. Nunoshita, M and Arai, H, Solid State Comm 11, p 337, 1972.

24. Nunoshita, M and Arai, J Non-Cryst Sol 12, p 339, 1973.

25. Weiser, K and Brodsky, M H, Phys Rev B 1, p 2632, 1970.

26. Kolomiets, B T et al, J Non-Cryst Sol 4, p 45, 1970.

27. Zallen, R et al, Phys Rev Lett 26, p 1564, 1971.

28. Butterfield, A W, Thin Solid Films, 21, p 287, 1974.

29. Main, C, PhD Thesis, University of Edinburgh, 1974.

30. Inoue, E et al, 'Non-silver Photographic Processes', (R J Cox, editor), Academic Press, 1975, p 71.

31. Howard, W E and Tsu, R, Phys Rev B 1, p 4709, 1970.

32. Tanaka, K, Appl Phys Lett 26, p 243, 1975.

33. Bluzer, N and Bahl, S K, Proc on the 5th International Conference on Amorphous and Liquid Semiconductors, Garmisch-Partenkirchen, Germany (J Stuke and W Brenig, editors), Taylor and Francis, London 1974, p 1207.

34. Fagen, E A et al, Proc on the 5th International Conference on Amorphous and Liquid Semiconductors, Garmisch-Partenkirchen, Germany (J Stuke and W Brenig, editors), Taylor and Francis, London 1974, p 601.

35. Kastner, M, Phys Rev B 6, p 2273, 1972.

36. Pantelides, S T, Phys Rev Lett, 35, p 250, 1975.

37. Wemple, S H and DiDomenico, M, Phys Rev Lett 23, p 1156, 1969.

38. Wemple, S H and DiDomenico, M, Phys Rev B 3, p 1338, 1971.

39. Wemple, S H, Phys Rev B 7, p 3767, 1973.

40. Galkiewicz, R K and Tauc, J, Solid State Comm 10, p 1261, 1972.

41. De Neufville, J P et al, Proc on the 5th International Conference on Amorphous and Liquid Semiconductors, Garmisch-Partenkirchen, Germany, (J Stuke and W Brenig, editors), Taylor and Francis, London 1974, p 737.

42. Berkes, J S et al, J Appl Phys 42, p 4908, 1971.

43. Tanaka, K and Kikuchi, M, Solid State Comm 11, p 1311, 1972.

44. De Neufville, J P et al, J Non-Cryst Sol 13, p 191, 1973.

45. Tanaka, K, Solid State Comm 15, p 1521, 1974.

46. Eisenberg, A and Tobolsky, A V, J Polym Sci 46, p 19, 1960.

47. Tobolsky, A V and Eisenberg, A, J Coll Sci 17, p 49, 1962.

48. Tobolsky, A V et al, J Coll Sci 17, p 717, 1962.

49. Urbach, F, Phys Rev 92, p 1324, 1953.

50. Dow, J D and Redfield, D, Phys Rev B 5, p 594, 1972.

51. Kolomiets, B T, Proc on the 5th International Conference on Amorphous and Liquid Semiconductors, Garmisch-Partenkirchen, Germany (J Stuke and W Brenig, editors), Taylor and Francis, London 1974, p 189.

52. Stuke, J, J Non-cryst Sol 4, p 1, 1970.

53. Hurst, C H, PhD Thesis, University of Cambridge, 1973.

54. Chopra, K L and Bahl, S K, Thin Solid Films 11, p 377, 1972.

55. Sussman, R S et al, J Phys C 8, L182, 1975.

56. Knights, J C, Solid State Comm 16, p 515, 1975.

57. Kolomiets, B T et al, J Non-Cryst Sol 4, p 289, 1970.

58. Kolomiets, B T et al, J Non-Cryst Sol 8-10, p 1004, 1972.

59. Street, R A et al, Phil Mag 29, p 1157, 1974.

60. Street, R A et al, Phil Mag 30, p 1181, 1974.

61. Street, R A et al, J Phys C 7, p 4185, 1974.

62. Street, R A et al, J Phys C 8, p 1293, 1975.

63. Bishop, R G and Guenzer, C S, Phys Rev Lett 30, p 1309, 1973.

64. Bishop, S G et al, Phys Rev Lett, 34 p 1346, 1975.

65. Kolomiets, B T et al, J Non-Cryst Sol 8-10, p 1010, 1972.

66. Weiser, G and Stuke, J, Phys Stat Sol (b) 45, p 691, 1971.

67. Yu, P Y and Cardona, M, Phys Stat Sol (b) 47, p 251, 1971.

CHAPTER 3 PHOTOCONDUCTIVITY IN AMORPHOUS CHALCOGENIDES

3.1 INTRODUCTION

At thermal equilibrium, electrons are constantly being excited from the valence band to the conduction band with the absorption of energy from the lattice (phonons) or of black body radiation. There is a dynamic equilibrium which keeps the number of excited carriers constant - thermal fluctuations excepted. The principle of detailed balance applies, ie, each process proceeds equally fast in both directions, independent of all other processes. Thus the same number of photons is emitted in the form of black body radiation as is absorbed again. When this equilibrium is disturbed, eg, by incident radiation, excess carriers are produced, or generated. The history of a carrier, from the time it is generated till it returns to the original band can be conveniently divided into generation and thermalization, transport (with trapping and detrapping) and recombination.

Optical absorption was discussed in the previous chapter. Some absorption events do not however produce charge carriers. A good example of this occurs in a-Se in which optical absorption sets in at photon energies about 0.5 eV less than the onset of photoconductivity. This is due to excitation from one localized state to another or to the formation of an exciton. The ratio of 'free' photogenerated electron-hole pairs to the number of photons absorbed is called the quantum efficiency, 'free' here implying free to contribute to conduction after the initial generation.

Transport is determined by the number of carriers at each energy, and their mobility. Thus in the dark the conductivity is

$$\sigma = e\int N(E)\ f(E)\ \mu(E)\ dE \qquad 3.1$$

where e is the electronic charge, N(E) the density of states, f(E) the probability of occupation and μ the mobility of a carrier at energy E. The integral is over all energies contributing to the transport process. In non-degenerate semiconductors it is convenient to consider conduction in the valence band as being due to positive holes. The probability of a state at energy E not being occupied by an electron, ie, of containing a hole, is

$$\overline{f}(E) = 1 - f(E) \qquad 3.2$$

When external excitation is applied the principle of detailed balance no longer holds although some fundamental parameters like the capture cross section are usually unchanged. When the excitation is constant in time a new dynamic quasi-equilibrium or steady state is established. Section 4 of this chapter is concerned with the quasi-equilibrium statistics, and the interpretation of steady state photoconductivity measurements.

Section 5 is an introduction to transient photoconductivity effects, especially the simple case of the initial linear photocurrent rise before deep trapping and recombination occurs. First, however, it is necessary to discuss, in some detail, transport in the dark in amorphous semiconductors and the processes of excess carrier generation, trapping and recombination.

3.2 EQUILIBRIUM STATISTICS AND CARRIER TRANSPORT IN THE DARK

3.2.1 DENSITY OF STATES AND TRAPPING

Several 'density-of-states-models' have been proposed for amorphous semiconductors. Some were discussed in Chapter 2 but they refer to the densities near the band edges and ignore localized states deep inside the gap. Indeed there is controversy about the number of states in the gap in chalcogenide glasses. Fritzsche[1] points out that optical absorption indicates densities of less than 5×10^{17} cm^{-3} eV^{-1} in simple chalcogenide glasses, while measurements of paramagnetism give an upper limit of 3×10^{16} cm^{-3} eV^{-1} and ESR $<10^{14}$ cm^{-3} eV^{-1}. On the other hand results on ac conductivity and glow curves indicate that the density is not less than 3×10^{17} and 1×10^{18} cm^{-3} eV^{-1} respectively. Fritzsche proposed a 'hills-and-valleys model', in which the band-edge energies vary spacially but the band *gap* is nearly constant, as a possible explanation. This gives rise to localized electron states in the conduction band valleys, which are spatially separated from the localized states in the valence band peaks. These spatial fluctuations in the bands are of the order of hundred $\mathring{A}$ or more, since any smaller fluctuations are averaged out by tunneling. According to this model there are very few states in the gap as far as optical experiments are concerned but ac conduction can be large due to carriers trapped in the valleys. This (after averaging) is consistent with the CFO model which is shown in Figure 3.1(a). Also shown, in Figure 3.1(b), is the model proposed by Mott and Davis[2] which has linear tails of limited extent *and* states at the Fermi level.

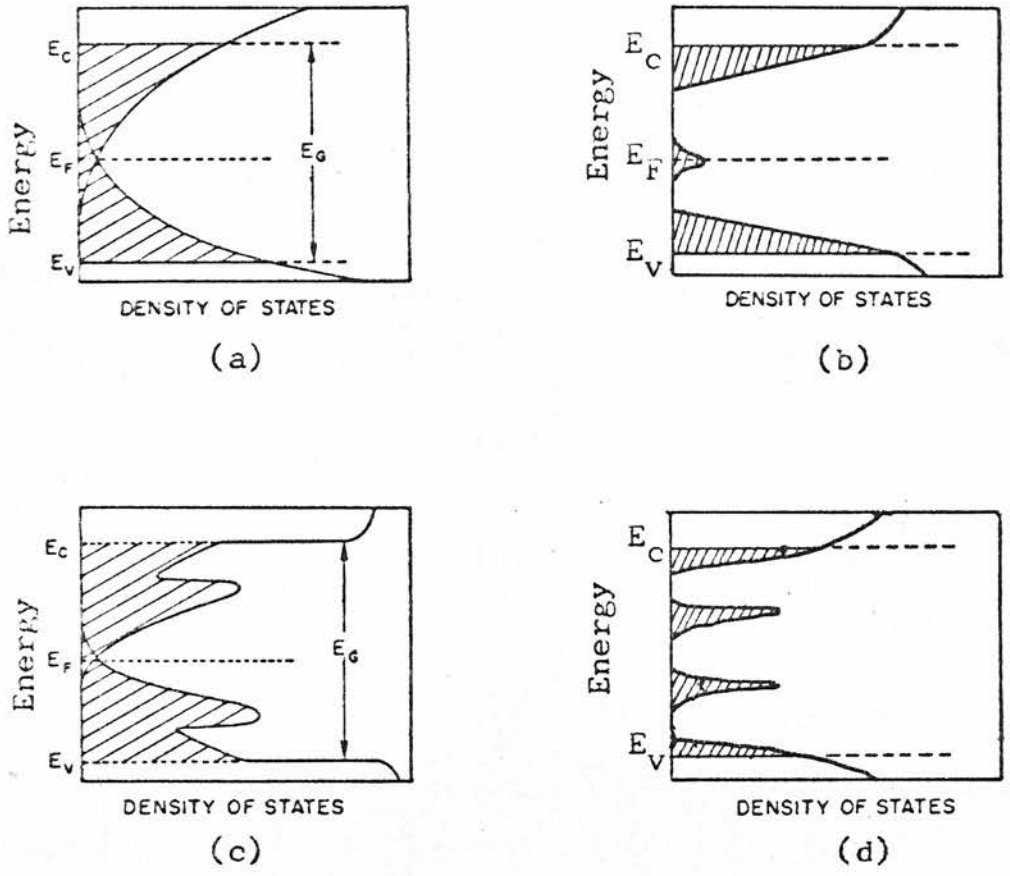

FIGURE 3.1

Four proposed density-of-states distributions for amorphous semiconductors.

(a) CFO model (Ref 29)

(b) linear tails of localized states (Ref 2)

(c) CFO model modified to include correlation effects (Ref 3)

(d) discrete-levels (Ref 4,11).

Localized states are shaded.

Figure 3.1(c) illustrates a model after Adler[3] which takes into account electronic correlation effects involving Coulombic repulsive splitting of localized states, making the density of states a function of electron occupation. Finally, Figure 3.1(d) shows a 'discrete-levels-model' which gives the simplest interpretation of experimental results on thermally activated drift mobility. This and similar models have been used to interpret photoconductivity measurements in As_2Te_3 and As_2Se_3 such as those to be described later in this chapter. Marshall[4] has also shown that results on photo-mobility and dark conductivity in As_2Te_3 and STAG glass are consistent with a discrete level model. It is interesting to note that there appears to be some correspondence between the discrete levels that have been observed in As_2Se_3 crystals[5] and those proposed for a-As_2Se_3. Voronkov et al[6] have proposed a model to explain their results on electroabsorption in As_2SeTe_2 which postulates a set of donors 0.50 eV above the valence band edge, nearly compensated by acceptors 0.66 eV below the conduction band edge. If these defect densities are large and roughly equal the Fermi level should be pinned midway between them at 0.42 eV above the valence band edge, a conclusion which is consistent with thermopower results of Arnoldussen et al[7]. Statistical fluctuations in the densities of the charged defects are expected to cause potential fluctuations which give rise to fluctuations of about $\pm$0.1 eV at the band edges and the donor and acceptor levels. This causes spatially separated regions of conduction and valence band states which in transport measurements appear as traps extending 0.1 eV into the gaps. This is rather similar to Fritzsche's 'hills-and-valleys' model.

Electron and hole motion within the bands of real crystals and amorphous semiconductors is interrupted by scattering events and the average distance between scattering is the mean-free-path. Thus the motion is of a diffusive nature and one can define a free mobility which is the average velocity of the carriers per unit field. In crystalline semiconductors this can be 10^3 cm^2/V-sec or greater. The free mobility may depend on energy, field and temperature. When localized states are present they act as capture centres for the free carriers. The captured carriers can either be re-emitted to the band or recombined with carriers of the opposite sign. When re-emission is more likely than recombination the localized states are called traps, otherwise they are recombination centres.

Release of a captured carrier back to the band requires energy and is therefore not likely when the energy difference is large. Traps can be subdivided into shallow traps which can establish thermal equilibrium with the band during the time of measurement and deep traps which have release times that are longer than the time of measurement. The sub-division into three kinds of localized states depends of course both on temperature and the type of measurement.

3.2.2 THE MOBILITY GAP AND DRIFT MOBILITY

At energies well within the band of extended states in an amorphous semiconductor, conventional transport with relatively long mean-free-path is likely and a carrier mobility in excess of 10^2 cm^2/V-sec is expected. At ordinary temperatures however,

the occupancy of those states will be very low and they will not contribute significantly to the conductivity. At an energy E_c (or E_v in the valence band) the mobility is expected to drop by perhaps three orders of magnitude. This is the energy where 'Anderson localization' sets in, ie, where the mean-free-path becomes comparable to the interatomic distance. Mott[8] suggests that this transition is sharp while Cohen[9] argues for a smoother variation. The energies E_c and E_v are called mobility edges or mobility shoulders and their difference is the mobility gap. It should be noted that the mobility gap is not in general the same as the optical gap.

For a given measurement time carriers in shallow traps and band states form a common reservoir and one can define a drift mobility, ie, average mobility including trapping events. Consider a discrete set of traps having energy E_t and density N_t. The effective density of extended states is N_c at energy E_c (this is roughly the density of states whithin one kT of E_c). Then with average trapping and release times equal to τ_t and τ_{tr} respectively

$$\mu_d = \mu_o \frac{N_c\, f(E_c)}{N_c\, f(E_c) + N_t\, f(E_t)} = \mu_o \left(1 + \frac{N_t}{N_c} \exp\left(\frac{E_c - E_t}{kT}\right)\right)^{-1} = \mu_o \frac{\tau_t}{\tau_t + \tau_{tr}} \qquad 3.3(a)$$

where μ_o is the free or microscopic mobility of a carrier in the band, and f(E) is the Boltzman occupancy function. This can usually be simplified further because normally $\tau_t \ll \tau_{tr}$, thus

$$\mu_d \simeq \mu_o \, \tau_t/\tau_{tr} = \mu_o \frac{N_c}{N_t} \exp(-\frac{E_c - E_t}{kT}) \qquad 3.3(b)$$

The hole drift mobility has been widely studied in the more insulating amorphous semiconductors by transit time measurements[10] and in a-Se and related materials, both the electron and the hole drift mobilities have been measured. The materials with a smaller mobility (or band) gap like As_2Te_3, are too conducting for transit time measurements to be possible and, therefore, a less direct 'photomobility' method has been used[11]. Direct measurements of the *free* mobility in amorphous semiconductors have not been possible so far because trapping effects are normally dominant.

A drift mobility limited by localized tail states, rather than discrete levels, is also possible. The expressions corresponding to equation 3.3(b) are :

for a linear tail - $$\mu_d = \mu_o \frac{\Delta E}{kT} \exp(-\frac{\Delta E}{kT}) \qquad 3.4(a)$$

and - $$\mu_d \simeq \mu_o \, (\frac{\Delta E}{kT})^{\frac{1}{2}} \exp(-\frac{\Delta E}{kT}) \qquad 3.4(b)$$

for a parabolic band,

where ΔE is the extent of the tailing. The pre-exponential product is approximately constant. The free mobility, just above the mobility edge, E_c, is estimated to be

$$\mu_o \simeq \frac{1}{6} \nu_{el} e R^2/kT \sim 10 \text{ cm}^2/\text{V-sec} \qquad 3.5$$

where ν_{el} is an electron frequency, of the order of 10^{15} sec^{-1}, and

R is an average jump distance.

3.2.3 DARK CONDUCTIVITY

Contributions to the dark conductivity can come from extended states at E_c as discussed previously, and also from hopping in localized band-tail states or in other localized states, eg, at the Fermi level. Just below E_c conduction may occur by thermally activated hopping of carriers between localized states[12]. This leads to a mobility of the form

$$\mu_{hop} = \frac{1}{6} \nu_{ph} \, e \, \frac{R^2}{kT} \, \exp(-\frac{W}{kT}) \, \exp(-2\alpha R) \qquad 3.6$$

where ν_{ph} is a phonon frequency $\sim 10^{12}$ sec^{-1}, $\exp(-2\alpha R)$ is a tunneling factor, and W a hopping activation energy. Hopping in a band of localized states inside the gap gives rise to an even lower mobility and a low activation energy for conductivity, about half the band width if the states are actually at the Fermi level. At very low temperature, Mott[13] argues that hopping to distant sites becomes more probable, ie, variable range hopping occurs, leading to a different temperature dependence from nearest neighbour hopping. This has been observed in tedrahedral amorphous semiconductors and in impurity bands in crystals but not in the materials of interest in this work.

Which kind of conduction process dominates depends on the relative mobilities, the densities of states and on the occupancy (and thus the temperature). The different contributions

can be summed to give a single equation for conductivity for each type of carrier

$$\sigma = \int eN(E)\ f(E)\ \mu_e(E)\ dE \qquad 3.7$$

for electrons and

$$\sigma = \int eN(E)\ \overline{f}(E)\ \mu_h(E)\ dE \qquad 3.8$$

for holes. This was in fact illustrated schematically in the last diagram in Figure 1.3 for the case of electrons in a situation where conduction in extended states dominates. The diagram also shows that a continuous tail of states does not give rise to a continuous tail in the $\sigma(E)$ vs E curve. This is because f(E) varies much faster than N(E). This will be the case for most conceivable distributions in the densities of localized states and the majority of states will be inactive because of low occupancy, thus effectively reducing the density of active states to a set of discrete levels. The discrete level approach can be looked upon as a method of analysis which ignores all inactive states, but there are in fact good reasons to believe that in the simpler chalcogenide glasses at least there are actually some discrete levels.

Normally, at a given temperature, there is one dominant contribution to the conductivity which can be written as

$$\sigma = \sigma_0 \exp(-\frac{E_d}{kT}) \qquad 3.9$$

where σ_o and E_d take on different values depending on the type of conduction process. For conduction just above E_c

$$\sigma = e\mu_o N_c \exp(-\frac{E_c - E_f}{kT}) \qquad 3.10(a)$$

where N_c is the effective density at E_c, $N_c \simeq N(E_c)kT$. In the case of discrete shallow traps this can be written as

$$\sigma = e\mu_d N_t \exp(-\frac{E_t - E_f}{kT}) \qquad 3.10(b)$$

Corresponding equations exist for other types of conduction, and an indication of which type actually dominates can sometimes be deduced from the experimentally determined value of the pre-exponential constants for the drift mobility and conductivity. It is necessary, however, to apply a correction to equation 3.10 arising from the temperature dependence of the optical gap, as discussed in Chapter 2. Thus for extended states

$$E_c - E_f = E_d' (1 - \phi(T)) \qquad 3.11$$

where, as in Chapter 2, $\phi(T)$ is the relative contraction of the gap at temperature T. In the present range of measurement $\phi(T)$ is usually linear, ie,

$$\phi(T) \simeq \phi_E \times T - \phi_o \qquad 3.12$$

and

$$E_c - E_f = E_d' (1 + \phi_o - \phi_E \times T) = E_d - \beta \times T \qquad 3.13$$

Hence, the experimentally determined pre-exponential constant contains the term $\exp(\beta/k)$ and this is typically about 30 in chalcogenide glasses.

3.3 EXCESS CARRIERS

3.3.1 GENERATION OF EXCESS CARRIERS

The principal methods for generating excess carriers are by absorption of light (internal photoeffect) or by injection at non-neutral contacts or junctions. Other methods include ionization by high energy quanta or particles, photoexcited injection (external photoeffect) and impact ionization. Only the first will be considered here, although ionization by electrons is of importance in drift mobility measurements in chalcogenide glasses.

Possible transitions in a semiconductor with a single defect level are shown in Figure 3.2. The transition labeled No 1 generates an electron-hole pair. Transitions 4 and 5 generate one carrier each and those No 2 and 3 none at all. Generation of electron-hole pairs which are bound to each other, ie, excitons is also possible. The fraction of absorbed photons that generate carriers, ie, electrons or holes that can take part in photo-conductivity, is called the quantum efficiency. For a photon flux F

$$\Delta G_n = \eta_n \alpha F \qquad 3.14(a)$$

$$\Delta G_p = \eta_p \alpha F \qquad 3.14(b)$$

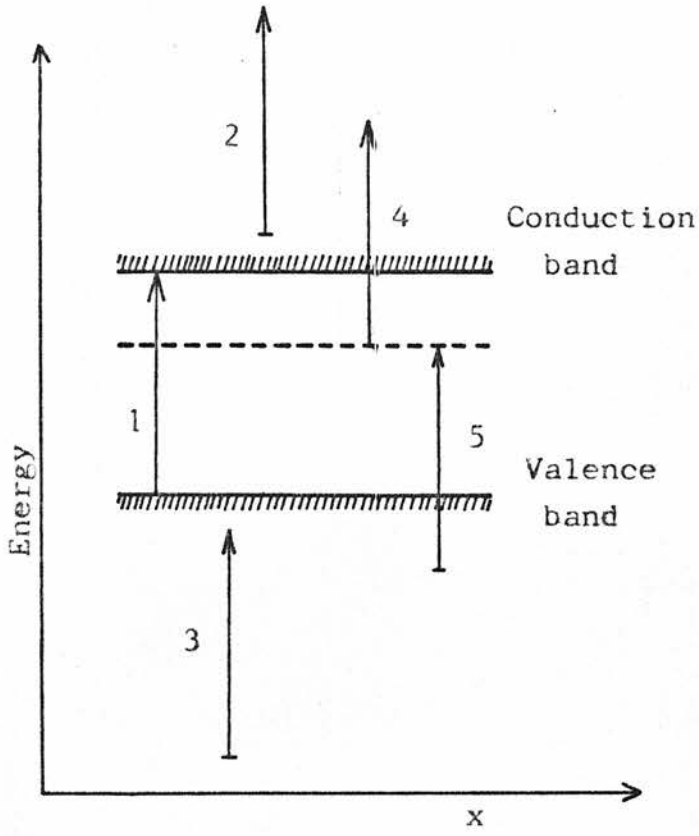

FIGURE 3.2

Possible transitions in the fundamental absorption region of a crystal with one set of defect levels.

where ΔG_n and ΔG_p are the generation rates of excess electrons and holes respectively and η_n and η_p are the quantum efficiencies. Transitions No 2 and 3 are not important in wide band-gap materials.

3.3.2 QUANTUM EFFICIENCY

According to Hartke and Regensburger[14] the 'photoconductivity edge' in a-Se is situated ~0.5 eV above the optical absorption edge as shown in Figure 3.3. Lanyon[15] proposed an explanation involving transitions between localized tail states and extended states at low energies, and interband transitions with unity quantum efficiency for higher energies. Thus a transition generating a free electron and a trapped hole could be followed either by a recombination of the hole which then never becomes a free hole, or it could be thermally excited into the valence band. This process would lead to $\eta_n = 1$ and $\eta_p < 1$. A similar process with the roles of electrons and holes interchanged would have $\eta_n < 1$ and $\eta_p = 1$. The approximate equality of electron and hole responses over a wide range of photon energies argues against this[16].

An alternative model due to Hartke and Regensburger[14] involves two processes, the ordinary interband transitions generating a free electron hole pair with unity quantum efficiency and a non-photoconducting generation of excitons which rapidly become self-trapped and cannot be ionized. The quantum efficiency (for either band) is then

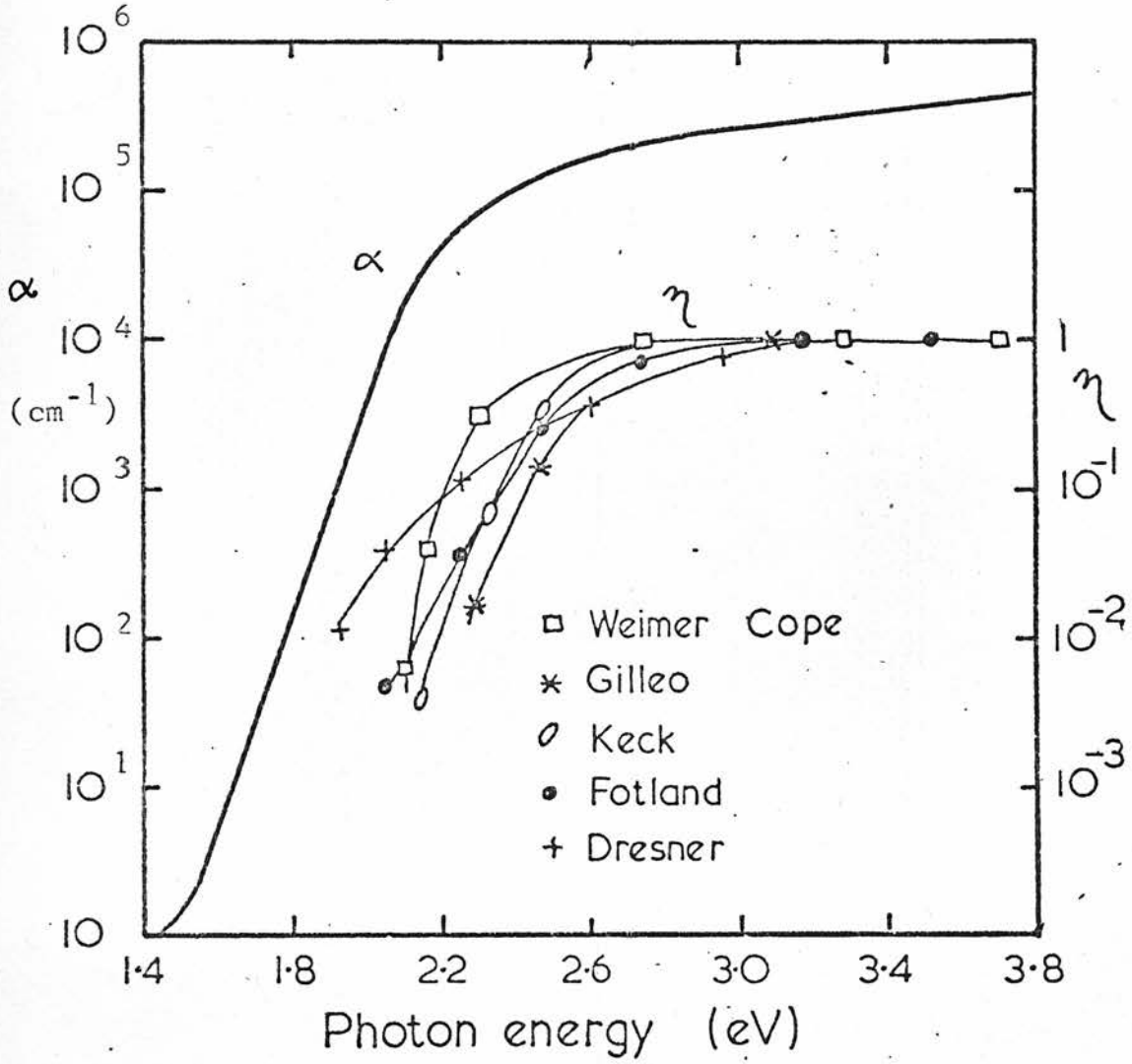

FIGURE 3.3 Optical absorption and quantum efficiency in amorphous Se. (Ref 14).

$$\eta(\nu) = \frac{\varepsilon_2^P(\nu)}{\varepsilon_2^P(\nu) + \varepsilon_2^N(\nu)} \qquad 3.15$$

where ε_2 is the imaginary part of the dielectric constant. The superscripts 'P' and 'N' refer to the photoconducting and non-photoconducting absorption processes respectively. Lucovsky[17] has suggested that bound excitons may form as excited states of molecular Se_8 rings but these exciton models are not consistent with the observed field dependence of η. Models involving a single process consider the probability of separating a photogenerated electron-hole pair from their mutual coulomb attraction. This has been discussed classically by Tabak and Warter[18], Davis and Mott[12] and by Knights and Davis[16]. The features of this model are illustrated in Figure 3.4. The excess kinetic energy of the carriers is

$$K.E. = (h\nu - E_o) + \frac{e^2}{\varepsilon r} \qquad 3.16$$

where E_o and ε are the optical gap and permittivity respectively. This excess energy is lost rapidly by thermalization, ie, emission of phonons. The rate of emission of phonons is of the order of the phonon frequency when the k-selection rules are relaxed. The thermalization time can thus be found and random walk theory gives the separation of carriers during that time. If the coulomb binding energy at that separation is of the order of kT or less ionization will take place and the quantum efficiency is unity. For higher binding energies, the quantum efficiency depends on the relative probabilities of ionization which is activated, and

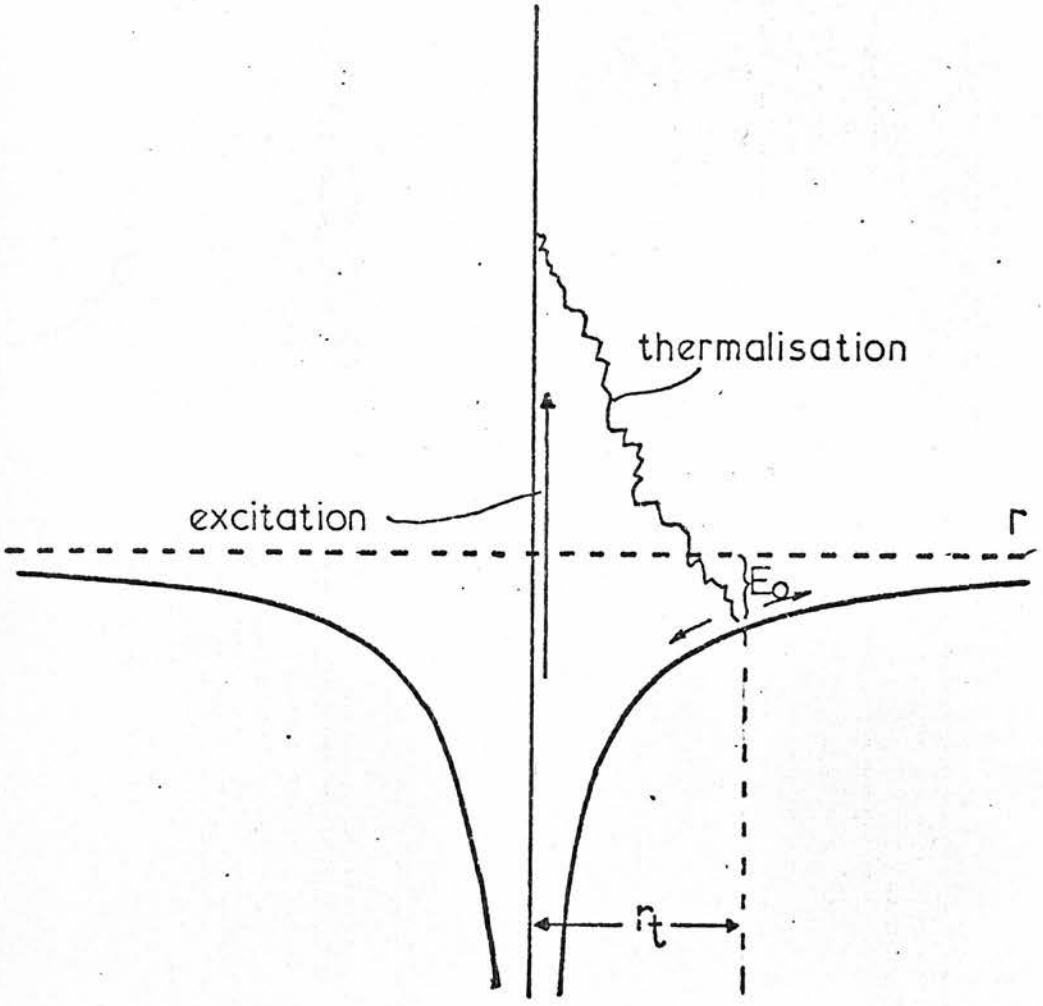

Photogeneration in Se

FIGURE 3.4

(Ref 16).

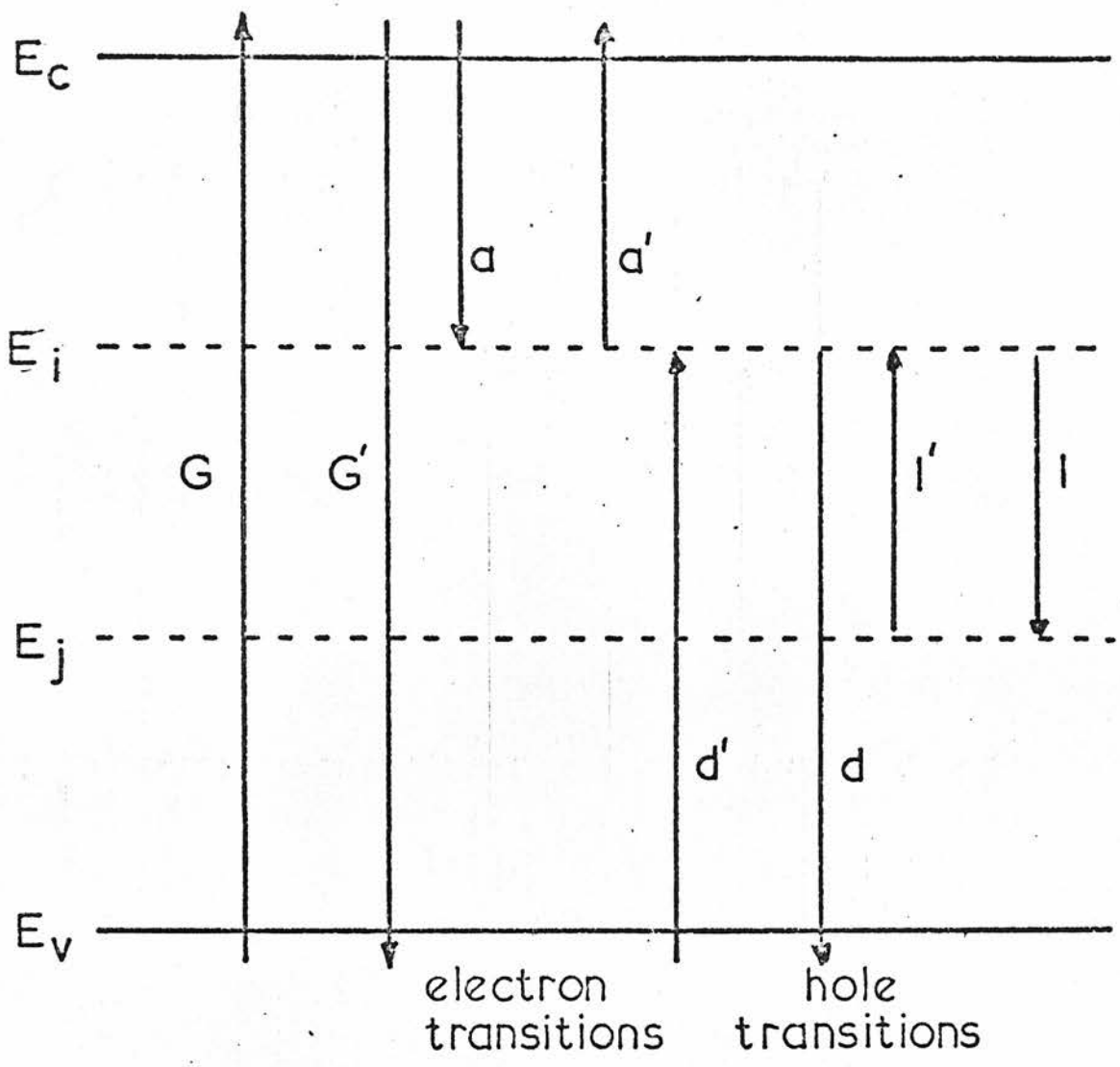

Carrier Transitions

FIGURE 3.5

(Ref 2o).

on geminate recombination. An electric field will obviously aid in separation of the electron-hole pairs and, qualitatively at any rate, this explains the field dependence of η.

3.3.3 TRAPPING AND RECOMBINATION OF EXCESS CARRIERS, RATE EQUATIONS

Some possible transitions are shown in Figure 3.5. G is the interband generation and includes both thermal excitation and internal photoeffect generation. G' is the reverse process, called interband recombination. The processes labelled a and a' are trapping of electrons by a localized state and re-emission to the band; d' and d denote trapping and re-emission of holes; 1' and 1 denote electron loss from and electron capture into states at E_i respectively. From the principle of detailed balance each process and its reverse proceed with the same speed at thermal equilibrium. The capture and release rates for each type of carrier can be written as

$$r_a = v\, S_n\, n\, N_i\, (1 - f) = \frac{n}{\tau_t^n} \qquad 3.17$$

$$r_a' = e_n N_i\, f = \frac{N_i\, f}{\tau_{tr}^n} \qquad 3.18$$

$$r_d' = v\, S_p\, p\, N_i f = \frac{p}{\tau_t^p} \qquad 3.19$$

$$r_d = e_p\, N_i (1 - f) = N_i (1 - f)/\tau_{tr}^p = N_i \bar{f}/\tau_{tr}^p \qquad 3.20$$

where the subscripts refer to the labels in Figure 3.5, v = thermal velocity of free carriers, S_n and S_p are the capture cross sections for electrons and holes respectively by a state at E_i, f is the occupancy at E_i ; e_n and e_p are the emission probabilities from a single trap containing an electron or a hole respectively and τ_t and τ_{tr} denote the average trapping and trap release times. The products of velocity and cross section are called capture coefficients.

$$C_n = v\, S_n \qquad 3.21(a)$$

$$C_p = v\, S_p \qquad 3.21(b)$$

Localized to localized transition rates can be written as

$$r_1' = K'\, N_i\, f_i\, N_j(1 - f_j) \qquad 3.22$$

$$r_1 = K\, N_i(1 - f_i)\, N_j\, f_j \qquad 3.23$$

where K' and K are transition coefficients.

At thermal equilibrium each transition rate can be equated to its reverse. This leads to expressions for e_n and e_p

$$e_n = C_n\, n \exp\left(\frac{E_i - E_f}{kT}\right) = C_n\, N_c \exp\left(-\frac{E_c - E_i}{kT}\right) \qquad 3.24$$

$$e_p = C_p\, p \exp\left(-\frac{E_i - E_f}{kT}\right) = C_p\, N_v \exp\left(-\frac{E_i - E_v}{kT}\right) \qquad 3.25$$

where N_c and N_v are the effective densities of states at the conduction and valence band mobility edges, E_c and E_v respectively. The emission is a phonon controlled process which can be written alternatively as

$$e_n = \nu_e \exp(-\frac{E_c - E_i}{kT}) \qquad 3.26$$

and similarly for holes. In equation 3.26, ν_e is an attempt to escape frequency related to the highest phonon frequency. The transition coefficients for localized to localized transitions are related by equating r_l' and r_l at thermal equilibrium, thus

$$K = K' \exp(-\frac{E_i - E_j}{kT}) \qquad 3.27$$

These parameters may depend on the energy of the localized states. The localized states considered here are assumed to be monovalent.

Although the principle of detailed balance only applies under conditions of thermal equilibrium equations 3.17 to 3.27 are generally true. Only the occupation functions and the trapping and release times are changed under non-equilibrium conditions in a wide-band non-degenerate semiconductor. The band-to-band spontaneous recombination rate is

$$G' = C_{np}\, np = C_{np}\, N_c\, N_v \exp(-\frac{E_c - E_v}{kT}) \qquad 3.28$$

Radiative capture by a free carrier or a localized state usually gives a capture cross section of about 10^{-19} cm^2 and using a free electron thermal velocity gives $C_{np} \doteq 10^{-12}$ cm^3 sec^{-1}. It can be shown that radiative recombination is negligible under most conditions compared to multiple phonon recombination via one or more sets of localized states, ie, transitions such as those in equations 3.17 to 3.23 dominate.

The above discussion can be extended to an arbitrary distribution of localized states. Ignoring all transitions between two localized states and assuming that C_n/C_p is independent of energy, the rate of increase of conduction electrons can be written as

$$\frac{dn}{dt} = G - \int_{E_v}^{E_c} n\, C_n(E)\, N(E)\, [1-f(E)]\, dE + \int_{E_v}^{E_c} e_n(E)\, N(E)\, f(E)\, dE \qquad 3.29$$

Similarly for holes

$$\frac{dp}{dt} = G - \int_{E_v}^{E_c} p\, C_p(E)\, N(E)\, f(E)\, dE + \int_{E_v}^{E_c} e_p(E)\, N(E)\, [1-f(E)]\, dE \qquad 3.30$$

Under steady state conditions n and p are constants and G can be eliminated.

$$\int_{E_v}^{E_c} N(E)\, \{- n\, C_n(E)\, [1-f(E)] + e_n(E)\, f(E) + p\, C_p(E)\, f(E) - e_p(E)\, [1-f(E)]\}\, dE = 0 \qquad 3.31$$

Since this is valid for an arbitrary distribution the quantity in curly brackets must be identically zero and from that condition the occupation function is obtained as

$$f(E) = \frac{n\,C_n(E) + e_p(E)}{n\,C_n(E) + e_n(E) + p\,C_p(E) + e_p(E)} \qquad 3.32$$

The same equation can be derived by considering the rate of change of occupation of one particular trap level. Thus two kinds of traps at the same energy but with different capture coefficients will have different values of f(E), ie, f(E) can be multivalued.

3.4 QUASI-EQUILIBRIUM STATISTICS

3.4.1 QUASI-FERMI LEVELS

At all energies below the equilibrium Fermi level E_f, e_n in equation 3.32 may be neglected in comparison with $n\,C_n$, $p\,C_p$ and e_p to give

$$f(E) = \frac{n\,C_n + e_p}{n\,C_n + p\,C_p + e_p} \quad , \; e_n \ll n\,C_n,\; p\,C_p,\; e_p \qquad 3.33\,(a)$$

Similarly for $E > E_f$, e_p may be neglected,

$$f(E) = \frac{n\,C_n}{n\,C_n + e_n + p\,C_p} \quad , \; e_p \ll e_n,\; n\,C_n,\; p\,C_p \qquad 3.34\,(a)$$

The last equation can be re-arranged to give

$$f(E) = \frac{n\,C_n}{N\,C_n + p\,C_p} \left\{ \frac{1}{1 + e_n/(n\,C_n + p\,C_p)} \right\}$$

From equation 3.24 we can write

$$e_n/(n\,C_n + p\,C_p) = \frac{\exp\left(\frac{E - E_f}{kT}\right)}{1 + \frac{p\,C_p}{n\,C_n}} \equiv \exp\left(\frac{E - E_{ft}^{n}}{kT} \right) \qquad 3.35(a)$$

where E_{ft}^{n} is defined by equation 3.35(a) and called the quasi-Fermi level for trapped electrons. Combining the above equations gives

$$f(E) = \frac{1}{1 + \frac{p\,C_p}{n\,C_n}} \left\{ 1 + \exp\left(\frac{E - E_{ft}^{n}}{kT} \right) \right\}^{-1} \qquad 3.34(b)$$

Similarly, for holes equation 3.35(a) can be rewritten as

$$\bar{f}(E) = 1 - f(E) = \frac{1}{1 + \frac{n\,C_n}{p\,C_p}} \left\{ 1 + \exp\left(\frac{E - E_{ft}^{p}}{kT} \right) \right\}^{-1} \qquad 3.33(b)$$

The quasi-Fermi levels for free electrons and holes are defined by

$$n = N_c \exp\left[- \frac{E_c - E_f^{n}}{kT} \right] \qquad 3.36$$

and

$$p = N_v \exp\left[\frac{E_v - E_f^{p}}{kT} \right] \qquad 3.37$$

They are different from E_{ft}^{n} and E_{ft}^{p} except under thermal equilibrium conditions, when all Fermi levels coincide with E_f. Examples of the trap occupancy function are shown in Figure 3.6. The diagrams assume one species of traps, ie, that the ratio C_n/C_p is constant, otherwise f(E) would be multivalued. The quasi-Fermi levels for trapped carriers are always outside those for free carriers and both move further from E_f with increasing illumination.

In theory the trap occupancy function can be calculated with localized-localized transitions included but the mathematics for an arbitrary trap distribution is much more difficult in that case. The so-called demarcation levels can be defined by the condition that a trapped carrier at those levels will have equal probabilities of re-emission and recombination, ie,

$$e_n(E_{dn}) = p\, C_p(E_{dn}) \qquad 3.38(a)$$

$$e_p(E_{dp}) = n\, C_n(E_{dp}) \qquad 3.38(b)$$

This gives

$$E_{dn} = E_v + (E_c - E_f^{p}) + kT \ln(C_p N_v/C_n N_c) \qquad 3.39(a)$$

$$E_{dp} = E_c - (E_f^{n} - E_v) + kT \ln(C_p N_v/C_n N_c) \qquad 3.39(b)$$

The significance of these equations is that states between E_c and E_{dn} act as electron traps most of the time, ie, transitions a and a' dominate. Likewise states between E_{dp} and E_v act as hole traps. This is not to say that recombination or localized-localized

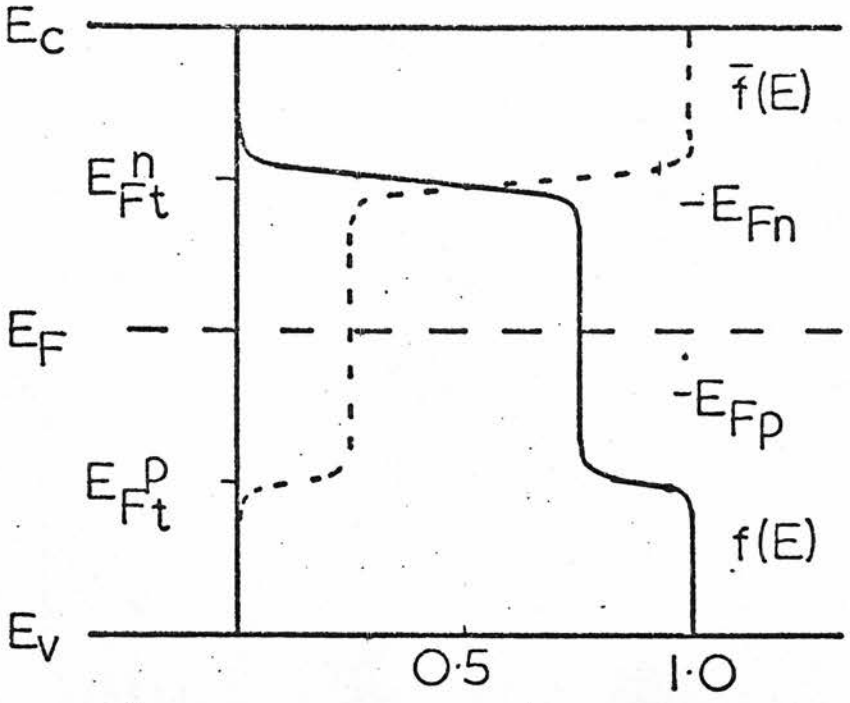

(a) $nC_n > pC_p$

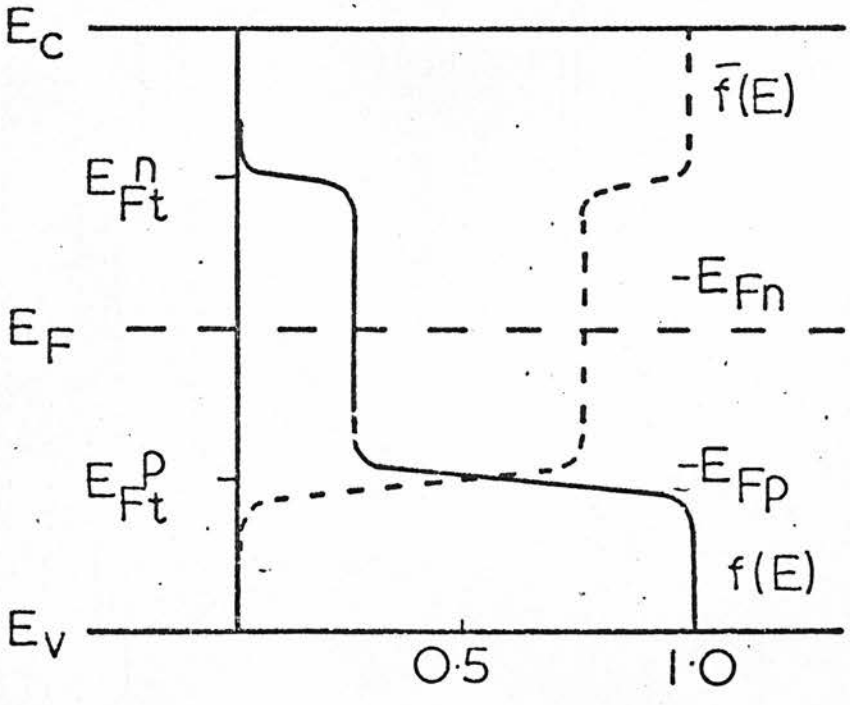

(b) $pC_p > nC_n$

Trap Occupancy (Constant Species) under Illumination.

FIGURE 3.6 (Ref 2o).

transitions cannot take place, only that a carrier experiences, on the average, many trapping and re-emission events before recombining or making a transition to another localized state.

When more than one recombination path is possible the one with highest probability will dominate and the overall recombination rate is controlled by the slowest step in that path. The relative probabilities of different paths depend on temperature and the level of illumination.

By using the rate equations developed earlier, together with the concepts of quasi-Fermi levels and some assumptions about the distribution of traps and their capture coefficients, it is possible to calculate the densities of carriers in the bands and at localized levels. Before this can be compared with experiment, however, it is necessary to consider where the conduction is taking place, ie, by free holes or electrons or hopping, etc, and to make assumptions about mobilities. It is also necessary to consider the effects of non-uniform excitation.

Lack of space does not allow a full development of the theory by this approach. In the following sections typical results on photoconductivity in chalcogenide glasses will be discussed and related to the rate equation formalism. It is convenient to consider the limiting cases where the number of photogenerated carriers is either small or very large compared to the thermally generated carriers.

3.4.2 STEADY STATE PHOTOCONDUCTIVITY IN CHALCOGENIDE GLASSES

Some typical results of steady-state photoconductivity measurements as a function of temperature 1/T, with intensity as a parameter are shown in Figure 3.7. They are for sputtered films of $As_2Se\ Te_2$ and are taken from a paper by Arnoldussen et al[7]. The main features are the following. For a constant intensity the photocurrent goes through a maximum near the temperature at which it equals the dark current. At higher temperatures the photoconductivity increases exponentially with 1/T; this is denoted region I. In region II the photocurrent decreases exponentially with 1/T until, in region III, it gradually levels off. At a constant temperature the photoconductivity increases linearly with illumination in regions I and III but in region II it increases as the square root of illumination, ie,

$$I_{pn} \propto F^n \qquad 3.40$$

where $n = 1$ in region I, $\frac{1}{2} \leqslant n$ in region II and $n \leqslant 1$ in region III. At low levels of illumination in region II, linear behaviour ($n \doteq 1$) is observed. In general, these features have been interpreted in terms of trapping and recombination kinetics. The recombination is said to be 'monomolecular' in the linear regimes and 'bimolecular' in the square root regime.

According to Spear et al[19] the activation energy in the bimolecular region is identical to the drift mobility activation energy in a-Si films. This is not the case for chalcogenide glasses. For example, according to Main[20], in a-As_2Se_3, after

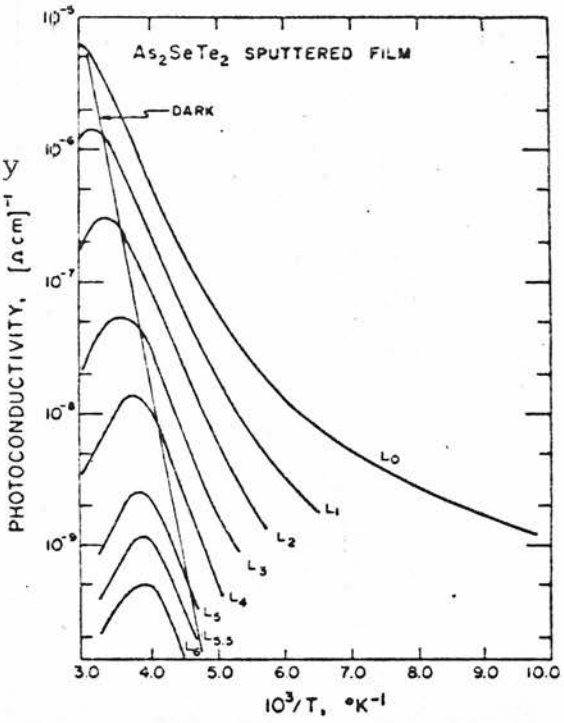

FIGURE 3.7

Typical photoconductivity results (Ref 7).

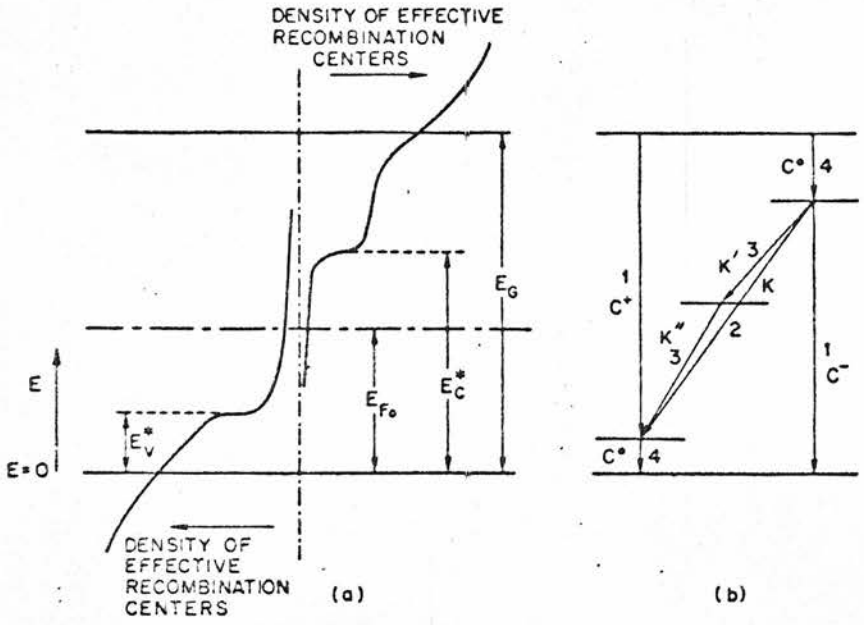

FIGURE 3.8

The recombination scheme used by Arnoldussen et al to explain the photoconductivity in As_2SeTe_2 (Ref 7).

correcting for the temperature shift of the absorption, the photocurrent activation energy is 0.33 eV in region II, whereas the drift mobility activation energies at zero field is either 0.44 eV or ~0.65 eV depending on which trapping levels have time to come into equilibrium with the band during the transit time[21,22]. These values of activation energy are in agreement with those derived from the photomobility measurements of Main[20] to be discussed in the next section.

3.4.3 INTERPRETATION OF THE STEADY-STATE PHOTOCONDUCTIVITY

Weiser et al[23] interpret photoconductivity in a-As_2Se Te_2 in terms of the CFO model and localized-localized transitions. According to this model the excess carriers thermalize in the tails of localized states with decreasing probability as the depth increases. It is assumed that the probability of recombination (via localized transitions) decreases more slowly than the thermalization probability. Hence an energy will be reached where the two are equal and below that energy (for electrons) the probability of recombination is greater. Weiser et al[23] call this critical energy the 'recombination edge'. An important consequence of the model is that the *trap occupancy* is a maximum at the recombination edges.

To obtain agreement with the experimental data it is necessary to further assume that the thermalization probability decreases with energy (for electrons) much more rapidly than seems likely and as a result the trap occupancy would peak very sharply at the recombination edges. This model is then almost indistinguishable from a discrete-trap-level model, with levels situated at energies

corresponding to the recombination edges. Moreover, the spatial separation of localized levels will make localized-to-localized transitions much less likely than transitions between a band and a localized state.

Arnoldussen et al[7], using the density-of-states model described at the beginning of the chapter, invoke both band-to-localized and localized-to-localized transitions between the recombination edges and the Fermi level, ie, effectively a five level model, as illustrated in Figure 3.8.

Arnoldussen et al interpret their photoconductivity data for $As_2Se\ Te_2$ in terms of this scheme. In the high temperature region either transitions 1 or 2 may govern the recombination. In the intermediate region transitions 2 dominate at high intensities and transitions 3 at low intensities. At low temperature transitions 4 control the recombination. Their modified model[6] is effectively a discrete level model plus a 'chaotic potential' which causes spatial fluctuation of the bands. Averaged spatially, this gives a continuum of states on both sides of the Fermi level and localized band-edge states as shown schematically in Figure 3.9. In the high temperature region the number of excess carriers, both in the traps and the bands is much smaller than the number of thermally generated carriers. Since the capture rate depends on the product of occupied states at one level (or band) and unoccupied at the other, it will increase linearly with increased generation until the excess generation becomes comparable to the thermal generation, after that the increase in capture rate becomes proportional to the square of the excess carrier density,

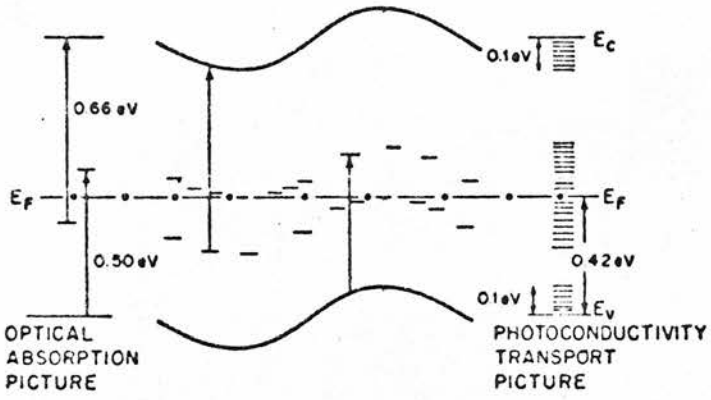

FIGURE 3.9

Discrete levels and sharp band edges broadened into a continuum of localized states and band tails by chaotic potential fluctuations (Ref 6).

with the result that the steady-state densities increase with the square root of the generation rate. This can perhaps be better illustrated by referring to the equations derived by Main[20] who employs a discrete level model involving the transitions shown in Figure 3.10. Main also introduces some band tailing and states at the Fermi level E_f, effectively pinning it; both have some influence on the charge neutrality condition but do not take part in the recombination traffic, ie, the transitions labelled No 3 in Figure 3.8 do not occur. It is assumed that the traps are in a quasi-equilibrium with the nearer band and lie outwith the appropriate trap quasi-Fermi levels under all experimental conditions, ie, $n_i = N_i f_i = n \frac{N_1}{N_c} \exp [- \frac{E_c - E_1}{kT}]$ etc. Only the basic recombination transitions are shown in Figure 3.10. The charge neutrality condition is approximately

$$N_1 f_1 \triangleq N_2 f_2 \qquad 3.41$$

Combining this condition with the recombination equation for holes, equation 3.30 and a quasi-Fermi function which includes localized-to-localized transition rates, gives

$$G-G_o = \Delta G = [\, 2p_o \,.\, \Delta p + \Delta p^2 \,] \{ C_{p1} \frac{N_2}{p_2} + C_{n2} (\frac{N_2}{p_2})^2 \frac{n_1}{N_1} + K_{12} (\frac{N_2}{p_2})^2 \} \qquad 3.42$$

where $p - p_o = \Delta p$ and p_2 and n_1 are the 'effective densities' of free holes and electrons which would exist if the Fermi level were coincident with the traps E_2 and E_1 respectively. This equation can then be solved for Δp and clearly there is a small signal case where

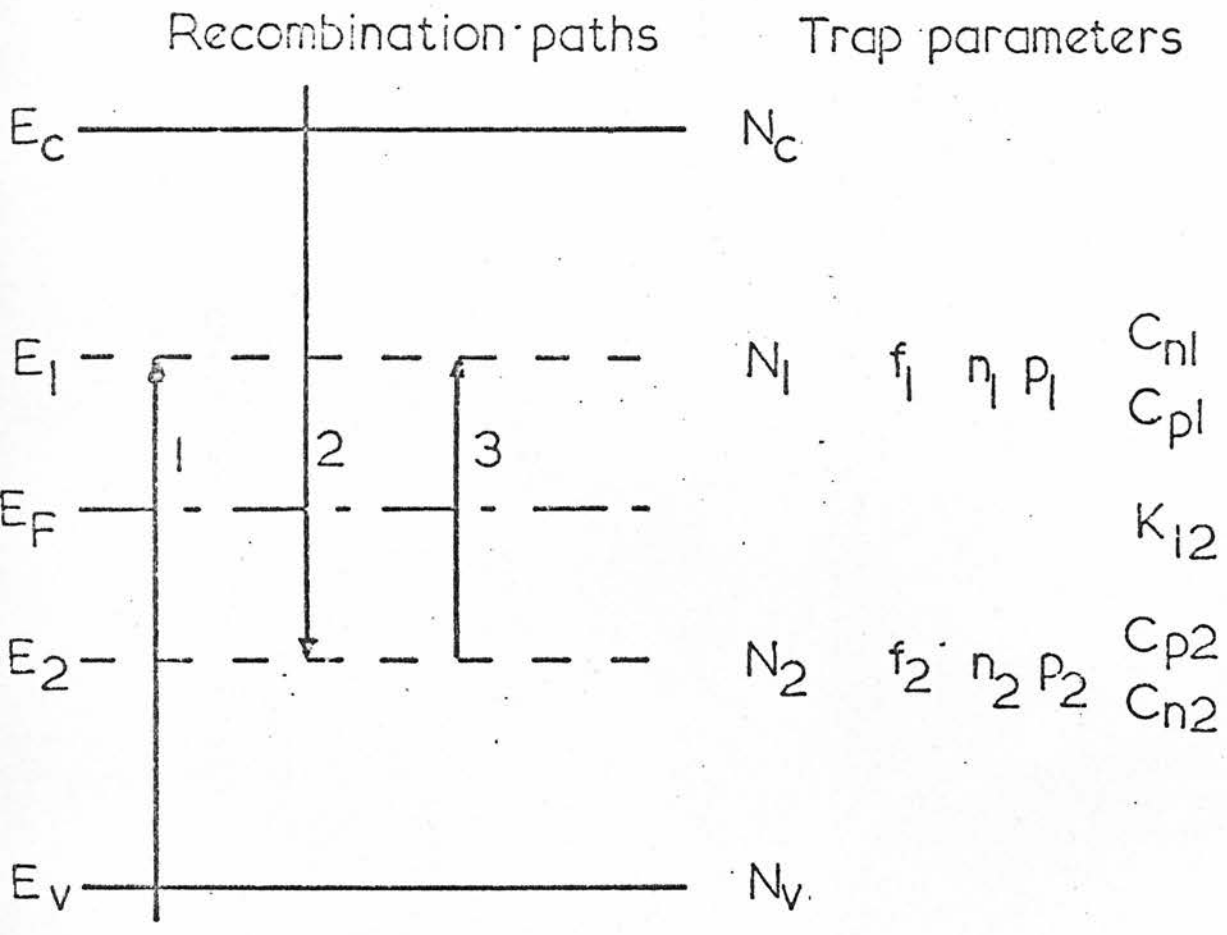

FIGURE 3.1o

(Ref 2o).

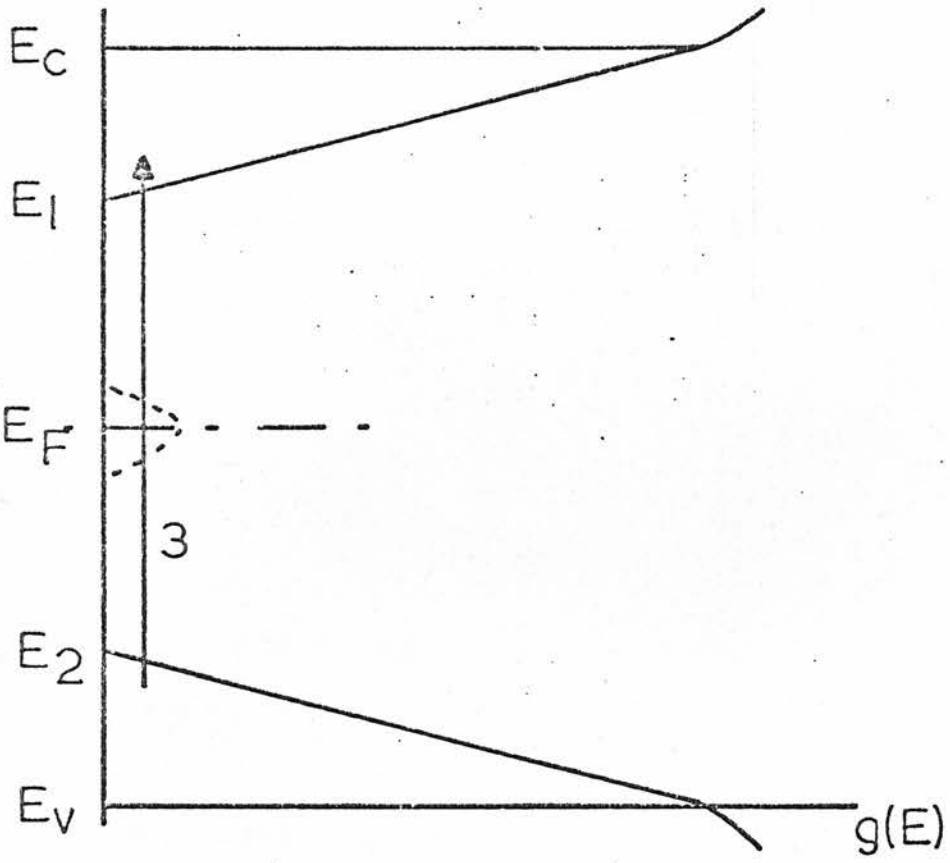

Model of Mott and Davis

FIGURE 3.11 (Ref 2).

$\Delta p \ll p_o$, $\Delta p \propto \Delta G$ and a large signal case where $\Delta p \gg p_o$ and $\Delta p \propto \Delta G^{\frac{1}{2}}$. The three terms in curly brackets represent the three recombination paths in Figure 3.10 and normally one dominates at a given temperature.

Equation 3.42 can be solved for each path separately and the solutions checked against experimental data. The activation energy of each solution is a combination of two or more of the energies E_c, E_1, E_2 and E_v. To determine which solutions are appropriate to the experimental observations it is necessary to analyse the data carefully and make comparisons with other electrical properties, eg, dark conductivity, transient photoconductivity, etc. The above analysis can only explain the photoconductivity regions I and II. Main[20] finds that in region III the photoconductivity has a constant activation energy which is less than in region II (in the case of a-As_2Te_3), and he argues that the trapped hole quasi-Fermi level approaches E_2 at low temperatures although he does not find the expected transition to a linear current intensity behaviour. However, following Marshall[4], it seems more likely that in the case of a-As_2Te_3 a transition to hopping conduction at E_2 occurs at low temperatures while another set of states, which could be the bottom of the valence band tail, controls drift mobility.

Mott and Davis[2] discuss photoconductivity kinetics using the limited-tail model of Figure 3.11. The analysis reduces to the discrete level case in Figure 3.10 and 'effective discrete' densities may be substituted in the recombination equations. To explain the data of Main, however, a'tailing' of 0.35 eV in the conduction band and 0.32eV in the

valence band of a-As_2Te_3 would be necessary according to this model; this is rather more than the 0.1 - 0.2 eV tailing expected in simple chalcogenide glasses. Another model which requires some mention is that of Simmons and Taylor. In their earlier papers[24,25,26] they treat the theory of steady-state statistics for an arbitrary trap distribution and a CFO type distribution. Only band-to-localized transitions are considered and there is no 'recombination edge' in this model since the transition coefficients do not vary rapidly with energy at any point. This means that the peaks in occupation, which are due to the density-of-states tailing *and* the fall-off in occupancy beyond the trap quasi-Fermi levels, will move outwards with increasing illumination. As a result, a plot of Δp vs I/T is curved, and the intensity relation is between square root and linear. More recently, Simmons and Taylor[27,28] have interpreted their results on photoconductivity in amorphous Si:Te:As in terms of a discrete-level-model with two discrete levels and this is similar to that used by Main for a-As_2Te_3 except that for simplicity Simmons and Taylor assume a symmetric case where

$$E_c - E_1 = E_2 - E_v \qquad 3.43$$

They consider that their data is not consistant with the CFO model and that in general a discrete level model is more appropriate for amorphous chalcogenides.

3.4.4 EFFECT OF TEMPERATURE DEPENDENT ABSORPTION

Figure 3.12 shows the sample geometry used in some of the experiments. The generation rate in the sample *at depth* x is

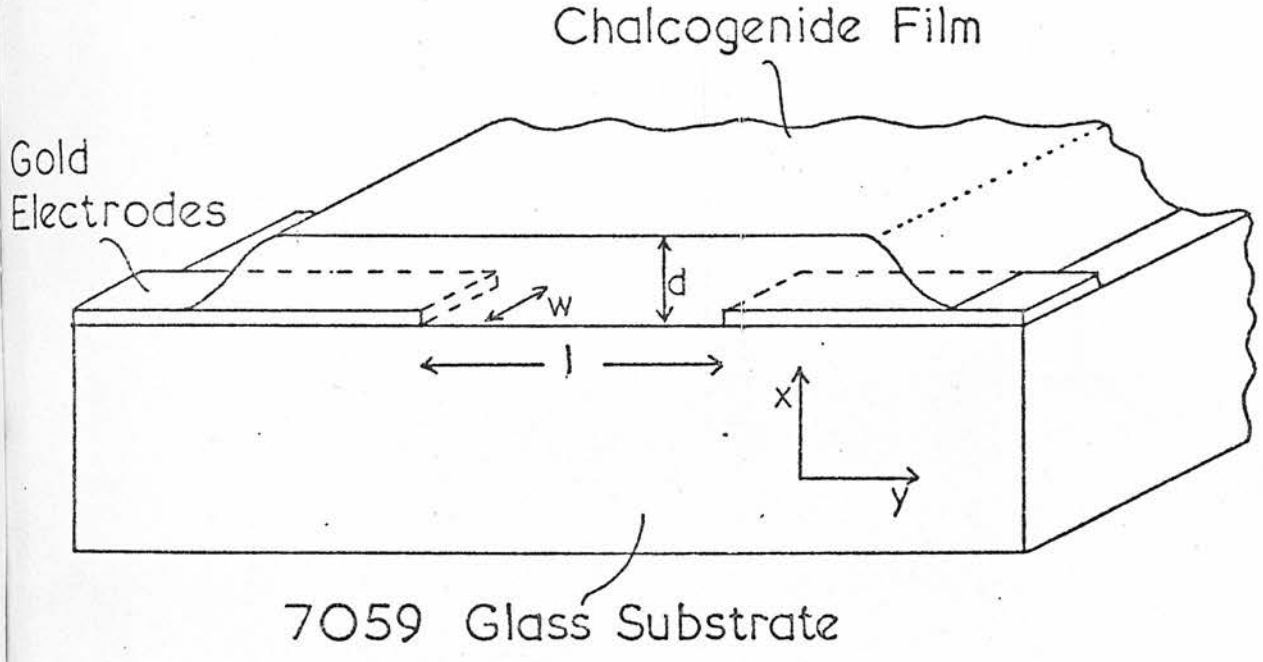

Sample Geometry.

FIGURE 3.12

$$\Delta G(x) = \eta\alpha\, F(x) \qquad 3.44$$

where α is the absorption coefficient and $F(x)$ the photon flux at x. If F_o is the incident light intensity then

$$F(x) = (1-R_1)\, F_o \exp[-\alpha x] \left(\frac{1 + R_2 \exp[-2\alpha(d-x)]}{1 - R_1 R_2 \exp[-2\alpha d]} \right) \qquad 3.45(a)$$

where R_1 is the air-film reflectance, and R_2 the film-substrate reflectance. Multiple reflection effects are included in equation 3.45(a) but not interference. If αd is sufficiently large, back reflections are unimportant and

$$F(x) = (1 - R_1)\, F_o \exp[-\alpha x] \qquad 3.45(b)$$

Obviously therefore, the generation rate and excess carrier densities vary with x. The observed photocurrent must be compared with the integral

$$I_{ph} = we\mu_{po}\mathcal{E}\int_o^d \Delta p(x)\, dx \qquad 3.46$$

in the case of free holes. Diffusion effects have been neglected although they may be important, especially for high α.

Equations 3.42, 3.44 and 3.46 lead, for the monomolecular case, to

$$I_{ph} \propto \eta(1 - \exp[-\alpha d]) \qquad 3.47$$

If $\exp[-\alpha d] \ll 1$ then all excess holes make equal contributions wherever they are generated and even if $\exp[-\alpha d] \lesssim 1$ the change in α will have a negligible effect. On the other hand the quantum efficiency may be dependent on temperature but the important point is that spatial and temperature effects can be separated.

The bimolecular case is more difficult. Integration with respect to x gives

$$I_{ph} \propto 2(\eta/\alpha)^{\frac{1}{2}} \left(1 - \exp\left[-\frac{\alpha d}{2}\right]\right) \qquad 3.48$$

ie, the photoconductivity depends approximately inversely on the square root of the absorption. Since at a given wavelength the absorption increases with temperature, especially when $\alpha \gtrsim 10^4$ cm^{-1}, it is clear that this must be taken into account. This is very important when considering the variation of quantum efficiency with temperature and wavelength. When $\alpha > 10^4$ cm^{-1}, at the lowest temperature the *relative* change in α is smaller than η is more likely to be unity and constant. On the other hand the effect of diffusion and possible surface states will be more important for large values of α. Figure 3.13 shows some results by Main[20] on the activation energy for photoconductivity in a-As_2Se_3 in the bimolecular region, with and without the correction for the shift of the absorption edge with temperature. The correction is very small above 2.1 eV where the absorption at 104 K is $\sim 10^4$ cm^{-1}, but at lower photon energies the correction is substantial.

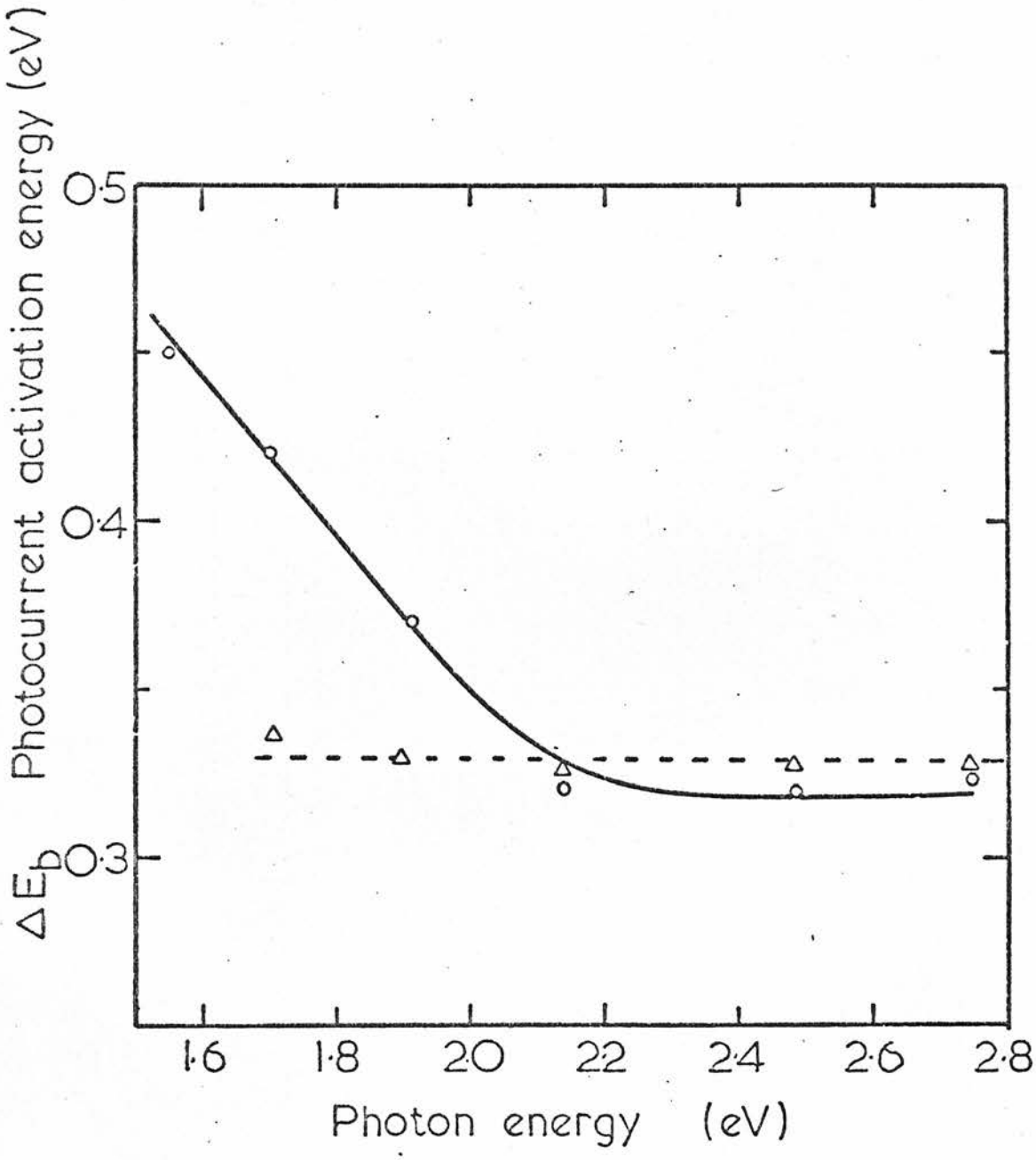

As_2Se_3 ΔE_b Photocurrent activation energy vs Photon energy

∘ original data

△ data corrected for absorption edge shift with Temperature

FIGURE 3.13 (Ref 2o).

3.4.5 SPECTRAL DEPENDENCE OF PHOTOCONDUCTIVITY

The dependence of quantum efficiency and absorption on temperature and photon energy have been discussed before. The effect on the spectral response can be considered in terms of the proportionalities 3.47 and 3.48 except for the case of $\alpha d < 1$, when multiple reflections should be taken into account (equation 3.45(a)). Main[20] has suggested that the quantum efficiency in a-As_2Se_3 is not thermally activated and that the decrease in spectral response above 2.2 eV is due to a decreasing recombination lifetime with increasing α. For a-As_2Te_3 he observed a similar decrease at 143 K where bimolecular recombination prevailed but *not* at room temperature where the recombination was monomolecular. Main concludes that theories involving 'geminate recombination' of the photogenerated electron-hole pair, resulting in an activated field-dependent quantum efficiency are not appropriate for a-As_2Se_3, even though the quantum efficiency reaches unity about 0.5 eV above the absorption edge as in a-Se.

When measuring spectral response, it is of course necessary to keep the photon flux density constant with wavelength or if that is not possible to normalize the photocurrent to a constant flux, in which case it is necessary to know the I_{ph} vs F relation at the temperature and values of F involved.

3.5 TRANSIENT PHOTOCONDUCTIVITY

3.5.1 PHOTOMOBILITY

Consider a step-function illumination applied to a sample in thermal equilibrium.

$$\Delta G(x) = \eta \alpha F(x) \tag{3.49}$$

In times shorter than the trapping time for the shallowest traps

$$\frac{d\Delta p}{dt} = \Delta G \tag{3.50}$$

$$\frac{dI_{ph}}{dt} = e \mu_{po} \mathcal{E} \frac{d\Delta p}{dt} \tag{3.51}$$

Such short measurement times have not been experimentally possible so far. For times longer than a given trapping time τ_t and a corresponding trap release time τ_{tr}, but shorter than the trapping time for another (deeper) set of traps and shorter than the recombination time, a quasi-thermal equilibrium will be established between the band and the traps so that

$$\Delta p + \Delta p_t = \Delta G \times t \tag{3.52}$$

and

$$\Delta p / \Delta p_t = \frac{N_v}{N_t} \exp \left[- \frac{E_t - E_v}{kT} \right] << 1 \tag{3.53}$$

where Δp_t is the increase in holes trapped at the level E_t. It follows that

$$\frac{dI_{ph}}{dt} = e\mathcal{E}\,\Delta G\,\mu_{po}\,\frac{N_v}{N_t}\,\exp\left[-\frac{E_t - E_v}{kT}\right] = e\mathcal{E}\,\Delta\,G\,\mu_d \qquad 3.54$$

where μ_d is the hole drift mobility. Figure 3.14 shows how the photocurrent is expected to grow with time. The steep slope in part (a) corresponds to the short interval before any trapping occurs, part (b) to band-trap quasi-equilibrium and part (c) shows the turnover resulting from recombination. In theory there could be linear regions corresponding to other trap levels.

In the regions which are important, ie, parts (a) and (b) in Figure 3.14, Δp is increasing linearly with time and therefore

$$\frac{dI_{ph}}{dt} \propto \int_0^d \eta\,\alpha F(x)\,dx = \eta(1 - R_1)F_0(1 - \exp\left[-\alpha d\right]) \qquad 3.55$$

so that, at high absorption the only temperature dependent term is the drift mobility.

3.5.2 LIFETIMES AND RISE AND DECAY OF PHOTOCURRENT

In materials containing high densities of traps each carrier will on the average undergo many trapping events before recombination, except at very low temperatures. When the traps are in a quasi-thermal equilibrium with the respective bands, rate equations must be

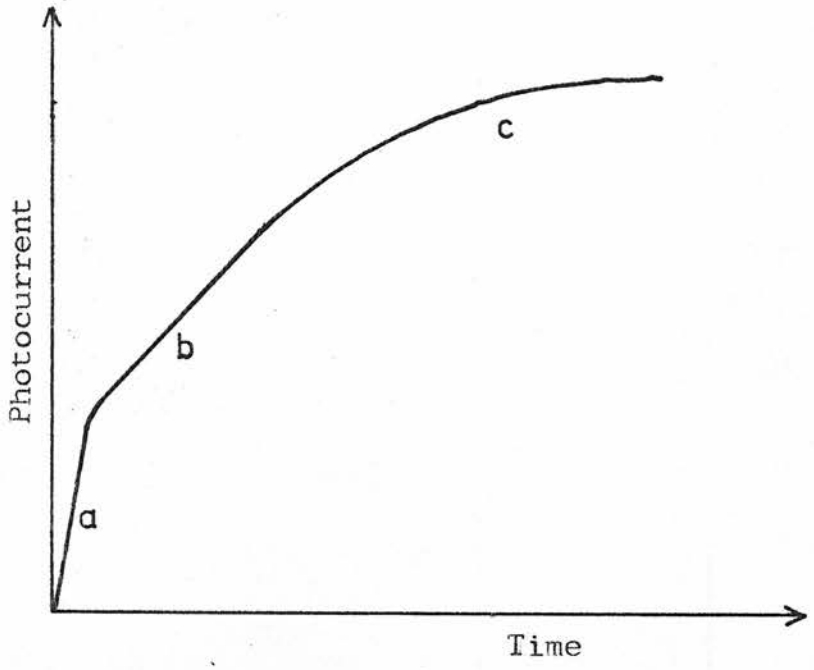

FIGURE 3.14

The response of photocurrent to a stepfunction illumination (a) before trapping, (b) after quasi-equilibrium has been established with a set of traps but before recombination becomes significant, (c) recombination limited growth.

written for the whole reservoir of carriers and for all paths, ie, eliminating intra reservoir transitions. Thus

$$\frac{d}{dt}(\Delta p + N_2 \Delta \bar{f}_2) \triangleq \frac{d}{dt}\left(\frac{N_2}{p_2}\Delta p\right) =$$

$$\Delta G - [\,2p_o\,\Delta p + \Delta p^2\,]\,\frac{N_2}{p_2}\{C_{p1} + C_{n2}\frac{N_2}{p_2}\,\frac{n_1}{N_1} + K_{12}\frac{N_2}{p_2}\} \qquad 3.56$$

describes the rate of change of free and trapped hole density taking part in hole conduction processes. The right hand side is the generation rate for excess holes, free and trapped at E_2, minus the various recombination rates through the paths shown in Figure 3.10. The instantaneous hole recombination lifetime can be defined in terms of the instantaneous recombination rate and hole density (free and trapped), since

$$R_p\,\tau_p = \Delta p + N_2\,\Delta\,\bar{f}_2 \triangleq \frac{N_2}{p_2}\,\Delta p \qquad 3.57$$

where R_p is the recombination rate. But R_p is just the second term on the right hand side of equation 3.56; hence substituting into equation 3.57 and solving for τ_p gives

$$\tau_p = [\,2p_o + \Delta p\,]^{-1}\{C_{p1} + C_{n2}\,\frac{N_2}{p_2}\,\frac{n_1}{N_1} + K_{12}\frac{N_2}{p_2}\}^{-1} \qquad 3.58$$

In the monomolecular region ($2p_o >> \Delta p$), the recombination lifetime is independent of excitation. Equation 3.56 can now be written as

$$\frac{N_2}{p_2}\frac{d\Delta p}{dt} = \Delta G - \frac{N_2}{p_2}\frac{\Delta p}{\tau_{pm}} \qquad 3.59$$

where τ_{pm} is the constant monomolecular recombination time. This equation can be solved easily, eg, for a step function illumination

$$\frac{N_2}{p_2}\Delta p = \Delta G\, \tau_{pm} g(t) \qquad 3.60$$

and

$$\frac{dI_{ph}}{dt} = e\, w \mathcal{E} \mu_d\, \tau_{pm}\, g(t) \int_o^d \Delta G(x)\, dx \qquad 3.61$$

where diffusion is neglected, and

$$g(t) = 1 - \exp\,[-t/\tau_{pm}] \qquad 3.62(a)$$

or

$$g(t) = \exp\,[-t/\tau_{pm}] \qquad 3.62(b)$$

depending on whether the excitation is switched on or off at $t = 0$, respectively.

Equation 3.59 can be applied in general if τ_p is understood to be the instantaneous lifetime, but it is more useful to write the bimolecular case as

$$\frac{d}{dt}\left(\frac{N_2}{p_2}\,\Delta p\right) = \Delta G - \Delta p^2\,\theta\,N_2/p_2 \qquad 3.63$$

where θ is the term in curly brackets in equation 3.56.

For rise : $$\Delta p = \left(\Delta G\, p_2/\theta N_2\right)^{\frac{1}{2}} \tanh\left[t\left(\theta\Delta G\, N_2/p_2\right)^{\frac{1}{2}}\right] \qquad 3.64$$

For decay : $$\Delta p = \left(\Delta G\, p_2/\theta N_2\right)^{\frac{1}{2}} \left[t(\theta\Delta G\, N_2/p_2)^{\frac{1}{2}} + 1\right]^{-1} \qquad 3.65$$

ie, the rise curve is a hyperbolic tangent and the decay curve a hyperabola. To obtain the rise and decay in photocurrent it is necessary to integrate these expressions with respect to x because of spatial variation in ΔG.

The steady state recombination lifetime in the bimolecular case can be found from equations 3.59 and 3.42 to be

$$\tau_{p\,st} = N_2\,\Delta p/p_2\Delta G = \left(\Delta G\, N_2\,\theta/p_2\right)^{-\frac{1}{2}} \qquad 3.66$$

In this chapter, a brief account of carrier transport and photoconductivity has been given. Some aspects were included for the sake of completeness and will not be referred to further. The concepts that are of importance in this work, and will be made use of later, are those discussed in Sections 3.2 and 3.4 and also photomobility discussed in 3.5.1.

3.6 REFERENCES

1. Fritzsche, H, J Non-Cryst Sol 6, p 49, 1971.
2. Mott, N F and Davis, E A, Electronic Processes in Non-Crystalline Materials, Clarendon Press, Oxford, 1971.
3. Adler, D, Amorphous Semiconductors, CRC, Cleveland, Ohio, 1971.
4. Marshall, J M and Owen, A E, Phil Mag 31, p 1341, 1975.
5. Kolomiets, B T, Proc 9th International Conference on the Physics of Semiconductors, Moscow, Vol 2, Acad Sci, USSR (Leningrad 'Nauka', 1968).
6. Voronkov, E et al, J Non-Cryst Sol 15, p 275, 1974.
7. Arnoldussen, T C et al, Phys Rev B 9, p 3377, 1974.
8. Mott, N F, Phil Mag 22, p 7, 1970.
9. Cohen, M H, J Non-Cryst Sol 4, p 326, 1970.
10. Spear, W E, Proc Phys Soc London 76, p 826, 1960.
11. Main, C and Owen, A E, Proc on the 5th International Conference on Amorphous and Liquid Semiconductors, Garmisch-Partenkirchen, Germany (J Stuke and W Brenig, editors), Taylor and Francis London, 1974, p 783.
12. Davis, E A and Mott, N F, Phil Mag 22, p 903, 1970.
13. Mott, N F, Phil Mag 19, p 835, 1969.
14. Hartke, J L and Regensburger, P J, Phys Rev 139, A970, 1965.
15. Lanyon, H P D, Phys Rev 130, p 134, 1963.
16. Knights, J C and Davis, E A, J Phys Chem Sol 35, p 543, 1974.
17. Lucovsky, G, Proc of the 10th International Conference on the Physics of Semiconductors (Keller, Hensel and Stern Editors), US Atomic Commission, 1970, p 799.
18. Tabak, M D and Warter, P J, Phys Rev 173, p 899, 1968.
19. Spear, W E, Proc on the 5th International Conference on Amorphous and Liquid Semiconductors, Garmisch-Partenkirchen, Germany (J Stuke and W Brenig, editors), Taylor and Francis London, p 1.
20. Main, C, PhD Thesis, University of Edinburgh, 1974.
21. Marshall, J M et al, J Non-Cryst Sol 8-10, p 760, 1972.

22. Fisher, F D et al, Phil Mag, to be published, 1975.

23. Weiser, K et al, Proc of the 10th International Conference on the Physics of Semiconductors (Keller, Hensel and Stern, editors), US Atomic Commission, 1970, p 667.

24. Simmons, J G and Taylor, G W, Phys Rev B 4, p 502, 1971.

25. Taylor, G W and Simmons, J G, J Non-Cryst Sol 8-10, p 940, 1972.

26. Simmons, J G and Taylor, G W, J Non-Cryst Sol 8-10, p 946, 1972.

27. Simmons, J G and Taylor, G W, J Phys C, 7, p 3051, 1974.

28. Taylor, G W and Simmons, J G, J Phys C, 7, p 3067, 1974.

29. Cohen, M H et al, Phys Rev Lett 22, p 1065, 1969.

CHAPTER 4 A REVIEW OF THE PHYSICAL PROPERTIES OF ARSENIC-CHALCOGENIDES

4.1 INTRODUCTION

This chapter is a survey of structural, thermodynamic and electrical properties of arsenic-chalcogenides in both their crystalline and amorphous forms, including the effects of doping with Cu or Ag. Those points which are directly relevant to the experimental results to be presented in Chapters 7 and 8 are discussed in some detail.

The physical properties of any material depend on the bonding between the atoms and molecules present; it is necessary therefore, to consider first the types and numbers of bonds formed by As, Se, Cu and other chemically similar atoms like S and Ag.

The valence shell configurations are $4s^2 4p^3$, $4s^2 4p^4$ and $3d^{10} 4s$ for the As, Se and Cu atoms respectively. The 3d electrons in Cu are very near in energy to the 4s electron. In covalent materials the spherical s-orbital and the three inversion-symmetric p-orbitals hybridize into highly directional orbitals which then interact with similar hybridized orbitals of other atoms to form bonding (σ) or antibonding (σ^*) states. These are broadened into bands in the solid. This is illustrated schematically in Figure 4.1(a) for the case of tetrahedrally bonded Ge in which the atomic $4s^2 4p^2$ structure is converted into tetrahedral sp^3 hybrids which split into bonding and antibonding states by interacting with hybrids on other atoms. The σ and σ^* bands are called valence and conduction band respectively. Tetrahedral solids are a special case however, since they contain

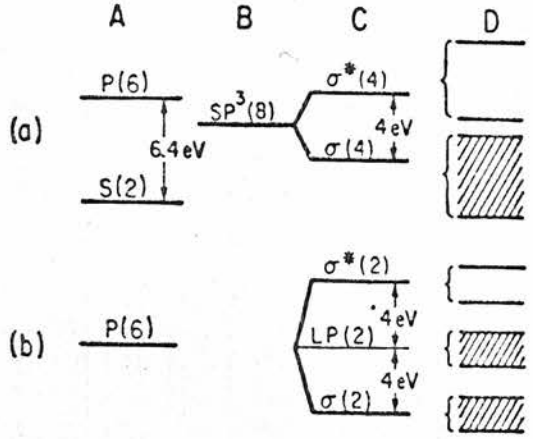

Bonding in (a) Ge and (b) Se. (*A*) atomic states, (*B*) hybridized states, (*C*) molecular states, (*D*) broadening of states into bands in the solid.

FIGURE 4.1 (Ref 1).

exactly half of the chemically stable 8 valence electrons per atom.

Arsenic has five valence electrons and Se six. If they were tetrahedrally bonded like Ge they would have one or two electrons per atom in the energetically unfavourable σ^* band. A state of lower overall energy occurs if some of the valence electrons form lone pair (LP) orbitals which do not form covalent bonds. The remaining unpaired electrons form σ and σ^* bands which have fewer states per atom than in tetrahedrally bonded materials. The question of how the atomic orbitals combine to form the LP, σ and σ^* bands is not fully resolved. Kastner[1] proposed the model shown in Figure 4.1(b) for the case of Se. He assumes that the 4s-states (not shown) do not interact with the p-states and form a LP band well below the p-bands. One of the three p-states forms a LP band at roughly the same energy as the original p-state; this leaves two p-states with only one electron each, and they tend to combine with p-states from other atoms to form σ and σ^* bands. The σ band lies below the LP band which thus becomes the valence band. Kastner explains the two peaks in the ε_2 spectrum of Se [2] as being due to the transitions from LP and σ bands. Arsenic has one fewer electron and therefore a similar picture for As would again have a separate LP band due to the 4s-state with all the p-states participating in bonding.

Although Kastner's model is useful as a first approximation it is not entirely realistic. This can be seen from the fact that the symmetry of the p-orbitals is not reflected in the bonding. Thus in all known crystalline forms of Se, As and As-Se compounds

have bond angles which are intermediate between the cubic symmetry (90^{o}) and the tetrahedral (109.5^{o}) symmetry and usually closer to the latter. This indicates that there must be hybridization between s and p states.

Chen[3] performed molecular-orbital studies of a-Se, As_2S_3 and As_2Se_3 where the amount of hybridization is related to the bond angles. He further assumed that a-Se contained a mixture of Se_8 rings and chains. Like Kastner he obtains a doubly peaked valence band but each peak is a mixture of LP and σ states. Thus the top of the valence band consists of both types of states. The calculated ε_2 spectra is in agreement with experiment[2]. For photon energies in the range 2 - 6 eV the σ states contribute about 30% of the ε_2 intensity. Chen's calculations also agree with Nielsen's[4] determination of the width of the valence band determined by photo-emission techniques.

Another indication that σ states contribute to the top of the valence band comes from the observation that band-gap radiation (~2 eV) can induce crystallization in a-Se[5], polymerization of As_2S_3 and As_2Se_3 [6] and phase separation of As_7Se_3 [7]. All these processes require breaking of bonds. Admittedly a hole could be thermally activated from a LP state to a σ state but the efficiency of the bond breaking would be very low, if the energy difference was appreciable, and in any case the observed activation energies relate to the density of holes in the valence band.

The interaction between chains in trigonal selenium or layers in crystalline As_2S_3 and As_2Se_3 is not purely by Van der Waals interactions. In the former[8] each atom is bonded to its two nearest

neighbours in the same chain, with a bond length of 2.32 Å. It also has 4 next-nearest neighbours in other chains, which are only 3.46 Å away. This suggests weak interchain bonds arising from some mixing of LP and hybrids of different chains.

Arsenic has a strong tendency to form, in addition to its three normal bonds, three other weaker bonds due to next-nearest neighbour interactions and in the 'backward' direction of the stronger bonds. This is why rhombohedral As is a semimetal[9]. In amorphous and orthorhombic As the next nearest neighbours are further away so these bonds will be even weaker but may still be as important as Van der Waals bonds. Similar considerations apply in crystalline and amorphous As_2Se_3. Even tetrahedral materials show some tendency to form bidirectional bonds. Thus liquid Ge and Si are metals with coordination number $\doteq 6$. In such a liquid a mobile bonding system is needed[9], ie, one in which bonds are easily broken. This is achieved by a reversible transformation of bidirectional p-orbitals into unidirectional sp hybrids. This process needs only a small amount of energy compared with the dissociation energy.

The bond interchange mechanism discussed by Eisenberg and Teter[10] in connection with viscosity measurements on polymeric sulfur may be of similar nature.

Atomic Cu has one 4s electron a few eV above the ten 3d electrons. Because of the spherical symmetry of the 4s state Cu can easily form bonds in any direction. Moreover, mixing with the empty 4p levels and with the 3d levels can occur. Thus Cu can change both its bonding and coordination and may be expected to

diffuce easily through networks which contain a sufficient quantity of atoms that have tendency to form mesomeric bonds, such as As.

4.2 STRUCTURAL AND THERMODYNAMIC PROPERTIES

4.2.1 CRYSTALS

Trigonal Se is the stable polymorph of Se. It consists of closely packed, infinite and parallel helicoidal chains with trigonal symmetry. The values of the dihedral and bond angles in the chain are $\delta = 102^{o}$ and $\theta = 105^{o}$; the bond length is 2.32 Å. Four next nearest neighbours lie at 3.46 Å. Figure 4.2 illustrates the alignment of chains[11] and weaker second-neighbour bonds are also shown.

In monoclinic Se the mean dihedral angle is the same as in the trigonal form but changes sign at every bond. This results in eight-membered puckered ring molecules; Se_8. In practice the rings are slightly distorted due to the influence of neighbouring rings. The rings arrange themselves in either of two polymorphs, α- or β-monoclinic Se, which may be considered as two different close-packed arrangements, of Se_8 ring molecules. The 8-fold rings and their spatial arrangement is illustrated in Figure 4.3 [12]. The next-nearest neighbours in both α- and β-Se lie at about 3.8 Å, but different Se atoms have different environments.

Sulfur is a group VI element like selenium. No trigonal polymorph for S exists, however, since sulfur chains are unstable below $160^{o}C$ [13], a temperature which is well above the melting point. Therefore, crystalline S consists of S_8 rings; below $96^{o}C$ the rings

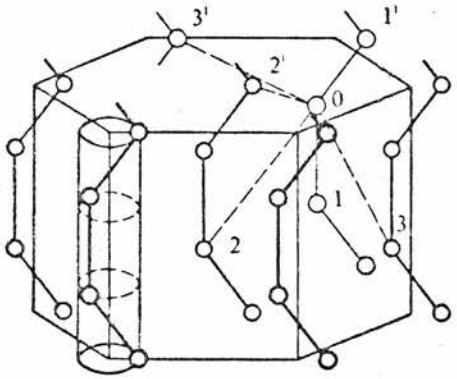

Structure of trigonal Se. First-neighbour bonds (2.32 A): 0–1,1'. Second-neighbour bonds (3.46 A): 0 - - - 2, 2', 3, 3'.

FIGURE 4.2

(Ref 11).

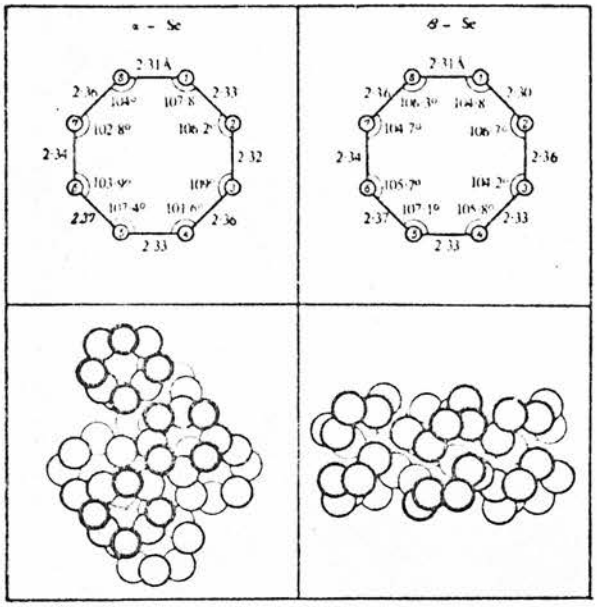

8-fold rings and their spatial arrangement in α- and β-monoclinic Se.

FIGURE 4.3

(Ref 8).

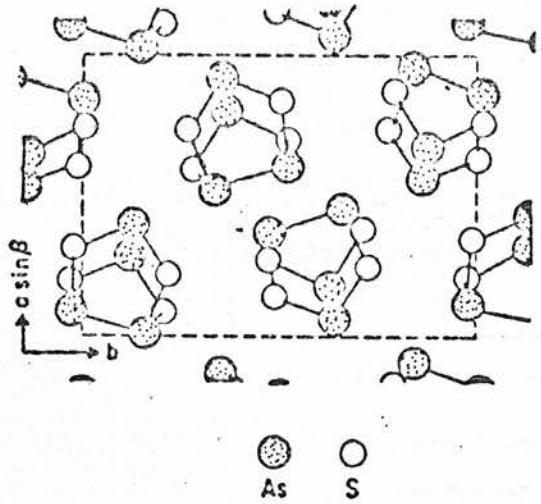

FIGURE 4.5
The realgar (As_4S_4) structure shown in a (ool) projection (Ref 17).

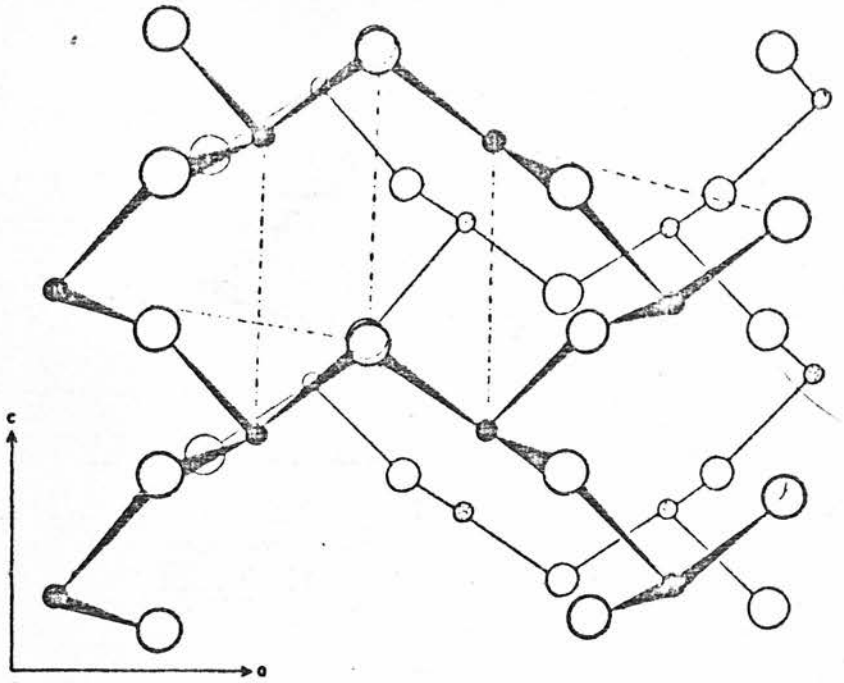

As atoms in upper sheet
S atoms in upper sheet
As atoms in lower sheet
S atoms in lower sheet
C_o translation cross-ring correlation
intra-sheet correlation between unlike atoms

FIGURE 4.4
The sheet structure of orpiment viewed along the b_o axis. The relative orientation of two adjacent sheets is shown, atoms in the upper sheet being linked by directional bonds (Ref 22).

form an orthorhombic (α) and a monoclinic array in the range 96 - 115°C (β).

There are three known structures of elemental As. Rhombohedral or α-As consists of double layers in which each atom is bonded to three neighbours[9]. Layers are bonded together by weak mesomeric bonds and α-As is a semimetal. The other two forms are vitreous (β) As and orthorhombic As (arsenolamprite). In both cases the second nearest neighbour distance is larger, the interlayer bonds are weaker, and they are semiconductors[14,15]. Orthorhombic As has a distorted black phosphorus structure.

Crystalline As_2Se_3 is isomorphous with the naturally occurring crystal orpiment As_2S_3, the structure of which is illustrated in Figure 4.4. It is monoclinic and consists of parallel sheets of 12-membered puckered rings. As in the elements the intermolecular (ie, interlayer) bonding is not purely by Van der Waals forces. Each As atom is bonded to 3 Se (or S) atoms which form an irregular triangular pyramid, and each Se (or S) atom is bonded to two As atoms. The unit cell parameters of the two compounds only differ by ~5% and, therefore, true crystalline solid solutions can be formed over the whole composition range[16].

Another crystalline phase in the As-S system is realgar which consists of cage-like As_4S_4 molecules as shown in Figure 4.5. The corresponding compound in the As-Se system also exists but is less stable as is indicated by a different phase diagram in the latter system[17,18].

Not much is known about crystalline compounds in the As-Se-Cu system. A compound Cu_2Se is found in nature as the mineral

berzelianite; it has a cubic structure and melts at 1120°C [19]. Khvorostenko et al[19] constructed a phase diagram for the system As_2Se_3-Cu_2Se in which they identify two intermediate compounds, ie, $CuAsSe_2$ and Cu_3AsSe_3. According to Liang[20] tetrahedral $CuAsSe_2$ complexes are formed in the As-Se-Cu system. Crystalline $CuAsSe_2$ has the sphalerite structure, with a cell dimension a = 5.49 Å. It is narrow gap semiconductor and melts at 415°C [19,20]. It is important to note that in $CuAsSe_2$ all atoms are tetrahedrally coordinated and it can be quenched into a glass in bulk form. It should therefore be classified as a tetrahedral glass former like $CdGeAs_2$.

4.2.2 THE PRESERVATION OF SHORT RANGE ORDER

The structure of glasses and RF sputtered films in the As-Se system has been studied by X-ray diffraction methods by Renninger and Averbach[18] and Renninger et al[21] who compared the experimental results with calculations based on computer-generated Monte Carlo models. Apling[22] and Leadbetter and Apling[23] compared X-ray and neutron diffraction results with model peak functions of bond lengths and simple considerations of probable local bonding configurations. They also studied As-S glasses. Several important conclusions emerge from the work of these authors.

(a) Se remains two-fold coordinated and As three-fold coordinated in glass and vapour-deposited films at all compositions investigated (0 - 50% As, atomic).

(b) The results are consistent with the assumption that the number of like-atom bonds formed is the minimum number

consistent with composition and covalency requirements.

(c) a-Se is a mixture of chains and rings, the latter mostly eight-membered.

(d) Microcrystal models, even heavily distorted, do not give acceptable agreement with experiment.

(e) Sheet structures occur in As-Se and As-S glasses, the sheet separations being larger than in the corresponding orpiment structures, and the intersheet correlation perpendicular to the sheets extends for 15 Å in As_2S_3 and 20 Å in As_2Se_3. For the selenide glasses the sheet structure becomes more pronounced with increasing As concentration. This may be explained in terms of steric factors. Increased chalcogen content means as increased number of chalcogen atoms in a link between AsS_3 or $AsSe_3$ pyramidal units, which in turn increases flexibility and may provide cross-linking between sheets (Figure 4.6).

(f) There is no feature in the RDF for the glasses corresponding to the cross ring distance along the C-axis in the crystal, indicating that the sheets are more or less disordered in the glasses.

(g) In the As-Se glasses the average nearest-neighbour distance increases from r_1 = 2.34 Å in a-Se to r_1 = 2.41 Å in glasses with 36 - 50% As. This means that in As_2Se_3 the average bond length is less in the glass than the crystal.

(h) Within the sheets the atomic density is much the same as in

the corresponding crystal, the decrease in density is predominantly achieved by wider separation of layers. According to Leadbetter and Apling[23] the intrasheet correlation in glassy As_2S_3 and As_2Se_3 is ~10 Å.

The picture that emerges from these studies and comparisons with other work such as Raman scattering[24] is the following. The short-range-order is similar to that in the crystals out to next-nearest neighbours. a-Se consists of chains, which may be folded, and Se_8 rings. Addition of As breaks up the rings until at about 20% As concentration no rings are left. Thus at low As concentrations the most significant change is the reduction in the ring concentration with increasing As content. In the range 10 - 30% As a network of $AsSe_3$ pyramids begins to form but some Se chains also exist. Above 30% As concentration the network or sheet structure dominates and its continuity increases up to 40 - 45% As. At still higher As concentrations the sheets gradually break down into smaller molecular units containing As-As bonds, ie, the basic building block of the sheets, $AsSe_3$ gives way to other units, possibly As_4Se_4 molecules.

In the As-S system the basic difference is that sulfur chains are absent and therefore the glass contains S_8 rings and As branched networks in various proportions from pure S to As_2S_3.

Smith et al[14] showed that the structure of a-As is much closer to that of orthorhombic than rhombohedral As. Greaves and Davis[15] constructed a three-fold coordinated CRN model of As which gave good agreement with the experimental values of density and RDF. This model is open and 'cavern-like' and the probability of

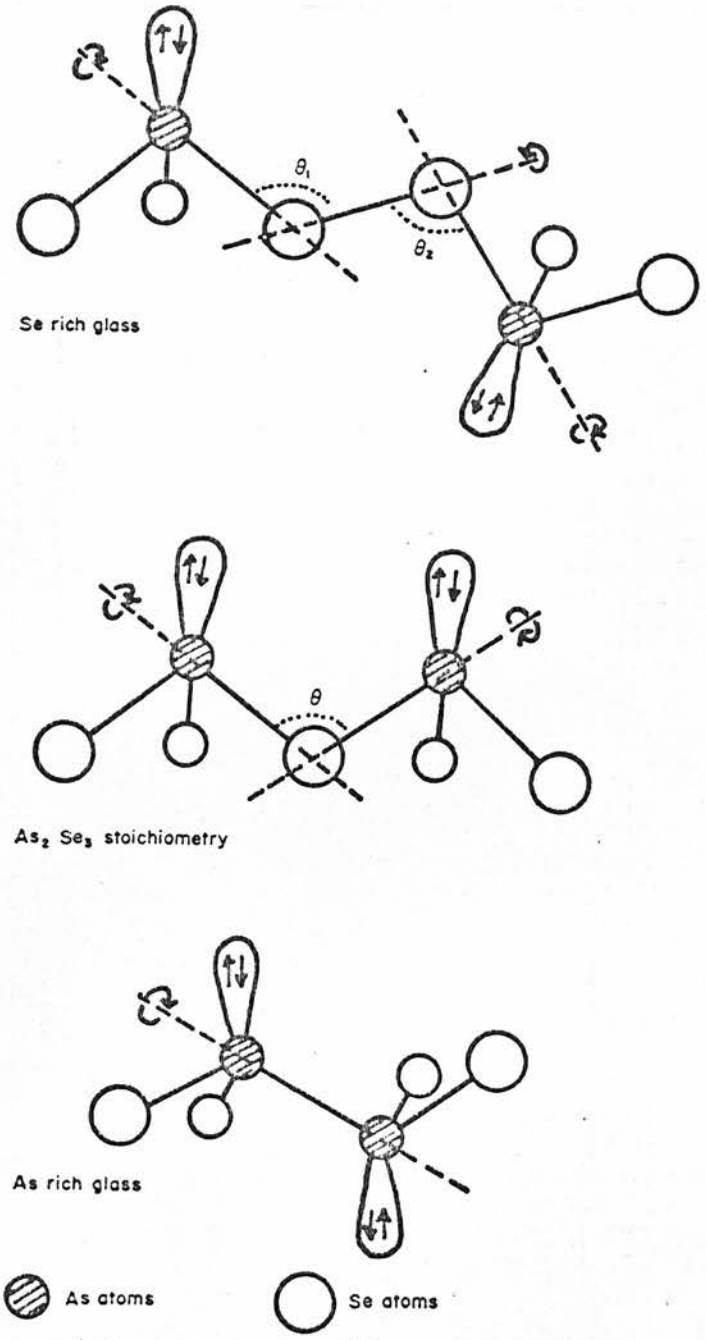

FIGURE 4.6

Atomic arrangements in As-Se glasses (Ref 22).

orbital overlap between atoms not directly bonded is small. The second peak in the RDF for the crystalline forms is at 3.15 - 3.2 Å and is not present in the a-As.

The RDF's for crystalline and a-$CuAsSe_2$ were obtained by Liang[20] and are shown in Figure 4.7. Like other tetrahedrally bonded materials, the third peak in the RDF for the crystal is absent in the amorphous form. The area of the first peak corresponds to a coordination number of about four. When Cu is added to As_2Se_3 the average coordination increases, suggesting that $CuAsSe_2$ complexes are formed in which all atoms are tetrahedrally bound, or alternatively that the Cu atoms act as interstitials (ie, are not covalently bound). The latter interpretation is unlikely[20], however, since the Cu atoms are singly ionized (Cu^+) and Tg increases with Cu concentration above 10% (atomic).

4.2.3 THE POLYMERIC NATURE OF CHALCOGENIDES

Tobolsky and Eisenberg[13,25,26] have developed a theory of equilibrium polymerization from the law of mass action which they applied to liquid S and Se. The conditions at equilibrium at any temperature may be written as

$$M \overset{K}{\rightleftharpoons} M^* \quad ; \quad M^* = KM \qquad 4.1$$

where M is an S_8 (or Se_8) ring and M* an S_8 diradical or broken ring.

$$M^*_n + M \overset{K_3}{\rightleftharpoons} M^*_{n+1} \quad ; \quad M^*_{n+1} = K_3{}^n \, KM^{n+1} \qquad 4.2$$

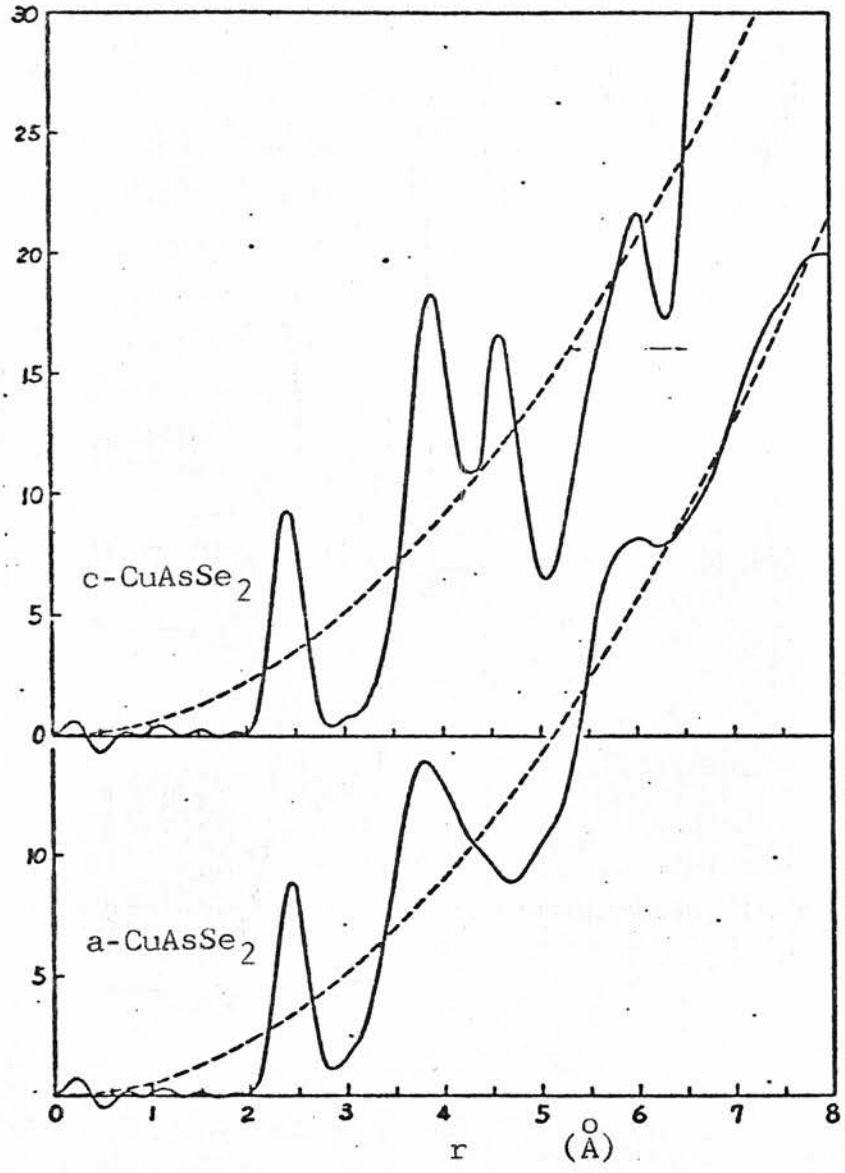

FIGURE 4.7

Radial distribution functions for crystalline and amorphous $CuAsSe_2$ (Ref 2o).

The first equation describes the initiation step, ie, a break-up of S_8 rings. The second equation is the n^{th} step of the propagation of polymerization, ie, chain growth. It is assumed that chains contain only integral numbers of monomer (S_8) units. K and K_3 are rate constants for the two reactions and it is assumed that K_3 is independent of n. Several useful equations can be derived from these assumptions, one of which gives the average chain length D in terms of S_8 units.

$$D = (1 - K_3M)^{-1} \qquad 4.3$$

where M is the concentration of unbroken rings. Also

$$M_o = M + KMD^2 \qquad 4.4$$

where M_o is the total (constant) number of S_8 units. The rate constants can be expressed as

;

$$K = \exp\left(\frac{\Delta S}{k}\right) \exp\left(-\frac{\Delta H}{kT}\right) \qquad 4.5$$

and

$$K_3 = \exp\left(\frac{\Delta S_3}{k}\right) \exp\left(-\frac{\Delta H_3}{kT}\right) \qquad 4.6$$

where ΔS and ΔS_3 are the increases in entropy and ΔH and ΔH_3 the increases in energy associated with initiation and propagation of the polymerization. It follows from equation 4.3 that $D \backsim 1$ when

$$1 >> K_3M \doteq K_3 M_o \qquad 4.7$$

and $D >> 1$ when $K_3M \doteq 1$. This transition occurs when the free energy of the polymerization reaction changes sign. For S and Se ΔH_3 is positive and therefore the polymerization proceeds *above* the transition temperature T_λ and the monomeric phase is stable *below* T_λ. D and M can be determined if K and K_3 are known and vice versa. Figure 4.8 shows the chain length as a function of T for S and Se [13]. The curves should only be taken as an approximation since it is difficult to determine the quantities involved experimentally. It is clear, however, that at T_λ the average chain length increases by about four orders of magnitude, reaches a maximum 10 - 20° above T_λ and then decreases slowly with increasing temperature. In sulfur T_λ = 160°C and above that temperature sulfur is highly viscous. Below 160°C it consists mostly of S_8 rings and is much more fluid. For Se on the other hand $T_\lambda \doteq 80$°C which is 140° below the melting point. Therefore, a-Se ought to be monomeric but probably can never reach that state because $Tg \doteq T_\lambda$. DTA measurements by Cornet and Rossier[27] on aged a-Se showed an endotherm starting at about 54°C, which they identify with the onset of polymerization. Thus $T_\lambda \doteq 54$°C is probably the best estimate for Se.

The values of ΔH and ΔH_3 as estimated by Eisenberg and Tobolsky[13] are given in Figure 4.8. Although $\Delta H \doteq 10\ \Delta H_3$ the energy needed to build a chain with 10^3 - 10^4 units is mostly due to the propagation reaction. An upper limit on the energy of polymerization at T_λ is therefore ΔH_3 per monomer unit or $\Delta H_3/8$ per atom. This is 17 meV and 12 meV per atom for sulfur and selenium respectively and it corresponds to an upward shift of 3 - 2 meV of the valence band as a whole (since there are 6 valence electrons/atom). It is to be expected, however, that the shift is non-uniform and may be represented as a broadening

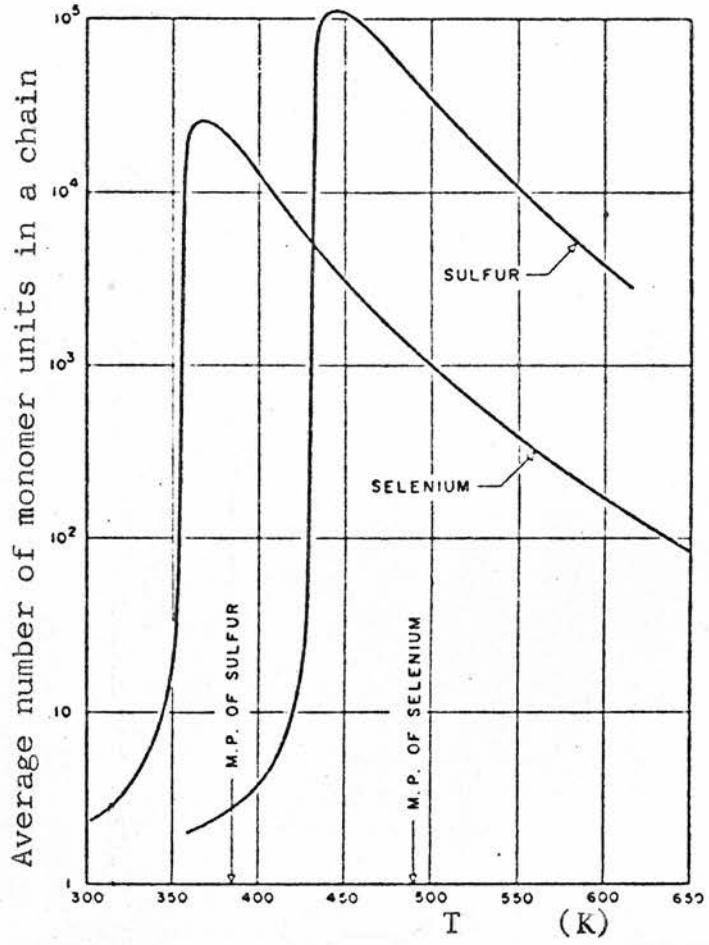

FIGURE 4.8

Sulfur (S_8)	Selenium (Se_8)
$\Delta H = 1.42\,eV$	$\Delta H = 1.08\,eV$
$\Delta H_3 = 0.138\,eV$	$\Delta H_3 = 0.10\,eV$
$\Delta S = 1.0\times10^{-3}\,eV/K$	$\Delta S = 1.0\times10^{-3}\,eV/K$
$\Delta S_3 = 2.0\times10^{-4}\,eV/K$	$\Delta S_3 = 2.4\times10^{-4}\,eV/K$

Equilibrium polimerization curves for sulfur and selenium (Ref 13).

of the upper valence band edge; thus reducing the optical gap and the steepness of the absorption curve.

Tobolsky and Owen[28] have extended the above theory to the more general case of copolymerization of a material containing two different kinds of monomer units. Applying this to various S-Se compositions they obtained good agreement with viscosity measurements. The D vs T curves are similar to those in Figure 4.8 although the transition is less sharp. T_λ increases with the S/Se ratio.

Myers and Felty[17] observed T_λ in the S-As system by DTA and volume-temperature measurements. Their results are shown in Figure 4.9, together with the glass transition temperature and the liquidus temperature. It is clear that T_λ decreases sharply by 30^o with the addition of 2% As and then stays constant up to 20% As. Myers and Felty interpret T_λ in this system as being due to polymerization of the S_8 rings, only, ie, the aggregates of AsS_3 linkages are not expected to participate. An alternative interpretation seems more probable, however, namely that each As atom breaks up one to three rings and that above T_λ three chains will grow from each As atom. Thus the As will act as an initiator for the polymerization, replacing the reaction represented by equation 4.1 and explaining the lowering of T_λ .

It is not known whether compounds like As_2S_3 and As_2Se_3 possess a polymerization temperature since it would be much lower than Tg, but it seems reasonable to expect that polymeric sheets of AsS_3 or $AsSe_3$ units will have some average size which is dependent on temperature. Thus there should be an equilibrium degree of polymerization. The number of broken bonds, ie, holes, should

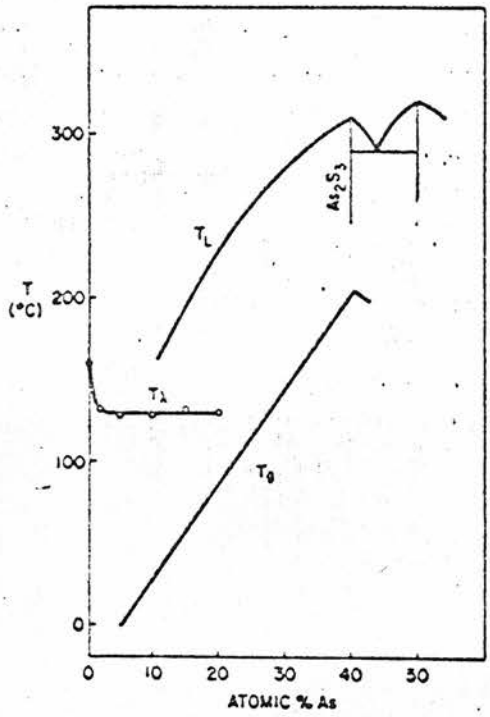

FIGURE 4.9
Liquidus temperature, polymerization temperature and the glass transition temperature in the As-S system (Ref 17).

FIGURE 4.1o
Isoviscosity curves for As-Se alloys (Ref 31).

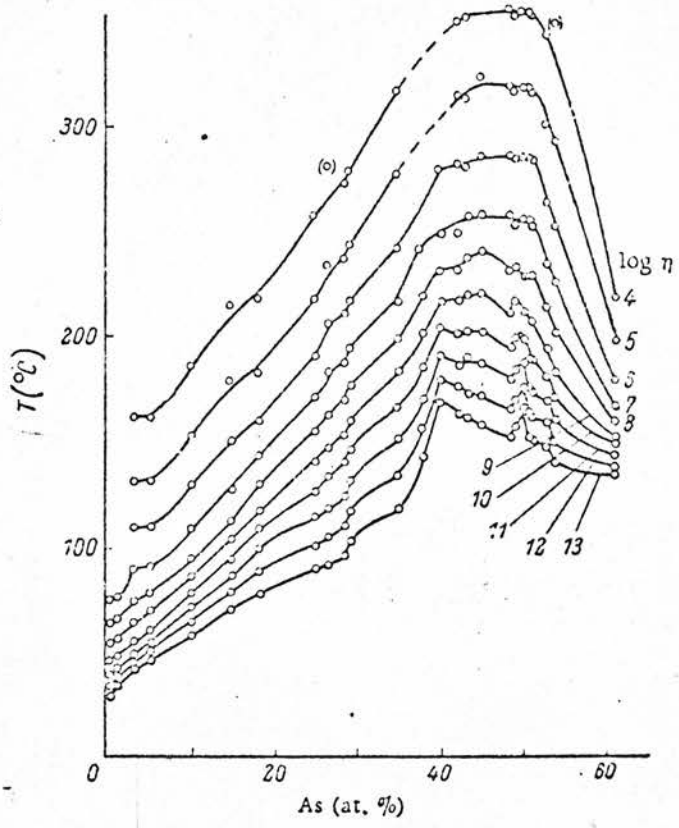

depend on the polymerization.

Eisenberg[29] has treated the case of polymerization of sulfur under pressure. T_λ decreases with pressure and is equal to the melting point of sulfur at ~850 Atm.

4.2.4 VISCOSITY AND THE GLASS TRANSITION

The viscosity at any given temperature depends on how easily molecules or segments of molecules can flow past each other. This in turn depends on their size, shape and flexibility, and on the strength of intermolecular bonding. The two extreme cases are materials like S, which below 160°C consists of S_8 rings held together by weak Van der Waals bonds, and tetrahedrally bonded materials in which no flow or re-arrangement is possible without breaking of bonds since they form a fully connected 3-dimensional network. The former materials are very fluid while the latter tend to retain their rigidity until the temperature is high enough to completely break down the tetrahedral covalent bonding and replace it with metallic and highly mobile bonding. Mobile or interchangeable bonding can also reduce the viscosity in polymeric materials[10]. Since viscosity, like the glass transition temperature, is a measure of structural relaxation, these quantities are closely related. It is indeed common to define Tg as the temperature at which the viscosity has some arbitrarily chosen value, usually $\eta = 10^{13}$ poise or $\eta = 10^{14.6}$ poise [30]. Although such a definition gives similar values for Tg to definitions in terms of the change in specific heat or expansivity, they should not be regarded as equivalent.

Considering that crystalline As_2Se_3 and As_4Se_4 consist of sheets and As_4Se_4 molecules respectively it might be expected that in glasses of similar compositions similar units could flow pasteach other without the breaking of covalent bonds. Figure 4.10 shows isoviscosity curves as a function of temperature and composition as measured by Nemilov and Petrovskii[31]. Nemilov[32] found that the activation energy for viscosity is considerably lower than the average chemical bond energy for selenium. In As_2Se_3 the two energies are similar. He interpreted this by assuming that bond breaking was necessary to achieve viscous flow in As_2Se_3 but not in Se. The activation energy and entropy of viscous flow were determined by Nemilov and Petrovskii[33] and are shown in Figure 4.11. There are clear signs of structure in these curves at 40% and 50% As (atomic), and the high viscosity at the latter composition rules out As_4S_4 molecules as a major constituent. Fischer and Krebs[34] measured viscosity in nine chalcogenide compositions, including four in the As-Se system. They concluded that these melts contained widely branched bonding system and that the concept of independent molecules was inappropriate. They also observed changes in bonding and coordination at high temperatures, from covalent to metallic bonding.

Myers and Felty[17] measured the glass transition and liquidus temperatures in the As-Se, As-S and As-S-Se systems. Some of their results are reproduced in Figures 4.9 and 4.12. The shape of the Tg vs composition curve (Figure 4.12) of As-Se is similar to that of the isoviscosity curves (Figure 4.10) as expected. The maximum is at ~43% As which indicates that the initial addition of As to stoichiometric As_2Se_3 increases the cross-linking. Myers and

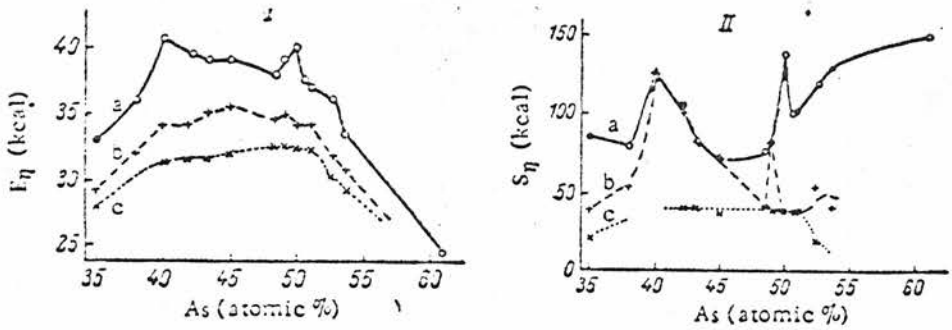

Values of E_η (kcal/mole) and S_η (kcal/mole ·deg) in the region of 35-61 atomic % As. Temperature, °C: a) 180; b) 230; c) 280. I) Values of E_η; II) values of S_η.

FIGURE 4.11 (Ref 33).

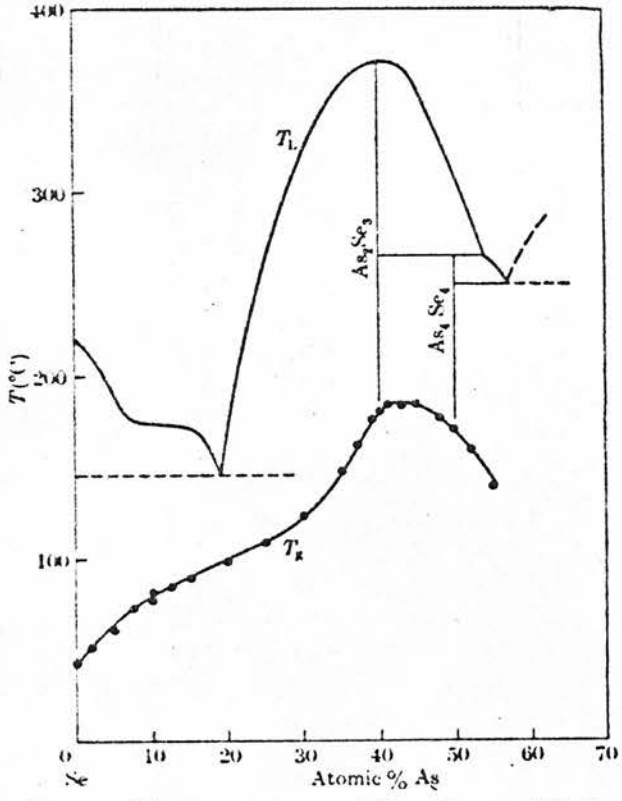

Glass transition temperatures and phase diagram of the Se–As system

FIGURE 4.12

(Ref 17).

Felty[17], following Nemilow and Petrovskii[31], explain the structure of the T_g curve for Se rich compositions in terms of mixtures of the polymer chains and monomer rings of pure Se and networks of $AsS_{3/2}$ linked rings or chain molecules. T_g varies less with composition between 10 and 30% because two polymer structures are being modified. The As-S system is different because there are no sulfur chains; only S_8 rings and $AsS_{3/2}$ network.

Bagley et al[35] found that the annealing of As-Se glasses with 8-10% As, just below T_g, caused an increase of about 30^o in T_g. Moreover, they did not detect any evidence of the double glass transition which would be expected in a phase-separated medium with two glassy phases. These results can be interpreted therefore as a change in the state of polymerization by annealing, which in turn changes the rigidity of the material and therefore T_g. The endotherm in the DTA curves which coincided with the annealing temperature adds further support to this view. The process is shown schematically in Figure 4.13. These results clearly show that when T_g and T_λ are close the former will depend drastically on the measurement technique and on the thermal history of the sample. It is indeed conceivable that a material could have two different T_g's, one on either side of T_λ , but it would be difficult to achieve the depolymerization necessary to observe the lower T_g.

Liang[20] has determined T_g in the As_2Se_3-Cu system. His results are shown in Figure 4.14. He used a rather high heating rate, 20^oC/min, thus T_g for As_2Se_3 is ~10^oC higher than observed by Myers and Felty. Liang does not explain the drop in T_g with the addition of small amounts of Cu. He considers the increase

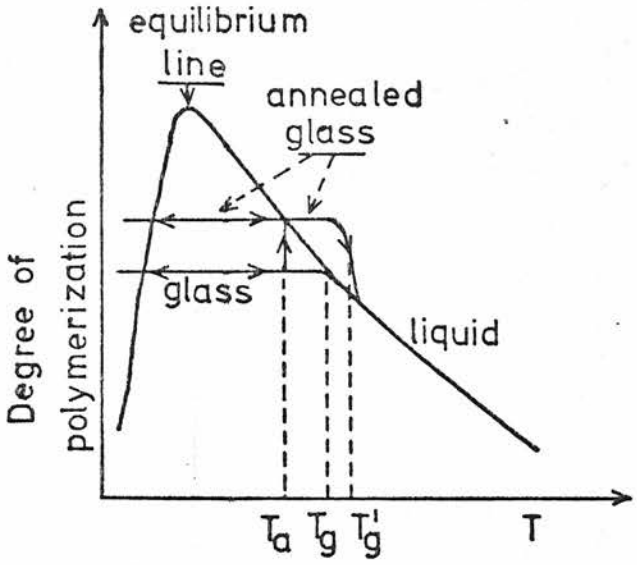

FIGURE 4.13

Explanation of the results of Bagley et al[35] . Annealing just below T_g allows the glass to relax to the equilibrium state of polymerization at the annealingtemperature T_a . This in turn increases the measured value of T_g to T'_g.

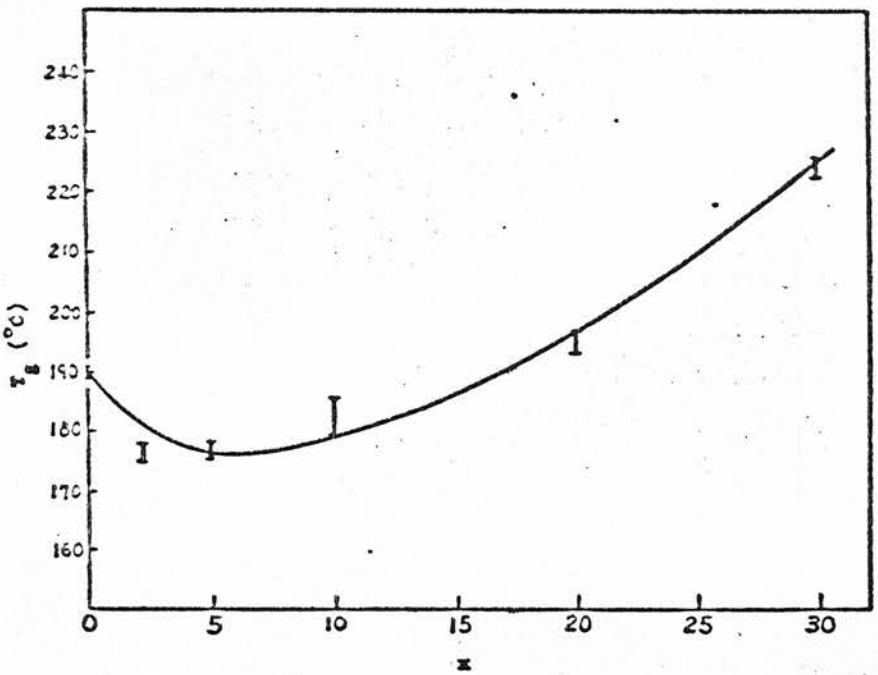

FIGURE 4.14

Plot of glass transition temperature vs atomic % Cu in a-$(As_{.4}Se_{.6})_{100-x}Cu_x$, (Ref 20).

in T_g at higher concentration to be due to the formation of a tetrahedral network based on $CuAsSe_2$ but it is difficult to see how T_g can actually be larger in As_2Se_3 doped with 20-30% Cu (atomic) than in a-$CuAsSe_2$ (T_g = 193°C). The low T_g at 2-10% Cu cannot be explained by the Cu taking out more Se than As atoms from the As_2Se_3 matrix because even with 10% Cu the remaining As:Se ratio is 43:57.

De Neufville and Rockstad[36] have discovered a correlation between T_g and the optical gap (defined by $\alpha \equiv 10^4$ cm^{-1}) of many amorphous compounds. This is illustrated in Figure 4.15. The results fall into groups according to the connectivity of the compounds, defined as $C = 8 - \bar{N}$ where $\bar{N}$ is the average coordination number. For two dimensional Se-Te compounds T_g is approximately independent of E_g. De Neufville and Rockstad interpret these results in terms of viscosity and the number and strength of bonds that must be broken to achieve viscous flow. They propose the following equation, derived from the Fulcher equation :

$$\phi = \phi_o \exp\left[\frac{-\delta(C - 2)E_g}{k(T - T_o)}\right] \qquad 4.8$$

where ϕ = fluidity, $\phi_o = 10^2$ $poise^{-1}$, $\phi(T_g) = 10^{-12}$ $poise^{-1}$, $\delta \doteq 0.5$ and T_o is the zero-gap extrapolation of the T_g vs E_g plot (Figure 4.15). Although the above results only refer to compounds it is interesting to consider whether equation 4.8 can be extended to intermediate compositions such as the As-Se system. It is easily shown that for As_xSe_{1-x}

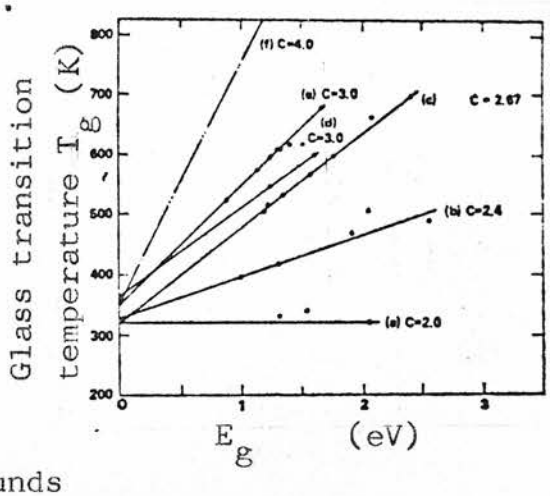

FIGURE 4.15

T_g vs the optical gap defined as the photon energy at which $\alpha = 10^4\ cm^{-1}$.
C is the connectivity.
All experimental points refer to amorphous compounds (Ref 36).

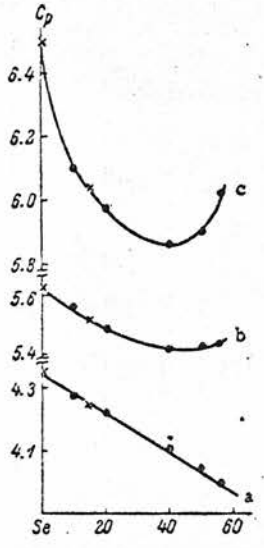

FIGURE 4.16

The specific heat of As-Se glasses as a function of composition,
(a) 1ooK
(b) 2ooK
(c) 3ooK
(Ref 43).

$$C - 2 = x \qquad 4.9$$

Combining this with equation 4.8 and taking logarithms gives

$$T_g = T_o + \frac{\delta . x\ E_g}{32.2\ k} \qquad 4.10$$

This equation will be compared to experimental results in Chapter 7.

4.2.5 HEAT CAPACITY

The specific heat of glassy and crystalline Se, As_2Se_3 and As_2S_3 has been measured by Tarasov and others[37,38,39] in the range 53 - 300 K. The results for crystals and glasses are remarkably similar although there are signs that C_p decreases more rapidly in the crystals below 100 K. Tarasov et al fitted linear chain functions to their data and obtained a characteristic cut-off temperature (θ_1) which they correlated with peaks in the IR spectra. They found θ_1 = 360, 410, 565 K for a-Se, As_2Se_3 and As_2S_3 respectively.

Chang and Bestul[40] measured C_p for both trigonal and glassy Se from 5 - 360 K and also found little difference between the two forms above 50 K. They found a nearly constant difference between 10 K and 40 K of 1 - 2 J/K-mole. At T_g the specific heat of the glass increases by a factor of 1.6. The same factor was found for a-As_2Se_3 and As_2S_3 [41,42]. The specific heat reaches the classical Dulong-Petit limit of 3k/atom below T_g in all cases[42]. The results of Zigel and Orlova[43] for C_p as a function of composition in the As-Se system at three different temperatures are reproduced in Figure 4.16.

The minimum for 40% As at 300 K indicates that the frequency of the optical modes is highest for that composition. The linear increase with Se concentration at 100 K is the result of an increasingly chain-like nature of the glasses, making more low-frequency acoustic modes available.

The ratio C_p/C_v is generally $\doteq 1.01$ according to the above authors[38, 42]. It is well known that below about 10 K many amorphous solids possess a specific heat C_v that is linear with temperature. Anderson et al[44] proposed an explanation in terms of tunneling of atoms or groups of atoms between pairs of local minima in energy vs a generalized coordinate curve.

4.2.6 DENSITY

Figure 4.17 shows the density ρ as a function of composition in the As-Se system[45] for 0 - 60% As. ρ rises linearly from 0 - 42% As has a maximum at 42% As and a *minimum* at 57.5% As. Other measurements give similar results[46]. It should be noted, however, that the density depends on thermal history. Thus Leadbetter and Apling[23] found that a sample of $As_{34}Se_{66}$ which was cooled from 800°C to room temperature in 20 hours had $\rho = 4.608$ g/cm^3 whereas for an $As_{37.5}Se_{62.5}$ sample air-quenched from 850°C to 150°C, held for 12 hours, then cooled to room temperature in 5 hours, $\rho = 4.582$ g/cm^3. If the straight line in Figure 4.17 for 0 - 42% As is extrapolated to pure As one obtains $\rho = 5.10$ g/cm^3, which is practically the same as in δ-As, one of the three different forms of a-As [15].

Figure 4.18 [20] illustrates how ρ increases linearly with atomic content of Cu in the As_2Se_3-Cu system. In the systems

FIGURE 4.17

Density vs composition in the As-Se system (Ref 45).

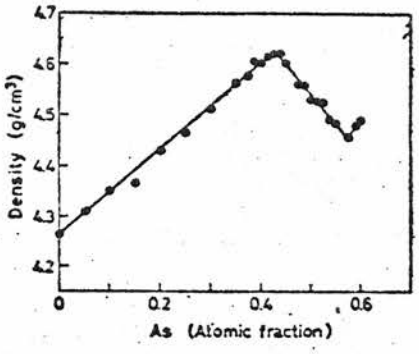

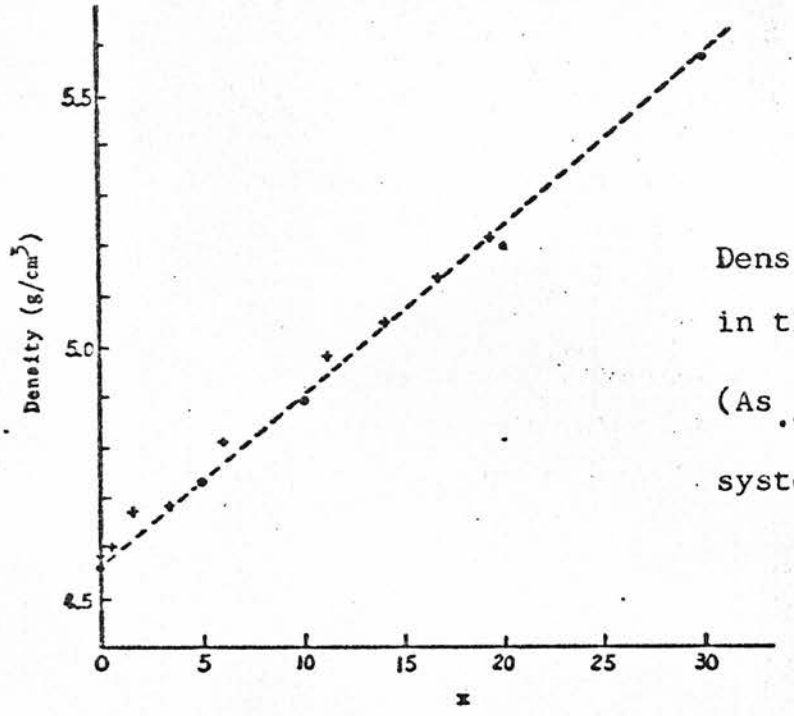

FIGURE 4.18

Density vs composition in the $(As_{.4}Se_{.6})_{100-x}Cu_x$ system (Ref 20).

FIGURE 4.19

Compressibility (adiabatic) vs composition in the As-Se system (Ref 46,73).

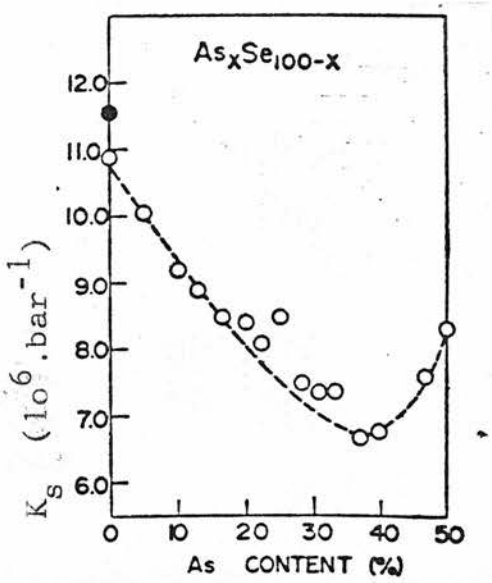

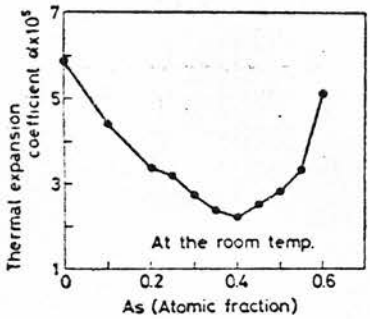

Thermal expansion coefficient of As-Se glasses.

FIGURE 4.2o

Thermal expansion coefficient vs composition in As-Se glasses (Ref 45).

$(As_2Se_3)_{(1-x)}(CuAsSe_2)_x$ and $(As_2Se_3)_{(1-x)}(CuSe_2)_x$ the density increases *sublinearly* with x [47]. The density of $CuAsSe_2$ is very similar in the crystalline and amorphous forms, $\rho \triangleq 5.28$ g/cm^3 [20].

4.2.7 COMPRESSIBILITY AND THERMAL EXPANSION

The compressibility in the As-Se system shows a distinct minimum near $As_{40}Se_{60}$ as shown in Figure 4.19. The points were calculated from the ultrasonic data of Chernov et al[46] and therefore give the adiabatic compressibility. The results for a-Se and a-As_2Se_3 agree very closely to those reported by Soga et al[48] who also found that the relation

$$K_s \cdot \rho^4 = \text{constant} \qquad 4.11$$

holds for crystalline As and Se and glassy Se and As_2Se_3. K_s is the adiabatic compressibility. Thus equation 4.11 relates compressibility and density as a function of composition and the glass-crystal transition.

The thermal expansion[45] of glasses in the As-Se system is shown in Figure 4.20 and again there is a minimum at 40% As. At this composition there is also a maximum in the microhardness[49] but the thermal conductivity shows a broad maximum between 20 and 40% As.

In the As-S system there is a sharp minimum in the expansion coefficient[50] and a maximum in the thermal conductivity[51] at 40% As (atomic).

4.3 ELECTRICAL PROPERTIES

4.3.1 DRIFT MOBILITY

Numerous accounts have been published on the trap-limited drift mobilities of carriers in a-Se[52,53,54,55] and in a-As_2Se_3 [54,56,57]. Some information is also available on nonstoichiometric compositions. Schottmiller et al[53] and Marshall et al[58] have, for example, measured the effect of additions of 0 - 9% As on the electron and hole mobilities. Fisher et al[59] have investigated μ_h for glasses in the range 30 - 50% As. Both electron and hole mobilities are normally thermally activated and depend strongly on electric field and composition. The magnitude of the pre-exponential terms is most simply explained in terms of trap-limited drift mobilities with traps at discrete levels or possibly in a tail of localized states, and conduction in extended states (see equations 3.3 and 3.4). Three other models have been proposed which are based on measurements of electrical properties of As_2Te_3 and As_2Te_3+Si, other than drift mobilities. Nagels et al[60] explained their observation of slightly temperature dependent activation energies of conductivity and thermoelectric power in As-Te-Si glasses by assuming significant contributions from both extended state conduction and thermally activated hopping in the valence band tail, the latter term giving an activation energy ~0.1 eV smaller than the former. Another model due to Grant and Davis[61] and others[62,63] proposes thermally activated hopping in a linear valence band tail as the dominant conduction mechanism. They also find a simple relation between E_σ and the activation energies of the photoconductivity in the monomolecular and bi-molecular regimes. This is however contradicted by the photo-

conductivity measurements of Main[64]. Seager et al[65] proposed a model involving polaron hopping conduction. From this model, Seager and Quinn[66] deduced values for the mobility activation energies in a-As_2Te_3 and a-As_2Se_3 which are lower than observed by photomobility measurements[64,67] and transit time measurements[54,56]. Marshall and Owen[67] compared photomobility and dark conductivity in a-As_2Te_3 and STAG glass and interpreted their results in terms of conduction in extended states above ~200 K with traps 0.22 eV below the Fermi level which limit the mobility. At lower temperatures the dominant conduction mechanism is hopping in a discrete set of localized states 0.13 eV below E_F. This model appears to be consistent with all available experimental results.

There appear to be three different sets of hole traps in the As-Se system, the dominant level depending on composition and the time scale of the measurement. The traps are thought to be associated with some structural features, such as As branch points, whose density depends on composition and the mobility is limited only by those traps with which the carriers can come into thermal equilibrium in a time less than the transit time $T_r = d/\mu_d \mathcal{E}$, where d = sample thickness and $\mathcal{E}$ = electric field. When the average number of trap-release events per carrier is ~1 a transit time is not well defined[56]. By using samples of different thicknesses and hence varying the transit time, it is sometimes possible to investigate different trap levels.

The hole mobility in pure Se is ~0.2 cm^2/volt-sec at room temperature[53,55] with a well-defined activation energy of 0.28 eV below 250 K, but tending to saturate at higher temperatures to a

value ~0.3 cm^2/volt-sec [55]. The latter value is associated with the *free* hole mobility[55].

The addition of As introduces deeper traps and it has not been possible to measure μ_h (the hole drift mobility) in the range 0.5 - 30% As. Up to 0.5% As μ_h is unchanged, but the hole lifetime is drastically reduced. Above 4% As the hole response is composed of a fast part characteristic of a-Se and a slow 'tail' characteristic of As_2Se_3 [53]. For thin samples of a-As_2Se_3 a zero-field mobility of ~10^{-5} cm^2/volt-sec is implied [56,58] with an activation energy 0.43 eV. In thicker samples $\mu_d \sim 10^{-6}$ cm^2/volt-sec at room temperature with activation energy $\triangleq$ 0.63 eV [59]. Similar results have been obtained from photomobility and noise measurements by Main[64] who identified levels at 0.44 eV and 0.65 eV. Kolomiets et al[69] resolved both these levels and another at 0.30 eV by depolarization measurements. Measurements on crystalline As_2Se_3 [70] have been interpreted in terms of traps at 0.49, 0.58 and 0.72 eV which, when scaled with the reduction in the optical gap, correspond roughly to those in a-As_2Se_3. Figure 4.21 shows the results of Fisher et al[59] on mobility and conductivity in glasses with 30 - 50% As. Both μ_d and the activation energy E_μ show a maximum near the stoichiometric composition. This indicates that the trap density has a sharp minimum at that composition. Fisher et al[59] estimate a trap density ~10^{16} cm^{-3} for As_2Se_3 at an energy 0.63 eV above the valence band mobility edge, increasing to ~10^{18} cm^{-3} in $As_{35}Se_{65}$ and $As_{50}Se_{50}$. The increase must occur nearer to the band edge to explain the maximum in E_μ. The electron drift mobility in a-Se is ~10^{-2} cm^2/volt-sec with an activation energy of 0.33 eV [53]. The addition of As causes a linear increase in the activation energy

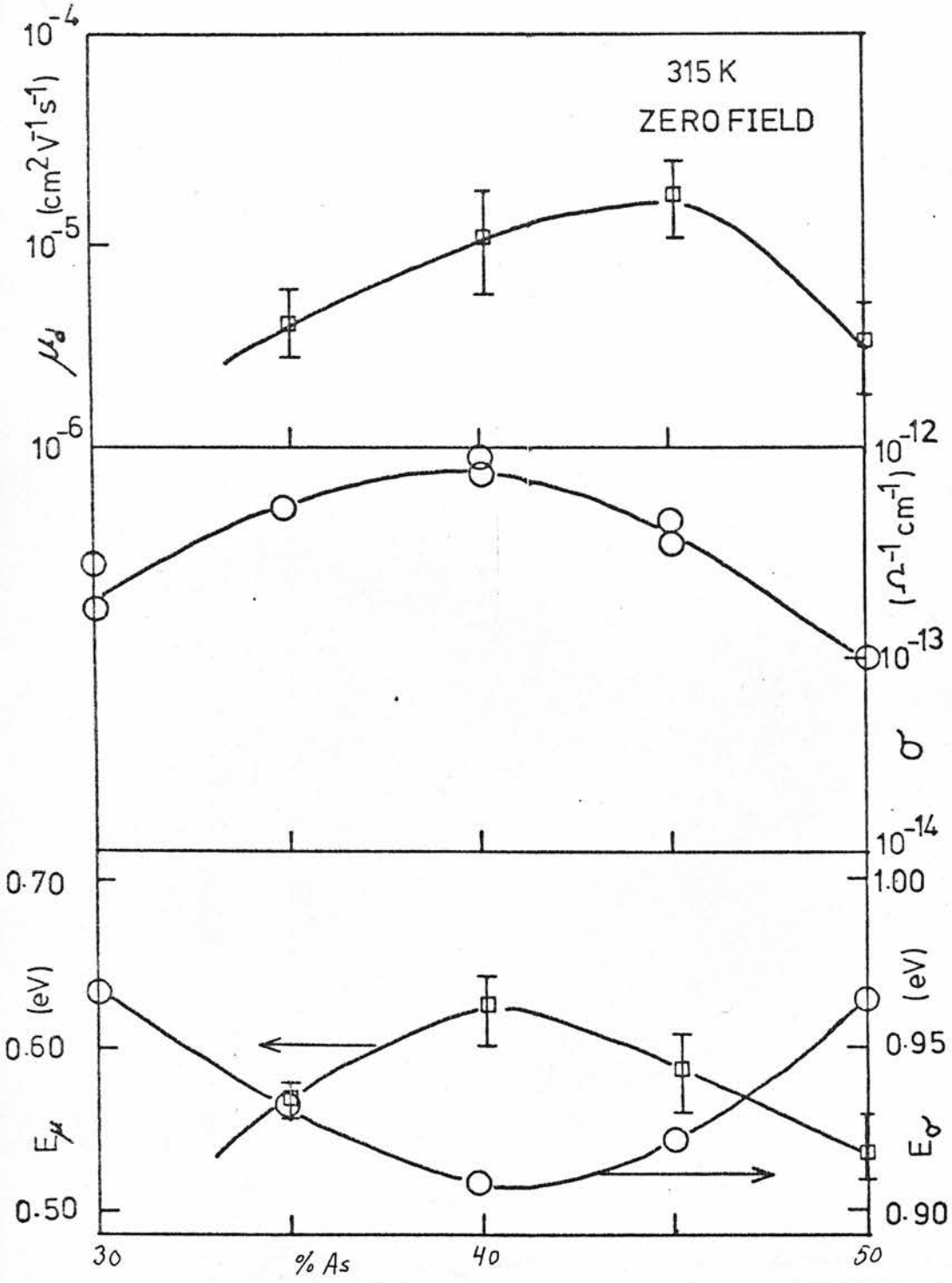

FIGURE 4.21

Compositional dependence of conductivity, mobility and their activation energies in As-Se glasses (Ref 59).

to 0.44 eV in As_8Se_{92}. The pre-exponential term is constant within a factor of 2 [58].

Marshall et al[58] suggest that disorder due to the As atoms causes the conduction band mobility edge E_c to move higher into the band, thus increasing E_μ. The trap density is supposed to remain nearly constant and conduction is expected to take place in the extended states at E_c. This model is consistent with any of the three cases considered in Figure 2.8, provided the trap level is below E_A. The density of states at which E_c occurs (ie, N_c' in the notation of Chapter 2) can be expected either to be constant or increase slightly with composition. Therefore $\frac{N_c'}{\Delta E_c}$ should decrease with composition and so should C_2 in the Davis and Mott interpretation, assuming other factors remain constant. Taking $\Delta E_c \doteq 0.1$ eV in a-Se requires $\Delta E_c \geqslant 0.2$ eV in As_8Se_{92}.

4.3.2 DARK CONDUCTIVITY

The dark conductivity shows a maximum for As-Se glasses 2 - 3% on the selenium rich side of stoichiometry[59,71-75]. This is associated with a minimum in the activation energy but its effect is somewhat reduced by a minimum in the pre-exponential term. Collected results showing the behaviour of these parameters are given in Figures 4.22 and 4.23. Both parameters differ between different authors but it may be concluded that the minimum in E_σ is very broad and occurs either at the stoichiometric composition or slightly on the As rich side. The minimum of the pre-exponential term is in the range 40 - 45% As. The asymmetry in the pre-exponential term, agreed by all the authors, is probably the main cause of the position of the conductivity maximum being on

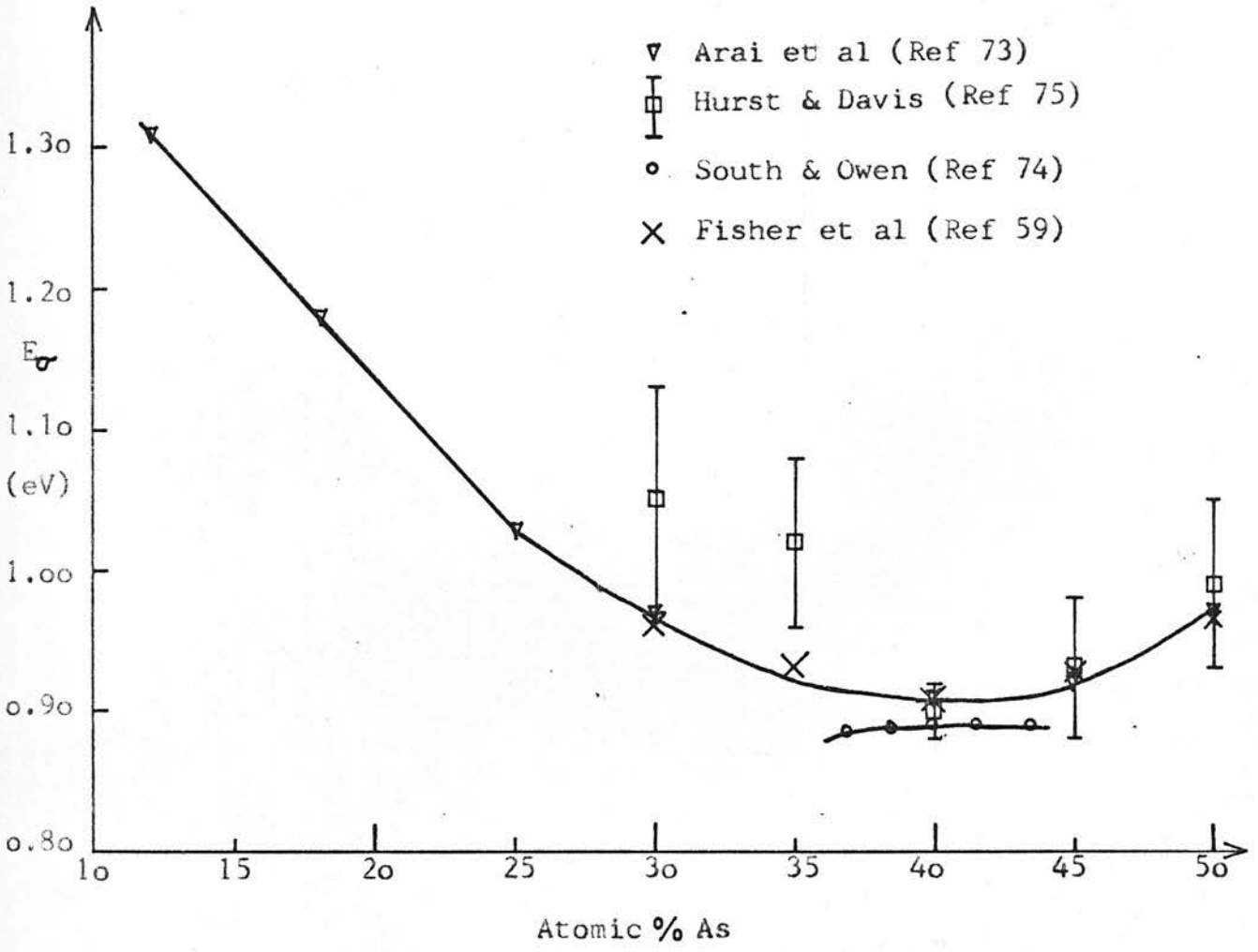

FIGURE 4.22

E_σ vs composition in the As-Se system.

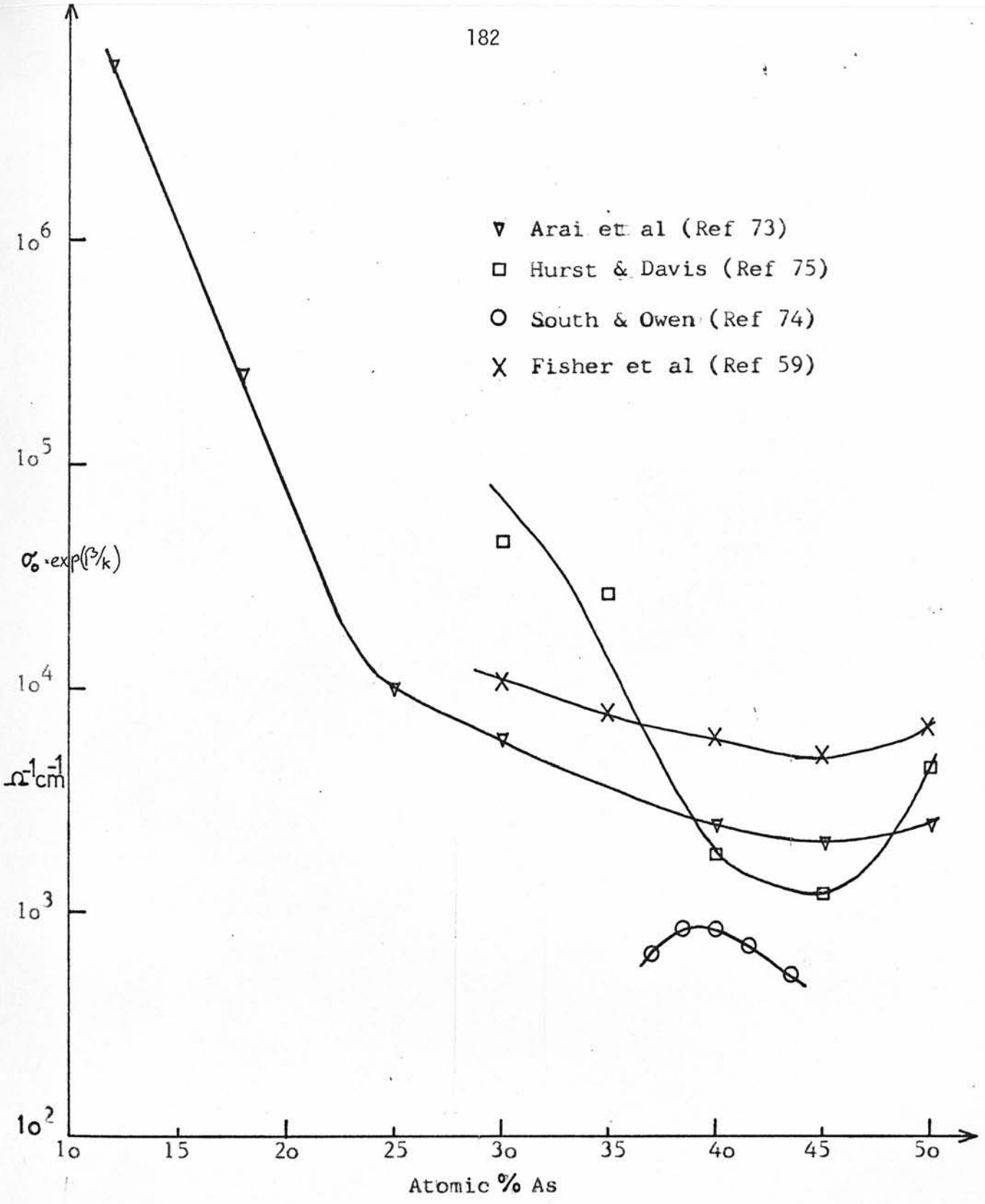

FIGURE 4.23

The conductivity pre-exponential σ_0 as a function of composition in As-Se glasses.

the Se-rich side. It has been suggested [72.76] that E_σ and the pre-exponential σ_0 in As-Se and As-S glasses are related by an empirical equation (the so-called compensation rule) of the form

$$E_\sigma = a \ln \sigma_0 + b \qquad 4.12$$

where a and b are constants independent of composition. This would imply that the conductivity can be written as

$$\sigma = \text{constant} \cdot \exp\left[E_\sigma \left(\frac{1}{a} - \frac{1}{kT}\right)\right] \qquad 4.13$$

and that plots of $\log \sigma$ vs $1/T$ for different compositions would cross at $T = a/k$. Furthermore, the extrema in σ and σ_0 would coincide with that in E_σ contrary to the conclusion reached earlier that the extrema in σ and σ_0 are on opposite sides of stoichiometry. Thus equation 4.12 cannot be an exact description for As-Se glasses in the range near As_2Se_3. To account for the minimum in E_σ near the stoichiometric composition, as well as corresponding minima in optical absorption (which was discussed in Chapter 2) and thermopower, Hurst and Davis[75] argue that because the As-Se, As-As and Se-Se bond strengths are very similar the predominant effect in the As-Se system is that of disorder. They suppose As_2Se_3 to be the most ordered composition and that deviations from stoichiometry increase disorder and shift the mobility edges further into the bands, thereby increasing $E_\sigma = E_F - E_V$ and the band gap.

If any changes in the densities of states well into the bands are ignored, reference to Figure 2.8 and Table 2.3 indicates that :

Figure 2.8(a) - $C_2 \propto \Delta E_v$ and E_{02} should increase by the same amount as E_σ.

Figure 2.8(b) - This case is not consistent with the Hurst and Davis model since E_{02} would decrease and E_σ remain unchanged with deviations from stoichiometry.

Figure 2.8(c) - This is a more complicated case but a careful comparison of changes in E_σ , E_{02} and C_2 should reveal whether the results are compatible with the Hurst and Davis model and Figure 2.8(c).

4.3.3 THE EFFECT OF ELECTRICAL FIELD

It has been shown[55,58,77] that both the dark conductivity and the drift mobilities of amorphous chalcogenides increase exponentially with the applied field. Many earlier reports assumed a field dependence of the Poole-Frenkel type, ie

$$\ln \sigma(\mathcal{E}) = \ln \sigma(0) + \beta \mathcal{E}^{1/2}/kT \qquad 4.14$$

but neither the experimentally determined value of β nor the low field behaviour agreed with theory. The currently accepted empirical form is

$$\sigma(\mathcal{E}) = \sigma(0) \exp [a(T) e \mathcal{E}/kT] \qquad 4.15$$

where e is the electronic charge and a(T) is a temperature dependent parameter which has the dimension of length. Grant and Davis[61]

express the temperature dependence of a(T) by writing $a(T) = L(1-T/T_o)$ where L is related to the effective hopping length in their model. Usually a is 5 - 50 Å and decreases with increasing temperature. The drift mobility obeys a similar equation. Moreover, the parameter a(T) as determined by conductivity or drift mobility measurements is approximately the same. This indicates that the carrier density is not field dependent. Marshall and Miller[68] have considered in detail the possible mechanisms causing the field dependence. They suggest that the field dependence may be due to a field modification of parameters controlling carrier motion in the region of the mobility edges. It is also of interest that a(T) is identical within experimental limits for the electron and hole drift mobilities in a-Se. Figure 4.24 illustrates the compositional behaviour of a(T) at 280 K in the As-Se system as determined from drift mobility and conductivity measurements[59].

Photoconductivity appears to show similar field dependence but with values for a(T) lower than from the dark conductivity, and intensity dependent.

4.3.4 PREPARATION AND CHANGES IN STRUCTURE

Arai et al[78] investigated the effects of densification on optical and electrical properties in four glasses including $As_{25}Se_{75}$ and $As_{40}Se_{60}$. They found a decrease in the optical gap and E_σ which corresponded to the pressure coefficients of these quantities which will, therefore, depend on preparation as a result of variations in density. The state of polymerization, ie, the average chain length and ring concentration etc depends on preparation and may be

expected to affect electrical properties by, for example, altering trap densities. Marshall and Owen[55] observed some differences in the hole drift mobility in vitreous and evaporated Se. Ast[79] surveyed the literature and found reported conductivities and activation energies varied wildly for unannealed evaporated a-As_2Se_3; in some cases E_σ ~ 0.4 eV, less than half the value for bulk samples.

4.3.5 GLASSES CONTAINING Cu

It has been known for a number of years that 1% or less (atomic) of Cu or Ag in chalcogenides drastically affects the electrical properties of those glasses[80,81] (See Figure 4.24). How these metals combine with the chalcogenide glass matrix is not clear. The possibility of complexes based on compounds like $CuSe_2$ and $CuAsSe_2$ being formed was discussed earlier in connection with structural studies. Nielsen[82] found evidence for Ag_2Se, Cu_2Se and CuSe compounds in photoemission experiments and Kawamoto et al[83] suggested that the compound Ag_2S exists in glasses containing As or Ge. They also showed that there is a transition from electronic to ionic conduction with increasing Ag content. In the As_2S_3-Ag_2S system this occurs at ~6% Ag (atomic) but at less than 1% Ag in the GeS_2-$2GeS$-Ag_2S system. Kawamoto et al[83] found that the ion involved is Ag^+. This agrees with work on the diffusion of Ag in a-As_2Se_3 with and without an electric field[84.85]. In the absence of a field

$$D_{Ag} = 3\ cm^2/sec \times \exp[\ -0.89\ eV/kT\ ] \qquad 4.16$$

where D_{Ag} is the diffusion coefficient of Ag in As_2Se_3 [84]. Comparison of this result with the Nernst-Einstein equation and the measured

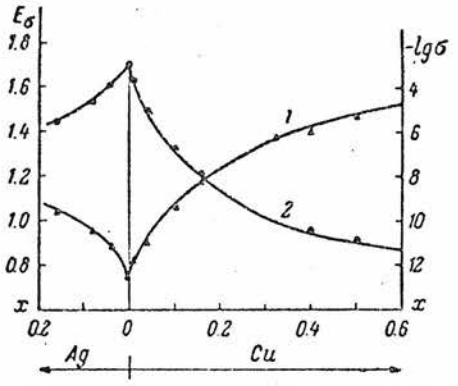

Dependence of the electrical conductivity and its activation energy on the composition of $M_xAsSe_{1.5}$ glasses. 1) Electrical conductivity σ ($\Omega^{-1} \cdot cm^{-1}$); 2) activation energy, determined from measurements of σ, E_σ (eV). The numbers along the abscissa give the value of x in $M_xAsSe_{1.5}$.

FIGURE 4.24

Log conductivity and E_σ in As_2Se_3 doped with varying amounts of Cu and Ag (Ref 80).

mobility shows that the ionic charge is equal to e during the jumps[85]. The activation energy of the ionic mobility is ~0.8 eV or slightly less than for D_{Ag}, but Lebedev et al[85] argue that this is due to non-uniform field distribution. In Table 4.1 these results are compared to those of Arai et al[73] who measured the d.c. conductivity in $As_{40}Se_{60}Ag_1$ glass.

T	μ_{ion} (Ag^+)	σ = Ne μ_{ion}*	σ; Arai et al[73]
180° C	1.1×10^{-8} cm^2/V-sec	6.4×10^{-7} Ω^{-1} cm^{-1}	2×10^{-7} Ω^{-1} cm^{-1}
120°C	5.2×10^{-10} cm^2/V-sec	3.0×10^{-8} Ω^{-1} cm^{-1}	9×10^{-9} Ω^{-1} cm^{-1}

* $N = 3.6 \times 10^{20}$ cm^{-3} for 1% Ag

TABLE 4.1

The comparison indicates that As_2Se_3 + 1% Ag is indeed an ionic conductor, the difference by a factor of 3 between the two columns for conductivity in Table 4.1 is no more than expected when comparing results from different authors. The measurements by Arai et al[73] of the influence of pressure on the conductivity reveal an initial reduction in σ in Ag-doped glasses as pressure is applied, followed by a rise at higher pressures. The pressure at which the minimum in σ occurs decreases with increasing temperature. Undoped As_2Se_3 shows a steady increase in σ with applied pressure, which is characteristic of pure electronic conduction. Pressure is expected to reduce ionic conduction. Thus the doped glasses show the characteristics of both types of conduction although in the temperature range measured

the conductivity has a single activation energy. Furthermore, the doped glasses also show a dielectric relaxation at low frequencies, that scales with the d.c. conductivity according to the equation

$$\sigma = \varepsilon_o \, \Delta\varepsilon 2\pi\nu_m \qquad 4.17$$

where ε_o is dielectric constant for vacuum, $\Delta\varepsilon$ is the contribution of the loss mechanism to the dielectric constant and ν_m the frequency of the maximum in the loss peak. Apart from the failure to observe a change in the activation energy there is thus strong evidence in favour of the conclusion that $As_{40}Se_{60}Ag_1$ is an ionic conductor.

Kolomiets et al[86] found that addition of $\leqslant$0.2% atomic of Ag or Cu to a-As_2Se_3 actually caused a slight *decrease* in σ and *increase* in E_σ, exactly opposite to the effect of higher concentrations. Similar changes were observed for the photoconductivity spectra. This may well be related to the behaviour of T_g [20]. Amrhein et al[87] investigated mechanical damping in $Si_{35}As_{25-x}Ag_xTe_{40-y}Se_y$ glasses and found a peak whose magnitude was approximately proportional to the Ag content. This peak shifted to lower temperatures and split into two overlapping peaks with increasing Se content. They also observed a shoulder in the damping constant vs temperature plot for Ag-containing glasses at ~0.7 T_g which they postulated was due to relaxation of chain segments formed when Ag is present.

4.3.6 PHOTODOPING

When a binary layer of Ag or Cu metal and a chalcogenide glass is exposed to bandgap illumination the metal diffuses rapidly into the glass until the metallic layer is completely used up. This phenomenon has been investigated in detail by Inoue et al[88]. They found that the photodoping rate is proportional to light intensity and is thermally activated with the activation energy equal to 0.033 eV for the Ag-$As_2S_{9.6}$ system. The conductivity and optical absorption increase drastically as a result of the photodoping; E_σ, E_{02} and C_2 are all reduced (see Table 2.2).

The density of photodoped metal was uniform from the surface layer to the doping front and the doping depth extended beyond the absorption depth. The metal does not migrate laterally, ie, perpendicular to the light beam and in the case of Ag at least, the photodoping stops as soon as the surface layer of Ag is exhausted. This last observation is a clear indication of the formation of some compound, such as Ag_2S.

Salik[89] has suggested a simple model in which electrons from the metal layer'spill over' into the glass, where they recombine with photogenerated holes, leaving behind Ag^+ or Cu^+ ions and setting up a photo-e.m.f. which acts on the ions.

4.4 REFERENCES

1. Kastner, M, Phys Rev Lett 28, p 355, 1972.
2. Stuke, J, J Non-Cryst Sol 4, p 1, 1970.
3. Chen, I, Phys Rev B 7, p 3672 and 8, p 1440, 1973.
4. Nielsen, P, Phys Rev B 6, p 3739, 1972.
5. Dresner, J and Stringfellow, G B, J Phys Chem Sol 29, p 303, 1968.
6. De Neufville, J P et al, J Non-Cryst Sol 13, p 191, 1973.
7. Asahara, Y and Izumitani, T, J Non-Cryst Sol 16, p 407, 1974.
8. Grigorovici, R, 'Amorphous and Liquid Semiconductors' (J Tauc, editor), Plenum Press, London and New York, 1974, p 53.
9. Krebs, H, J Non-Cryst Sol 1, p 455, 1969.
10. Eisenberg, A and Teter, L A, J Phys Chem 71, p 2332, 1967.
11. Grigorovici, R, see Ref 8, p 52.
12. Wyckoff, R W G, Crystal Structures, 2nd ed, Wiley, New York, 1964.
13. Eisenberg, A and Tobolsky, A V, J Polym Sci 46, p 19, 1960.
14. Smith, P M et al, Phil Mag 31, p 57, 1975.
15. Greaves, G N and Davis, E A, Phil Mag 29, p 1201, 1974.
16. Street, R A et al, J Phys C 7, p 4185, 1974.
17. Myers, M B and Felty, E J, Mat Res Bull 2, p 535, 1967.
18. Renninger, A L and Averbach, B L, Phys Rev B 8, p 1507, 1973.
19. Khvorostenko, A S et al, Neorg Mater 8, p 73, 1970.
20. Liang, K, PhD Thesis, Stanford University, 1973.
21. Renninger, A L et al, J Non-Cryst Sol 16, p 1, 1974.
22. Apling, A J, 'Electronic and Structural Properties of Amorphous Semiconductors', (P G Le Comber and J Mort, editors), Academic Press, London and New York, 1973, p 243.
23. Leadbetter, A J and Apling, A J, J Non-Cryst Sol 15, p 250, 1974.
24. Schottmiller, J et al, J Non-Cryst Sol 4, p 80, 1970.
25. Tobolsky, A V and Eisenberg, A, J Am Chem Soc 81, p 780, 1959.

26. Tobolsky, A V and Eisenberg, A, J Coll Sci 17, p 49, 1962.

27. Cornet, J and Rossier, D, 'Proc on the 5th International Conference on Amorphous and Liquid Semiconductors', Garmisch-Partenkirchen, Germany (J Stuke and W Brenig, editors), Taylor and Francis, London 1974, p 267.

28. Tobolsky, A V and Owen, G D T, J Polym Sci 59, p 329, 1962.

29. Eisenberg, A, J Chem Phys 39, p 1852, 1963.

30. Bagley, B G, 'Amorphous and Liquid Semiconductors', (J Tauc, editor), Plenum Press, London and New York, 1974, p 8.

31. Nemilov, S V and Petrovskii, G T, J Appl Chem USSR 36, p 932, 1963.

32. Nemilov, S V, Soviet Phys Sol State 6, p 1075, 1964.

33. Nemilov, S V and Petrovskii, G T, J Appl Chem USSR, 36, p 1855, 1963.

34. Fischer, M and Krebs, H, Glastechn Ber 47, p 42, 1974.

35. Bagley, B G et al, ' Proc on the 5th International Conference on Amorphous and Liquid Semiconductors' Garmisch-Partenkirchen, Germany, (J Stuke, and W Brenig, Editors), Taylor and Francis, London 1974, p 1169.

36. DeNeufville, J P and Rockstad, H K, Ibid, p 419.

37. Tarasov, V V et al, Russ J Phys Chem 43, p 249, 1969.

38. Tarasov, V V and Zhdanov, V M, Russ J Phys Chem 44, p 1349, 1970.

39. Vinogradova, V Z, and Dembovsky, S A, Neorg Mater 1, p 1838, 1965.

40. Chang, S S and Bestul, A B, J Chem Thermodynamics 6, p 325, 1974.

41. Thornburg, D D and Johnson, R I, J Non-cryst Sol 17, p 2, 1975.

42. Shnaus, U E et al, Phys Chem Glasses 11, p 231, 1970.

43. Ziegel, V V and Orlova, G M, Zh Prikl Khim 46, p 721, 1973.

44. Anderson , P W et al, Phil Mag 25, p 1, 1972.

45. Kunugi, M et al, Zairyo 18, p 807, 1969.

46. Chernov, A P et al, Neorg Mater 4, p 1658, 1968.

47. Alimbarashvili, N A and Baidakov, L A, Neorg Mater 9, p 2108, 1973.

48. Soga N et al, J Phys Chem Sol 34, p 2143, 1973.

49. Rozov, I A et al, Soviet Phys Semic 1, p 969, 1968.

50. Kawamoto, Y and Tsuchihashi, S, Yogyo Kyokai Shi, 78, p 173, 1970.

51. Hattori, M et al, Kogyo Kagaku Zasshi 69, p 1737, 1966.

52. Dolezalek, F K and Spear, W E, J Non-Cryst Sol 4, p 97, 1970.

53. Schottmiller, J et al, J Non-Cryst Sol 4, p 80, 1970.

54. Marshall, J M et al, J Non-Cryst Sol 8-10, p 760, 1972.

55. Marshall, J M and Owen, A E, Phys Stat Sol (a) 12, p 181, 1972.

56. Marshall, J M and Owen, A E, Phil Mag, 24, p 1281, 1971.

57. Pfister, G, Phys Rev Lett 33, p 1474, 1974.

58. Marshall, J M et al, Phys Stat Sol (a), 25, p 419, 1974.

59. Fisher, F D et al, Phil Mag 1975, to be published.

60. Nagels, P et al, 'Proc on the 5th International Conference on Amorphous and Liquid Semiconductors', Garmisch-Partenkirchen, Germany (J Stuke and W Brenig, editors), Taylor and Francis, London, 1974, p 867.

61. Grant, A J and Davis, E A, Solid State Comm 15, p 563, 1974.

62. Grant, A J et al, 'Proc on the 5th International Conference on Amorphous and Liquid Semiconductors', Garmisch-Partenkirchen, Germany (J Stuke and W Brenig, editors), Taylor and Francis, London, 1974, p 325.

63. Weiser, K et al, Ibid, p 335.

64. Main, C, PhD Thesis, University of Edinburgh, 1974.

65. Seager, C H et al, Phys Rev B 8, p 4746, 1973.

66. Seager, C H and Quinn, R K, J Non-Cryst Sol 17, p 386, 1975.

67. Marshall, J M and Owen, A E, Phil Mag 31, p 1341, 1975.

68. Marshall, J M and Miller, G R, Phil Mag 27, p 1151, 1973.

69. Kolomiets, B T et al, Mat Res Bull 5, p 655, 1970.

70. Kolomiets, B T et al, Proc on the 9th International Conference on the Physics of Semiconductors, Moscow, Vol 2, Acad Sci USSR (Leningrad 'Nauka'), 1968.

71. Edmond, J T, J Non-Cryst Sol 1, p 39 , 1968.

72. Minami, T et al, J Ceram Soc Jap 78, p 299, 1970.

73. Arai, K et al, Jap J Appl Phys 11, p 1080, 1970.

74. South, R B and Owen, A E, 'Proc on the 5th International Conference on Amorphous and Liquid Semiconductors', Garmisch-Partenkirchen, Germany (J Stuke and W Brenig, editors), Taylor and Francis, London, 1974, p 305.

75. Hurst, C H and Davis, E A, J Non-Cryst Sol 16, p 343, 1974.

76. Baidakov, L A et al, J Appl Chem USSR 34, p 2316, 1961.

77. DeWit, H J and Crevecoeur, C, J Non-Cryst Sol 8-10, p 787, 1972.

78. Arai, K et al, Jap J Appl Phys 12, p 1717, 1973.

79. Ast, D G, J Vac Sci Techn 10, p 748, 1973.

80. Danilov, A V and El'Mosli, M, Fiz Tverd Tela 5, p 2015, 1963.

81. Owen, A E, Glass Ind 48, p 637 and 695, 1967.

82. Nielsen, P, Thin Solid Films 15, p 309, 1973.

83. Kawamoto,Y et al, J Am Ceram Soc 57, p 489, 1974.

84. Suptitz, P and Willert, I, Phys Stat Sol (a), 28, p 223, 1975.

85. Lebedev, E A et al, Phys Stat Sol (a) 28, p 461, 1975.

86. Kolomiets, B T et al, J Non-Cryst Sol 5, p 389, 1971.

87. Amrhein, E M et al, J Non-Cryst Sol 16, p 46, 1974.

88. Inoue, E et al, 'Non-silver Photographic Processes'(R J Cox editor), Academic Press, 1975, p 71.

89. Salik, J, J Appl Phys 45, p 501, 1974.

CHAPTER 5 EXPERIMENTAL TECHNIQUES

5.1 INTRODUCTION

This chapter is a brief description of the methods used to produce samples, of the equipment used for experiments and of the experiments themselves. Most of these methods have been used by other workers in this laboratory and elsewhere, although some modifications were made for the present work. An excellent and more detailed description of similar electrical experiments has been given by C Main[1]. The optical experiments are the most important part of the work described here, but since these are conceptually very simple, and most of the equipment was commercially made, a long description is not necessary.

5.2 PREPARATION OF SAMPLES

5.2.1 PREPARATION OF BULK INGOTS

The glasses were prepared in bulk form in the departmental chemistry laboratory, either by or under the supervision of an experienced chemist.

Thick-walled quartz tubes (2 mm), of 11 mm or 26 mm bore and with a 'neck' or narrowing at least 10 cm from the closed end, were cleaned in Deacon 90 for 24 hours, followed by rinsing with deionized water and this was followed by overnight baking at 110°C. Conical quartz plugs that fitted the tube necks received the same treatment. The materials used were 6N elemental As and Se from Kock Light Limited, and Annalar Cu from BDH Limited. Initial attempts to prepare As_2Se_3-Cu films failed, mainly, it transpired,

because the commercially available compound was not stoichiometric, ie, some lumps were almost pure As while others were rich in Se. Hence, only compounds made in our own laboratory were used and usually 200 - 250 gms of As_2Se_3 were prepared in a single melt. Other compositions were prepared from As_2Se_3 and As, Se or Cu, by weighing out on an Oertling R20 microbalance, predetermined amounts, less about 10 mg, into small trays made by folding pieces of filter paper. When all the materials had been weighed out, the quartz tube was weighed and the contents of one tray emptied into it. Then the tube was put on the balance pan again and the weight made up by gradually adding with tweezers the extra 10 mg. This procedure was then repeated until all required materials were in the tube. Care was taken never to touch the tube or the materials except with tube tongs or tweezers since finger-marks can cause weighing errors. Powdered material was not used since oxygen contamination increases with the surface to volume ratio. When pure As was used it was left in the open air for as short a time as possible to minimise oxidation. With all the materials loaded, the quartz plug was put in its place and the tube evacuated to approximately 10^{-5} Torr and sealed with an oxy-propane blow torch. The tube was then put in a rocking furnace (See Figure 5.1) and heated up to about 500°C and kept at that level for some time to allow the arsenic to react. This was necessary because the high vapor pressure of elemental arsenic above 800°C might have caused the tube to explode. Next, the tube was heated at 800 - 1000°C for 24 hours before quenching in air or water. Between 10 and 50 gm were prepared of each composition.

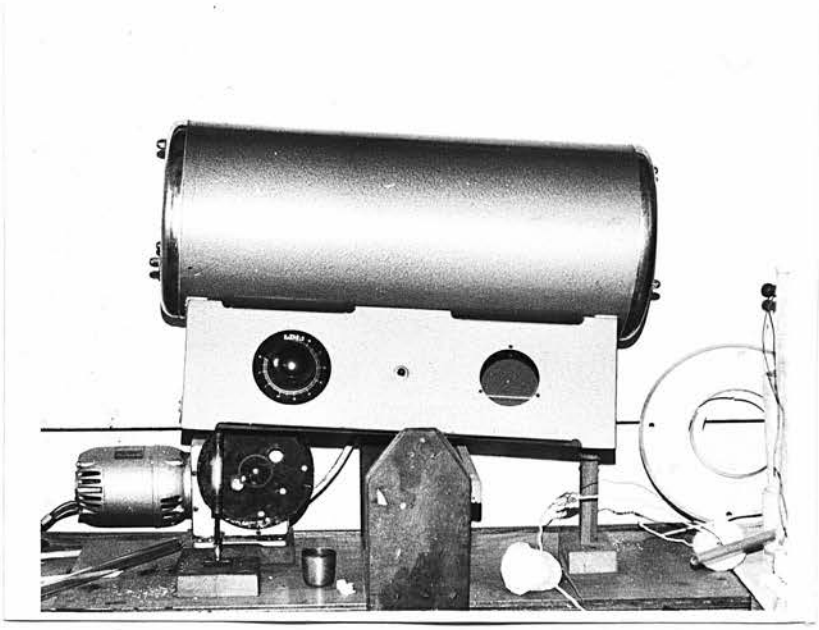

FIGURE 5.1

Temperature controlled rocking furnace used for production of glass melts.

5.2.2 EVAPORATION OF FILMS

Figure 5.2 shows the mask used for most of the simple preparations by evaporation and sputtering. Usually the middle gap (Figure 5.2) contained three ½" x 1" 7059 Corning glass substrates, two with gold electrode patterns for electrical measurements and a clear one for optical measurements. The two large gaps in the mask each contained three 1" x 1" substrates cut from ordinary microscope substrates. The films on these were used for the chemical analysis to be described later. All substrates were cleaned in Deacon 90 followed by rinsing in clean water and methanol before finally drying with blasts from a cylinder of compressed argon. The mask was placed in a vacuum system 25 - 30 cm vertically above the source. The source was a few lumps of the material to be evaporated placed in a quartz crucible which had been through the same cleaning process as the substrates. A coil of tungsten wire supported and surrounded the crucible; current passed through this coil and controlled by a variac provided the heating. The pressure was reduced to 4×10^{-6} Torr or better by means of a rotary and a diffusion pump, and usually kept at that pressure for at least half an hour before evaporation in order to outgas the source and substrates. An externally controlled metal plate or mask was used to blank off the initial and the final parts of the evaporation and it was found that this gave films nearer to the original composition, with less graded composition, than otherwise. The thickness of the films could be controlled approximately by counting the number of interference fringes in areas between screened and exposed parts of the

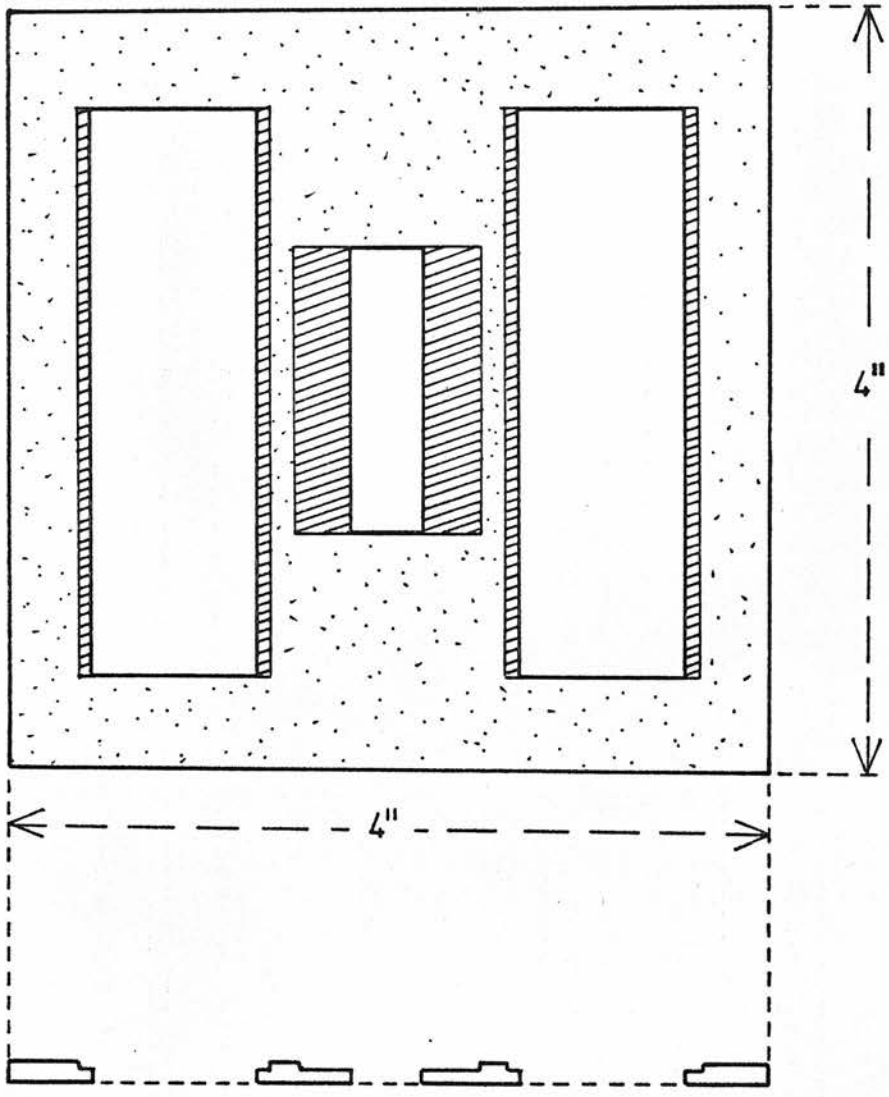

FIGURE 5.2

A brass mask for supporting substrates during deposition of amorphous films by evaporation or RF sputtering. A cross section is also shown. Three o.5"x1" and six 1"x1" substrates were used each time.

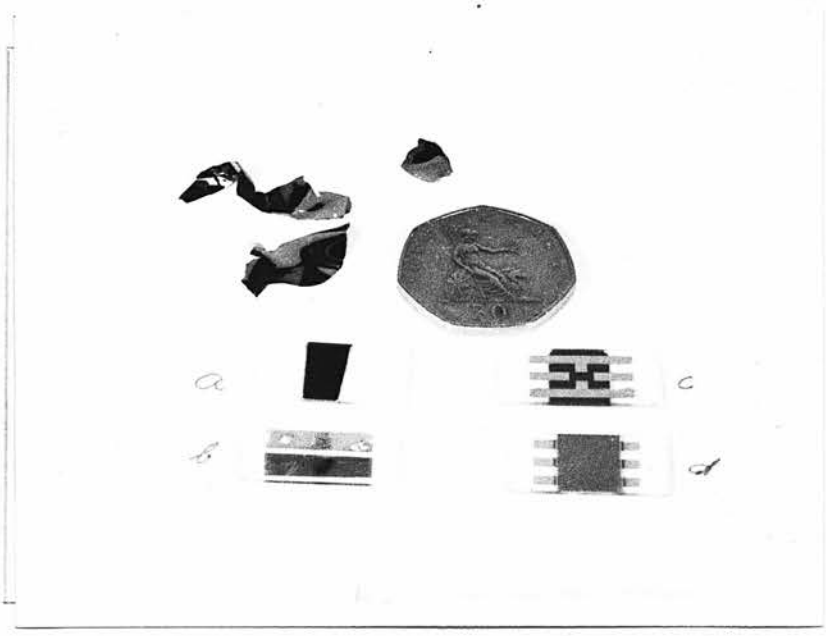

FIGURE 5.3

Chalcogenide films for optical and electrical work, top left: pieces of blown bubbles,
(a) RF sputtered optical sample,
(b) bubble pieces mounted on a substrate, electrodes deposited on top surface,
(c) RF sputtered film with electrodes, as wieved through the 7o59 Corning substrate
(d) same as (c), seen from abowe.

bell jar.

Attempts to evaporate As_2Se_3 glasses that had been doped with Cu failed because of the low vapor pressure of Cu. The Cu concentration of the films as determined by chemical analysis was usually 1 - 10% of that in the source material. Attempts were also made to coevaporate As_2Se_3 from a crucible and Cu from a molybdenum boat but although it is easy to produce films with high concentrations of Cu in this way it is very difficult to avoid a graded composition.

Therefore, the only thermally evaporated films used were of Se and As_2Se_3 (approximately). Electron beam evaporation of Cu-doped As_2Se_3 was more successful than ordinary (lower temperature) thermal evaporation; the concentration of Cu in the film was then about $\frac{1}{3}$ of that in the starting material. However, there was still some danger of graded composition and in the end other methods seemed more suitable, eg, sputtering, pressing or the blowing of bubbles.

5.2.3 RF SPUTTERING

High quality films with properties very similar to bulk materials were produced by RF sputtering using a RDM Mark III, 13.56 MHz, 1 kW generator and a RDM Mark III impedance matching unit. The sputtering was done in an argon atmosphere at a pressure of ~8 x 10^{-3} Torr. The target was a $3\frac{1}{2}$" aluminium disc covered with a powder of the glass to be deposited. Because the thermal conductivity of powders is very low and As-Se-Cu glasses

have rather low softening temperatures it was found that high power levels caused softening and thermal evaporation, but by sputtering at 50 Watts for 1 - 2 hours good films were obtained reproducibly. At this power the Cu content was only slightly less in the film than in the starting material. If the power was reduced to only 20 - 30 watts As seemed to be preferentially deposited, giving As rich films and the Cu content of the films sputtered at 25 watts was $\frac{1}{3} - \frac{1}{2}$ that of the starting material. It is well-known that different elements sputter at different rates; thus chalcogens sputter faster than silicon even if they come from the same source. It seems reasonable however, that these differences will be less when the target glass is heated above its softening temperature as was the case with the As-Se-Cu glasses at 50 watt sputtering power. This was evident from the fact that the particles in the powdered source became fused together on the surface of the powder. Examples of sputtered films are shown in Figure 5.3 in which (a) is an optical sample, (c) and (d) are films sputtered onto a substrate (7059) with photolithographically produced electrodes seen from below and above respectively.

5.2.4 PRESSED SAMPLES

This is a standard method of producing 20 - 100 μm thick 'bulk' samples of known composition. A suitable piece of bulk material, 2 - 3 mm across, is put between two plates of mica and held with tweezers in a bunsen flame but turned around frequently so as to heat both plates at similar rates. When the piece of glass becomes soft it deforms and can be pressed into a film between

the mica plates. The pressing is done on a hot plate with a preheated pressing tool. Good samples are obtained when hot plate and pressing tool are at a temperature low enough for the glass to become rigid after a few seconds of pressing but high enough to allow the pressing to take place before the glass becomes too viscous. The materials of concern in the present work are very easily prepared in this way. After pressing, the mica can be flaked off and the glass rubbed clean with soft tissue, to give a high quality optically smooth surface. Usually the pressed samples are slightly wedge-shaped which makes them less suitable than other films for optical transmission measurements.

5.2.5 THIN FILMS PREPARED BY THE BLOWING OF A BUBBLE

This was found to be a highly successful method of making thin films of known composition and of the order of 1 μm in thickness, for optical absorption measurements. Most of the measurements described in this work were in fact performed on small pieces of glass bubbles. A few grams of the glass were put in a small porcelain cup on an electrical hot plate inside a glovebox, which also contained clean quartz tubes of 3 mm bore and about 8 cm long, several containers with liquid N_2 , and a balloon hand pump. First, some liquid N_2 was poured out, which evaporated instantly to produce higher pressure inside the box than outside. This was repeated several times before the box door was firmly closed. The pressure was then always maintained above atmospheric by the nitrogen evaporating from its containers, which were usually paper cups. A safety valve prevented the pressure from rising too high

and also produced a noise when the nitrogen escaped, thus serving as a check that the pressure difference was being maintained. After the pump and the porcelain cup had been thoroughly flushed out with nitrogen the cup was covered with a sheet of mica and slowly heated until the glass melted and formed a highly viscous liquid. A quartz tube was attached to the baloon via 30 cm of rubber tubing and the free end dipped into the melt, kept there for a while to warm the quartz and then pulled out with a drop of melt on the end. After 2 - 4 seconds the balloon was vigorously pressed. If all conditions were right an elongated bubble, several inches long and $\frac{1}{2}$" - 2" in diameter was formed which solidified instantly and burst. The bubbles were collected on clean paper tissues and good pieces selected for measurement. Blowing of glass bubbles requires some practice and experimenting before success is achieved. If the melt is too viscous, it blocks the tube and cannot be blown. If it is too fluid, it shoots out of the tube without forming a bubble. Obviously therefore, this method is not suitable for materials which change from an almost rigid to a highly fluid state in a narrow temperature range but this presented no problems with the glasses used in this study. It is important to keep the time between the melting of the glass and the blowing of the last bubble as short as possible to avoid contamination. There is some water in the liquid nitrogen but most of it solidifies on the outside of the nitrogen containers and any water that may be left inside the porcelain cup will boil off before it can react with the chalcogenide. Liquid N_2 also usually contains some liquid O_2 but if the above precautions are taken very little oxidation will take place. Furthermore, one

must avoid heating the melt too much since then it will start evaporating and this could lead to a change in composition of the remaining material.

The newly-blown bubbles were extremely difficult to handle because of static charge but storage overnight usually overcame that problem. With a scalpel, tweezers and much patience, it was possible to choose good pieces of bubbles of varying thicknesses and cut them into suitable samples. For optical transmission measurements samples of suitable size were placed on top of a 2 mm hole in the sample holder. The metal around the hole had previously been smeared with silicon vacuum grease and most of the grease was wiped off again with tissue. The glass film was pressed gently with tissue to squeeze out bubbles of air and give the silicon grease a good grip. Usually several attempts had to be made before a sample could be mounted without cracking. Once mounted, these films usually lasted well, withstanding thermal cycling and the vibrations caused by handling the sample holder. For electrical measurements the failure rate is higher. Rectangular pieces of bubbles 3 - 6 mm across were glued to ½" x 1" 7059 glass substrates with silicon grease, two pieces on each substrate. More than half of the pieces cracked during this process. The substrates with uncracked bubbles were then sellotaped onto a 4" x 4" glass plate and 25 μm diameter tungsten wire stretched across the bubbles. The bubbles and substrates were suitably masked with aluminium foil and sellotape to give well-defined gold electrodes deposited by evaporation and with a 25 μm gap defined by the tungsten wire. There was a discontinuity in the gold film at the edge of the sample which caused some problems. A drop of silver dag over the edge was

enough to connect the gold on the substrate and the sample, but the dag seemed to contract and cracks tended to form in the sample around the dag. This was especially pronounced at low temperatures. Thus, a sample would often give good results around room temperature but on cooling the cracks would widen to cause an open circuit. Heating back to room temperature sometimes caused electrical contact to be re-established. Experiments with colloidal graphite gave better results although it tended to diffuse between the sample and the substrate. Some pieces of blown film are shown at the top left hand of Figure 5.3. Also shown are two pieces of blown film (item b) on a 7059 substrate with evaporated gold electrodes.

5.2.6 DEPOSITION OF ELECTRODES AND THEIR GEOMETRY

The technique described in the previous paragraph, ie, that of defining the gap by a thin tungsten wire, is convenient for providing coplanar electrodes on the top surface of samples. It was used in the case of bubbles, which were less than 5 μm thick, and since the electrode gap was 25 μm across and 2 - 5 mm wide, fringing fields and non-uniform field distribution were not significant. This method was also used to make coplanar electrodes on the surface of pressed samples and even bulk samples taken directly from quenched melts. In this case the thickness of the sample was greater than the gap width and it was not possible to assume a uniform field distribution throughout the thickness of the sample. However, at low fields, ie, when the glass is approximately ohmic, this should only change the geometrical factor connecting conductance and conductivity. Thus, the thermal activation energy should be the same as for a thinner sample.

No attempt was made to estimate the geometrical factor and therefore the conductivity preexponential could not be determined for such samples. These samples were also used for steady state photoconductivity and photomobility measurements. The wavelengths used for excitation were short enough to be in the high absorption region so that the effective sample thickness was the absorption depth, ie, practically all the light was absorbed in the first 1 - 2 μm and the rest of the sample was effectively an insulator. Furthermore, the amount of absorbed light is just the incident light minus the light reflected from the top surface, independent of back reflections, transmission or temperature shift of the absorption edge. Indeed, comparison of results on bubbles and thick samples indicated no differences in dark current activation energies, photoconductivity or photomobility.

The evaporation of electrodes was performed in the same vacuum system as the thermal evaporation of the chalcogenide films. Pieces of gold wire were suspended on a tungsten wire through which current was passed until it became red hot and the gold melted and wetted the tungsten. Continued heating caused the gold to evaporate slowly. Sometimes a Birvac T300-RG2 vacuum system with an electron beam evaporator was used. In this case the gold was placed in a molybdenum crucible. In either case the start and finish of evaporation onto the film were controlled by a mask which could be rotated from the outside.

This method of producing electrodes can of course be used for samples produced by thermal evaporation or sputtering. In this case, however, it is more convenient to first deposit the electrodes

onto the substrate and then the glass. This should ensure a cleaner electrode-glass interface and avoid possible damage of the film from the tungsten wire and the heat emitted during gold evaporation.

When the electrodes are deposited first, it is possible to use either the same method or to use photolithography. The latter makes it possible to produce electrodes of different gap sizes and in exactly known widths. Figure 5.4 shows the electrode pattern that was produced by photolithography. Two 4 mm long gaps were produced, 10 μm and 25 μm wide. The two central electrodes, each 2 mm wide, were intended as bottom electrodes in sandwich configuration. A very thin film of Nicrome was evaporated onto clean substrates followed by a thicker layer of gold; the Nicrome sticks better to the glass than the gold which tends to flake off during etching if it is used alone. The gold was then covered with photoresist and dried by heating. Next, the mask was placed on top of the substrate and it was exposed to ultraviolet light for about 10 secs, followed by developing, rinsing, drying and etching in 'Nicrome etch and a gold etch', and finally cleaning in acetone. This process removes all gold and Nicrome in the areas exposed to the UV light but leaves the rest untouched. Attempts to use photolithography to put down electrodes on top of bubbles or pressed samples failed because the etchant dissolves the chalcogenide glasses.

The use of gold electrodes for chalcogenide glasses is widespread. Shaw[2] observed no diffusion of gold and states that gold forms consistently good ohmic contacts to As_2Se_3 glasses.

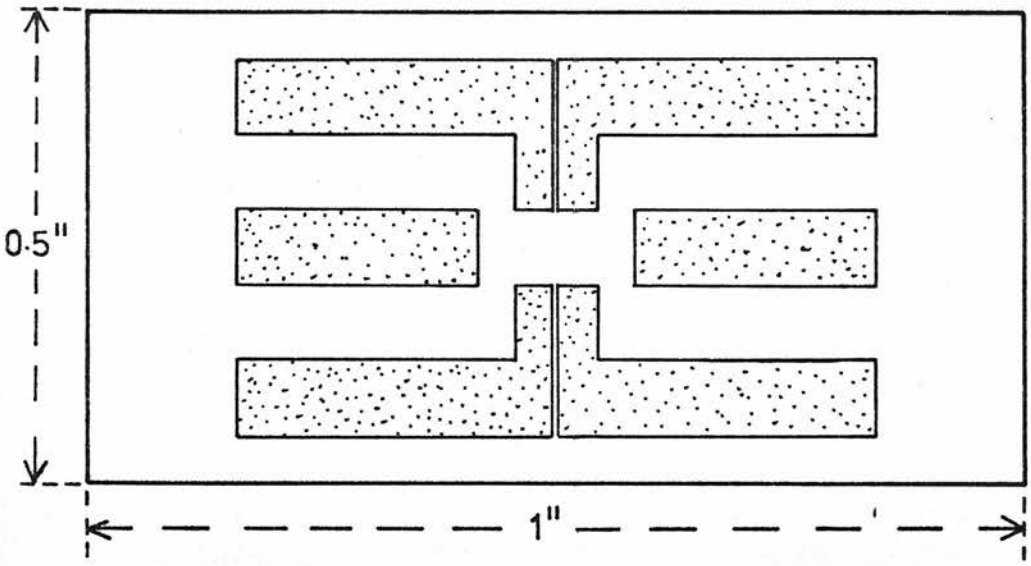

FIGURE 5.4

A mask for producing coplanar electrodes by photolithography. Dotted areas correspond to the electrodes. The gaps are 10μm and 25μm.

Suptitz and Willert[3] have measured the diffusion coefficient of gold in glassy As_2Se_3 and obtain $D_{Au} = 6 \exp\left(-\frac{1.15\ eV}{kT}\right)\ cm^2/sec$ for pure As_2Se_3. In Cu doped As_2Se_3 the diffusion coefficient of gold is lower than in the 'pure' glass. Using Einstein's relation

$$\mu = \frac{qD}{kT} \qquad 5.1$$

where q = the charge on the migrating Au ions, assumed to be e = one electronic charge, the mobility μ_{Au} of gold in As_2Se_3 can be calculated. At 120°C, $\mu_A = 3 \times 10^{-15}\ cm^2/V\ sec$ and at 180°C $\mu_A = 2.7 \times 10^{-13}\ cm^2/V\ sec$. Using $N_{Au} = 2 \times 10^{19}\ cm^{-3}$, the solubility of Au in As_2Se_3 [4] the ionic conductivity due to Au ions in As_2Se_3 can be estimated. The result is

$$\sigma_{Au}(120^oC) = N_{Au}\ \mu_{Au}(120^oC) \times e = 1.0 \times 10^{-14}\ \Omega^{-1}cm^{-1}$$

ie, nearly four orders of magnitude less than the observed (electronic) conductivity of As_2Se_3 at that temperature. At 180°C $\sigma_{Au} \triangleq 9 \times 10^{-13}\ \Omega^{-1}cm^{-1}$ and $\sigma_{el} \triangleq 10^{-7}\ \Omega^{-1}cm^{-1}$ [5]. Biktimirova et al[4] obtain a somewhat higher activation energy for D_{Au} but even at 180°C their D_{Au} is only about 20 times higher than that of Suptitz and Willert. Furthermore, they derive the effective charge for the gold ions as 0.2 - 0.4 e. The conclusion is that ionic conduction due to gold ions is insignificant in As_2Se_3 - Cu glasses.

5.2.7 THICKNESS MEASUREMENTS

The thickness of all optical samples was measured by two methods. First, the optical thickness was determined from the separation of interference fringes in the region $1 < \lambda < 2.5$ μm using the condition for constructive or destructive interference

$$2\,nd = m\lambda$$

where n = refractive index, d = sample thickness, λ = wave length and m is the order, an integer for a constructive interference or maxima and a half integer for minima. Since m is not known it was necessary to use the differences in m and λ between two or more fringes. The exact procedure and its limitations will be described in the next chapter but basically it means that the value of nd is overestimated by a few per cent. This does not, of course, give an absolute thickness measurement since n is also not generally known.

After the optical experiments on each sample were finished, the thickness was measured mechanically on a Taylor-Hobson Talysurf type 4 machine which works on a principle similar to a gramophone pick-up, ie, a diamond stylus is moved across the sample and its vertical movements give a proportional electrical output which is amplified and displayed on a pen recorder. The Talysurf is calibrated by measuring the output of the recorder when the stylus moves over a standard, ie, a glass plate with grooves of known depth. Evaporated and sputtered samples could be measured directly on their substrates although it was necessary to scrape off the edges of sample films to obtain a sharp step. The thickness could usually be

measured with a maximum error of 0.05 μm for submicron samples and to within 5% for thicker samples. Blown samples were more difficult to measure accurately, for two reasons. First, since they were either mounted on substrates with silicon grease or not at all, the stylus tended to drag them along. Therefore, it was necessary to lower the stylus directly onto the sample and measure the displacement as it moved off the edge of the sample. Secondly, the blown samples were less uniform in thickness and often had small ridges on the surface. The method that was found to work best, was to cut the sample into small bits, about 0.2 cm across and 0.3 cm or more long and glue these to a microscope slide with silicon grease, pressing with considerable force to eliminate air bubbles and to squeeze out excess grease. Each piece was then measured individually and the average result used as a final answer. Even after this procedure, a comparison between different samples, of the same composition, of the ratio of nd determined optically to d determined mechanically sometimes gave a scatter of up to 20% in n. However, although the scatter in values of n obtained by this method was considerable, there was no significant variation with composition within the As-Se system, and hence it seemed a justified approximation to use throughout, the value obtained by averaging n over all compositions. This will be discussed further in the next Chapter. The thickness of pressed samples was measured with a micrometer.

5.2.8 CHEMICAL ANALYSIS

All chemical analyses were performed in the departmental chemistry laboratories by, or under the supervision of Mr D J Reynolds.

The samples for analysis normally consisted of 1-5μm films of amorphous As-Se or As-Se-Cu deposited on 1" square pieces of microscope slide glass. Of the six such films produced in each evaporation or sputtering, 2 or 3 were used for the analysis of the Cu content and the rest for analysis of the Se content. Colorimetry was the method normally used. Each sample film was treated as follows : Fingermarks and traces of adhesive were cleaned with acetone and dicloromethane followed by drying. Substrate and film were weighed accurately on a microbalance and placed in a preweighed 250 ml beaker. Concentrated nitric acid was added and the beaker warmed until the film was completely dissolved. Next, the clear substrate was removed, after rinsing into the beaker with deionized water, and cleaned and dried before reweighing to obtain the weight of the film. The contents of the beaker were then evaporated to dryness at 100^{o}C. For Se analysis, the contents of the beaker were dissolved by adding the appropriate amounts of 10% acacia solution, hydrochloric acid and, several hours later, hydroxlamine hydrachloride solution (25%) and sulfur dioxide solution (the acacia is a natural gum used to stabilize the colloid). This was allowed to stand for further 3 hours and then compared on an absorption spectrophotometer at 340 mμ wavelength, with standard solutions which had been made by putting precisely known amounts of As and Se in a preweighed beaker and then dissolving by the method

described above. The standard and sample solutions were made up to precisely the same weight. The colorimetric agent is elemental selenium. For the determination of Cu a solvent made up of deionized water, 35% ammonia solution and acacia solution was used. After half an hour or more, sodium diethyldithiocarbamate solution was added and colour allowed to develop for 2 hours. Next, the samples were compared to standard solution with known concentrations of Cu and As_2Se_3, the comparison being done at 440 mμ on the absorption spectrophotometer. In this case the colorimetric agent is copperdiethyldithiocarbamate. For an accurate determination, films of thickness 1 μm or more (1" square) were necessary. The mean of the results for the individual films was taken as the final answer. The accuracy of the Se:As ratio determination was within 2 atomic %. The concentration of Cu as a doping element was determined to within 2% in the range 0.01% - 5% Cu (atomic). Determinations of As and Cu concentration by atomic absorption were used occasionally and gave results in reasonable agreement with the colorimetric values. Acetylene was used as a fuel gas and nitrous oxide as oxidant.

5.3 OPTICAL EXPERIMENTS

5.3.1 THE ZEISS SPECTROPHOTOMETER

Figure 5.5(a) shows the Zeiss spectrophotometer used for all optical measurements. The individual units are identified on the outline diagram in Figure 5.5(b). The light source, monochromator, platform for sample chamber and the detector unit are all mounted on the same optical bench. Not shown are the power supplies for the

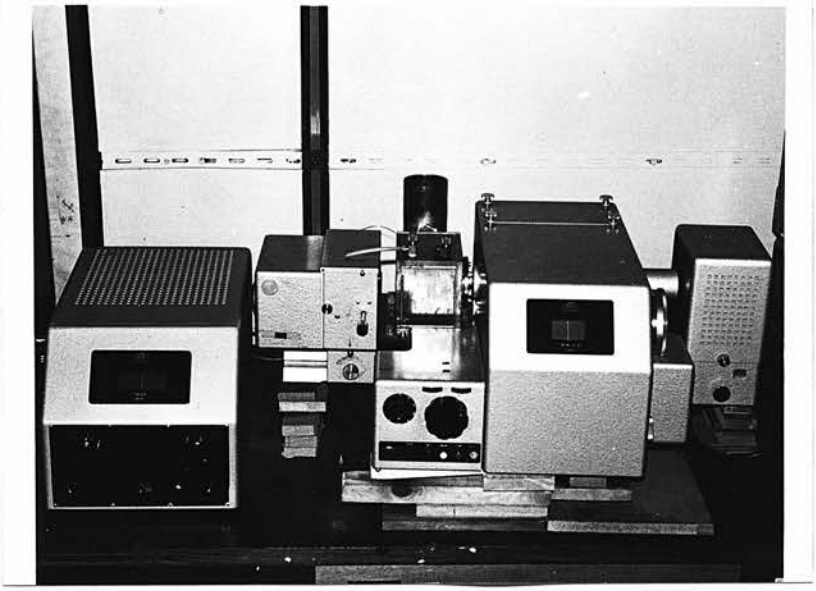

FIGURE 5.5(a)

The Zeiss spectrophotometer, see explanations below. Power supplies not shown.

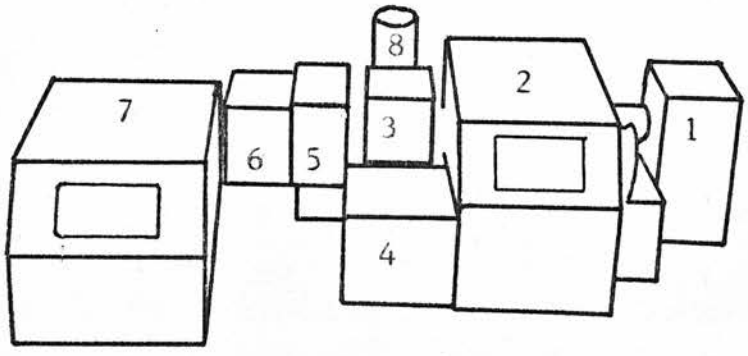

FIGURE 5.5(b)

1-light source, 2-monochromator, 3-vacuum chamber, 4-wavelength control unit, 5-Zeiss sample holder, 6-detector unit, 7-amplifier, 8-liquid nitrogen container.

light source and the detector and amplifier units. The light source is a 30 W, 6 V tungsten filament lamp. The Zeiss MM 12 d is a double-prism single-beam monochromator using glass prisms in the wavelength range of interest. A temperature controlled vacuum chamber, to be described in the next section, is mounted on a specially built platform whose height can be adjusted. Metal strips screwed into the platform on either side of the chamber confine it so that it is free to move only perpendicular to the light beam, ie, in and out of the picture. The extreme positions are adjusted by stop screws. The detector unit has a photo-multiplier tube (Zeiss 1P28) which was used for $\lambda \leqslant 0.670$ μm and a PbS photoconductive cell for the range 0.670 μm $\leqslant$ 2.5 μm. Finally, the amplifier unit (Zeiss PM QII) gives an output reading on a scale from 0 - 100. Just inside the entrance slit of the monochromator there is a chopper diaphragm which vibrates at 100 Hz to modulate the light beam and the amplifier unit is tuned to this frequency; this reduces the effects of ambient light. The widths of the entrance, centre and exit slits are always the same and can be controlled either manually or automatically by a servomechanism which, on the operation of a microswitch, automatically adjusts the slit widths so that the amplifier meter reads 100. Thus, when the sample is placed in the beam the transmission can be read off directly in %. In the case of very low transmission the meter reading can be amplified by up to 100 times by multipliers. Since the meter divisions are 0.5% this means one division per 0.005% transmission. By using interpolation the sensitivity is at least 0.002% transmission or 1:50000. The stated errors arising in the detector and amplifier units are within 2%. The

laboratory-built sample holder introduces some additional errors which will be discussed in the next section, but with care and frequent checking each reading is estimated to be within 5% of the true value. The bandwidth of the light beam increases with slit widths. In cases where there was a strong spectral dependence of absorption, the slit widths were kept within 0.2 mm, which according to graphs provided by the manufacturers indicates a maximum bandwidth of less than 0.010 eV, a figure considered to be adequate for transmission measurements on glasses. The calibration of the wavelength scale was checked against the Na D lines and several lines in the spectrum of the hydrogen lamp.

5.3.2 THE TEMPERATURE CONTROLLED VACUUM CHAMBER

This chamber was used both for optical and electrical measurements and is shown in Figure 5.6, together with the cold-finger and a sample holder for electrical measurements. A diagram of the sample holder for optical transmission measurements is shown in Figure 5.7. It is simply a 1 mm aluminium plate with 2 holes, 2 mm in diameter, as nearly identical as possible. The temperatures of the holder can be controlled to within $\frac{1}{2}^{o}K$ in the range from $\sim 80^{o}K$ to $430^{o}K$ by adjusting the heater current, and thus balancing the heat flow into and out of the sample holder. The chamber was always evacuated by a rotary pump, both to reduce heat convection and also to ensure that the relative position of the sample holder and the chamber was always the same. The light beam enters through one quartz window, goes through either the uncovered reference hole or the other hole covered with the sample and leaves via the other

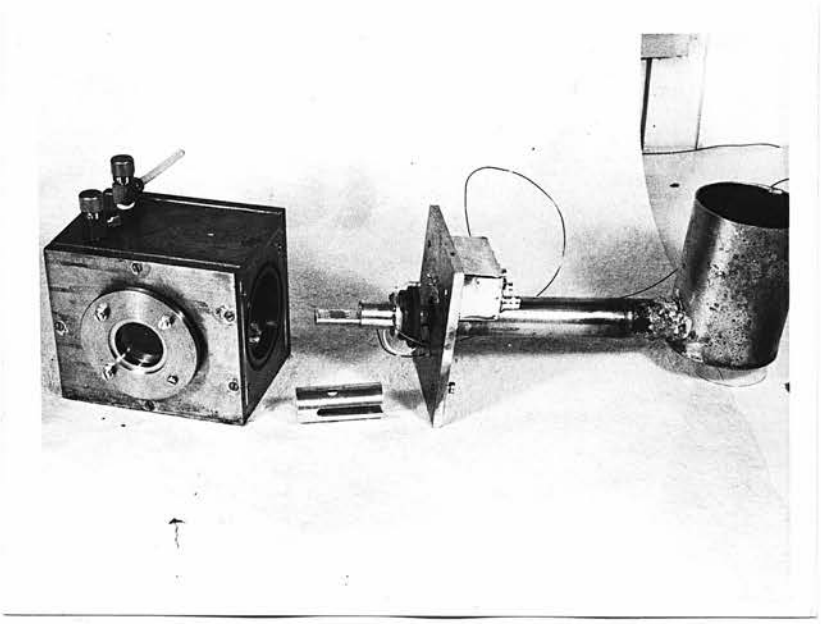

FIGURE 5.6

Vacuum chamber (left) with quartz windows. Coldfinger with sample holder for electrical work. In the foreground a shield that fits ower the sample holder.

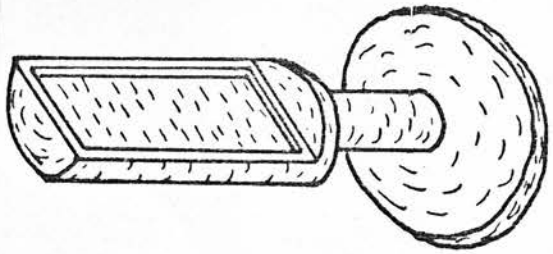

FIGURE 5.8

Sample holder for electrical measurements (aluminium).

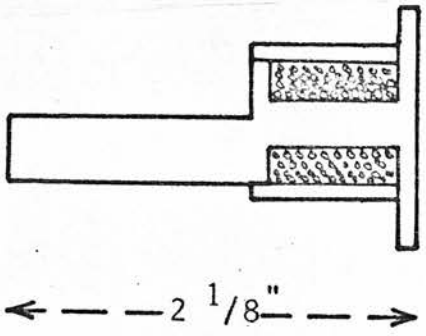

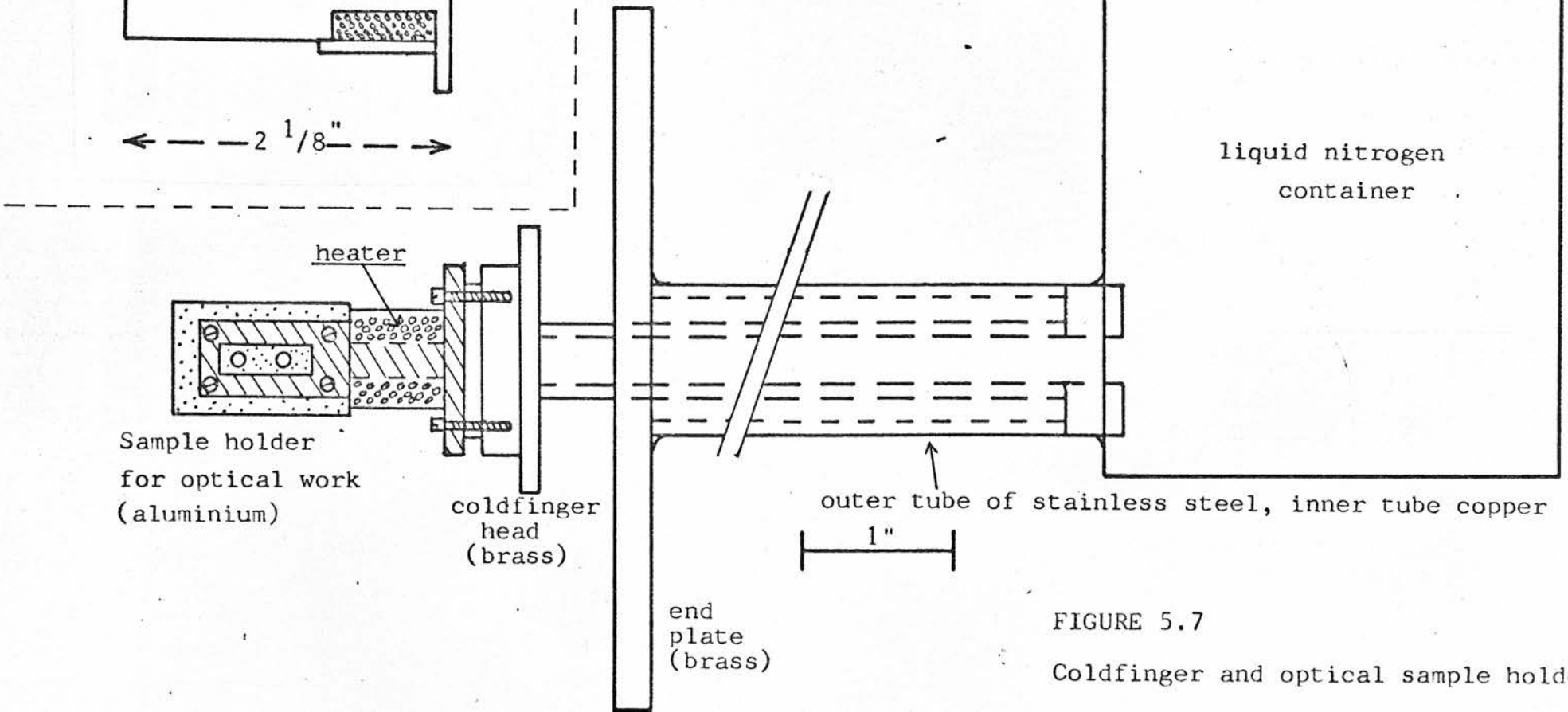

FIGURE 5.7

Coldfinger and optical sample holder.

quartz window to enter the detector unit. When mounting a sample, a piece of suitable size, was cut from a selected fragment of a blown film and carefully lowered onto the holder to cover the sample hole. It was then pressed gently with tissue. This made the film stick firmly to the silicon greased surface of the holder. The grease also provided a good thermal contact between sample and sample holder. After evacuation of the chamber, it was placed on its platform in the path of the light beam and the end positions adjusted to give maximum readings. The diameter of the beam is larger than that of the holes, but smaller than the hole separation. Furthermore, the light intensity is not quite uniform throughout the cross section of the beam. By adjusting both positions to maximum transmission (at one or two wavelengths of high transmission) it was thus assured that the same portion of the beam was transmitted through both holes. That this was actually so, was checked frequently by comparing the transmission with both holes uncovered, and furthermore, for each composition, at least one sample was measured in the Zeiss sample holder which is attached to the front of the detector unit. In this case the sample cross section was larger than that of the beam, so that the whole beam passed through the sample. Afterwards, a piece of the same sample was transferred to the temperature controlled sample holder and the measurement repeated. The agreement was usually good. The Zeiss sample holder could only be used at room temperature. Using the other holder, it was found necessary to re-adjust the stop screw positions every time the temperature was changed, to compensate for thermal contraction of the coldfinger tube. Normally, after adjustment of the stop screws, the sample was checked for cracks or pinholes by looking

for transmission at short wavelengths, where a good sample should not give detectable transmission. Then the transmission was measured in suitable steps of wavenumbers, starting at 0.0010% transmission, continuing into the high transmission region (longer wavelength) where interference fringes appeared. The measurements extended right up to 4.0×10^3 cm^{-1} wavenumber (λ = 2.5 μm), the limit set by the glass prism and the PbS detector. Finally, measurements at several wavelengths in the high absorption region were repeated to check that conditions had not changed during the run.

Possible sources of errors introduced by the chamber and sample holder are the following : Difference in size of reference and sample holes. This was definately less than 1%, as shown by frequent checks without a sample. Different parts of the beam passed by the two holes. This was checked by the same method, but there was always a danger of misalignment occurring during a run. This possibility was minimised by checking several times during each run that both positions resulted in maximum transmission. The errors due to this effect should not be more than 1 - 2% and usually less. A third possible source of error is diffuse reflected light inside the chamber. This was not thought to be significant, however, since the aluminium sample holder was not optically smooth and there was never any detectable change in readings at short, non-transmitted wavelengths, when the light source was switched off. Finally, during low temperature measurements it sometimes occurred that the whole chamber became so cold that water vapor condensed on the quartz windows. This

only happened after prolonged cooling and was usually avoided by completing the experiment before condensation started. In any case it was obvious when this did occur, because the readings tended to vary widely, and the readings that were checked again were different. This is not therefore considered to be a source of errors in the results presented here.

5.4 ELECTRICAL MEASUREMENTS

5.4.1 THE SAMPLE HOLDER

The same vacuum chamber was used for electrical and optical measurements. Figure 5.6 shows the chamber and the coldfinger with a sample holder for electrical measurements. Figure 5.8 shows the same in diagrammatic form. The sample holder is isolated from the colfinger head with a PTFE disc, apart from the presence of the four screws which can be either of brass or nylon. The latter were chosen to give correct balance between heat production in the heater windings and heat flow into the coldfinger head, which is at liquid N_2 temperature. The holder can be attached to the head in four different positions, with the sample facing upwards, or $\pm 90^{o}$ or 180^{o}. Normally it faces one of the chamber windows. The hole through the sample holder allows viewing of the light beam from the other side. The thermocouple wires are of very fine gauge copper and constantan, thus minimising heat conduction along the wires. One junction is embedded deep inside the sample holder, near the middle, and as near to the sample as possible. The other (reference) junction is outside in an icewater bath. The substrate is stuck down with silicon grease to give good thermal contact and

the ends are pressed down with blocks of PTFE and an Al plate which is held with two screws. Electrical contacts are made with 0.0024" varnished Cu wires; one end is soldered to the feed-throughs in the face plate and the other is stuck onto the uncovered parts of the gold electrodes with silver dag. The small gauge of the wires reduces thermal conduction to or from the sample.

5.4.2 DC DARK CONDUCTIVITY

Figure 5.9 is a block diagram of the system used for the measurement of dark current as a function of temperature and field. For such measurements it is vital to ensure that no stray light enters the chamber and this can be tested by shining a microscope illuminator on points where light could possibly enter. Thus, it was found necessary to cover feedthroughs with plasticine. There is a component of photoconductivity in As_2Se_3 which has a very large time constant[6] and this makes it necessary either to keep the sample in the dark overnight or to warm it above room temperature. It is also necessary to allow time for electrical relaxation processes every time the field across the sample is changed; a half hour is usually sufficient. This system, with the Keithley 610C electrometer, can be used to measure currents down to 10^{-14} Amps, although measurements in the 10^{-14} - 10^{-13} Amps range are often difficult due to electrical noise from the surroundings. The electrometer was normally used in the 'fast mode', which means that its input is virtually earthed. All measurements of current as a function of temperature were performed with discontinuous heating or cooling, ie, both

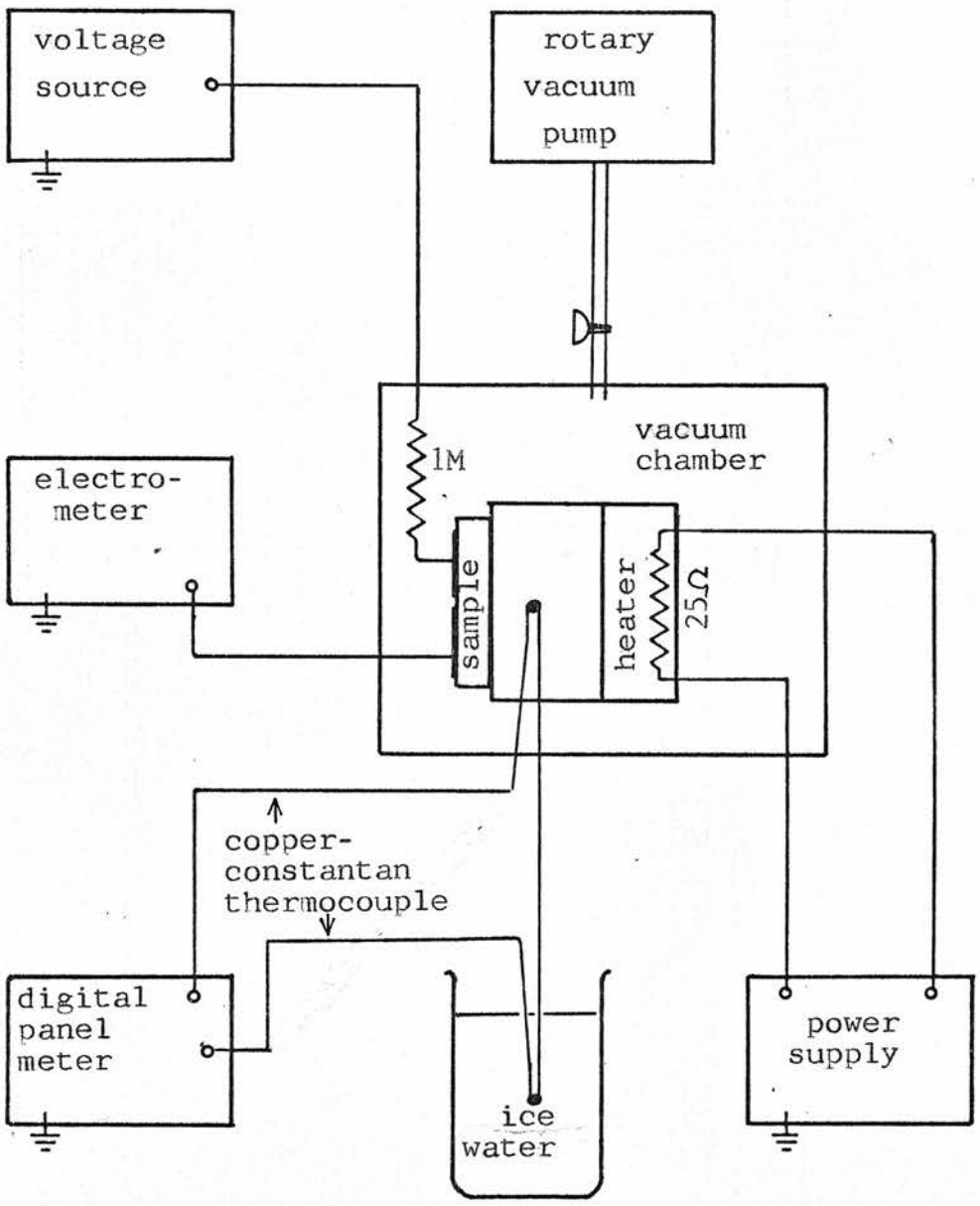

FIGURE 5.9

Block diagram of the system used for measurements of dark conductivity.

temperature and current were allowed to stabilize before readings were taken.

5.4.3 THE 'BIG RED' LIGHT-EMITTING DIODE (LED)

The Monsanto MV4H high intensity light emitting diode is an extremely convenient light source. Figure 5.10 is a photograph of an MV4H, together with a light-pipe LED assembly and a power amplifier for driving the LED with dc current, square waves or both simultaneously. Also shown is a PIN-3DP photodiode which was used to calibrate the LED and light-pipe combination in terms of the number of photons per cm^2 per sec leaving the light-pipe for a given LED drive current. A 5p coin is shown for comparison. When properly heatsunk, the LED can, according to the manufacturers data, withstand up to 1 Amp continuous or 25 Amps of suitably pulsed light (1 μsec pulses at 300 pps). The circuit diagram of the amplifier is shown in Figure 5.11; the transistor used has a risetime of about 1 μsec but this amplifier was not much used. It was found more convenient to drive the LED directly from a dc power supply (with a series resistor for protection and a reostat for accurate current adjustment), or from a Hewlett Packard model 214 pulse generator. Figure 5.12 shows, in a block diagram form, these three configurations. Figure 5.13 shows the spectral distribution of the LED radiation as given by the manufacturers. The wavelength at maximum intensity was found to be ~0.660 μm for the LED used in this work. This compares with 0.655μm found by Main[1] and 0.650 - 0.700 μm given by the manufacturer.

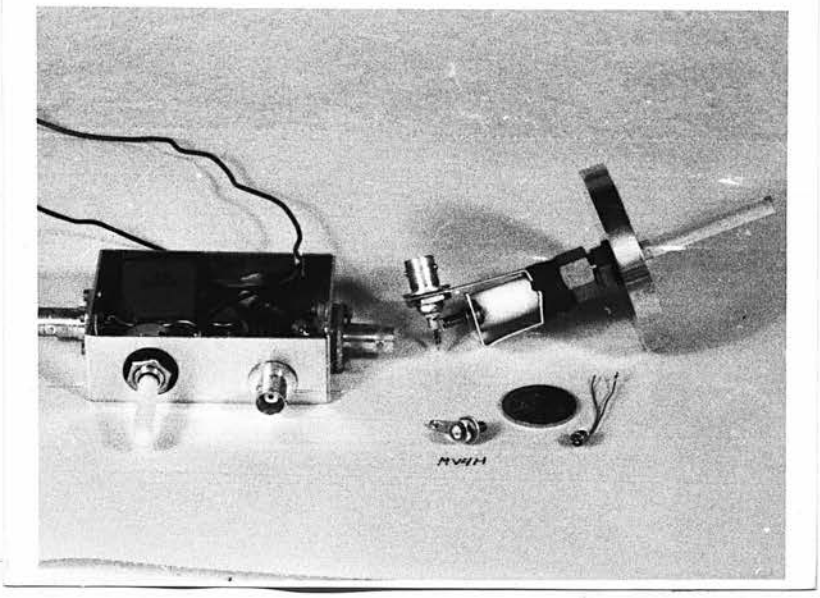

FIGURE 5.1o

On left: LED amplifier (circuit diagram below), right: LED assembly with a light pipe, in front: the 'BIG RED' light emitting diode, Monsanto MV4H, and (on left) a PIN-3DP silicon diode photodetector.

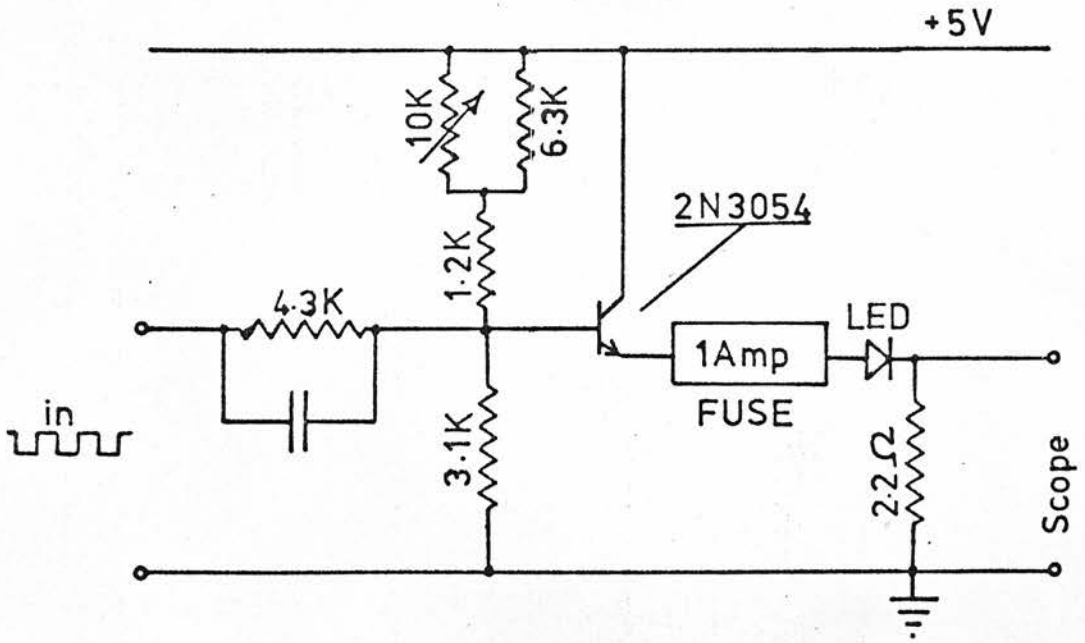

FIGURE 5.11

A circuit diagram of an amplifier used to obtain a square wave output of light superimposed on a DC light output, both are continuosly variable.

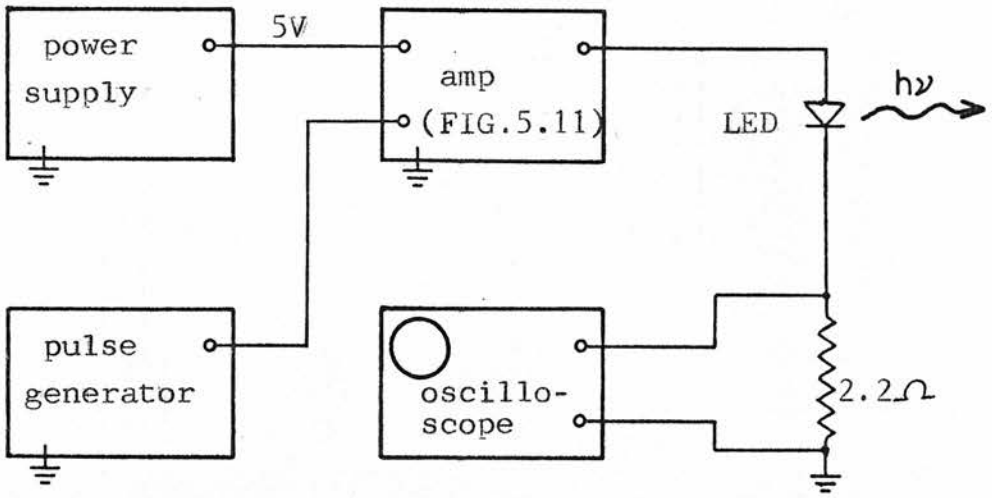

FIGURE 5.12(a)

This configuration gives a square wave light output superimposed on a DC output.

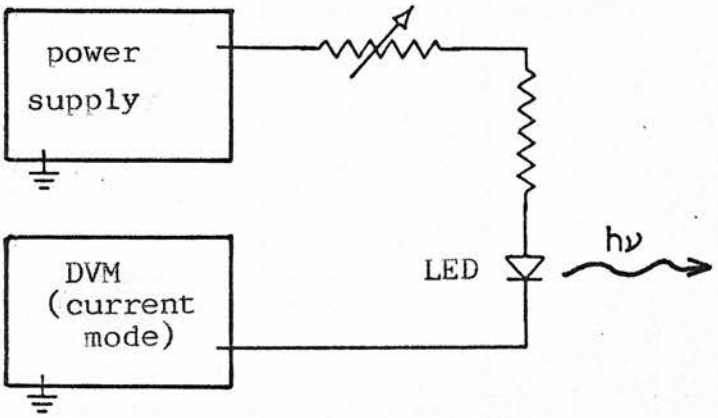

FIGURE 5.12(b)

The configuration used for most steady-state photoconductivity measurements.

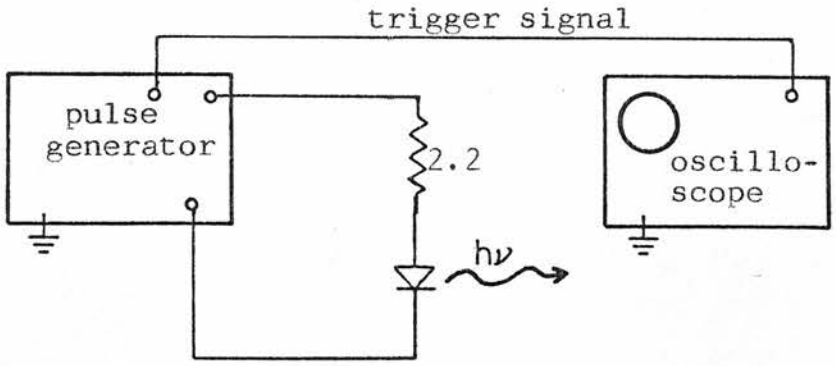

FIGURE 5.12(c)

LED drive system for photomobility measure ments.

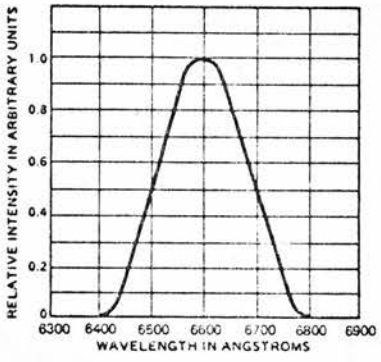

Spectral Distribution

FIGURE 5.13

Spectral distribution of the LED output as given by the manufacturer. The LED used in this work showed a maximum at 6600 Å.

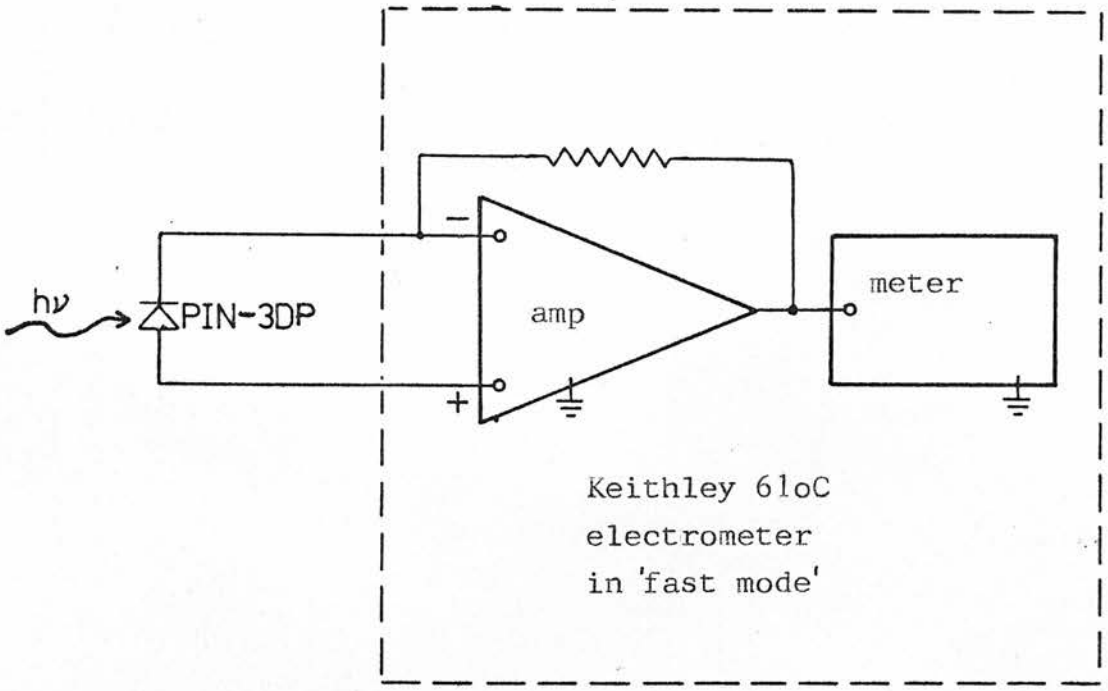

FIGURE 5.14

The silicon photodiode in the photovoltaic mode, using the electrometer as amplifier.

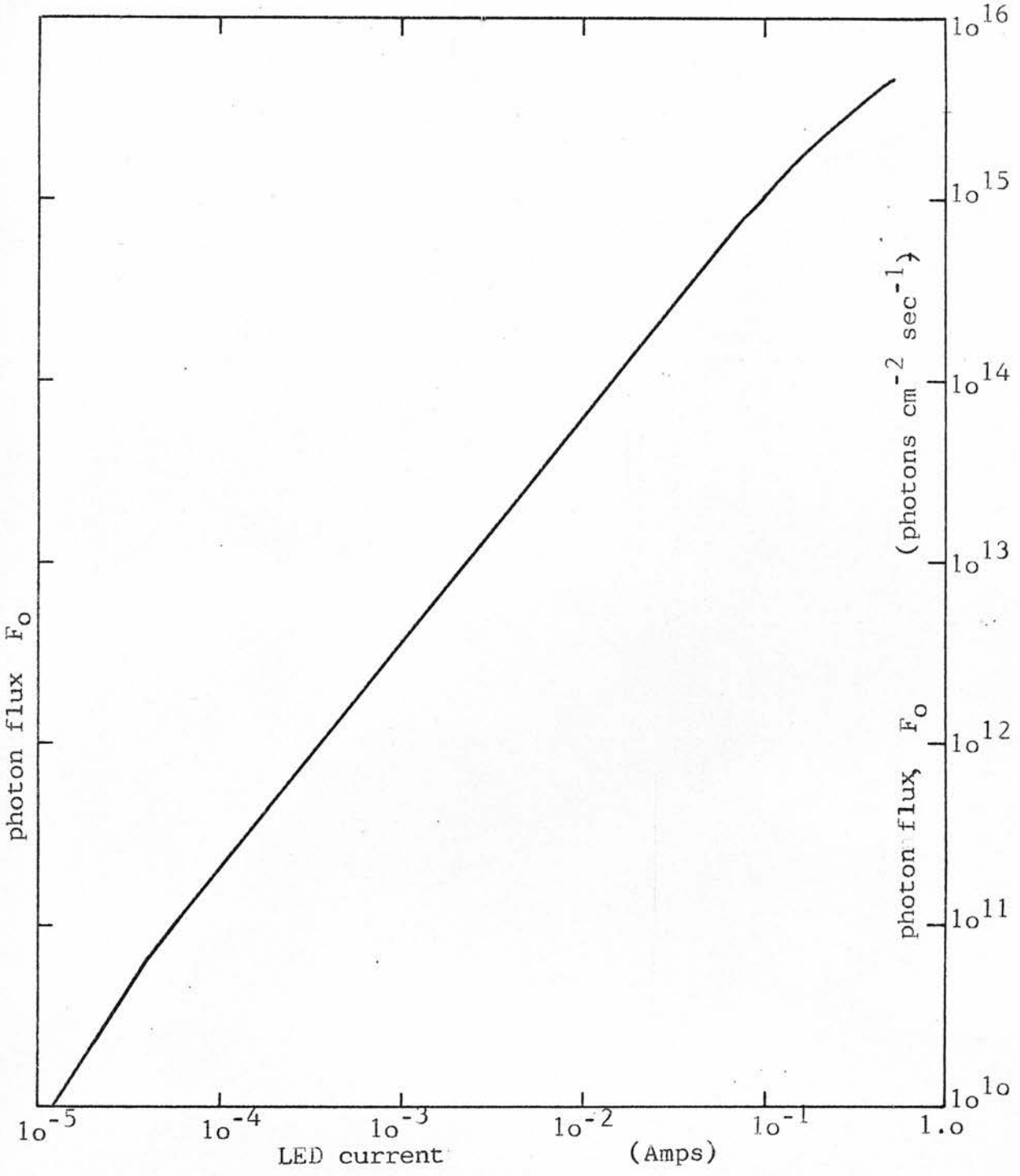

FIGURE 5.15

Calibration curve for the Monsanto MV4H light emitting diode + light pipe.

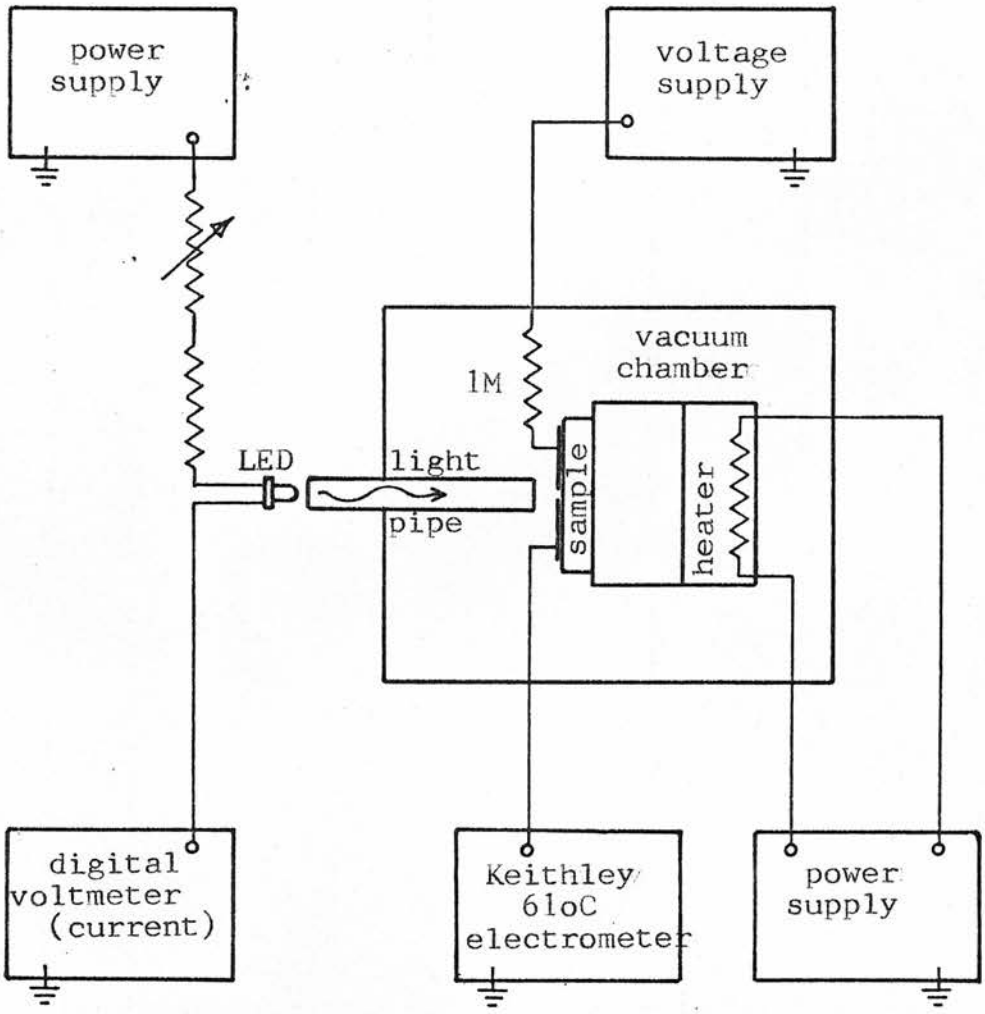

FIGURE 5.16

The system used for steady-state photoconductivity measurements.

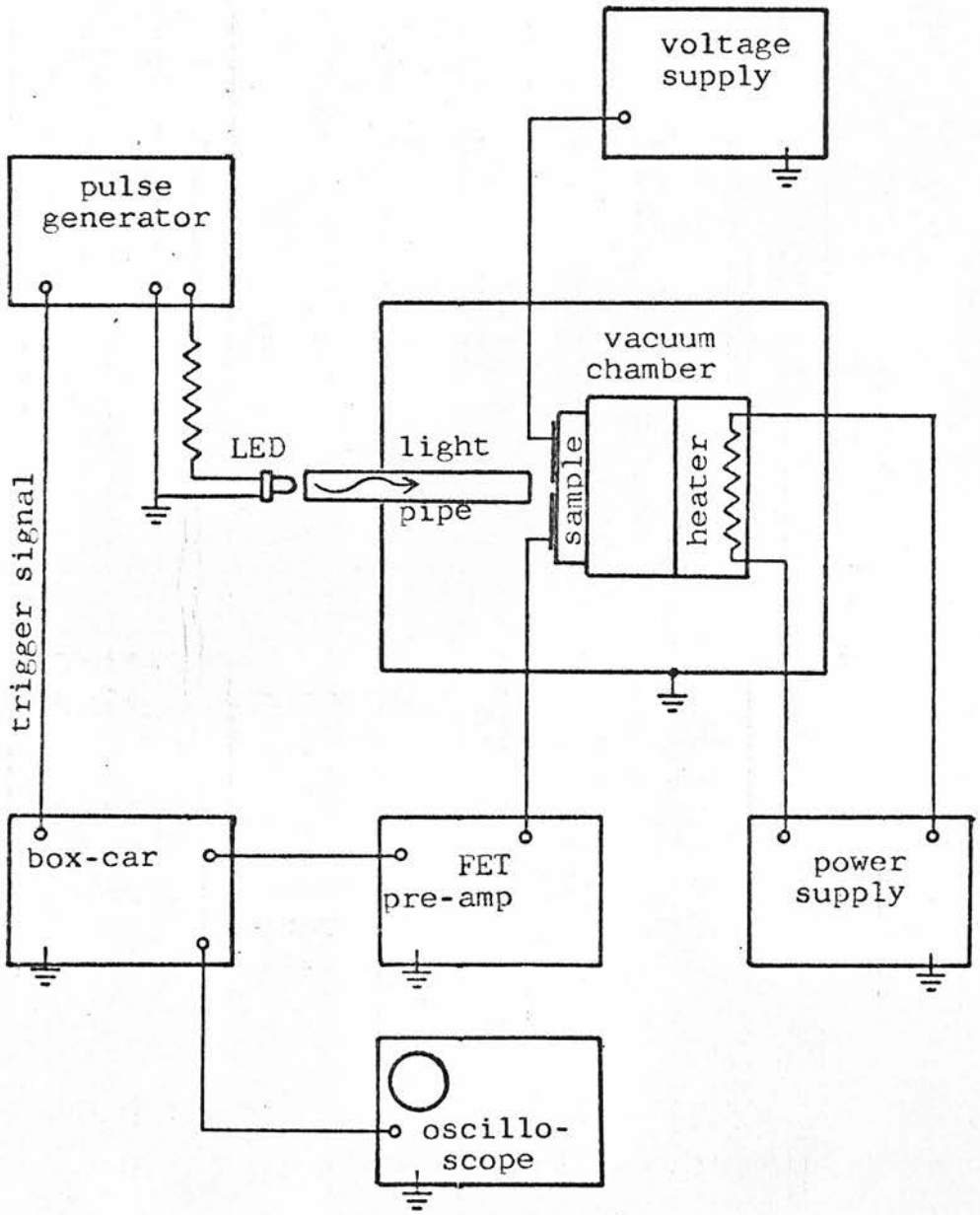

FIGURE 5.17

Block diagram of the photomobility system.

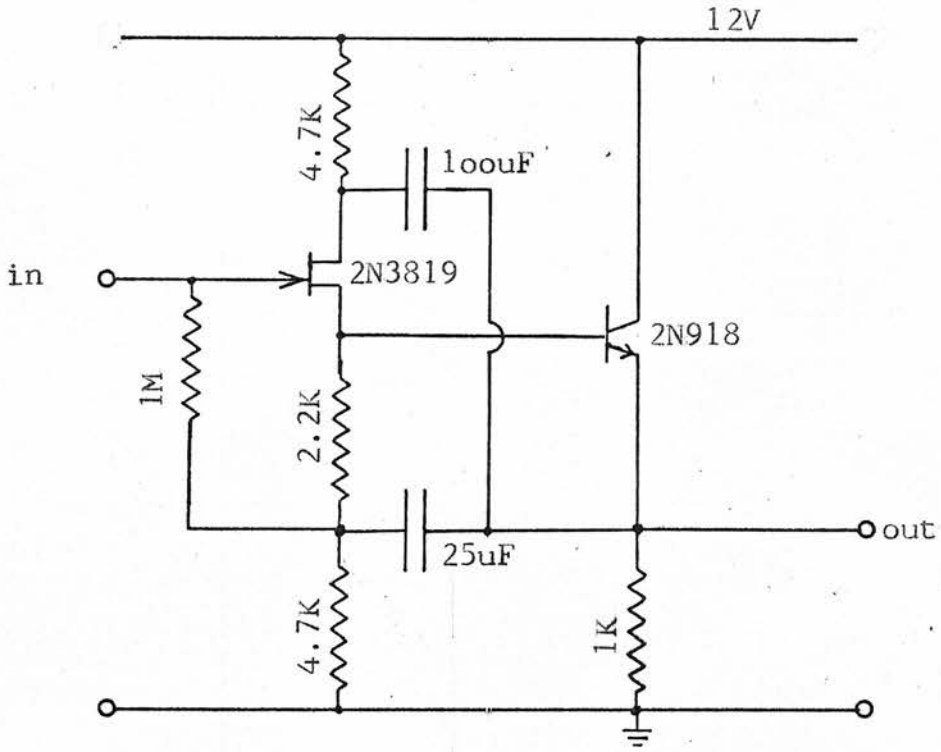

FIGURE 5.18

Circuit diagram of the FET high input resistance amplifier.

5.4.4 CALIBRATION OF THE LED

The PIN-3DP photodiode (from United Detector Technology Limited) has a linear relationship between light intensity and current over ten decades. It can be used either in a photocurrent mode with a fixed voltage applied across it, or in the photovoltaic mode. The latter configuration was used for the calibration of the LED, with the Keithley 610C electrometer in the 'fast mode' as an amplifier, as shown in Figure 5.14.

The photodiode only gives relative calibration and it was therefore necessary to obtain one or more absolute measurements of LED current vs intensity. This was done using a Hilger-Schwarz thermopile, model FT20, which gives an output voltage proportional to the total energy absorbed. Its dc sensitivity is 18 $\mu V/\mu W$, and thus it is suitable only for measuring fairly high intensities. A Fluke differential microvoltmeter model 885AB was used to measure the change in thermopile voltage as the LED was switched on and off. Some problems are caused by drift of the thermopile voltage but repeated measurements were used to obtain good average results. The final calibration curve for the LED is shown in Figure 5.15.

5.4.5 PHOTOCONDUCTIVITY AND PHOTOMOBILITY

A block diagram of the system used for measuring the steady-state photocurrent (I_{ph}) is shown in Figure 5.16. The light-pipe is a highly polished 6 mm pyrex rod and it extends into the vacuum chamber to within a few mm from the sample. The incident photon flux was obtained from the calibration curve in Figure 5.15. The

total current is the sum of I_d - the dark current, and I_{ph} - the photocurrent.

Photomobility is a term used for measurements of the initial rate of increase of photocurrent as a step function illumination is applied. Under certain assumptions the carrier drift mobility can be derived from initial rise of photocurrent. Figure 5.17 is a block diagram of the arrangement used for these experiments and a circuit diagram of the FET amplifier is given in Figure 5.18. The linear part of the photocurrent response is limited on one hand by the onset of recombination or deep trapping, and on the other by the RC time constant of the sample capacitance and the series resistor. This was estimated to be $\leqslant 0.5$ μsec. The As_2Se_3 - Cu glasses seem to have even lower drift mobilities than pure As_2Se_3 and it was necessary to use a boxcar noise recovery system consisting of a low noise amplifier type 450, a linear gate type 415 and a scan delay generator type 425A, all from Brookdeal Electronics Limited, for these measurements. This is basically a 'single channel analyser' which is triggered by the LED drive pulse and which repeatedly samples a narrow section of the output signal, slowly scanning the whole signal. The average output was displayed on the Tektronix 549 storage oscilloscope. Some problems were caused by pick-up of noise produced by the generator-LED system. This was minimised by avoiding earth loops as far as possible and earthing all equipment except the generator and the LED to a common point.

5.5 REFERENCES

1. Main, C, PhD Thesis, University of Edinburgh, 1974.
2. Shaw, R F, PhD Thesis, University of Cambridge, 1969.
3. Suptitz, P and Willert, I, Phys Stat Sol (a), 28, p 223, 1975.
4. Biktimirova, V Kh et al, Soviet Phys Semic 8, p 1412, 1975.
5. Hurst, C H and Davis, E A, J Non-Cryst Sol 16, p 343, 1974.
6. Fuchs, W and Meyer, D, Phys Stat Sol (a), 24, p 275, 1974.

CHAPTER 6 METHODS OF ANALYSIS

6.1 INTRODUCTION

This chapter describes how measured data was converted into results from which useful properties could be extracted. Various corrections which have been taken into account are described, the omission of others is justified, and errors are assessed as far as is possible. Section 2 discusses the conversion of optical transmission vs wave number data into quantities such as the dimensionless product αd - absorption times thickness, or α vs wave number or photon energy which in turn can be manipulated and plotted in terms of various optical absorption laws to give useful material parameters. A major simplifying assumption which needs some justification, is the use of a refractive index $n = 3.2$ in the highly absorbing region which is taken to be constant with photon energy and composition. The contribution of the extinction coefficient to the reflectivities is shown to be insignificant in the measurement range. The analysis of the interferometric data to obtain values for sample thicknesses is described and here again the assumption is made that the refractive index, or rather, the wavelength independent part of it, is independent of composition in the materials of interest. It is concluded that interferometric thickness measurements are more accurate than direct mechanical measurements.

Most of the electrical measurements were performed using well-known methods and equipment, and hence only a brief account of their analysis is given. The main points are the following : (a) the geometric factor arising from sample geometry and connecting

conductance and conductivity, (b) the variation of illumination and excess carrier density through the sample and perpendicular to the electric field, and (c) how this leads to an effective sample thickness for photoconductivity which is of the order of α^{-1}. This is shown to lead to a correction of the activation energy for steady-state photoconductivity, arising from the shift of α with temperature, but not the photomobility activation energy. Finally, the quantum efficiency, necessary to derive the drift mobility, is discussed.

6.2 ANALYSIS OF OPTICAL DATA

6.2.1 CONVERSION OF TRANSMISSION DATA TO ABSORPTION DATA

The diagrams in Figure 6.1 indicate the relations between refractive indices, reflection coefficients and transmission. The interface between two materials a and b, one of which (say a) is absorbing and with refractive indices n_a and n_b gives rise to a reflection coefficient

$$R_{ab} = \frac{(n_a-n_b)^2 + k_a^2}{(n_a+n_b)^2 + k_a^2} \qquad 6.1$$

at normal incidence, in which

$$k_a = \frac{\lambda\alpha}{4\pi} \qquad 6.2$$

is the extinction coefficient of the absorbing medium, whose absorption coefficient is α and λ is the wavelength. Thus, a beam

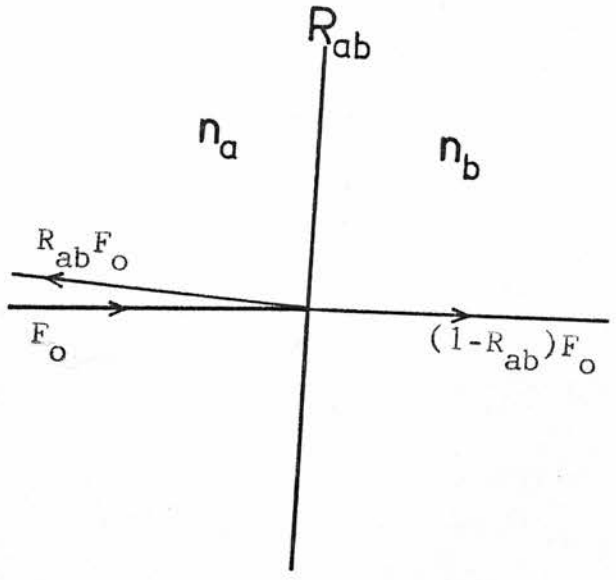

FIGURE 6.1(a)

Diagram showing how a light beam incident on an interface between two materials with different refractive indices is split into reflected and transmitted parts.

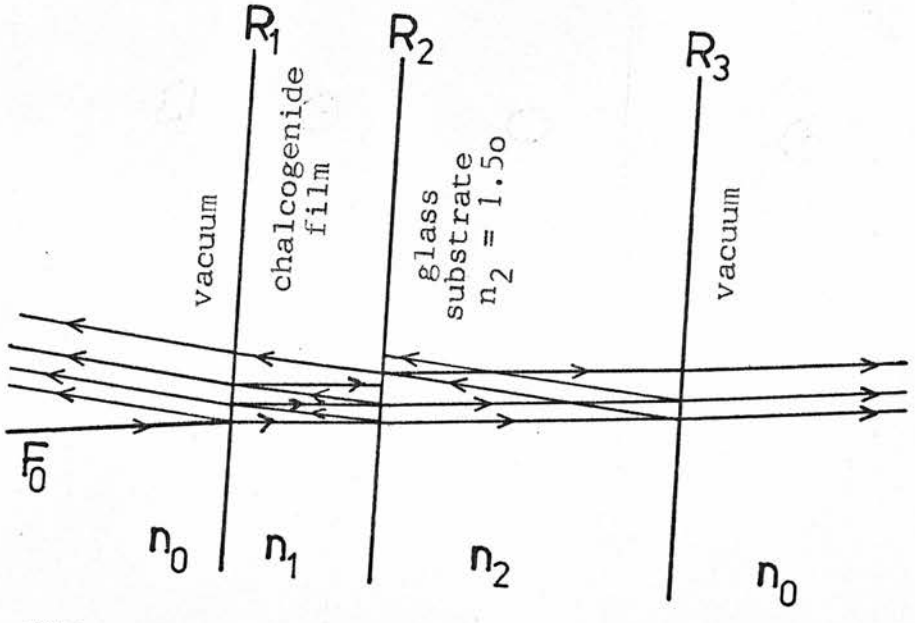

FIGURE 6.1(b)

A similar diagram for a sample on a glass substrate, some multiple reflections are shown.

of intensity F_o incident normally on the interface will be divided into a reflected part of intensity $R_{ab}F_o$ and a transmitted part $(1 - R_{ab})F_o$. The intensity will also be reduced by the absorbing medium so that after a distance d it has fallen to $e^{-\alpha d}$ times its original value.

The configuration in Figure 6.1(b) applies to a film on a substrate. Taking account of multiple reflections from all three interfaces, but neglecting interference effects one obtains for the transmission through a sample on a substrate

$$T = \frac{(1-R_1)(1-R_2)(1-R_3)}{(1-R_2R_3)} \quad \frac{\exp(-\alpha d)}{\{1 - [R_1R_2+R_1R_3(1-R_2)^2]\exp(-2\alpha d)\}} \qquad 6.3$$

where T is the ratio of transmitted light intensity to the incident light intensity. Most of the data obtained in this work was for unsupported samples, in which case the above equation simplifies since $R_3 = 0$ and $R_2 = R_1 = R$, ie,

$$T = (1-R)^2 \frac{\exp(-\alpha d)}{1-R^2 \exp(-2\alpha d)} \qquad 6.4$$

Both equations can be rewritten in the form

$$T = \frac{A/y}{1 - B/y^2} \qquad 6.5$$

where $y = \exp(\alpha d)$ but A and B are different in the two cases. Solving equation 6.5 for y and taking natural logarithms gives

$$\alpha d = \ln\left[\frac{A}{2T} \pm \sqrt{\left(\frac{A}{2T}\right)^2 + B}\right] \qquad 6.6$$

Only the + sign gives a meaningful answer. In most cases of interest B can be neglected since usually B exp(-2αd) << 1 in equations 6.3 and 6.4. It was included here, however, and a computer used to calculate the dimensionless quantity αd, as a function of T, with the refractive index n_1 as a parameter. Some examples are shown in Figure 6.2. The experimental data was obtained in the form T vs wave number x. This was converted into αd vs x data by reading the αd value of the αd vs T graph. It was of course necessary to make some assumptions about the values of R_1 and R_2, ie, for n_1 and k.

Neglecting the denominator in equation 6.4, one can write

$$\exp(\alpha d) = (1-R)^2/T$$

$$\alpha d = 2\ln(1-R) - \ln T$$

$$\Delta\alpha.\ d = -\frac{2\Delta R}{(1-R)} \qquad 6.7$$

by differentiating. This can be used to estimate the effect on α of errors in R arising from incorrect values of n and k. By differentiation of equation 6.7 with respect to either one of n or k, keeping the other constant one obtains

$$\Delta\alpha\ .\ d = -\frac{2\Delta n}{n}\left(\frac{n-1}{n+1}\right) \qquad 6.8$$

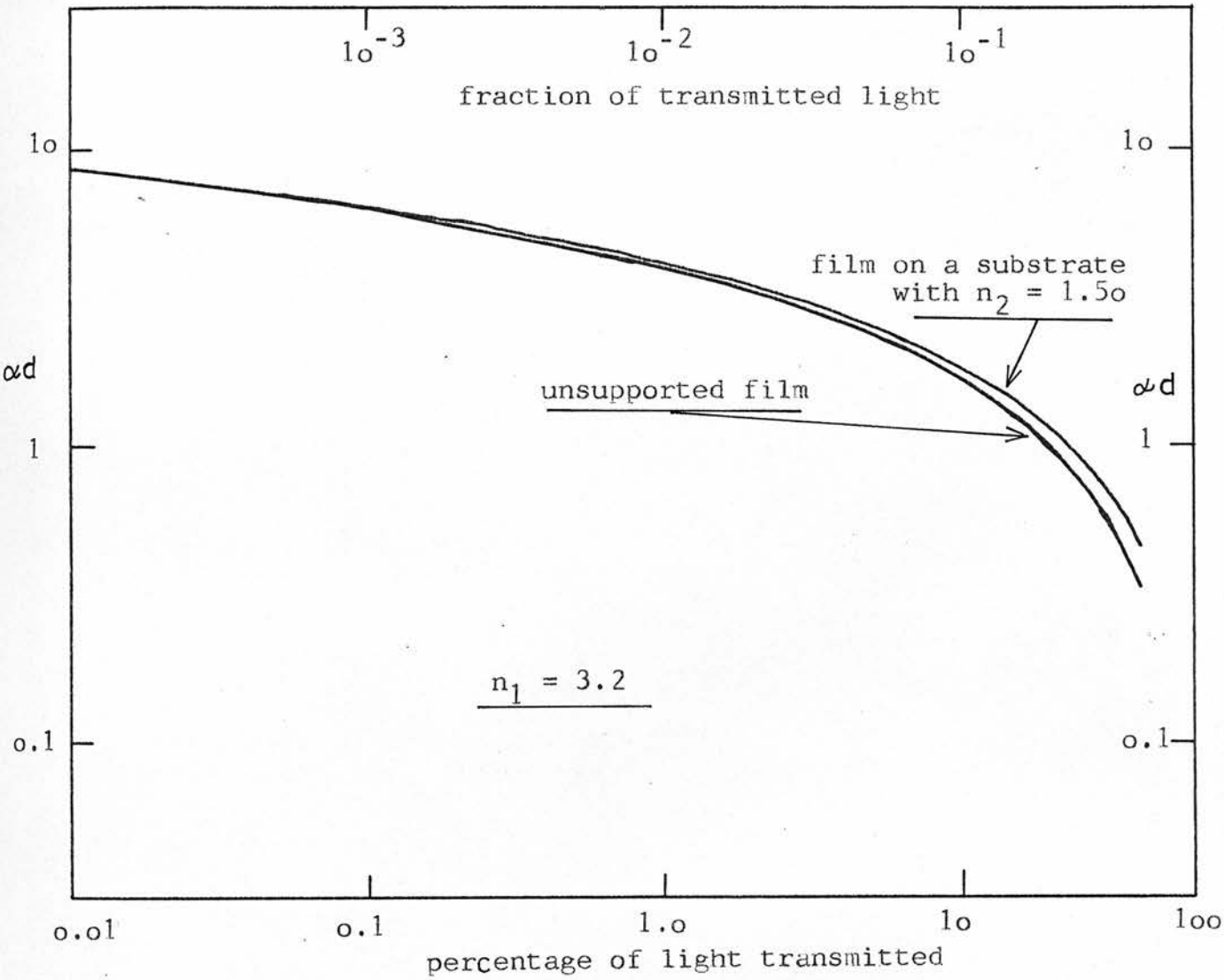

FIGURE 6.2

Calculated calibration curves used to convert transmission data into absorptiance: αd.

if $k \doteq 0$, and

$$\Delta\alpha \cdot d = - \frac{-2k^2}{(n+1)^2 + k^2} \qquad 6.9$$

as the error due to omission of k from the reflection coefficient if n = constant. Furthermore, since interference effects become significant for $T > 0.15$ and accurate measurements of transmission were only possible for $T > 1.0 \times 10^{-4}$, it follows from equation 6.4, again neglecting the second term in the denominator, that

$$2 \ln(1-R) - \ln 10^{-4} \geqslant \alpha d \geqslant 2 \ln(1-R) - \ln 0.15$$

For the values used, n = 3.2 and R = 0.27 this gives

$$8.6 \geqslant \alpha d \geqslant 1.2 \qquad 6.10$$

Combining this result with equation 6.8 gives

$$\left| \frac{\Delta\alpha}{\alpha} \right| \leqslant 1.7 \left| \frac{\Delta n}{n} \right| \left(\frac{n-1}{n+1} \right) \qquad 6.11$$

Since, from equation 6.9, $\Delta\alpha(k) \underset{\sim}{\propto} k^2 \underset{\sim}{\propto} \alpha^2$, it follows that $\left| \frac{\Delta\alpha(k)}{\alpha} \right|$ increases with α and we can use the upper limit in 6.10 to obtain

$$\left| \frac{\Delta\alpha}{\alpha} \right| \leqslant \frac{0.23\ k^2}{(n+1)^2 + k^2} \qquad 6.12$$

The reflectivity of a- As_2Se_3 has been measured by Zallen et al[1]

and that of a-Se by Weiser and Stuke[2]. Taking R = 0.27, ie, n = 3.2 appears to be a good approximation for a-Se but possibly slightly on the low side for a-As_2Se_3. Thus, Main[3] found n = 3.3 - 3.4 near the absorption edge. Since the conversion of transmission to absorption data is rather insensitive to small errors in R, and since the reflectivities of the non-stoichiometric glasses have not been measured it was decided to use n = 3.2 for all compositions. It is estimated that in the small range of energy covered the error is not more than ± 0.2.

Butterfield[4] has measured the refractive index of evaporated As-Se films for lower photon energies and extrapolation of his data supports the above choice for n. Substituting $|\Delta n| = 0.2$ in equation 6.8 and the inequality 6.11 gives

$$|\Delta\alpha| = \frac{0.066}{d} \quad , \text{and} \quad \frac{\Delta\alpha}{\alpha} \leqslant 0.056$$

ie, $\Delta\alpha$, the maximum error in α is constant and is less than 6% of the lowest value of α measured for each sample. For d = 1 μm one obtains $|\Delta\alpha| = 6.6 \times 10^2$ cm^{-1} and less for thicker samples.

The error in α arising from the assumption that $k \doteq 0$ is only important when α is high, ie $\alpha \doteq 10^6$ cm^{-1} and this is when errors arising from Δn are least important. The highest absorption coefficient measured in this work was for an evaporated Se film with $d \doteq 0.20$ μm. In this case $\alpha d = 8.6$ at $\lambda \doteq 0.5$ μm, leading to $k = \frac{\lambda\alpha}{4\pi} \doteq 1.6$. Substitution of this value into equations 6.9 and 6.12 gives $\Delta\alpha \cdot d = -0.26$ and $\frac{\Delta\alpha}{\alpha} = -0.030$, ie, an error of 3%. Thus the corrected value is $\alpha d = 8.3$. In all other cases the

correction is even smaller. It should be mentioned that equations 6.8 and 6.9 are not strictly applicable to samples on a substrate since they were derived from equation 6.4. However, corresponding equations derived from equation 6.3, and involving R_1, R_2, n_1 and n_2 do not lead to significantly different results. This can be seen by considering equation 6.7 which becomes

$$\Delta\alpha \cdot d = -\left(\frac{\Delta R_1}{1-R_1} + \frac{\Delta R_2}{1-R_2} \right)$$

Although $\Delta R_2 > \Delta R_1$ (for $\Delta n_1 = 0.2$) this is offset by the fact that $(1-R_2) > (1-R_1)$ and the second term turns out to be slightly smaller than the first.

6.2.2 REFRACTIVE INDICES IN THE INFRARED

As was mentioned in the last chapter the optical path length through each sample was determined from a plot of fringe order vs wavenumber. This method is based on the condition for constructive (or destructive) interference.

$$\frac{2\, n_m d}{\lambda_m} = m \qquad 6.13$$

where m is an integer for maxima and a half-integer for minima. Assuming that $n = n_i - \beta\lambda$, where β is independent of wavelength, one obtains

$$\frac{2\, n_m d}{\lambda_m} = \frac{2(n_i - \beta\lambda_m)d}{\lambda_m} = \frac{2\, n_i d}{\lambda_m} - 2\beta d = m \qquad 6.14$$

This means that the slope of a m vs $1/\lambda_m$ (or wavenumber) plot only gives $n_i d$, ie, the value of n determined this way is higher than the ture value (since $\beta > 0$). To determine n_m it is necessary to know the absolute value of m, then equation 6.13 can be used directly. The order m could only be assessed unambiguously in the case of relatively thin samples. For these it was indeed found that the refractive index n_m was smaller than n_i; typically the difference was about 10% and an example is shown in Figure 6.3. This difference is not important for the present work, because n_i is simply a parameter required in the determination of sample thickness. Figure 6.4 shows n_i for different compositions, determined by dividing the value of d obtained by direct mechanical measurements, into $n_i d$, the optical path in the wavelength range 1 μm < λ ⩽ 2.5 μm. For each composition the average over three to five samples is given, ie,

$$n_i = \sum_j \frac{(n_i d)_j}{d_j} \qquad 6.15$$

where j runs over all samples of that composition. There is considerable scatter, but no discernible compositional dependence of n_i. It was considered reasonable to use the average value $n_i = 2.80$ for all compositions.

6.2.3 EXTRACTION OF POWER LAWS DESCRIBING INTERBAND ABSORPTION

The empirical laws describing the interband absorption in amorphous materials (equations 2.29 and 2.30 in chapter 2) can be re-arranged as follows

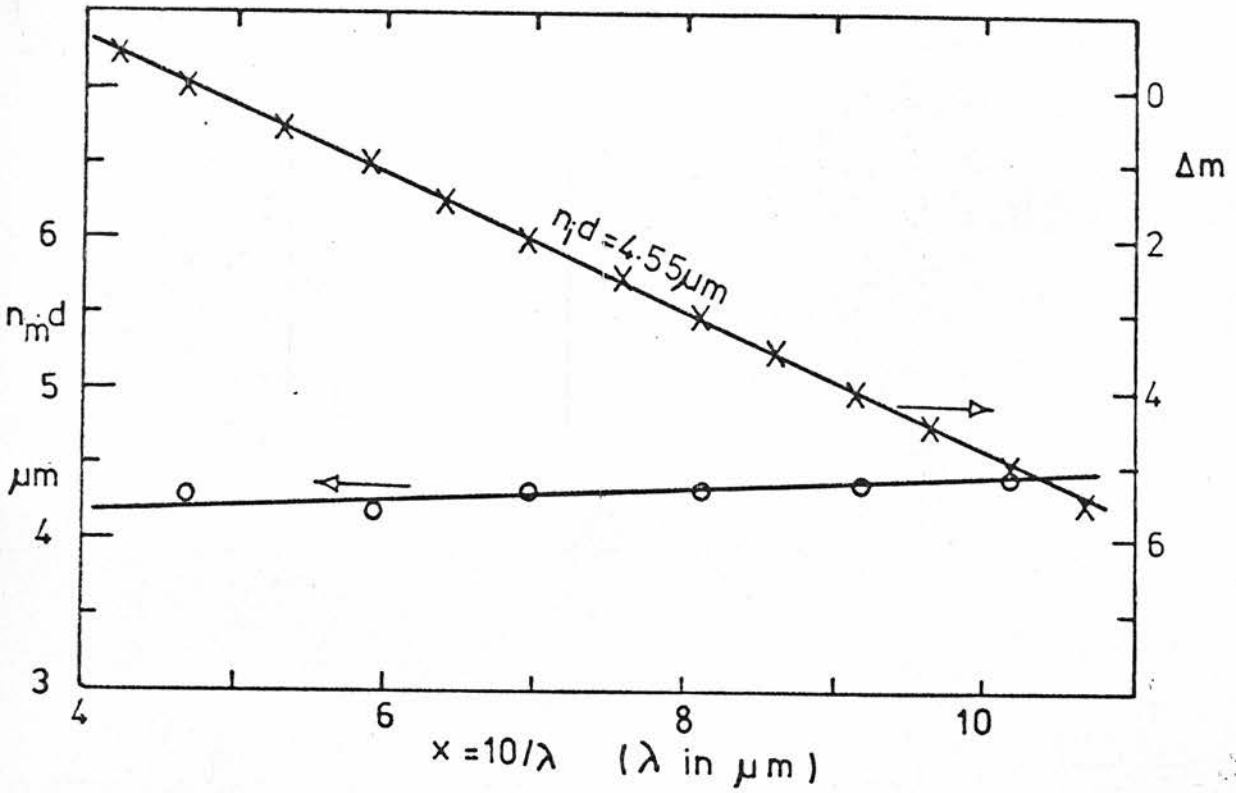

FIGURE 6.3

A plot of the changes in the order m vs the inverse wavelength. The slope gives $n_i d$ (see equation 6.14). The circles show $n_m d$, as determined from equation 6.13 directly.

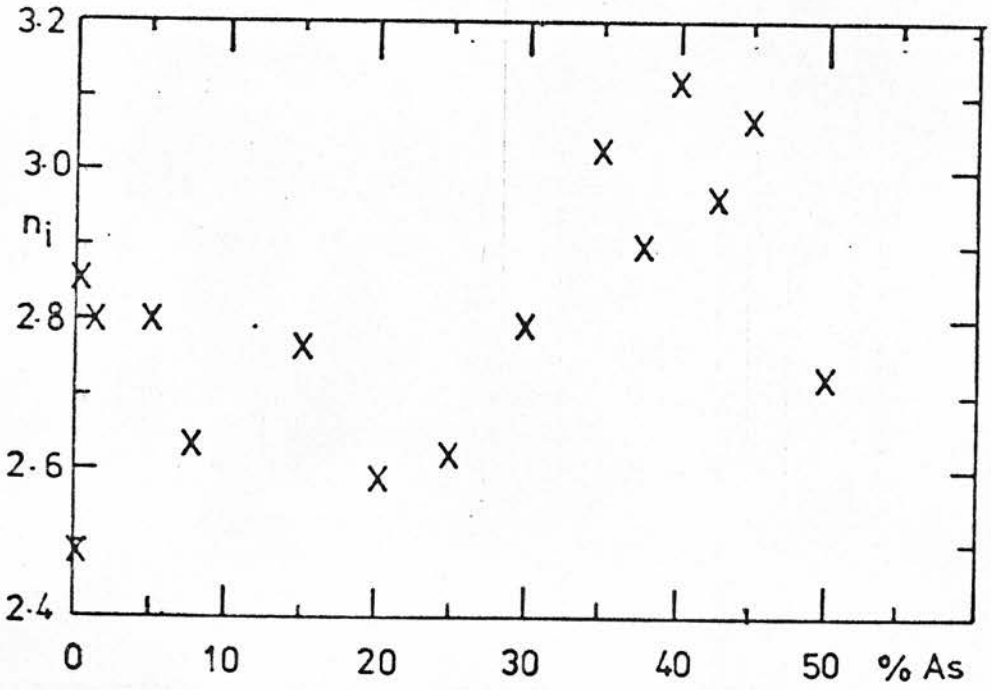

FIGURE 6.4

A plot of n_i vs composition in As-Se bubbles.

$$\alpha x = C_n(x - x_{on})^n$$

where x = wave number = $h\nu/1.24 \times 10^{-4}$ eV-cm and n = 1,2.
Multiplying through by the sample thickness gives

$$(\alpha d \cdot x)^{1/n} = (C_n d)^{1/n}(x - x_{on}) \qquad 6.16$$

It was found convenient to use this equation to determine x_{on} and $C_n d$ for each sample. Some examples of this procedure are given in Figures 6.5 and 6.6 for both values of n. For each composition and temperature the values of x_{on} were averaged over the samples measured and the average value multiplied by 1.24×10^{-4} eV-cm to give E_{on}. To determine C_n, the data was normalized with respect to thickness by dividing $n_i d$ into $C_n d$ to give C_n/n_i. Finally, $n_i = 2.80$ was used to obtain C_n. It is, of course, possible to have non-integral power laws, eg, $1 \leqslant n \leqslant 2$, but although slightly better agreement with experimental data for $As_{0.1}Se_{99.9}$ and $As_{1.0}Se_{99.0}$ would probably result from the use of non-integer powers it would decrease the usefulness of the results by increasing the number of adjustable parameters and making comparison with other compositions more difficult.

6.2.4 ASSESSMENT OF ERRORS

The effects of neglecting the contribution of the extinction coefficient to the reflection coefficients have already been shown to be neglegible, and the constant refractive index approximation has also been justified. Other factors can affect the effective

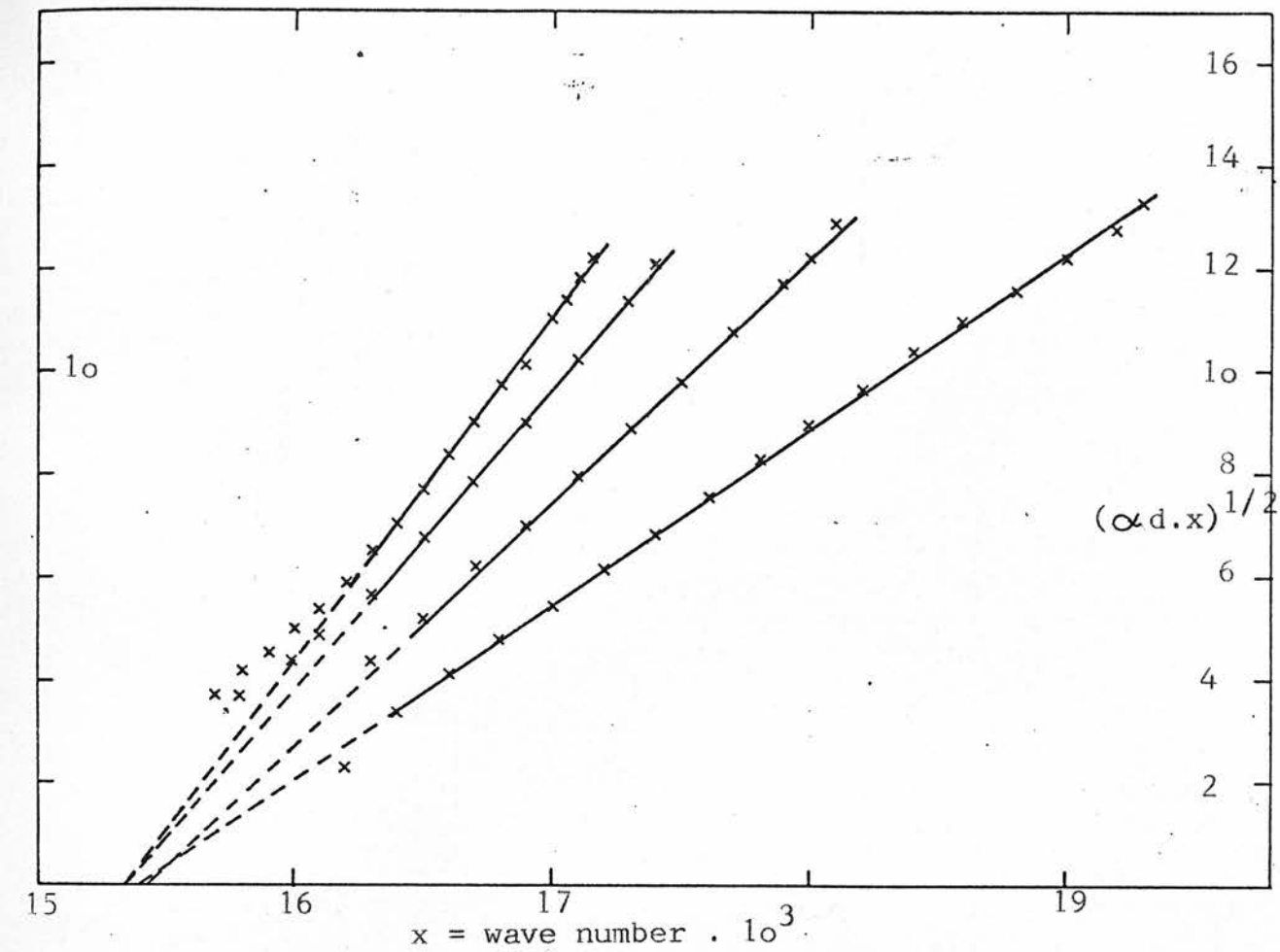

FIGURE 6.5 Method used to work out E_{o2} and C_2 d.

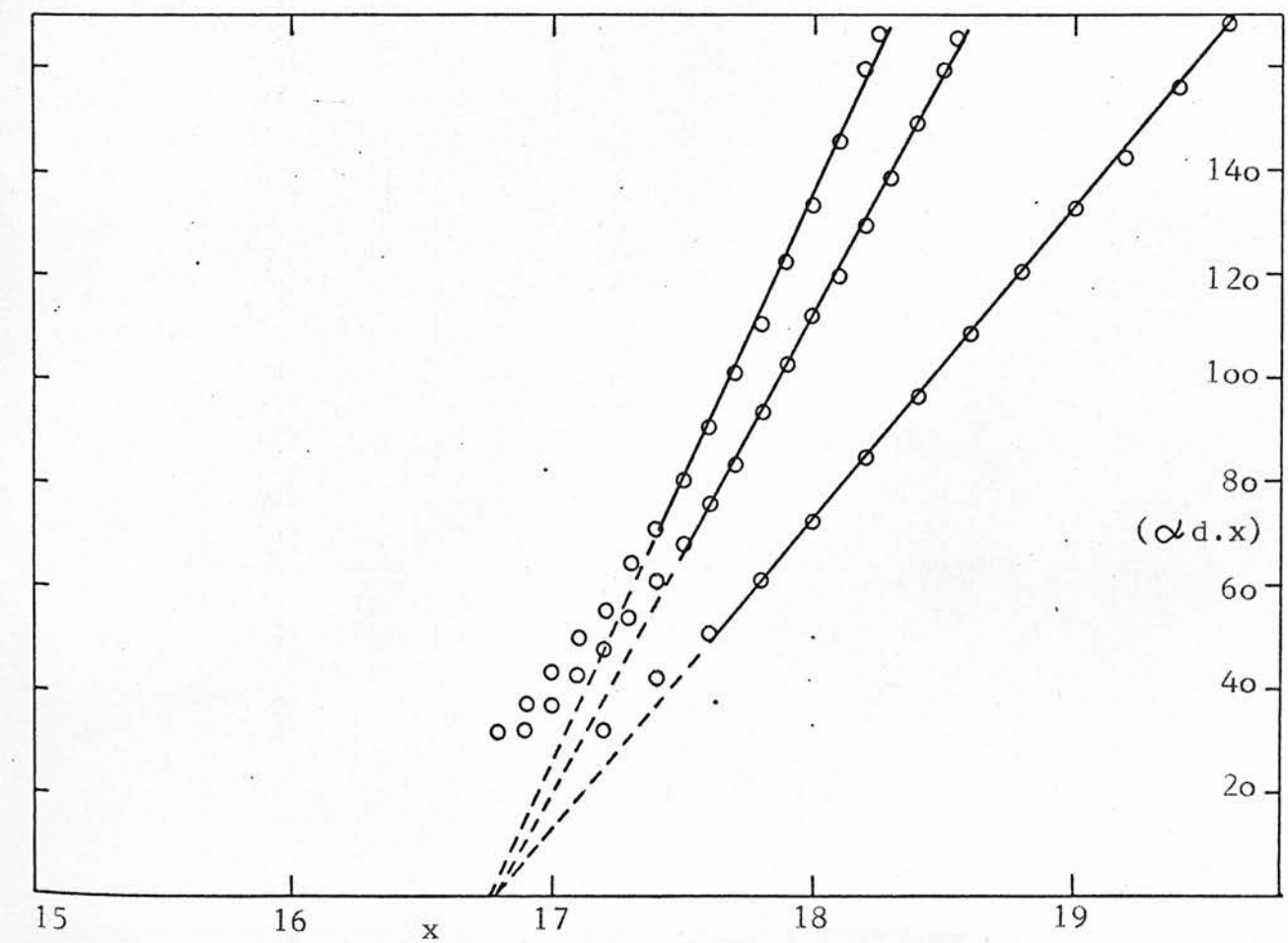

FIGURE 6.6 Method for finding E_{o1} and C_1.

reflection coefficients, however, namely scattering due to sample inhomogeneities and surface irregularities. Many of the blown films had inclusions of thicker regions, usually ridge shaped, which were clearly visible with the naked eye. Some were also wedge shaped. It was easy to select pieces of bubbles which were fairly uniform in thickness and with a negligible fraction of their surface area occupied by visible ridges, eg, less than 2%, but thickness measurements with the Talysurf indicated that even the surface of these was not completely smooth. A comparison of a typical bubble sample with a sputtered sample indicates that the latter has a considerably smoother surface and examples are shown in Figure 6.7. Nevertheless, in spite of these irregularities, the bubbles appear quite smooth, even under a microscope. Moreover, interference fringes are well-developed in the infrared, and it is assumed therefore that scattering is not significant except possibly in the UV. The scattering is expected to be Rayleigh scattering,

$$\text{ie,} \quad \frac{F_s}{F_o} \propto \left(\frac{\lambda_o}{\lambda}\right)^4$$

where F_o and F_s are the numbers of incident and scattered photons respectively, λ_o is the mean size of scatterers and d = wavelength. The consequence of neglecting this effect is an overestimate in α when $\lambda \lesssim \lambda_o$, and therefore one would expect steeper absorption curves if scattering is making a significant but neglected contribution. This is contrary to what is observed; the absorption rises more slowly with photon energy in bubble samples than in sputtered or evaporated films. It is concluded therefore that scattering is not significant in the present experiments.

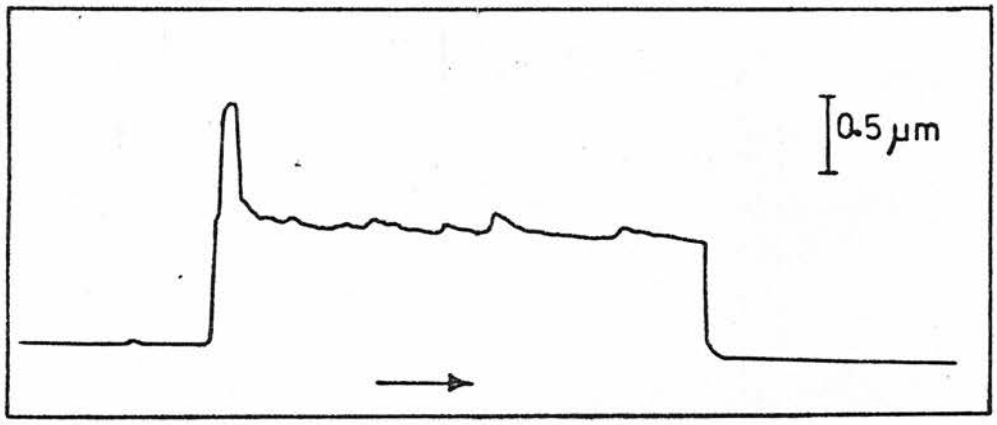

FIGURE 6.7(a)

A Talysurf trace for a bubble ($As_{42.5}Se_{57.5}$), the large peak corresponds to twice the thickness of the bubble.

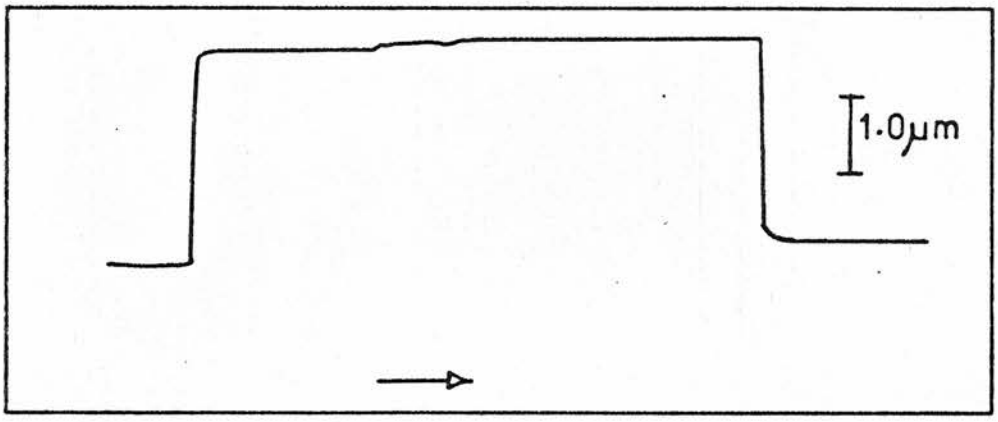

FIGURE 6.7(b)

A Talysurf trace for an RF sputtered film.

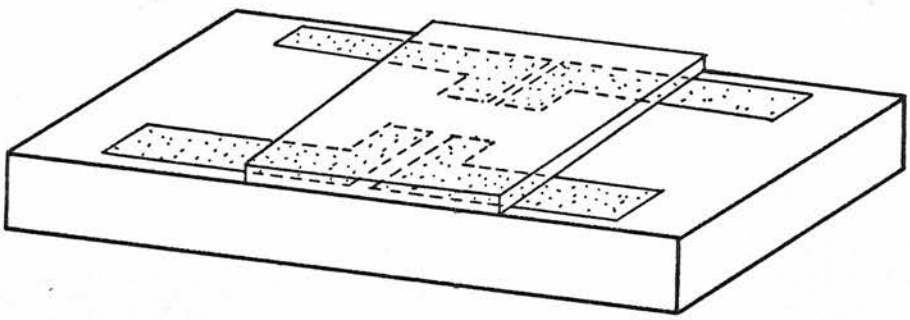

FIGURE 6.8(a)

A Corning 7o59 substrate with electrodes produced by photolithography, and a chalcogenide film deposited on top.

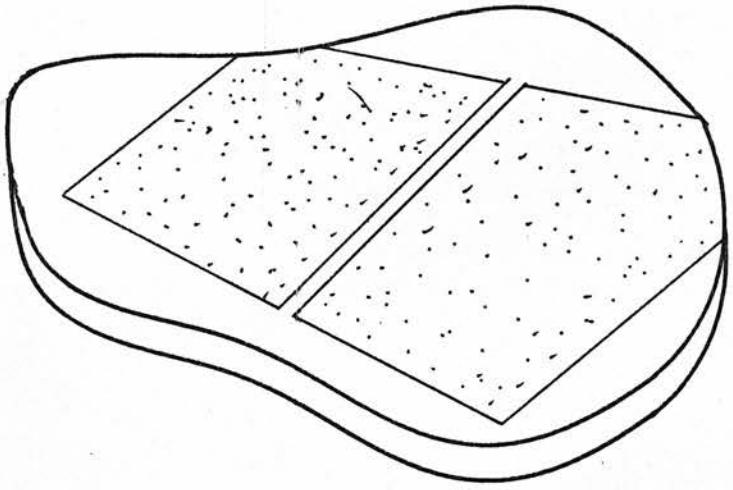

FIGURE 6.8(b)

A hot pressed sample with electrodes deposited afterwards. The gap was produced by stretching a 25μ wire across the sample during the evaporation.

6.3 ANALYSIS OF ELECTRICAL DATA

Figure 6.8 shows the two sample geometries used in this work. Both are coplanar configurations. When RF sputtering was used the films were deposited onto a 7059 substrate with photolithographically produced electrodes (Figure 6.8(a)). For bubbles, hot pressed samples and bulk samples the electrodes were deposited afterwards (Figure 6.8(b)). The two limiting cases that need to be considered are $d \ll l$ and $d \gtrsim l$ ($l \ll w$ always holds), where d, l and w are the sample thickness, electrode spacing and electrode width respectively. The first case is very simple since the field distribution can be assumed to be uniform and fringe fields neglected, thus

$$\sigma = \frac{l}{wd} \frac{I_d}{V} \qquad 6.17$$

where I_d is the dark current. For thicker samples ($d \gtrsim l$), the field is no longer uniform. Equation 6.17 may still be used, however, if d is replaced by an *effective* thickness, d_{eff}, which is less than the true thickness. No attempt was made to calculate d_{eff}. The purpose of measuring the dark current in thick samples was to find the activation energy (which is not affected by geometry if the sample is uniform in composition), and for use in analysing the photocurrent by subtracting the dark current from the total current under illumination.

It follows from equation 3.47 that the photoconductivity is independent of sample thickness and the absorption constant in the monomolecular region if $\alpha d \gtrsim 1$.

In the present work the photoconductivity was only measured in the bimolecular and low temperature regions. The photoconductivity averaged over the absorption depth is

$$\sigma_{ph} = \frac{l\alpha}{W} \frac{I_{ph}}{V} \qquad 6.18$$

This formula was used for thick samples, neglecting the temperature dependence of α. Because of the lack of detailed knowledge of the quantum efficiency in Cu-doped glass it was not practical to make corrections for the temperature dependence of η and α. It is likely that in the bimolecular region the net correction would lead to a value for the activation energy smaller than the measured value (equation 2.48).

In the low temperature region the situation is even more complicated because the photocurrent vs light flux dependence is not known although it is expected that $I_{ph} \propto F^n$ where $\frac{1}{2} < n \leq 1$.

The case of photomobility is much simpler since recombination effects are unimportant and this has already been discussed in Chapter 3. It follows from equations 3.54 and 3.55 that the simplest case is when $\alpha d \gtrsim 1$, a condition that was reasonably well satisfied in the present work, even for RF sputtered samples. It then follows from equations 3.54 that

$$\mu_d = [e\mathcal{E}w F_o \eta(1-R_1)]^{-1} \cdot \frac{dI}{dt} \qquad 6.19$$

where $\mathcal{E} = V/l$ is the electric field, F_o the incident photon flux (3×10^{16} photons cm^{-2} sec^{-1} in the present work within a factor of 3).

The measurements of Kolomiets et al[5] show that the peak in the photoconductivity spectral response shifts to *higher* energies with Cu-doping. This indicates that the quantum efficiency at the energy used in the present work is probably less than unity and may be dependent on temperature. The lack of direct measurements of η prevents an assessment of the errors introduced by any temperature dependence of η other than to say that the trap depth derived from the activation energy of $\frac{dI}{dt}$ may be larger than actual value. In calculating the mobility it was estimated that

$$\eta(1 - R_1) \triangleq 0.5 \qquad 6.20$$

which corresponds to $\eta \sim 0.7$.

6.4 REFERENCES

1. Zallen, R et al, Phys Rev Lett 26, p 1564, 1971.
2. Weiser, G and Stuke, J, Phys Stat Sol 35, p 747, 1969.
3. Main, C, PhD Thesis, University of Edinburgh, 1974.
4. Butterfield, A W, Thin Solid Films 21, p 287, 1974.
5. Kolomiets, B T et al, J Non-Cryst Sol 5, p 389, 1971.

CHAPTER 7 INTERBAND OPTICAL ABSORPTION IN As-Se GLASSES - RESULTS AND DISCUSSION

7.1 INTRODUCTION

Absorption data of the type described in the previous chapter were obtained for 15 different compositions in the As-Se system, at room temperature and at one or more other temperature, usually in the range 110-120 K. The range of absorption coefficients obtained was typically from below 6×10^3 cm^{-1} to 9×10^4 cm^{-1} and in no case covered less than one decade. The room temperature results on a-Se and a-$As_{40}Se_{60}$ are shown in Figures 7.1 and 7.2 together with results from the literature. The agreement is very close for evaporated Se and RF sputtered $As_{40}Se_{60}$. For films prepared from bubbles a slight shift is observed to higher photon energies for absorption in Se and to lower energies in $As_{40}Se_{60}$. A considerably larger shift is observed for evaporated $As_{43}Se_{57}$ compared to bubbles. This is in good agreement with the behaviour expected from a comparison of virgin and annealed films[1,2,3] as was discussed in section 2.2.7. According to Fritzsche[1] the absorption edge of sputtered or evaporated films of chalcogenide glasses usually lies at lower photon energies than it does in bulk glasses. Similarly, when evaporated tetrahedral films are annealed, the gap shifts to higher photon energies. Notable exceptions from this behaviour are $As_{40}Se_{60}$ and $As_{40}S_{60}$ where the opposite effect occurs. In all cases, according to Fritzsche, annealing of evaporated or sputtered films is reported to shift the edge towards that of the bulk materials.

Thus, it appears that the films prepared from bubbles used in

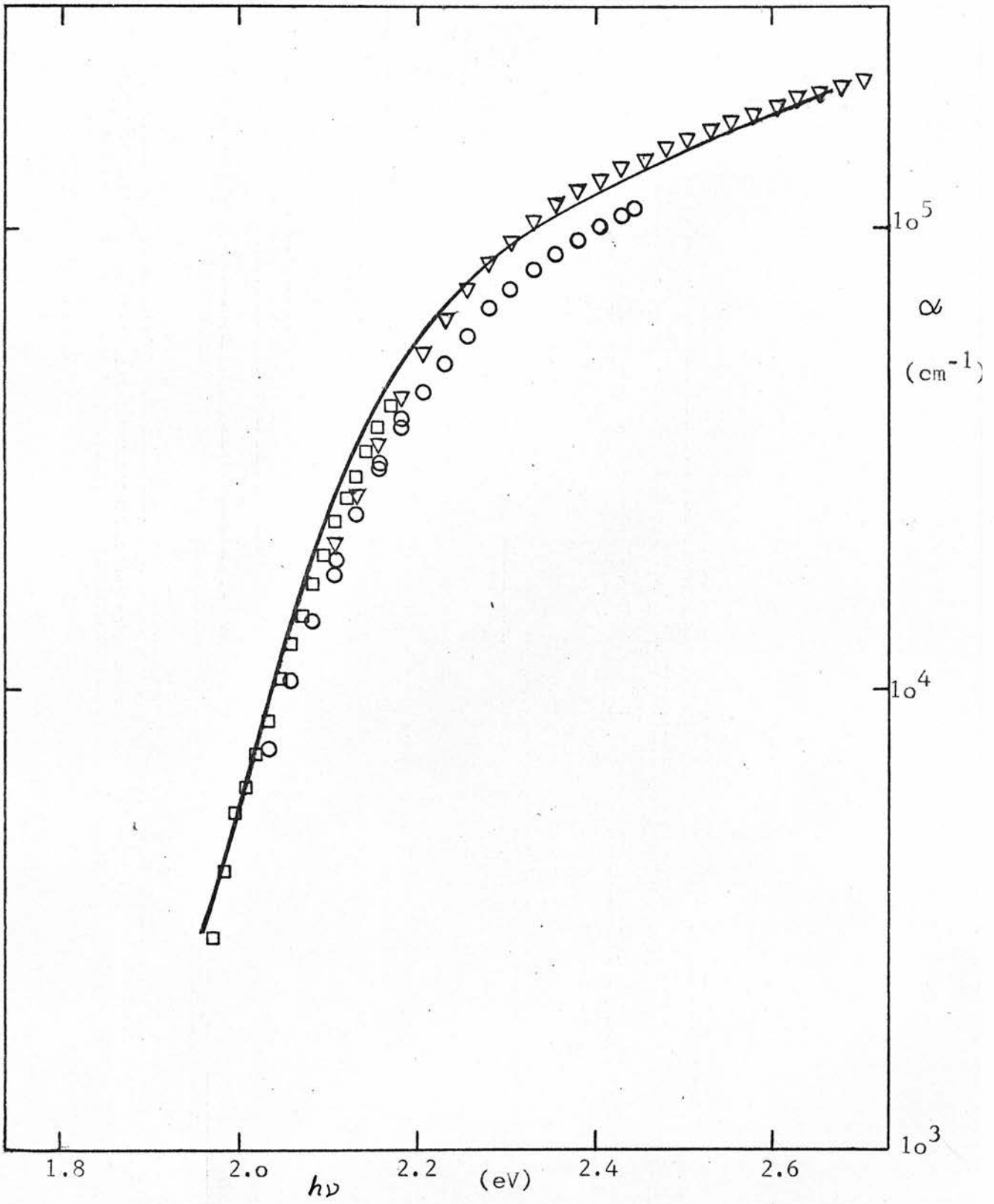

FIGURE 7.1

Log absorption vs photon energy for a-Se:
circles- bubbles at 296K, squares and triangles - evaporated samples at 295K, solid line - Knights & Davis (Ref 17).

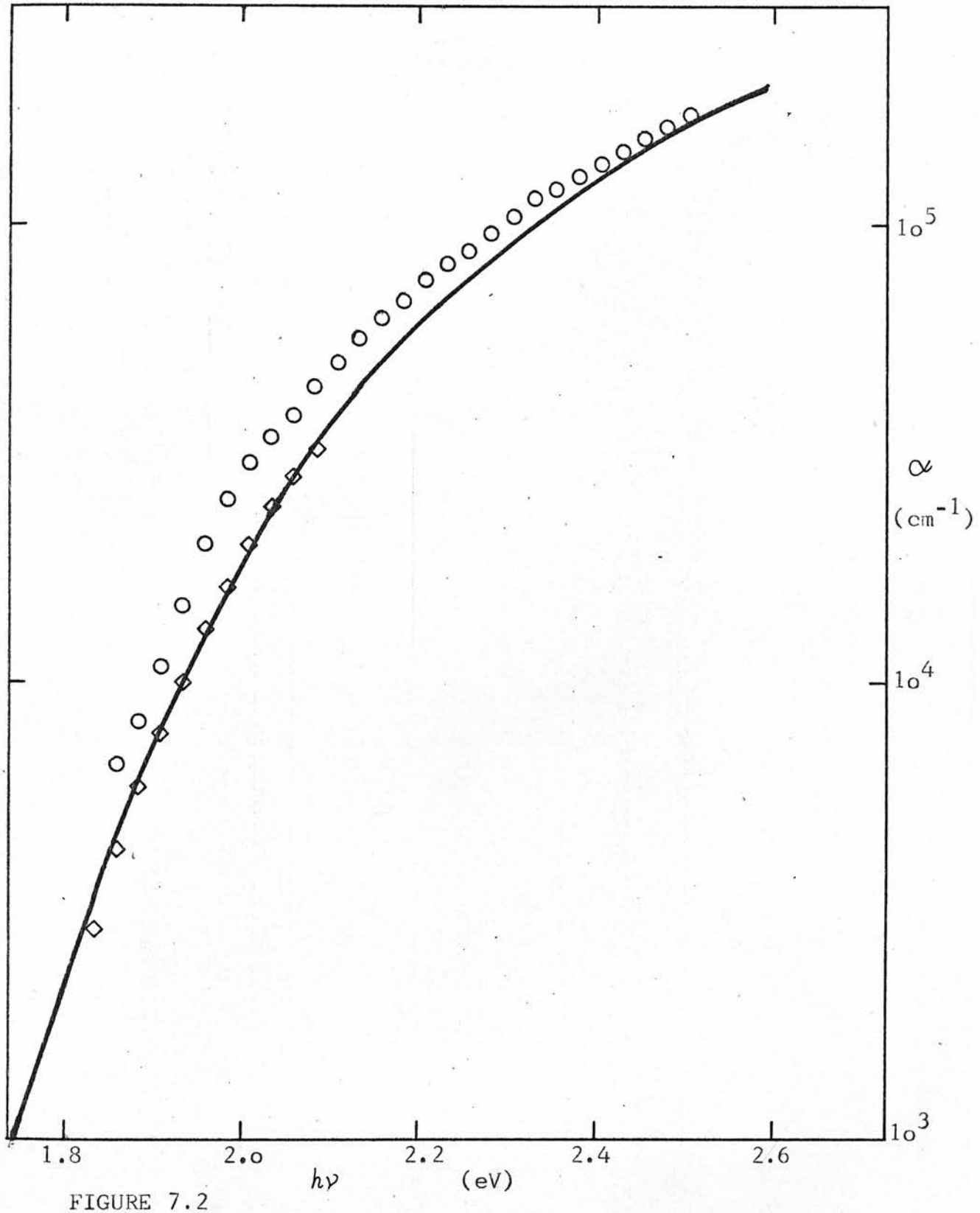

FIGURE 7.2

Log absorption vs photon energy.for a-$As_{40}Se_{60}$,

circles - bubbles

diamonds - RF sputtered film

solid line - Felty & Myers (Ref 34).

this study are close to bulk vitreous materials in their optical properties. This is consistent with the preparation method since it is estimated that during the bubble blowing process the material cools from a temperature near its liquidus temperature to well below T_g in 10^{-1} - 10^{-2} sec.

In the rest of this chapter, only typical examples of the various power law plots are included to illustrate specific points or trends but the absorption data for all compositions is tabulated in Appendix A.

7.2 INTERBAND ABSORPTION AND POWER LAWS

7.2.1 GLASSES CONTAINING As

It was found that the square law (equation 2.30) applies to all compositions with 1 - 50% As. Results typical of this region are shown in Figure 7.3 which is a plot of $(\alpha h\nu)^{\frac{1}{2}}$ vs $h\nu$ for $As_{20}Se_{80}$ at four different temperatures. Figure 7.4 is a similar plot for different compositions at room temperature. It is evident that both E_{02} and C_2 depend on composition and temperature. This will be discussed further in later sections. Thick samples of most compositions showed a deviation from the square law at photon energies slightly above E_{02}, which indicates a transition to an exponential form of absorption. For most compositions there was no deviation from the square law at the highest absorption values measured in this study, the exceptions being $As_{25}Se_{75}$ and films with 1% As or less. The solid columns in Figure 7.5 show the range of photon energies for which the square law was shown to hold in this work, as a function of composition. Open columns indicate that no deviation was observed at the highest energies measured and thus the square law is expected to continue to apply.

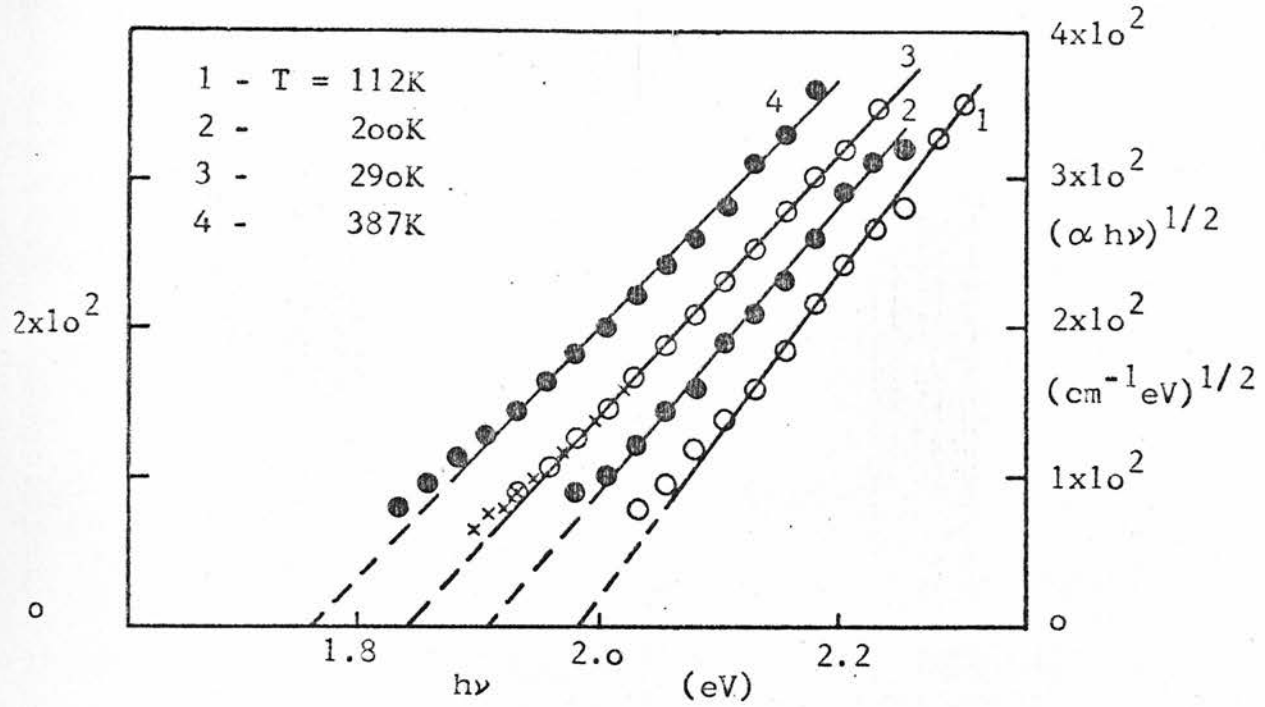

FIGURE 7.3

Absorption in $As_{2o}Se_{8o}$ bubble specimen with temperature as a parameter (square law plot).

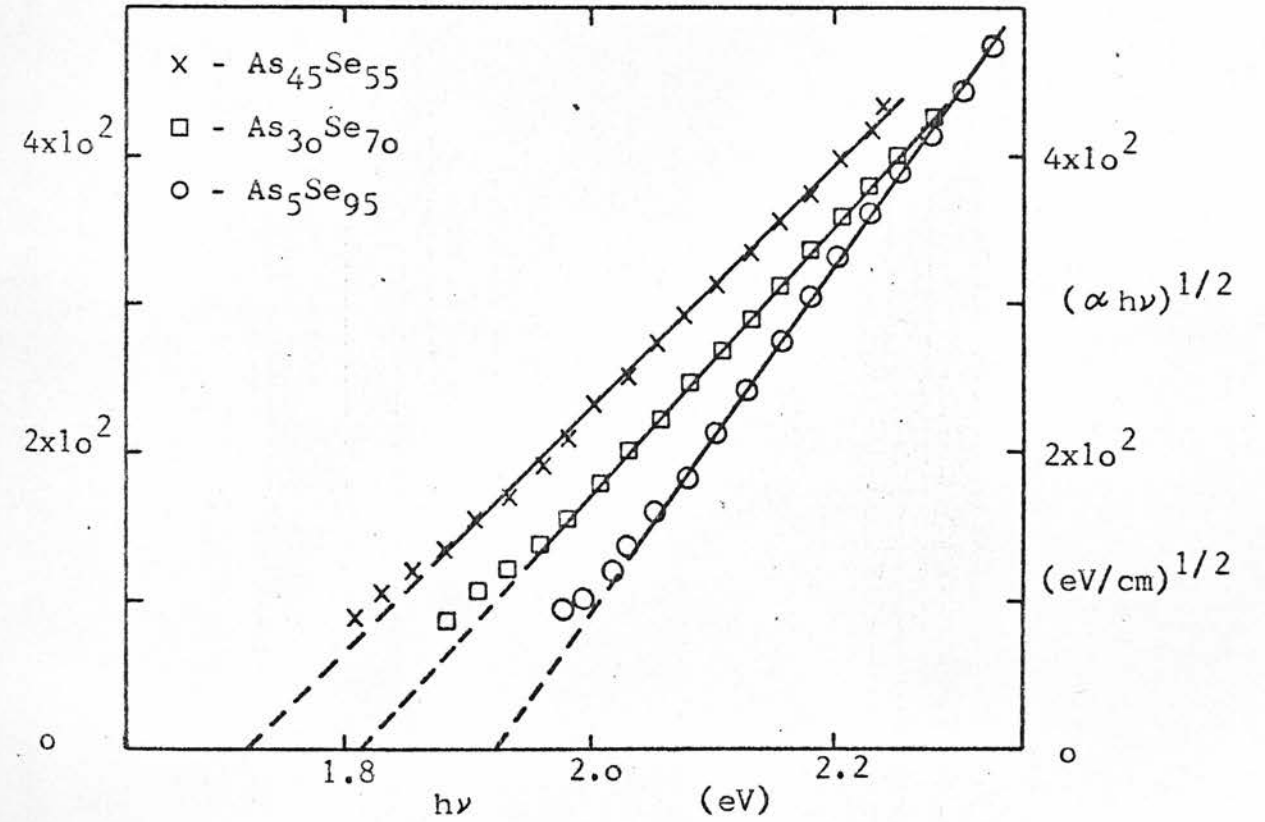

FIGURE 7.4

Square law plots for the absorption of three compositions at room temperature.

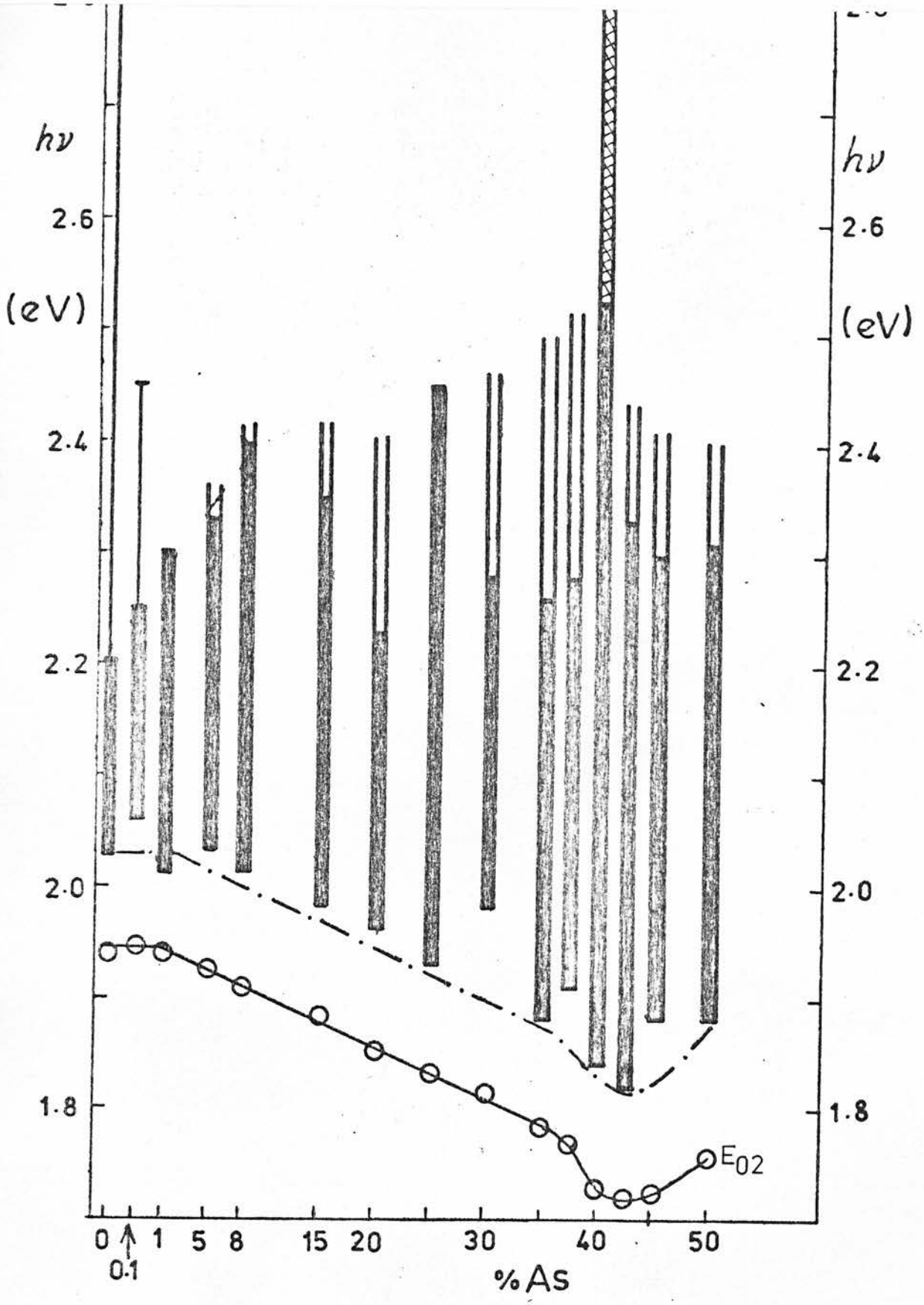

FIGURE 7.5

Histogram showing the photon energy range over which the square law for absorption holds: solid columns represent the present work, open columns expected continuation of the square law region and cross- hatched column the square law observed by Weiser (Ref 4).

Weiser et al[4] found no deviation from a square law for photon energies as high as 3.5 eV in evaporated $As_{40}Se_{60}$. This is indicated by the cross-hatched column. The dot-dash line indicates approximately the energy at which the transition from a square to an exponential law takes place. It is clear that this occurs ~0.1 eV above the E_{02} line which is also shown. Moreover, the upper limit increases with As content and published results[5] show that the square law holds up to at least 2.8 eV in the case of a-As.

7.2.2 SELENIUM

Bubbles of pure Se obey equation 2.29, the linear law, from slightly above the extrapolated gap E_{01} to the highest energy at which the absorption could be measured (2.4 eV). For evaporated Se the absorption curve follows the linear law up to ~2.9 eV and as Figure 7.6 shows becomes slightly superlinear at higher energies. Davis[6] found similar behaviour with superlinearity starting at 3.2 eV. Bubbles of $As_{0.1}Se_{99.9}$ also obey a linear law but over a more limited range of photon energies (~2.2 eV - 2.45 eV). The extent of the linear fit is indicated in Figure 7.5 by the solid lines.

Data for both these compositions can be fitted to a square law over a narrow range between the linear and the exponential regimes. Such an exercise would not be of much value were it not for the fact that the values of E_{02} and C_2 so obtained agree very closely with those extrapolated from glasses with higher As concentrations. Figure 7.7 gives a comparison of a linear and a square law plot of the same data (evaporated Se). The extrapolated gaps E_{02} and E_{01} occur at 1.94 eV and 2.08 eV respectively in bubbles and 0.02 eV

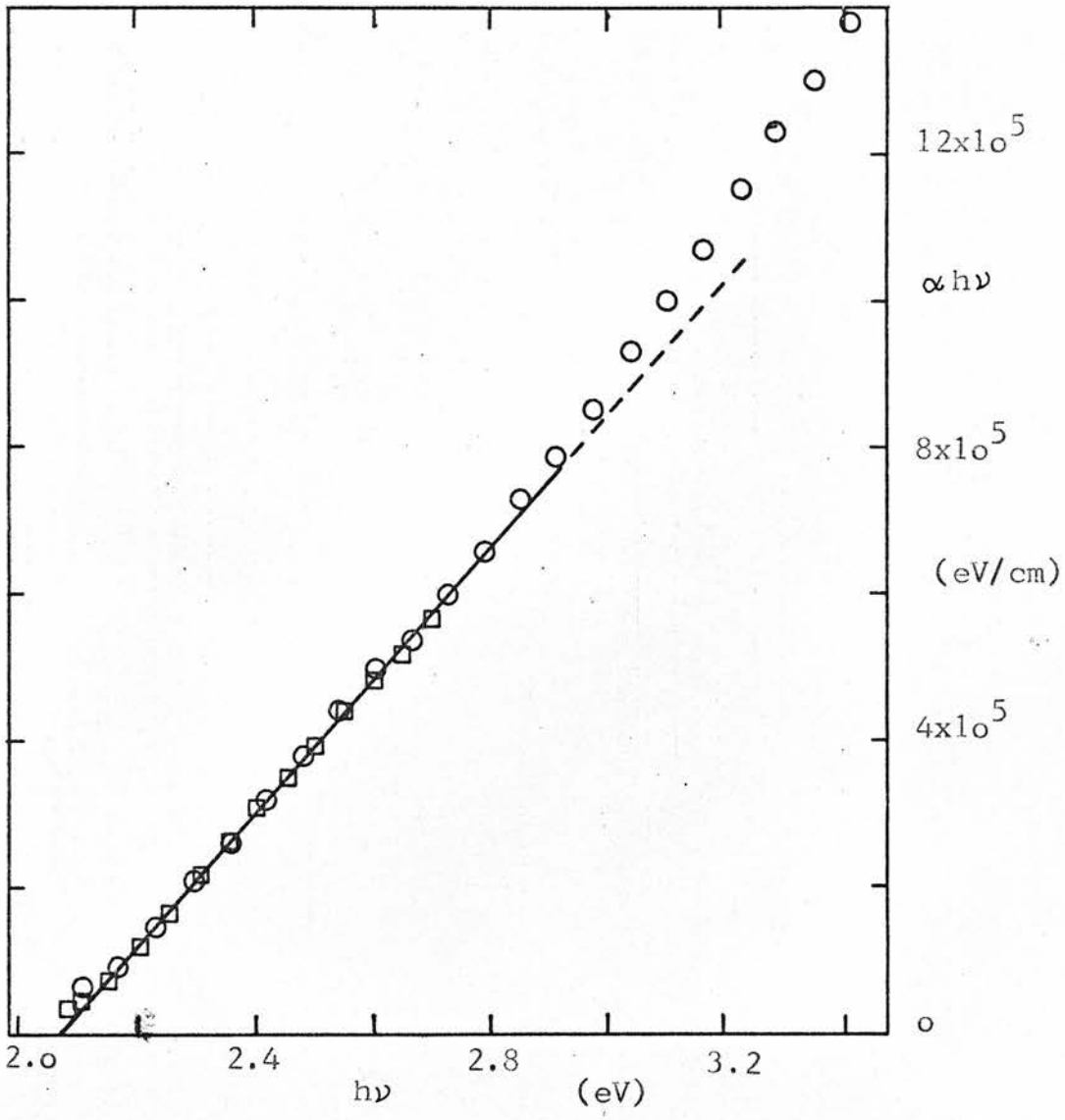

FIGURE 7.6

Optical absorption in thin films of evaporated Se on a linear law plot (room temperature).

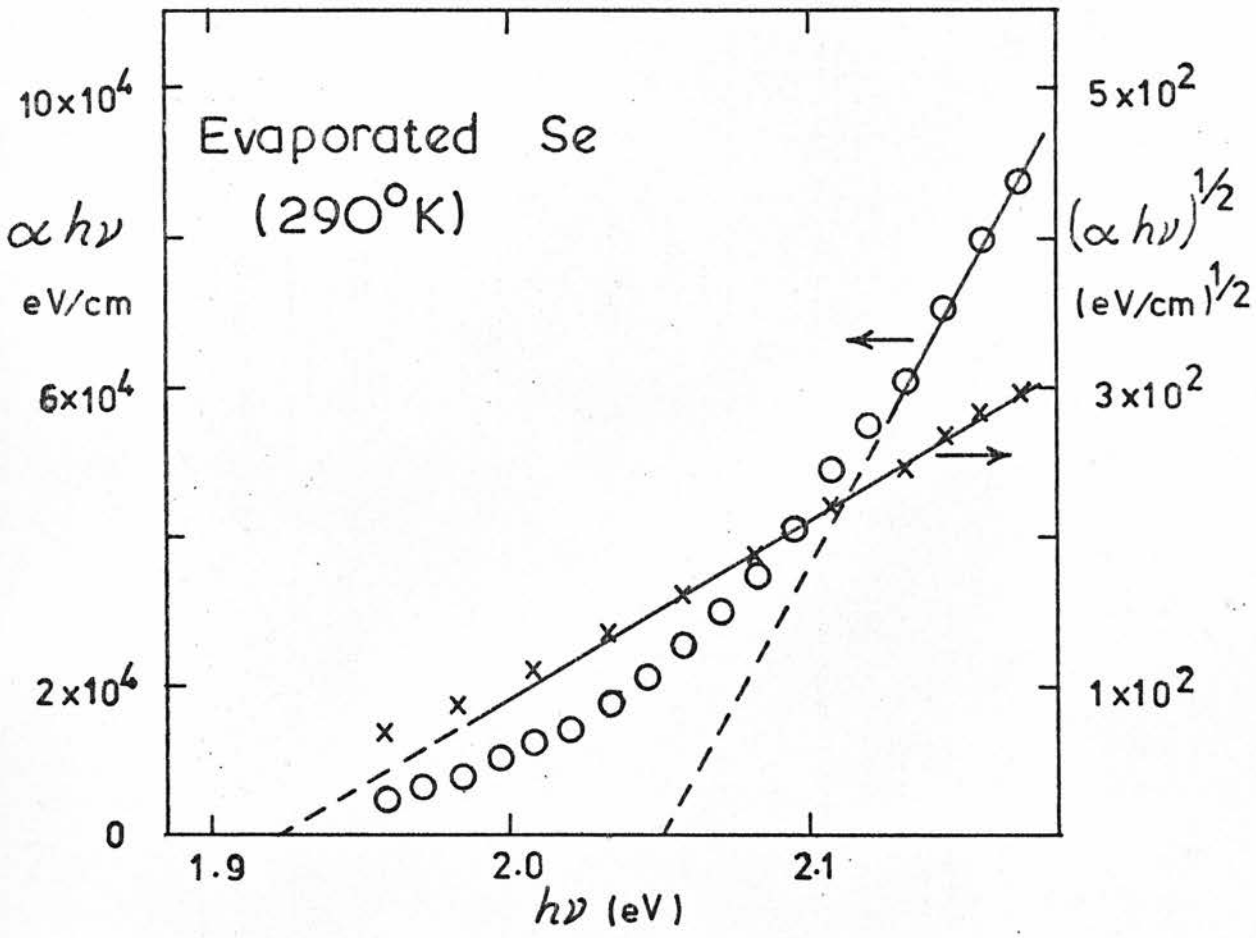

FIGURE 7.7

Absorption results for evaporated Se , a square-law plot gives better fit at low energies.

lower in energy in evaporated Se (a difference which is in agreement with the observations at the beginning of this chapter). It is interesting that these energies correspond closely to the energies at which Sussman et al[7] observed a kink and a maximum respectively in the electroabsorption spectrum for a-Se, as was discussed in section 2.4.2 and shown in Figure 2.20. It seems likely therefore that there is a relation between these results. If so then the maximum in the electroabsorption at 2 eV should disappear with the addition of 1% As and the electroabsorption should follow the dashed line in Figure 2.20.

In the linear region the absorption is *less* than an extraplation from the square law region would indicate, ie, it is as if part of the absorption is suppressed in Se compared to glasses with a few percent As.

7.3 THE OPTICAL GAP

7.3.1 VARIATION WITH COMPOSITION

Figure 7.8 shows the 'gap' E_{02} vs composition at room temperature, and extrapolated to absolute zero. E_{02} decreases linearly with increasing As content up to nearly 40% As and has a minimum at Ca 43% As. Each circle in Figure 7.8 represents an average of 3 - 5 and and each x and average of 2 - 4 bubbles. The different values of E_{02} for sputtered and especially for evaporated films are also included in Figure 7.8 as well as E_{01} for pure and slightly doped (0.1%) As. E_{02} is again plotted in Figure 7.9 together with several 'equiabsorption lines'. It is clear that the E_{02} curve, which is of course an extrapolated zero absorption line, follows very closely in shape the lines for $\alpha \leqslant 10^4$ cm^{-1}. The levelling-off shown by the high absorption

lines towards the Se end of the diagram is simply a reflection of the high values of C_2 for those compositions. Figure 7.9 includes some results on 'hot-pressed' samples obtained by Hurst[8] and the agreement with the present work is excellent. This supports the contention that the bubbles are close to bulk materials in their optical properties.

It is interesting to consider the above results in relation to arsenic-chalcogenides in general. Figure 7.10 again reproduces E_{02} for bubbles of As-Se glasses and includes results from the literature on E_{02} in $As_{70}Se_{30}$ [9], As [5], and the system As-S [11]; it also shows the photon energy corresponding to $\alpha = 10^2$ cm^{-1} for some of the above materials[12] and for As-Te films[13]. The broken lines represent the interpolations thought to reflect the most likely behaviour for intermediate compositions. There must be a maximum in the E_{02} curve for As-Se between 50 and 70% As, here put tentatively at 57% on account of the minimum in density at that composition[14]. In the As-Te system the optical gap is expected to vary approximately linearly throughout the composition range since there are no signs of extrema in the optical and electrical gaps, nor in T_g and other structural properties near stoichiometry or any other composition. The extrapolated ($\alpha = 10^2$ cm^{-1}) curve agrees well with the measured values for a-As. The As-S system on the other hand probably behaves similarly to the As-Se system because both have extrema in T_g and several other properties near stoichiometry. As was discussed in Chapter 4, the two systems have significantly different phase diagrams on the As-rich side and therefore there may well be two maxima in E_{02} in the As-S system, reflecting the two minima in the liquidus.

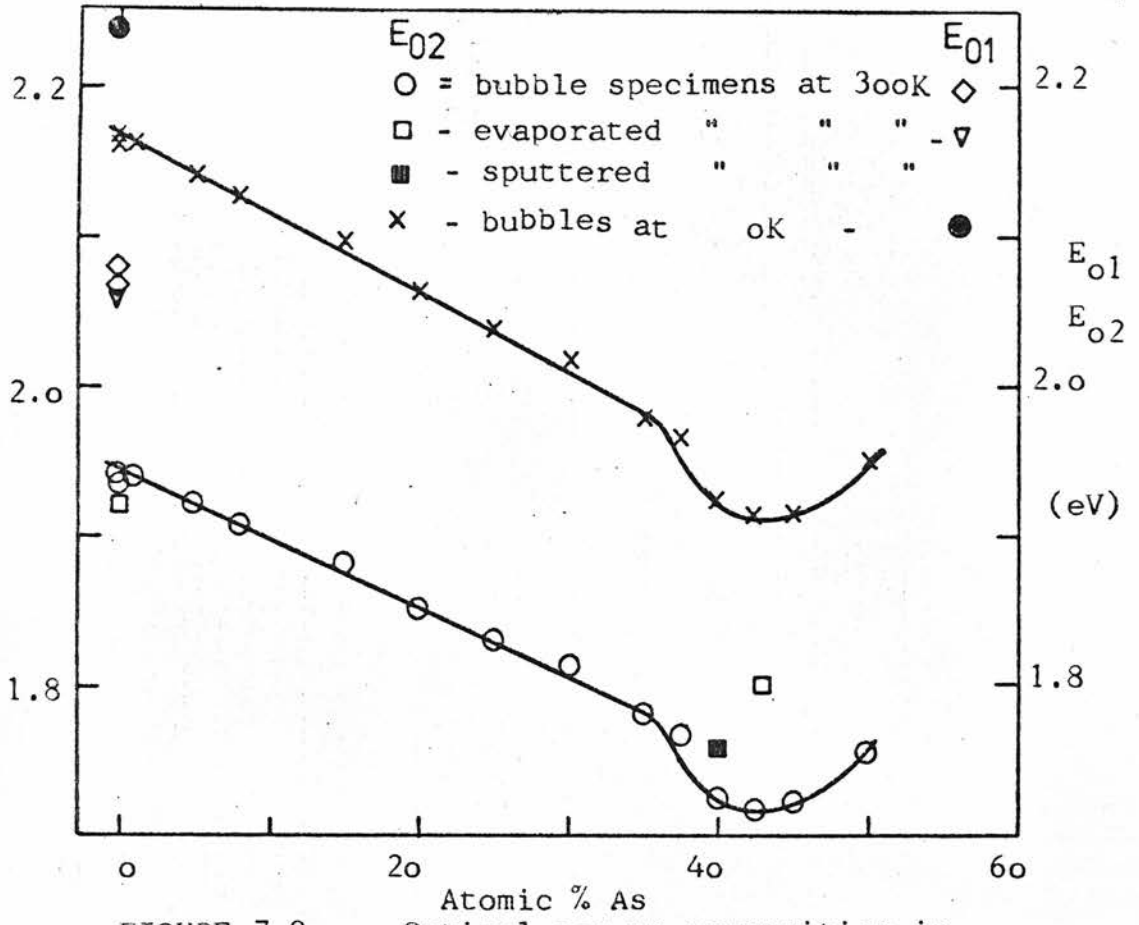

FIGURE 7.8 Optical gap vs composition in the As-Se system at 3ooK and extrapolated to oK.

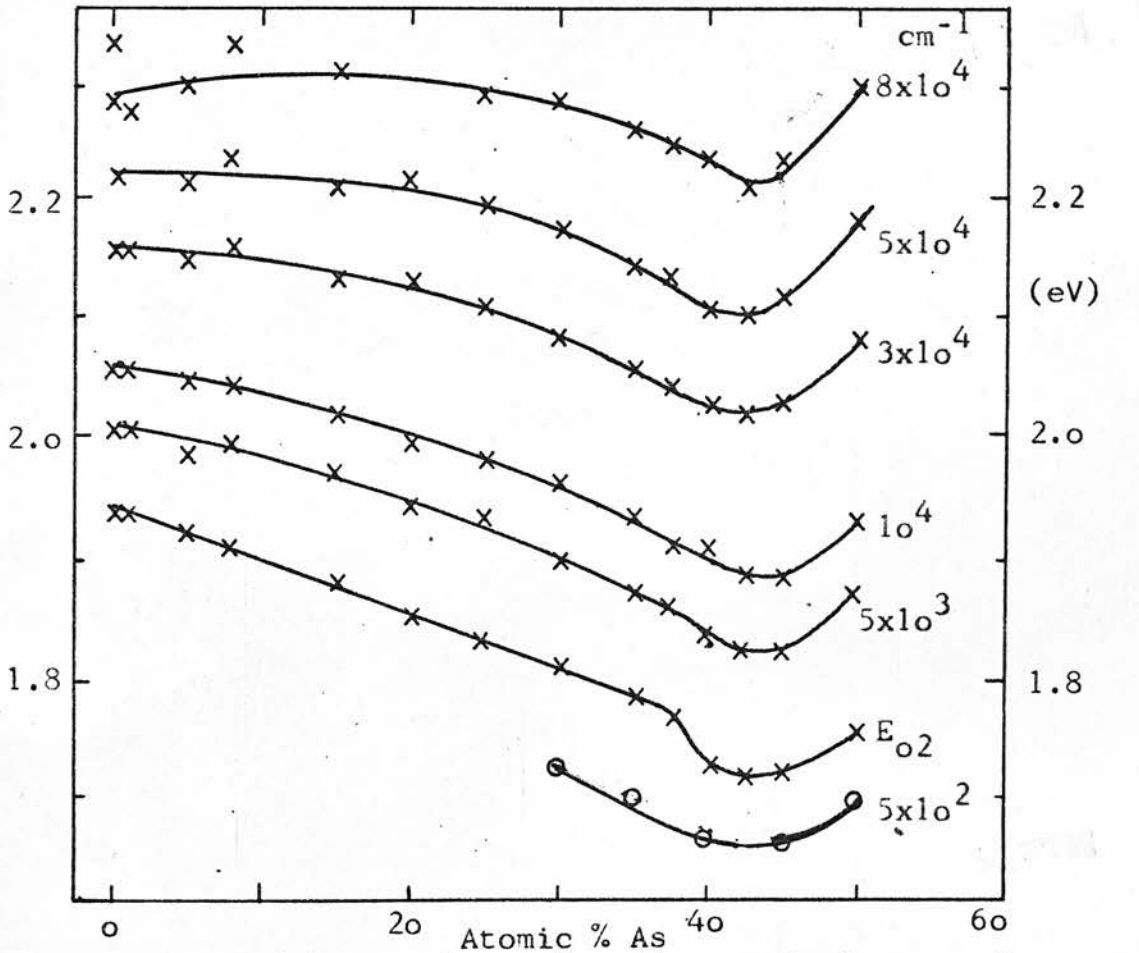

FIGURE 7.9 Equiabsorption lines, circles are from Hurst (Ref 8).

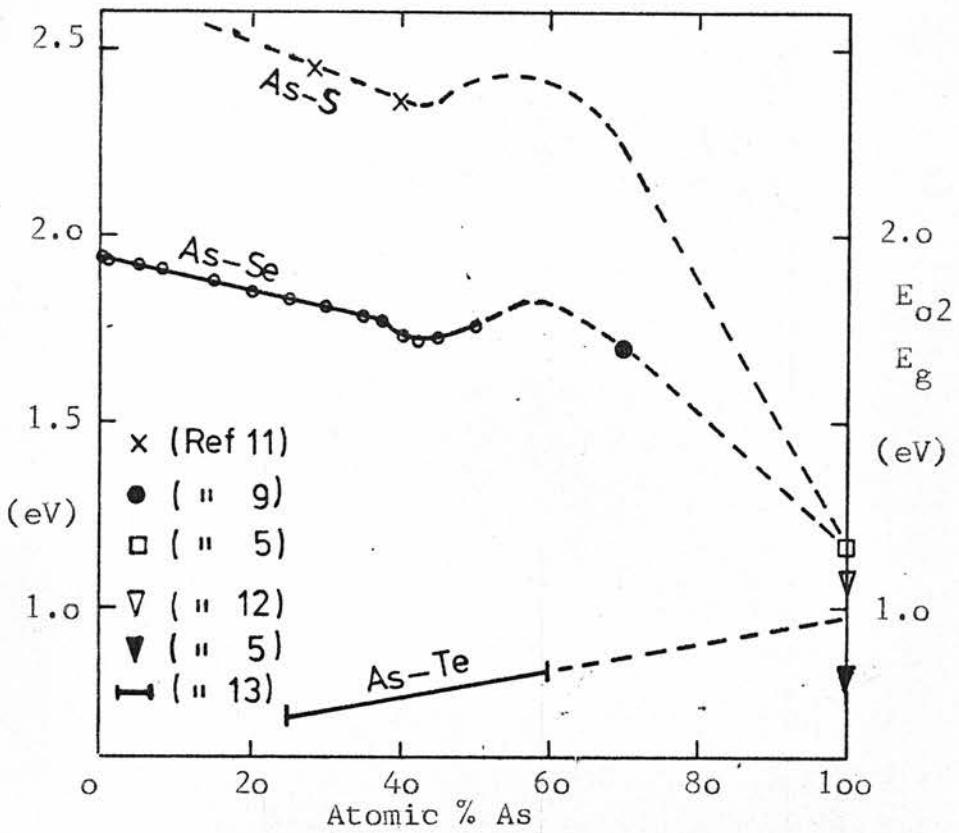

FIGURE 7.1o Present results on E_{o2} in As-Se glasses combined with other results to predict the compositional dependence of the gap in arsenic-chalcogenide glasses. Triangles and the As-Te results refer to E_g at $\alpha = 1oocm^{-1}$.

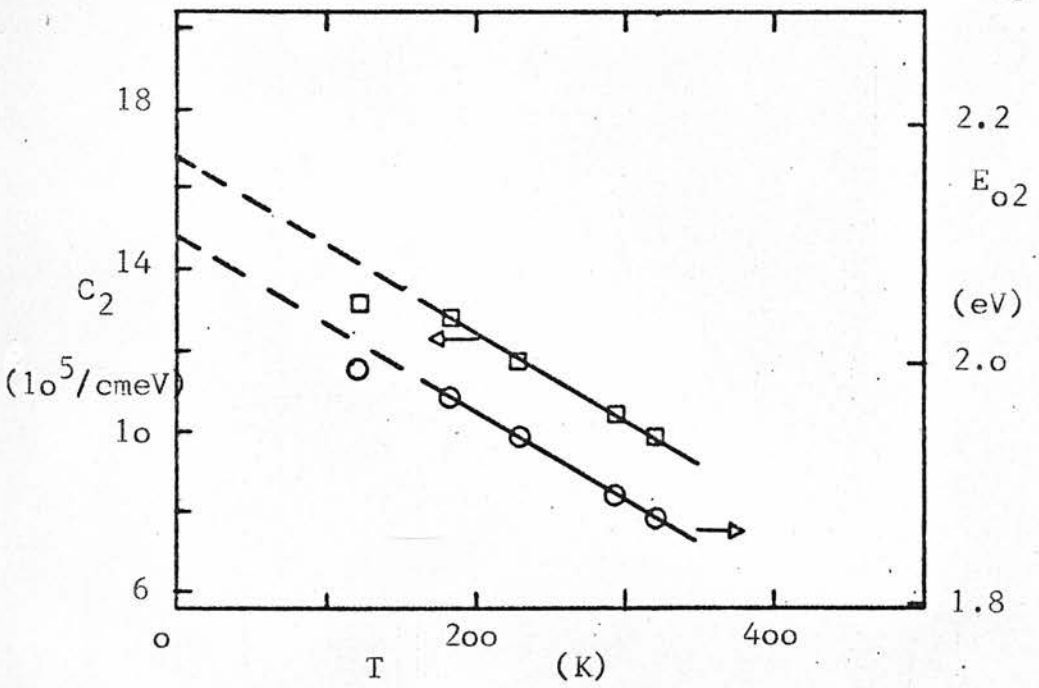

FIGURE 7.11

E_{o2} and C_2 as a function of temperature in $As_{15}Se_{85}$ bubbles.

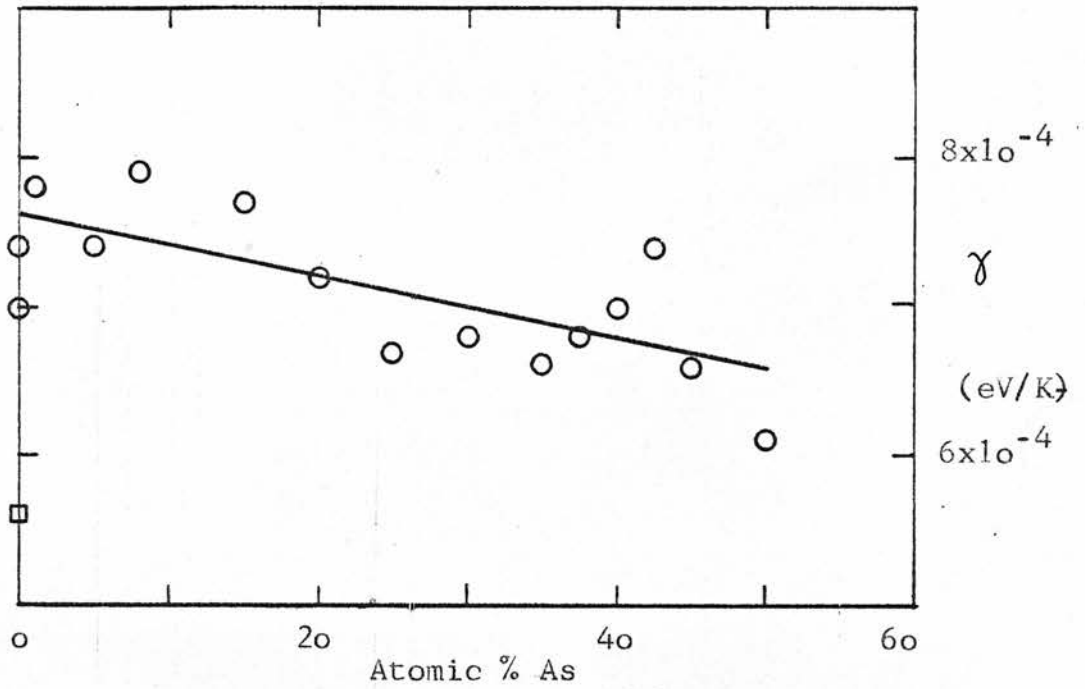

FIGURE 7.12(a)

The temperature coefficient of the gap E_{o2} (circles) as a function of composition. The temperature coefficient of E_{o1} in Se bubbles is also shown (square).

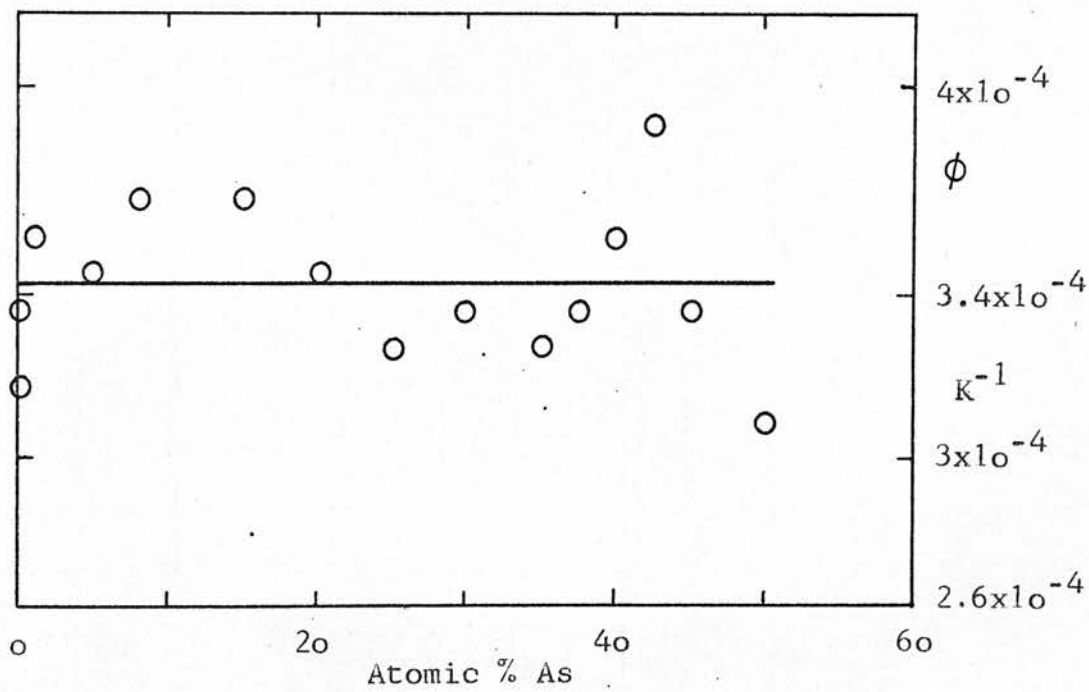

FIGURE 7.12(b)

The normalized temperature coefficient ϕ as a function of composition.

7.3.2 VARIATION WITH TEMPERATURE

The variation of E_{02} with temperature in $As_{15}Se_{85}$ is shown in Figure 7.11 (circles) and is typical of all compositions. E_{02} varies linearly with T above 150 K but is generally observed to vary more slowly at lower temperatures. The temperature coefficient of E_{02}, γ, varies with composition as illustrated in Figure 7.12(a). There is some indication of a local maximum near 43% As but the errors are too large to be certain. The solid line represents a least squares fit and can be expressed as

$$\overline{\gamma}(x) = (1.00 - 0.26\ x)\ .\ 7.60 \times 10^{-4}\ \text{eV/K} \qquad 7.1$$

where x is the atomic fraction of As.

Because of the uncertainty it is difficult to compare the compositional variation of γ with other properties such as the specific heat, as was suggested in Chapter 2 (equation 2.41). If these two quantities are proportional then γ, as determined here, relates to the average specific heat in the range 120 - 300 K. Referring to Figure 4.16 shows that C_p decreases with increasing As content up to ~40% As and increases thereafter (above 200 K), although only slowly until the As content is more than 50%. Figure 7.12(a) reveals no corresponding upturn in γ. Dividing the smoothed value $\overline{\gamma}$ taken from the line in Figure 7.12(a) by the specific heat per atom[15,16] at 220 K gives the constant 'a' in equation 2.41 as a = -2.64 for pure Se, decreasing slowly to a = -2.38 for $As_{50}Se_{50}$.

Figure 7.12(b) shows the *normalized* temperature coefficient

$$\phi = - \frac{1}{E_{02}(0K)} \left(\frac{\partial E_{02}}{\partial T} \right) \qquad 7.2$$

This time a least square fit gives a line independent of composition, suggesting that for the glasses investigated

$$E_{02}(T) = E_{02}(0) \ (1 - \overline{\phi} \ T) \qquad 7.3$$

where $\overline{\phi} = (3.50 \pm 0.10) \ . \ 10^{-4} \ K^{-1}$, independent of composition. As expected from the different definition of the optical gap the values of γ in the present study are slightly lower than obtained by Hurst[8] who found $\gamma \sim -8.1 \times 10^{-4}$ to -9.5×10^{-4} eV/K in the $As_{30}Se_{70}$-$As_{50}Se_{50}$ system at $\alpha = 500$ cm^{-1}. For pure Se the present value is $\gamma = -7.4 \times 10^{-4}$ eV/K or $\overline{\gamma} = -7.6 \times 10^{-4}$ eV/K. It is interesting that the temperature coefficient of E_{01} is smaller, ie, $\frac{\partial E_{01}}{\partial T} = -5.6 \times 10^{-4}$eV/K, which may indicate(since $E_{01} > E_{02}$) that the electron-phonon interaction decreases away from the band edges. This is consistent with $\frac{\partial C_2}{\partial T}$ being negative. Knights and Davis[17] reported a temperature coefficient $\sim -7 \times 10^{-4}$ eV/K for a-Se.

7.3.3 VARIATION WITH DENSITY

In Figure 7.13 E_{02} at room temperature is plotted vs density as suggested by the similarity in the composition dependence of these two parameters and by equation 2.45. The density data is the same as discussed in Chapter 4 [14,18]. The curve using the density results of Kunugi et al[14] is much closer to a straight line than the one comparing E_{02} to the densities reported by Chernov et al[18]. In

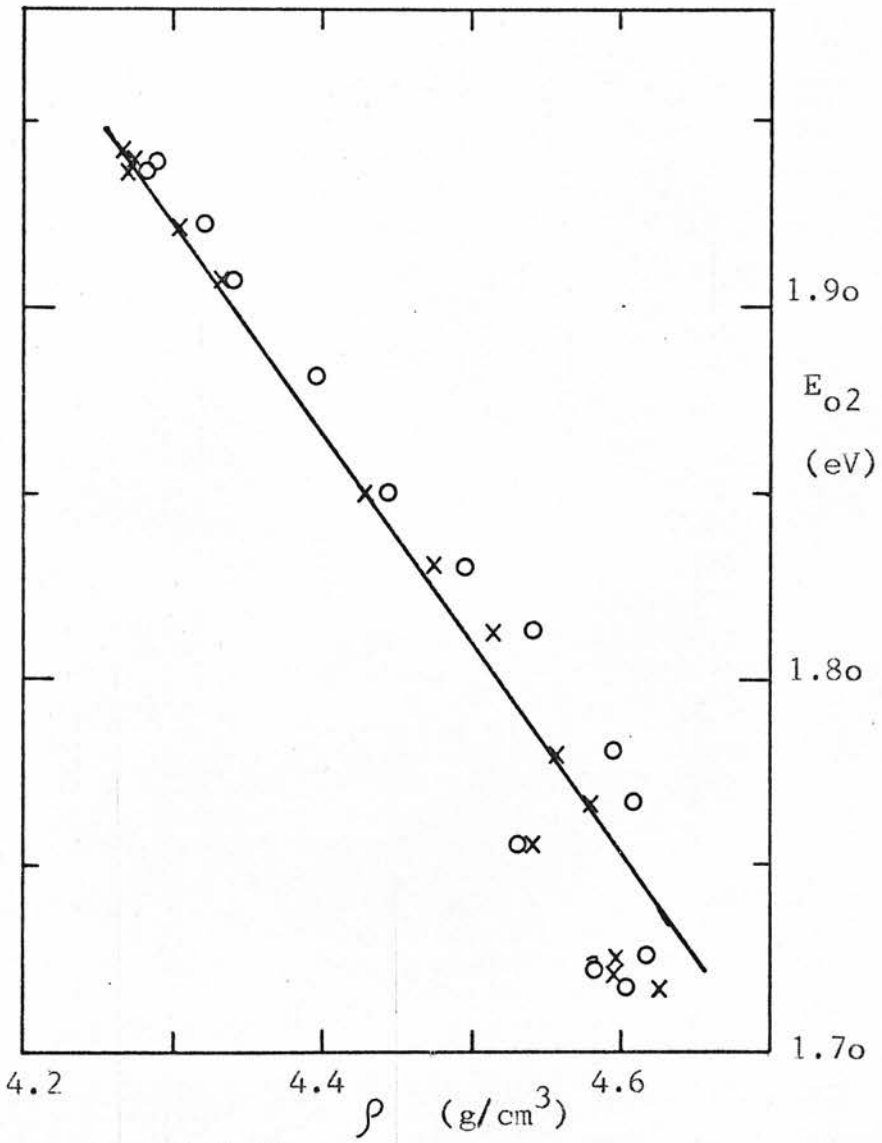

FIGURE 7.13

The gap E_{o2} (this work) in As-Se bubbles plotted vs the density as given by Chernov et al[18] (circles) and Kunugi et al[14] (crosses). The solid line is given by equation 7.4 .

both cases, however, the deviations from a straight line are less than the differences between the two sets of results. Using the results of Kunugi et al[14], therefore, equation 2.45 becomes approximately

$$E_{02} = 4.30 \text{ eV} - 0.55 \rho \text{ eV cm}^3/\text{g} \qquad 7.4$$

The density of a-As is 4.9 - 5.1 g/cm^3 which, when substituted in equation 7.4, gives E_{02} = 1.4 - 1.6 eV for a-As. This value is somewhat higher than observed[5,12]. Equation 7.4 can be differentiated to give

$$\left(\frac{\partial E_{02}}{\partial P} \right)_T = -\delta \rho K \qquad 7.5$$

where $\delta \triangleq 0.55$ eV cm^3/g and K is the isothermal compressibility. This gives -16 x 10^{-6} eV/bar and -24 x 10^{-6} eV/bar as the pressure coefficients of a-$As_{40}Se_{60}$ and a-Se respectively, whereas Kastner[19] reported -(13 $\pm$ 1) x 10^{-6} and -(20 $\pm$ 5) x 10^{-4} eV/bar for these materials. The difference means that δ has probably been over-estimated. Assuming that equation 4.11 relating compressibility and density applies, and neglecting the fact that it refers to the adiabatic rather than the isothermal compressibility, the following expression is obtained

$$\rho^3 \left(\frac{\partial E_{02}}{\partial P} \right)_T = \text{constant} \qquad 7.6$$

Using Kastner's value for the pressure coefficient of a-$As_{40}Se_{60}$ and ρ = 4.62 g/cm^3 [14] gives the constant as -(13 $\pm$ 1) x 10^{-4} eV g^3/bar cm^3.

This in turn gives $\left(\frac{\partial E_{02}}{\partial P}\right)_T = -(17 \pm 2) \times 10^{-6}$ eV/bar for a-Se, a more exact value than obtained by Kastner, provided equation 7.6 is valid. It should also be noted that, at least in the range 0 - 35% As, a compression of a-Se to the same density as any particular composition reduces the gap of a-Se to approximately the same value as for that composition.

The errors that arise when comparing results from differently prepared samples in different laboratories, make it difficult to conclude from the above analysis, whether or not density and the optical gap are linearly related in the As-Se system. It must, however, be considered very probable, bearing in mind Kastner's analysis of $\left(\frac{\partial E_g}{\partial P}\right)_T$ and $\left(\frac{\partial n}{\partial P}\right)_T$ in amorphous semiconductors and the observation by Arai et al (20, 21) of a relation of a similar kind for conductivity. Furthermore, there must be a local maximum in E_{02} in the range 50 - 70% As and Kunugi et al[14] observed a minimum in ρ at 57% As.

7.3.4 COMPARISON WITH d.c. CONDUCTIVITY

Figure 7.14 is a plot of the activation energy of the d.c. conductivity vs composition as measured by Fisher et al[22], taking the zero energy to be at the Fermi level, ie, $E_\sigma = -E_v$. Also shown is $E_{02}(0K) - E_\sigma$, the difference between the gap E_{02} at 0K and E_σ. This quantity is shown to decrease linearly with increasing As content in the composition range in question. It should be mentioned that in obtaining $E_{02}(0K)$ the smoothed values of γ were used. The values of E_σ, $E_{02}(0K)$ and their ratio are given in Table 7.1.

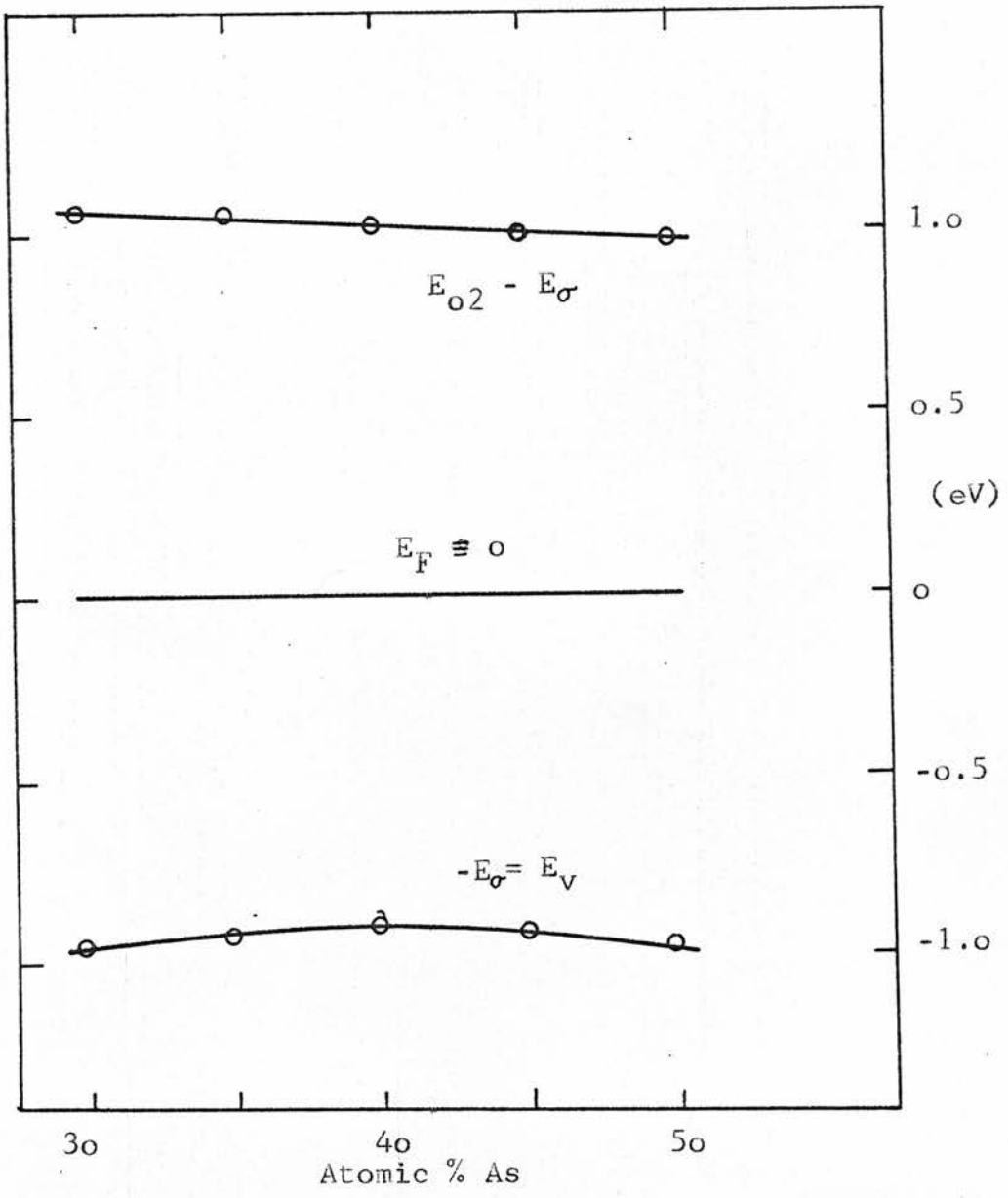

FIGURE 7.14

Comparison between the conductivity activation energy E_σ as measured by Fisher et al[22], and the optical gap E_{o2} (extrapolated to oK). The zero energy is taken at the Fermi level. E_{o2} is the difference between the top and bottom curves.

	$As_{30}Se_{70}$	$As_{35}Se_{65}$	$As_{40}Se_{60}$	$As_{45}Se_{55}$	$As_{50}Se_{50}$
$E_\sigma(22)$	0.963 eV	0.933 eV	0.910 eV	0.925 eV	0.968 eV
$E_{02}(0K)$	2.019 eV	1.980 eV	1.925 eV	1.916 eV	1.950 eV
E_σ/E_{02}	0.48	0.47	0.47	0.48	0.50

TABLE 7.1

The ratio is within 6% of $\frac{1}{2}$ in all compositions, the value expected for an intrinsic semiconductor, even though E_{02} is an extrapolated rather than actual band gap and the Fermi level is normally assumed to be 'pinned' in amorphous semiconductors. The validity of the comparison in Figure 7.14 can also be questioned on the grounds that E_v and the extrapolated optical valence band edge are in general expected to be different although in the Davis and Mott interpretation[23] they coincide if it is assumed that $E_{02} = E_A - E_v$, ie, that the conduction band tail is deeper than the valence band tail. Assuming the same to hold in Tauc's interpretation and applying the condition expressed in the inequality 2.33 and Figure 2.2 to the histogram in Figure 7.5, it is clear that since the square law fits until ~0.1 eV above E_{02} the valence band mobility edge is not more than ~0.03 eV above the extrapolated parabolic edge. The deviation from the square law is of course due to the exponential absorption tail but if the above condition was not satisfied there would be a *dip* in the absorption

curve between the exponential and square law regions. As far as is known such a dip has never been observed in any amorphous semiconductor and therefore similar analysis should apply to whichever band has the shallower tail. It is of course *possible* that the extrapolated parabolic edge lies further into the band than the mobility edge but not much further (eg,<< 0.1 eV) since that would constitute a tail of *extended* states and violate accepted ideas on Anderson localization. In any case equation 2.33 can be used (in Tauc's interpretation in terms of parabolic bands) to obtain an upper limit to the density of localized states at the mobility edge. If the extrapolated parabolic edge is at $E_v^{\,o}$ then

$$N(E_v) \leqslant N_v(E_v^{\,o} - E_v)^{\frac{1}{2}} \simeq 0.2\ N_v\ eV^{\frac{1}{2}} \qquad 7.7$$

Using the free electron mass and equation 2.32(a) to estimate N_v gives

$$N(E_v) \lesssim 5 \times 10^{20}\ eV^{-1}\ cm^{-3} \qquad 7.8$$

as the maximum density of states at the valence band mobility edge.

7.3.5 CORRELATION WITH T_g

Figure 7.15 is a plot of the glass transition temperature T_g as determined by Myers and Felty[24] vs $xE_{02}(x)$, which equation 4.10, suggests should be a straight line (x is the atomic fraction As). The fit is poor, the straight line actually drawn in Figure 7.15 connects the points corresponding to Se and $As_{40}Se_{60}$ and gives δ = 13.6

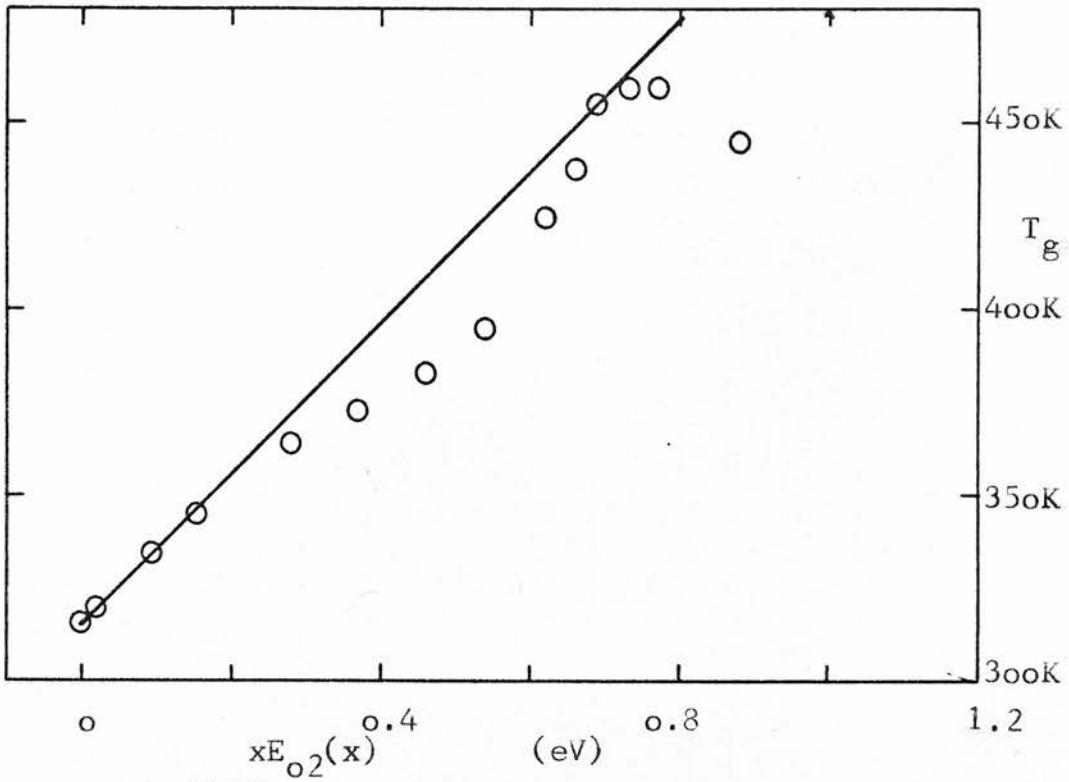

FIGURE 7.15

Plot of T_g (Myers & Felty[24]) vs xE_{o2} where x is the atomic fraction of As. The line joins Se and $As_{40}Se_{60}$.

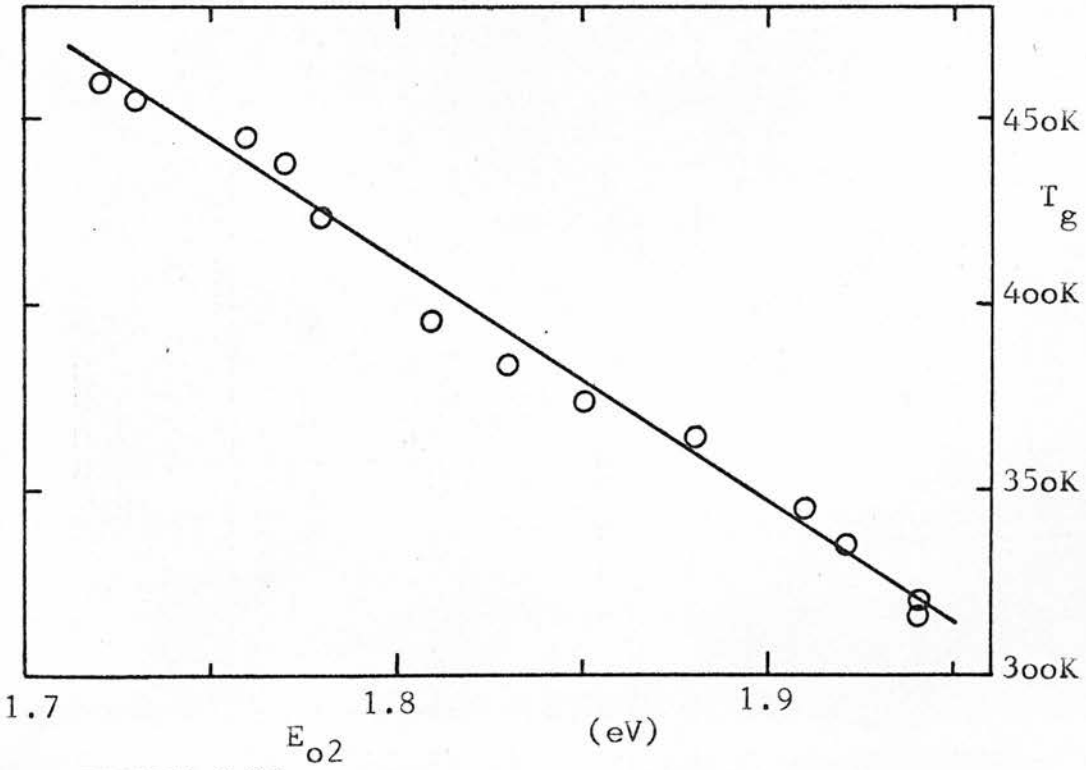

FIGURE 7.16

T_g plotted directly against E_{o2} gives a better fit to a straight line than in Figure 7.15.

as opposed to $\delta \sim 0.5$ obtained for amorphous compounds with constant connectivity[25].

A much better fit, extending over the whole composition range is obtained by plotting T_g directly against E_{02} at room temperature, as shown in Figure 7.16. The line in Figure 7.16 may be expressed as

$$T_g = 1600\ K - 660\ K/eV\ .\ E_{02} \qquad 7.9(a)$$

or

$$T_g = 320\ K + 660\ K/eV\ .\ \Delta E_{02} \qquad 7.9(b)$$

where

$$\Delta E_{02} = E_{02}(0) - E_{02}(x) \qquad 7.10$$

This means that in terms of equation 4.8

$$\delta(C - 2) = -18.3 \qquad 7.11$$

where C is the 'connectivity'.

It is therefore concluded that the variation in T_g in the As-Se system is directly related to the *change* in the optical gap but not to the increased connectivity except insofar as E_{02} may depend on connectivity. This throws serious doubts on the interpretation by De Neufville et al[25] of the observed correlation between T_g and E_g. Their model may also be critisized since the number of broken bonds at a given temperature increases exponentially and not linearly with

decreasing energy gap (E_σ to be exact). In fact Nunoshita and Arai[26] have found that $\ln T_g \propto E_\sigma$ in Si-As-Te glasses. The viscosity in partly cross-linked polymers depends on the size and shape of the molecular units and their flexibility and also on the free volume available. Therefore some rotational and translational degrees of freedom may become available above T_g with the breakage of a minimal number of covalent bonds. The rigidity and size of the polymeric units or sub-units increases, in general, with increased connectivity (not in As_4S_4). This may be the reason for the apparent correlation between T_g and connectivity observed by DeNeufville et al[25].

It is suggested that the present results as well as those of DeNeufville et al indicate a correlation between T_g and *changes* in the band gap in classes of materials, rather than the absolute value of the band gap. Inspection of compositions represented in Figure 4.15 reveals that in most cases all the materials corresponding to a single line contain a common group IV or group V element as a major constituent. The one point 25 K above the C = 2.4 line represents Sb_2S_3 and the other four points, much closer to the line, correspond to As_4X_6 where X is a mixture chalcogens. It is interesting to note that if T_g is plotted vs the gap $E_{02}(T_g)$ at the glass transition temperature, the fit is substantially improved. This is probably fortuituous, however, resulting from the fact that $\frac{dE_{02}}{dT_g}$ is negative.

A likely correlation between E_{02} and density has been discussed before. Since both the viscosity and T_g increase as the free volume decreases it appears likely that T_g as well as E_{02} depends directly on the density. Alternatively, it may be argued that the

compositional variation of E_{02} and T_g are caused by a variation in the degree of polymerization since a highly polymeric material will also be highly viscous and its internal energy content will be increased, as was discussed in Chapters 2 and 4. According to the 'internal energy model' $\Delta E_{02} \propto$ the energy of polymerization. The packing density also increases with polymerization.

Finally, it is worth noting that using T_g = 616 K [25] for a-As to extrapolate equation 7.9, gives $E_{02} \triangleq$ 1.5 eV for a-As which is higher than observed but is very close to the value obtained by extrapolating the E_{02} vs x curve (Figure 7.8) linearly from the $x < 0.4$ region. A similar value was obtained earlier by combining equation 7.4 with published values of density for pure a-As. This suggests that the average atomic volume of As is less in selenium rich compositions than in a-As itself.

7.4 THE PREFACTOR C_2

7.4.1 VARIATION WITH COMPOSITION

The most surprising result to emerge from the present work is the way in which C_2 is found to depend on composition. This is shown in Figure 7.17 which is a plot of C_2^{-1} vs composition for bubbles at 295 K and 115 K. Each point represents an average over 2 - 5 samples. The fit to a straight line is good for the whole composition range at both temperatures. Thus

$$C_2 = (ax + b)^{-1} \qquad 7.12$$

where $a = (2.0 \pm 0.1) \times 10^{-6}$ eV cm and is practically independent of

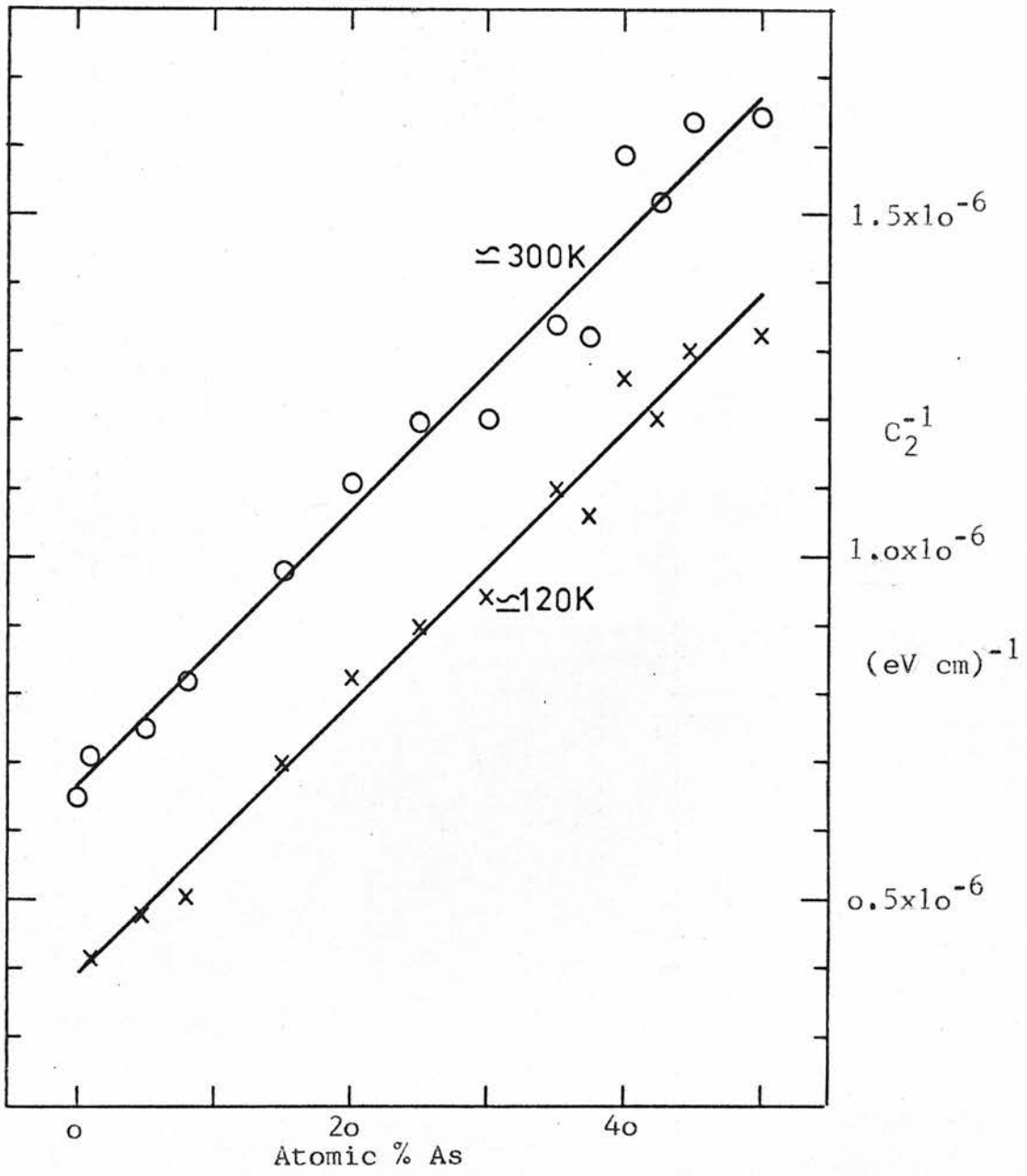

FIGURE 7.17

The inverse of the pre-factor C_2 is a linear function of As content.

temperature; $b = 6.6 \times 10^{-7}$ eV cm at room temperature and 4.0×10^{-7} eV cm at 115 K. That C_2^{-1} should vary linearly with composition over such a wide range is quite remarkable considering that almost all other properties exhibit extrema near the stoichiometric composition $As_{40}Se_{60}$, as was discussed in Chapter 4. It is even more remarkable when one considers the close relation between the changes in E_{02} and C_2 with preparation, that was shown to exist in Chapter 2 and is further supported by the present work. Table 7.2 compares the values obtained for these two parameters in films prepared by different methods.

COMPOSITION	PREPARATION	E_{02}	C_2
Se	bubbles	1.94 eV	15.4×10^5 eV^{-1} cm^{-1}
Se	evaporated	1.92	14.0
$As_{40}Se_{60}$	bubbles	1.73	6.3
$As_{40}Se_{60}$	sputtered *	1.76	6.2
$As_{42.5}Se_{57.5}$	bubbles	1.72	6.6
$As_{43}Se_{57}$	evaporated *	1.80	8.1

* one sample only

TABLE 7.2

Just as in Table 2.2, both parameters vary in the same direction with preparation for each particular composition, except for sputtered $As_{40}Se_{60}$ where E_{02} is significantly larger than in the bubbles but C_2 is the same within experimental error. As before the

direction of the shift in both parameters is determined by which of the two competing processes of reduction in disorder or increase in polymerization dominates on going from evaporated to films prepared from bubbles (bulk material).

An extrapolation of the curve in Figure 7.17 to pure As gives $C_2 = 3.8 \times 10^5$ eV^{-1} cm^{-1} at room temperature. A similar extrapolation based on the two evaporated compositions gives $C_2 \simeq 5 \times 10^5$ eV^{-1} cm^{-1} for pure As, a value which compares favourably with $C_2 = 5.2 \times 10^5$ eV^{-1} cm^{-1} obtained from the optical absorption results of Greaves et al[5]. It is not clear, however, whether they used annealed films for their measurements. The same value was reported by Cornet and Rossier for evaporated As-Te films. It seems likely, therefore, that C_2^{-1} will vary, if not linearly then at least monotonically with As content, from pure Se to pure As. This is illustrated in Figure 7.18. There may also be a connection between the independence on composition of C_2 in the As-Te system and the absence of extrema in parameters such as E_{02} and T_g near the composition $As_{40}Te_{60}$.

7.4.2 COMPARISON OF C_2 AND E_{02}

The compositional variation of C_2 and E_{02} may be compared in terms of the density-of-states diagrams in Figure 2.8 and the relations in Table 2.3. It follows immediately from equation 7.12 that the cases shown in Figure 2.8(a) and (b) are ruled out because equation 7.12 is incompatible with the observed minimum in E_{02} in these two cases. Case (c) is difficult to analyse because it contains more possibilities than the others. Combining the observed linear decrease in E_{02} with x for $x \leqslant 0.35$ and the linear increase in

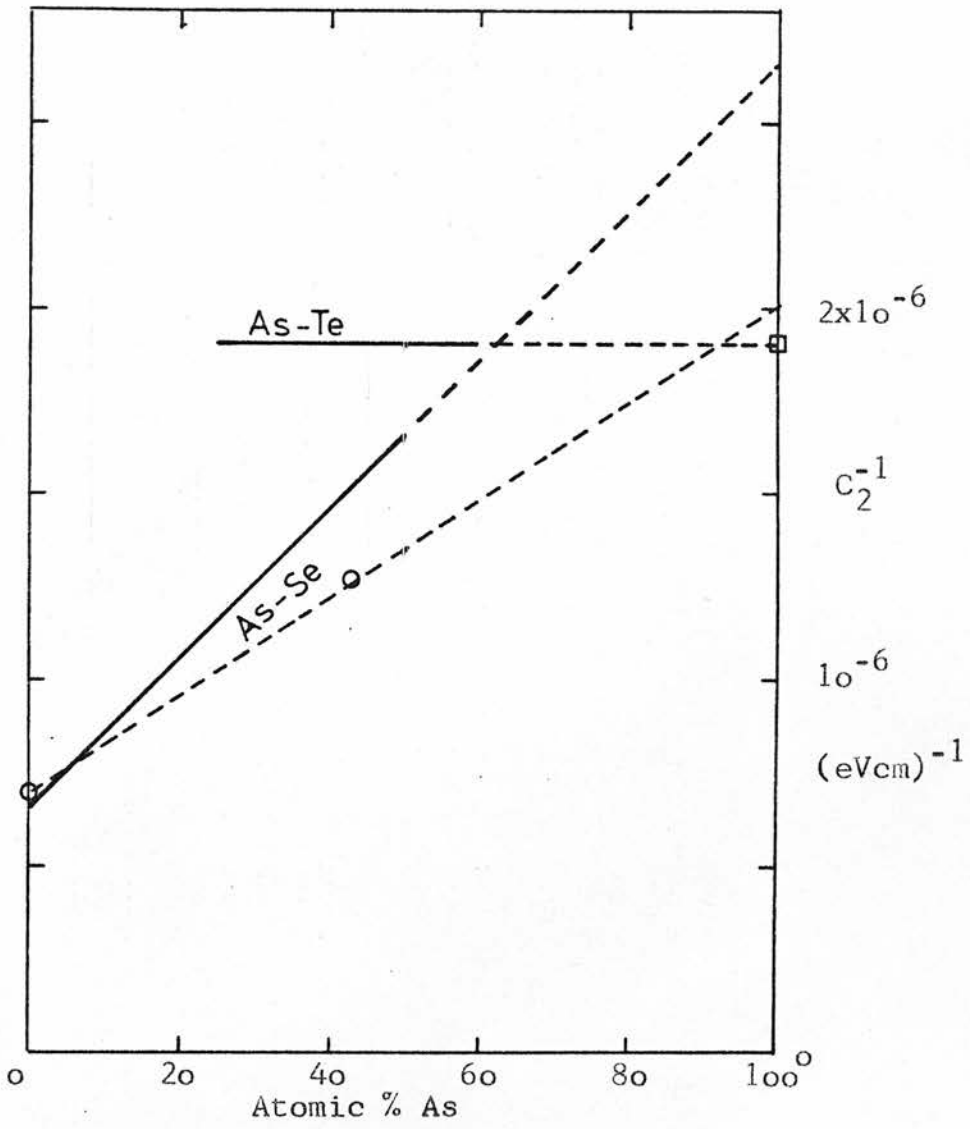

FIGURE 7.18

Expected compositional variation of C_2^{-1} in arsenic chalcogenide glasses. The result for As is from Greaves et al[5] (square), for As-Te from Cornet & Rossier[13]. Circles are for evaporated films. Broken lines are extrapolations.

The figure corresponds to room temperature.

ΔE_c necessary to explain the change in the electron drift mobility[27], gives an increase of ~0.15 eV in ΔE_c as the As content increases from zero to 8%. Of that increase, 0.11 eV corresponds to a shift of the mobility edge into the conduction band, increasing E_μ from 0.33 eV to 0.44 eV. A quarter of the increase in ΔE_c, ie, 0.04 eV corresponds to a deepening of the tail into the gap, thus reducing E_{02} by that amount. The actual reduction in E_{02} is 0.03 eV indicating that ΔE_v has increased by only ~0.01 eV. (For a given change in ΔE_v, E_{02} changes by $\frac{3}{4}$ of the change in ΔE_v - see equation 2.51(a)). The above analysis assumes that the electron traps are at a discrete level whose energy is not altered. A possible alternative interpretation[27] is that the electrons are trapped at the foot of the linear conduction band tail, ie, that $E_\mu = \Delta E_c$. A similar analysis in this case gives an increase of 0.11 eV in ΔE_c, which contributes $\frac{1}{4}$ x 0.11 eV $\triangleq$ 0.03 eV to the reduction in E_{02} and thus accounts for the total change in E_{02}, implying that ΔE_v does not change at all. In either case equations 2.50 and 7.12 imply that

$$\Delta E_c/\Delta E_v \propto (ax + b)^2 \qquad 7.13$$

where a and b are positive and b depends on temperature.

This proportionality is consistent with either of the above cases in that the expanded bracket is approximately linear in x in the composition range considered above. Difficulties arise, however, when it is attempted to apply this result in the whole range over which E_{02} varies linearly. Furthermore, it is not clear how to accommodate the temperature dependence of b with this kind of analysis since presumably $E_\mu(x)/E_\mu(0)$ and $\Delta E_c(x)/\Delta E_c(0)$ are

independent of temperature.

Considering compositions in the range 30 - 50% As and Figure 7.14, the simplest interpretation in terms of Figure 2.8(c) is to assume that E_F is fixed in this composition range, that ΔE_c increases approximately linearly with x and that ΔE_v has a minimum near $As_{40}Se_{60}$. According to equation 2.50, however, this would imply a local minimum or at least a change of slope in C_2 in the range 40 - 45% As, contrary to observations. It is *possible* to postulate a changing Fermi level and minima in both ΔE_c and ΔE_v so that the proportionality 7.13 is satisfied. It seems hardly worthwhile however since the result would have to be compatible with the behaviour for Se-rich glasses and the temperature dependence of C_2 poses a difficult problem throughout the range investigated.

The above analysis has ignored the probable variation of the parameters N_v and N_c in equation 2.50. It is probably more reasonable to expect these to vary monotonically throughout a wide range of compositions than $\Delta E_v / \Delta E_c$, and, in addition, thermal broadening of the bands due to the electron-phonon interaction may be expected to reduce $N_v N_c$. An analysis in terms of $N_c N_v \propto (ax + b)$ and $\Delta E_v / \Delta E_c$ constant is difficult however without further assuming that the extrapolated parabolic band gap $-E_p$ in equation 2.51 - is also a function of composition. Because of this and the additional argument against the Davis and Mott interpretation - namely that the observed range of validity of the square law is much wider than the expected extent of linear tails - it is concluded that a simpler and probably more correct interpretation can be given in terms of Tauc's parabolic bands (Figure 2.7). It should be mentioned first that in

terms of Figure 2.8(c) and equations 2.50 and 2.51(a), it would be possible to have a square law at low photon energies due to a linear tail followed by another square law at higher energies due to the parabolic bands. The extrapolated gaps for the two regions would be different, however, unless $3\Delta E_v = \Delta E_c$, in which case C_2 would be smaller by a factor of $\sqrt{3}/4$ in the low energy range. Thus it is not possible to have a 'Davis-Mott' type square law merging into a square law derived from parabolic bands without a change in either or both of C_2 and E_{02}.

In Tauc's interpretation C_2 and E_{02} are related, as indicated in Figure 2.7, by the fact that the total number of states must remain constant for a particular composition. As was discussed in Chapter 2, however, the relative position of the bands or the position of the ε_2-maximum can change as a function of composition and therefore E_{02} can change while C_2 remains constant. Alternatively, the average oscillator strength, ie, the matrix element can change, and with it C_2. It has already been argued from Figure 7.5 that for one band at least the mobility edge cannot be more than 0.03 eV further into the band than the extrapolated parabolic edge. This is assumed to be the valence band because the overlap of atomic wave functions is less than in the conduction band and therefore the effect of disorder should be smaller, ie, the tail shallower. There is no restriction on the other (conduction) band tail. Since E_σ increases by 0.1 eV in going from $As_{40}Se_{60}$ to a composition ~10% on either side it follows that the extrapolated parabolic valence band edge must be composition dependent, ie, the minimum in E_σ cannot be explained by a minimum in disorder, near the stoichiometric composition. The alternative explanation

must be related to the degree of polymerization and the density, and the problem is to account for the absence of any minimum in C_2 near the composition which has smallest E_{02}.

7.4.3 VARIATION WITH TEMPERATURE

Combining equations 2.35 and 7.12 gives

$$N_c N_v M^2 \propto (ax + b)^{-1} = C_2 \qquad 7.14$$

with a proportionality factor which is independent of composition and temperature. According to this and Figure 7.17 the temperature dependence of C_2 arises from the temperature dependent term b.

Figure 7.11 is a plot of C_2 vs T as well as E_{02} vs T for $As_{15}Se_{85}$. It suggests strongly that these two parameters vary in a similar way with temperature although the relative change in C_2 is much larger. Figure 7.19 shows the same data, this time plotted directly as C_2 vs E_{02}. The resulting straight line can be expressed as

$$E_{02} = 1.50 \text{ eV} + 0.37 \text{ cm eV}^2 \cdot C_2 \qquad 7.15$$

Similar behaviour is found for other compositions but with different constants. In general it was found that C_2 decreases linearly with increasing temperature above 110 - 150 K, ie, over the same range as E_{02} varies linearly. It was not possible to measure these parameters at sufficiently low temperatures to determine whether they are actually linearly related or whether equation 7.15 is simply

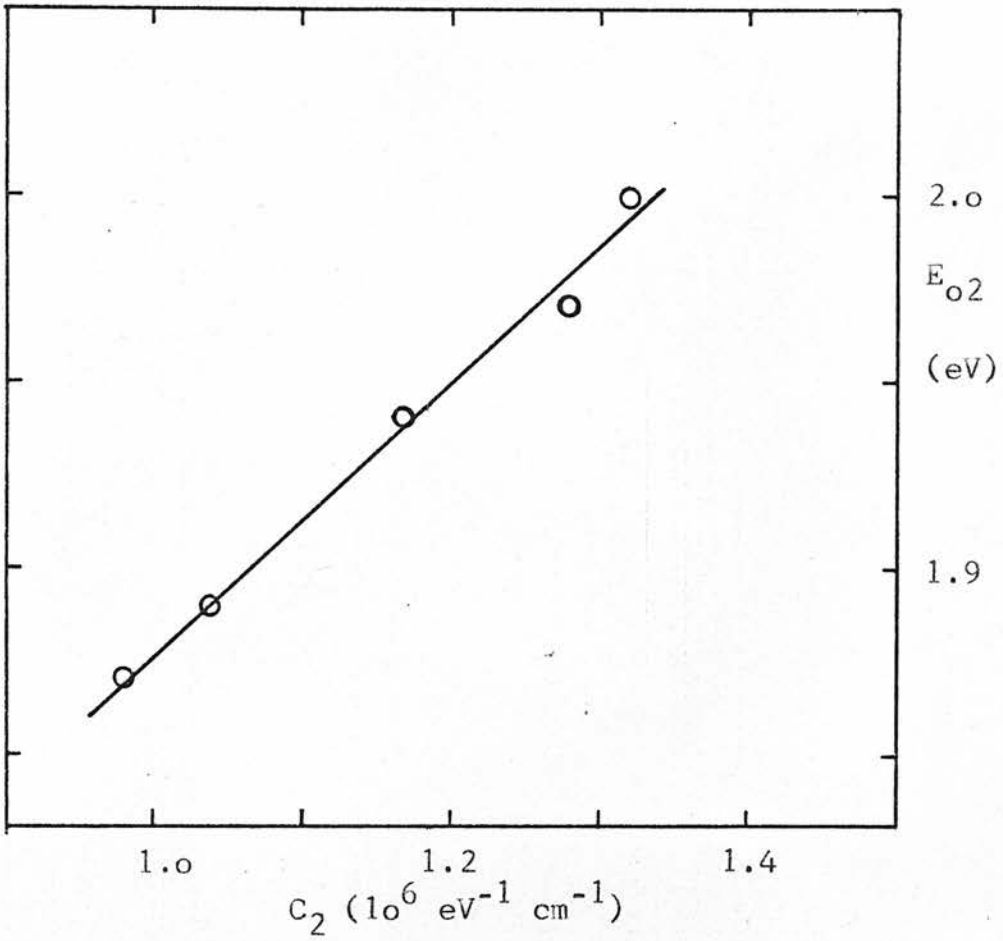

FIGURE 7.19

Comparison of the temperature variation of E_{o2} and C_2 (see Figure 7.11) in a bubble specimen, $As_{15}Se_{85}$.

a consequence of both varying linearly but independently. The fact that both deviate from linear behaviour at similar temperatures would seem to indicate however that they are actually related. Furthermore, Figure 7.19 only indicates that C_2 and the *change* in E_{02} are linearly related, ie, the constant 1.50 eV in equation 7.13 must be taken as arbitrary. The significance of Figures 7.11 and 7.19 is that they suggest that the same mechanism is responsible for the temperature dependence of both parameters. It is generally agreed that the electron-phonon interaction causes the shift of the gap with temperature. The above evidence strongly suggests that it is also responsible for the change in C_2 with temperature. C_2 changes by 30% over the measurement range in Figure 7.19. In terms of equation 7.12 'ax' for this composition is 3.0×10^{-7} eV cm and b increases from 4.0×10^{-7} eV cm to 7.6×10^{-7} eV cm. The relative change is not sufficient to determine how b varies with temperature. Assuming that $\frac{db}{dT}$ is linear and expanding equation 7.12 would, within the experimental errors, give an approximately linear $\frac{dC_2}{dT}$. To determine which of C_2 or b, if either, varies exactly linearly with T at high temperatures would require accurate measurements at many temperatures for samples such as As_5Se_{95} with low As contents, in which the term ax in equation 7.12 is small. Unfortunately, such data was not obtained in the present study. Insufficient data is available to determine whether the main contribution to $\frac{dC_2}{dT}$ comes from temperature dependent matrix elements or densities-of-states or both. The same applies to the compositional dependence. In terms of Figure 2.7 and the correlations between changes in E_{02} and C_2 it would seem however that the bands broaden as a result of increased density, pressure or temperature, ie, that the densities-of-states decrease. The dispersion energy E_d in a-As_2S_3

has a positive pressure coefficient[28] which presumably means that the average matrix element increases with pressure. Information is not available on the temperature coefficient of E_d in chalcogenide glasses; this could give some indication, together with $\frac{dC_2}{dT}$, about temperature dependent matrix elements.

The temperature dependence of C_2 in this work is in qualitative agreement with the deduction from the results of Kosek and Tauc[11] that C_2 is more affected by temperature in a-As_2S_5 than in As_2S_3, indicating that a relation similar to equation 7.12 may apply to the As-S system also. If that is the case and if the results for both systems extrapolate to the same value for a-As, then it is more instructive to rewrite equation 7.12 as

$$C_2^{-1} = b' - a(1 - x) \qquad 7.16$$

where $b' = (a + b)$ equals C_2^{-1} for As, a is a different constant for each system and $(1 - x)$ is the fractional content of chalcogen atoms. In the As-Te system presumably $a \doteq 0$.

7.5 DISCUSSION

7.5.1 SUMMARY OF CONCLUSIONS

The following conclusions have been drawn from the experimental results presented above and from comparison with previously published results on the properties of amorphous arsenic chalcogenides.

1. Films prepared from bubbles closely approximate bulk or annealed glass in their optical properties.

2. A square law for optical interband absorption (equation 2.30) applies to all the films investigated in the composition range 1 - 50% As and can also be fitted over a narrow range in photon energies in pure Se and Se doped with 0.1% As, giving square law parameters in good agreement with those extrapolated from glasses with higher As content.

3. A linear law for optical interband absorption (equation 2.29) applies to both evaporated films and bubbles of pure Se, over a wide range of photon energies at energies higher than the limited square law region. The same law applies over a much narrower range in Se doped with 0.1% As.

4. The extrapolated gaps are E_{02} = 1.94 eV and E_{01} = 2.08 eV for bubbles of Se and 0.02 eV less for evaporated Se.

5. These energies correspond closely to a shoulder and a maximum in the electroabsorption data of Sussman et al[7]. It is suggested that these are related and a prediction of the effect of As-doping on the electroabsorption spectrum is made.

6. E_{02} decreases linearly with increasing As-content up to ~35% As and has a shallow minimum of $E_{02} \triangleq 1.72$ eV near $As_{43}Se_{57}$. Lines of equal absorption show a similar composition dependence except at very high absorption levels where the absorption in Se rich compositions is enhanced by a steeper absorption curve.

7. Comparison of these results with published works suggests that

E_{02} also has a local maximum near $As_{57}Se_{43}$ and then decreases rapidly to 1.2 - 1.4 eV for pure As. Similar behaviour is predicted for the As-S system but in the As-Te system E_{02} probably varies linearly throughout the composition range.

8. E_{02} varies linearly with temperature for $T \gtrsim 150$ K but more slowly at lower temperatures.

9. γ - the temperature coefficient of E_{02} decreases with increasing As-content. The normalized or fractional temperature coefficient $\bar{\gamma}/E_{02}(0K) = (3.5 \pm 0.1) \times 10^{-4}\ K^{-1}$ and is independent of composition.

10. It seems likely that E_{02} and the density ρ are linearly related, although optical and density measurements on similarly prepared samples are needed to be certain of this.

11. Such a relation is further supported by published results on compressibility and the shift of the optical gap E_g with pressure.

12. The ratio $E_\sigma/E_{02}(0K)$ is very close to $\frac{1}{2}$, the intrinsic value.

13. $E_{02}(0K) - E_\sigma$ decreases approximately linearly from $As_{30}Se_{70}$ to $As_{50}Se_{50}$.

14. Comparison of $E_{02}(0K)$ and E_σ in this range strongly suggests that, *relative to the Fermi level*, the optical conduction band edge is lowered linearly as the As-content increases, while the

valence band optical and mobility edges are symmetric about $As_{40}Se_{60}$.

15. Using Tauc's model of parabolic bands and the low energy limit of the square law region, it is deduced that the valence band mobility edge is less than 0.03 eV below the extrapolated parabolic edge, assuming a longer tail in the conduction band.

16. It follows from this that the density-of-states at the valence band mobility edge has an upper limit of 0.2 N_v $eV^{\frac{1}{2}}$ which gives $\doteq 5 \times 10^{20}$ eV^{-1} cm^{-3} if the free electron mass is used to evaluate N_v.

17. The interpretation by DeNeufville et al[25] of their observation of a linear relation between T_g and E_g for amorphous compounds cannot be extended to nonstoichiometric As-Se glasses and is probably incorrect.

18. A simple linear relation between T_g and E_{02} is observed for *all* compositions investigated.

19. It is clear that E_{02} decreases and ρ and T_g increase with increased polymerization.

20. Three different and independent extrapolations from the range 0 - 40% As to pure As all suggest $E_{02} \doteq 1.5$ eV for As, which is higher than observed.

21. A simple linear relation between composition and the inverse of C_2 is observed for all compositions investigated (Se-$As_{50}Se_{50}$), without extrema at any composition.

22. Extrapolation of the linear C_2^{-1} curve to pure As gives reasonable agreement with published values. Other arsenic-chalcogenides are also considered.

23. Comparison of C_2 and E_{02} with electrical data virtually eliminates the Davis and Mott interpretation of the square law for absorption in terms of linear band tails. Tauc's model of parabolic bands seems to be more appropriate, although some additional conditions must then be invoked to explain the linear law for a-Se.

24. The extrema in many properties, particularly E_{02} and E_{σ}, near the composition $As_{40}Se_{60}$ cannot be explained satisfactorily by a model which invokes only compositional disorder.

25. E_{02} and C_2 change in a related manner as the temperature and the preparation conditions are varied.

26. The temperature dependence of C_2 is probably due to the electron-phonon interaction.

7.5.2 RELATION WITH OTHER WORK

As was discussed in Chapter 2, Street et al[29] observed a

photoluminescence (PL) peak in As-Se glasses, with an intensity proportional to the As-content. Furthermore, the energies at which the PL peak and the excitation peak occur scale with E_g between all the As-chalcogenides investigated. Street et al[29] argue that these observations indicate that the PL peak is associated with As atoms only. If that is so then it is tempting to speculate whether there might be a connection between the photoluminescence and the present optical results. A simple assumption would be to postulate that PL intensity is proportional to the product ax in equation 7.12 and that b in that equation represents absorption which does not lead to radiative recombination. Street et al[30] also noticed that the PL intensity depends on preparation but further experiments are needed before these arguments can be developed much further. It would be interesting, for example, to know whether the PL intensity continues to grow linearly when the As-content increases from 40 - 100%.

The dispersion oscillator energy E_o (which was disussed in some detail in section 2.2.6) is identical in a-Se and a-$As_{40}Se_{60}$ [3,31], E_o = 3.85 eV, but increases sharply to E_o = 4.4 eV in $As_{50}Se_{50}$ [3]. Since E_o is sensitive to the shape of the absorption curve at low energies ($E_{02} \leqslant h\nu \leqslant E_o$), ie, to E_{02} and C_2, it is suggested that E_o is approximately constant in the range 0 - 40% As, because the compositional variations of E_{02} and C_2 have opposite effects on the absorption. In the composition range where E_{02} is increasing with As-content while C_2 is still decreasing, both effects tend to decrease the absorption at a given energy with the result that E_o shifts to higher energies. This further suggests that measurements of the dispersion parameters as a function of composition may give important information which could help to gain understanding of the

compositional variation of C_2.

7.5.3 A MODEL FOR AMORPHOUS ARSENIC CHALCOGENIDES

It has already been implied several times in this and earlier chapters that the degree of polymerization is a dominant factor in determining the optical as well as mechanical and thermodynamic properties of compositions in the As-Se and As-S systems. It has been suggested moreover that variations of the optical gap are directly related to either the internal energy content or the density. Considering first the former possibility. In Chapter 4.2.3, it was shown that the increase in internal energy associated with complete polymerization is 12 meV/atom in selenium. Re-arranging equation 2.41 gives

$$\Delta E_g = a\, C_A\, \Delta T = a\, \Delta U_A \qquad 7.17$$

where C_A is the specific heat per atom and ΔU_A is the change in thermal energy per atom associated with a change ΔT in temperature. From section 7.3.2; a = -2.64 for Se. Assuming that equation 7.15 can be extended to relate changes in E_{02} and internal energy due to polymerization, gives $\Delta E_{02} \doteq 0.03$ eV as the maximum change in E_{02} due to polymerization of Se. The energy gap E_{02} is 0.2 eV smaller in a-$As_{40}Se_{60}$ than in Se. In As_3S_3 E_{02} has been observed to decrease by ~0.17 eV as a result of photopolymerization[32]. In order to make the 'internal energy' model consistent, it is necessary therefore to postulate either a much larger value of ΔH_3, or that the parameter 'a' in equation 7.15 is larger for changes in structural energy than thermal energy. An increase by at least one order of magnitude is required. Thus it

seems more likely that the optical gap is related to density - the second of the two possibilities mentioned in the previous paragraph. This is now considered in more detail.

The temperature coefficient of the optical gap in chalcogenides is similar to those in amorphous and crystalline tetrahedrally bonded semiconductors. On the other hand the pressure coefficients are very different for the two classes of materials and, as was discussed earlier, there is a close relation between the pressure coefficient, the density and the compressibility in chalcogenides. With this in mind it is concluded that two different mechanisms influence E_{02} and C_2 in amorphous chalcogenides. One is the electron-phonon interaction which is purely thermal and the other is interaction between atoms which do not form a common bond, ie, either by Van der Waals interactions (equation 2.42) or more likely through the overlap of non-bonding orbitals. Bond bending may also contribute. Following the discussion in Chapter 2, it is further assumed that this latter interactions manifests itself in a linear relationship between E_{02} and the average atomic density. Since the atomic masses of Se and As are very similar, it follows that ρ and E_{02} are also linearly related in the As-Se system. This mechanism explains, qualitatively at least, the close similarity in compositional behaviour of different physical parameters such as the extrema near $As_{43}Se_{57}$, the most highly interconnected and densest composition.

It does not explain, however, why the close relation between changes in C_2 and E_{02} for any particular material does not extend to changes with composition, ie, why C_2 does not show a local minimum near $As_{40}Se_{60}$. But this is equally true of other models, such as

the compositional disorder model. It is instructive to consider that it is possible in theory, by using *different* preparation conditions for different compositions, to prepare a series of samples for which E_{02} vs x plots would have no minimum near 40% As but for which the corresponding C_2^{-1} vs x plot *would* show a local minimum at that composition. In the present work the preparation conditions are very similar for all compositions, in terms of the viscosity of the melt and the cooling rate. This suggests that C_2 depends only on the concentration ratios of the constituent elements, the temperature and the *deviation* from thermal equilibrium, whereas E_{02} and ρ, and most other properties depend on these as well as the actual equilibrium state.

To explain the linear law for interband absorption in a-Se it is necessary either to assume that the density-of-states falls below the expected parabolic curves above E_{02} or, which seems more likely, that the matrix element is energy dependent. A matrix element which decreases with increasing photon energy in the range 2 - 5 eV was calculated for a-Se by Maschke and Thomas[33] from the averaged crystalline matrix elements. A linear absorption law will then result if the square of the matrix element is approximately proportional to the inverse of the photon energy. At lower energies (<2 eV) the matrix element is expected to decrease again because of increased localization of the wave functions. Therefore, there should be a maximum in the M^2 vs $h\nu$ plot near 2 eV. Over a narrow region on either side of this maximum the matrix element can be assumed constant, giving the observed square law for absorption in a-Se in the range 2.0 - 2.2 eV. It is envisaged that the addition of As causes a rapid change to an energy independent matrix element.

SUMMARY : A model is proposed for the As-Se system in which the interaction between atoms which do not form a common bond, governs the width of the gap. This interaction probably arises mainly from overlap between non-bonding orbitals. Polymerization tends to increase the density without changing the covalent bond lengths. This in turn increases the non-covalent interaction and thereby reduces the optical gap. An increase in the degree of polymerization reduces the flexibility of the network and, therefore, the compressibility and the thermal expansivity decrease while the glass transition temperature increases. As a result all the above-mentioned parameters are closely related and tend to show simple variation with each other. An example is the linear variation of T_g as a function of E_{02} over the whole range Se to $As_{50}Se_{50}$. More complicated relations are expected in systems such as As-S because the masses of the constituent atoms and the strength of the possible bonds between them are very different from each other.

It is suggested that C_2, in contrast to the parameters discussed above, is independent of the equilibrium degree of polymerization.

An amorphous arsenic-chalcogenide solid is in general not in a state of equilibrium polymerization, but can approach it under illumination through polymerization or photodepolymerization. Careful measurements of as many physical properties as possible on the same sample or samples prepared under similar conditions should give further information on the relationships between these properties and on the interactions responsible for their behaviour. It is recognized that atoms of different elements do not have the same tendency for non-covalent interaction. This may in some instances

result in deviations from otherwise simple relationships between different physical parameters. This model refers primarily to the macroscopic physical properties and the band edges. Traps are not considered although their number and energy distribution is no doubt influenced by the degree of polymerization as their main source is probably compositional and structural disorder.

7.5.4 NEW DEVELOPMENTS

The previous analysis is based on the assumption of one-electron densities-of-states functions derived from ordinary covalent bonds. The Davis-Mott interpretation of the optical gap in terms of linear tails of localized states does not appear to be consistent with the experimental results and therefore Tauc's parabolic band model is adopted by default. Furthermore it is argued that the optical gap and many other properties are not determined primarily by disorder but rather by interaction between orbitals which do not form a common covalent bond.

Recently there has been much interest in fundamentally different models for the electronic structure of amorphous semiconductors. Thus Anderson[35] proposed an 'attractive Hubbard interaction' model in which the distortion of the lattice by two electrons at the same site (but with opposite spins) causes a lowering of energy that more than compensates for the repulsive Coulomb interaction, making the net interaction attractive. In this model, with certain assumptions, each state is either unoccupied (by electrons) or doubly occupied thus explaining the absence of paramagnetism in most semiconducting glasses as well as the linear term in the specific heat at low

temperatures. The optical gap is the energy needed to remove one electron from a doubly occupied site and at the same time change the energy of the remaining electron to the higher lying single electron state. This energy is just the difference between the electron-lattice interaction caused by the second electron and the Coulumb interaction between the first and second electron. The Fermi level is pinned near the middle of the gap. All carriers in doubly occupied (or doubly unoccupied) states are localized while those in singly occupied, or excited, states have extended wave functions. In this model the gap will depend on pressure or density because the electron-phonon coupling and Coulumb interaction depend on those terms. The large negative pressure coefficient of the optical gap of chalcogenides shows that either the Coulumb energy increases or the energy due to lattice distortion decreases or both (a zero gap corresponds to the two energy terms being equal).

Although still in their infancy, it seems likely that Anderson's model, or similar models, are a better description of the electronic structure of amorphous semiconductors than the conventional assumptions used in the present work. More theoretical work is needed, however, before detailed comparisons with experimental work can be made. In any case it is considered that such a reinterpretation of the present work would not change the predictions and correlations discussed previously although new assumptions about the fundamental physical reasons for them would have to be made. For example, a linear relation between density and optical gap is, if anything, easier to explain in terms of Anderson's model than conventional models. Similarly, the predicted local maximum in E_{02} at ~60% As would still be expected to occur on the grounds of optical measurements for other

compositions and density[14] and conductivity[36] measurements as a function of composition.

The considerable amount of knowledge that exists on the arsenic-chalcogenides should serve as a testing ground for the new models, which in turn might suggest new experiments. It must be stressed, however, that it is necessary to consider many different properties at once and not just say electrical or optical properties on their own.

7.6 REFERENCES

1. Fritzsche, H, Electronic and Structural Properties of Amorphous Semiconductors (P G LeComber and J Mort, editors), Academic Press, London and New York, 1973, p 579.

2. DeNeufville, J P et al, J Non-Cryst Sol 13, p 191, 1973.

3. DeNeufville, J P et al, Proc on the 5th International Conference on Amorphous and Liquid Semiconductors, Garmisch-Partenkirchen, Germany (J Stuke and W Brenig, editors) Taylor and Francis, London, 1974, p 737.

4. Weiser, K, 1970, cited by Owen, A E, Cont Phys 11, p 257, 1970.

5. Greaves, G N et al, Proc on the 5th International Conference on Amorphous and Liquid Semiconductors, Garmisch-Partenkirchen, Germany (J Stuke and W Brenig, editors), Taylor and Francis, London, 1974, p 369.

6. Davis, E A, J Non-Cryst Sol 4, p 107, 1970.

7. Sussman, R S et al, J Phys C 8, p L182, 1975.

8. Hurst, C H, PhD Thesis, University of Cambridge, 1973.

9. Asahara, Y and Izumitani, T, J Non-Cryst Sol 15, p 343, 1974.

11. Kosek, F and Tauc, J, Czech J Phys B 20, p 94, 1970.

12. Knights, J C, Solid State Comm 16, p 515, 1975.

13. Cornet, J and Rossier, D, Phil Mag 27, p 1335, 1973.

14. Kunugi, M et al, Zairyo 18, p 807, 1969.

15. Tarasov, V V et al, Russ J Phys Chem 43, p 249, 1969.

16. Ziegel, V V and Orlova, G M, J Appl Chem USSR 46, p 771, 1973.

17. Knights, J C and Davis, E A, J Phys Chem Sol 35, p 543, 1974.

18. Chernov, A P et al, Inorg Mater USSR 4, p 1658, 1968.

19. Kastner, M, Phys Rev B 7, p 5237, 1973.

20. Arai, K et al, Jap J Appl Phys 12, p 1717, 1973.

21. Arai, K et al, J Non-Cryst Sol 13, p 131, 1973.

22. Fisher, F D et al, Phil Mag 1975, to be published.

23. Davis, E A and Mott, N F, Phil Mag 22, p 903, 1970.

24. Myers, M B and Felty, E J, Mat Res Bull 2, p 535, 1967.

25. DeNeufville, J P et al, Proc on the 5th International Conference on Amorphous and Liquid Semiconductors, Garmisch-Partenkirchen, Germany (J Stuke and W Brenig, editors), Taylor and Francis, London 1974, p 419.

26. Nunoshita, M and Arai, H, Solid State Comm 11, p 213, 1972.

27. Marshall, J M et al, Phys Stat Sol (a), 25, p 419, 1974.

28. Galkiewicz, R K and Tauc, J, Solid State Comm 10, p 1261, 1972.

29. Street, R A et al, Phil Mag 30, p 1181, 1974.

30. Street, R A et al, J Phys C 6, p 1830, 1973.

31. Yu, P Y and Cardona, M, Phys Stat Sol (b) 47, p 251, 1971.

32. Tanaka, K, Appl Phys Lett 26, p 243, 1975.

33. Maschke, K and Thomas, P, Phys Stat Sol 41, p 743, 1970.

34. Felty, E J and Myers, M B, cited by Mott, N F and Davis, E A in Electronic Processes in Non-Crystalline Materials, Oxford, 1971, p 244.

35. Anderson, P W, Phys Rev Lett 34, p 953, 1975.

36. Mackowsky, J M et al, J Non-Cryst Sol 15, p 279, 1974.

CHAPTER 8 GLASSES DOPED WITH Cu - RESULTS AND DISCUSSION

8.1 INTRODUCTION

The results presented in this chapter are of a preliminary nature. More extensive experiments are required before the different measurements can be intercorrelated into a common framework. Some interesting features do, however, emerge from the present work, which have not been reported before. One is an annealing effect at ~340 K which changes the electrical properties. Most published works on the electrical properties of As-Se glasses containing Cu or Ag impurities refer to measurements which extend to temperatures above 340 K, ie, they refer to annealed samples only.

It is shown that electronic conduction in extended states cannot be the dominant conduction mechanism and in the discussion of possible alternative conduction mechanisms, frequent reference is made to glasses doped with Ag on which more results have been published. It is assumed that these two metals have similar effect on the parent glass but this may not be so - for example, four different Cu-As-Se or Cu-Se compounds are thought to exist in Cu-As-Se glasses while $AgSe_2$ is the only silver compound reported.

8.2 STEADY STATE CHARACTERISTICS

8.2.1 OPTICAL ABSORPTION

Figure 8.1 is a plot of $(\alpha h\nu)^{\frac{1}{2}}$ vs $h\nu$, showing the optical absorption behaviour of two films containing Cu. Curve 1 is for a

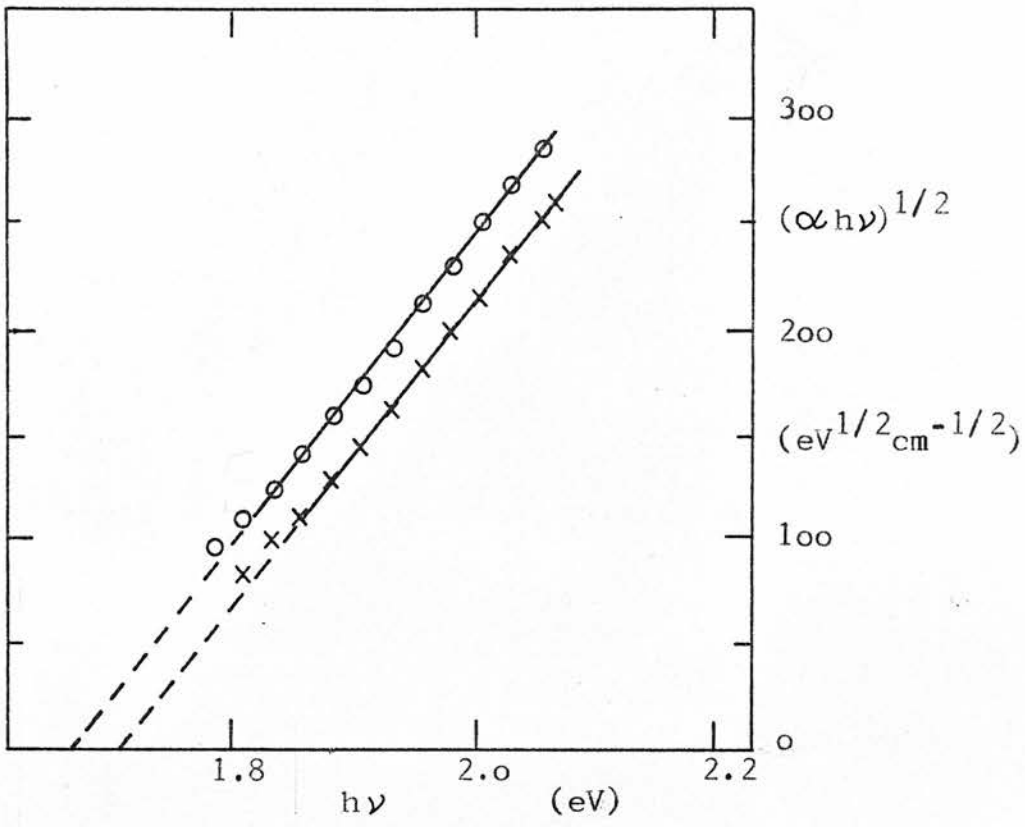

FIGURE 8.1

Optical absorption in Cu doped films.

circles - bubble sample, $As_{4o}Se_{6o}Cu_{1.o}$

crosses - electron beam evaporated sample, $As_{46}Se_{54}Cu_{.o23}$

film prepared from a bubble of $As_{40}Se_{60}Cu_{1.0}$ and curve 2 for a film produced by electron-beam evaporation. Chemical analysis gave the composition of the latter film as $As_{46}Se_{54}Cu_{0.023}$ (the source material had the same composition as the bubble). The optical parameters of these films are collected in Table 8.1, which also includes for comparison, results from the previous chapter on undoped films with similar As:Se ratios.

COMPOSITION	PREPARATION	E_{02}	C_2
$As_{40}Se_{60}$	bubble	1.73 eV	6.3×10^5 eV^{-1} cm^{-1}
$As_{40}Se_{60}Cu_{1.0}$	bubble	1.67 eV	5.5×10^5 eV^{-1} cm^{-1}
$As_{45}Se_{55}$	bubble	1.72 eV	6.1×10^5 eV^{-1} cm^{-1}
$As_{46}Se_{54}Cu_{0.023}$	electron-beam	1.70 eV	5.0×10^5 eV^{-1} cm^{-1}

TABLE 8.1

It is clear from the table that E_{02} is reduced by the addition of Cu, even in small amounts. This is in agreement with the results obtained on silver doped glasses by Inoue et al[1] and by Kolomiets[2]. On the other hand, Kolomiets et al[3] observed an increase in the energy at which the spectral response curve for photoconductivity shows a maximum for small levels of doping ($\lesssim$ 1%) followed by a decrease at higher levels[4]. This implies that initially the 'photoconductivity gap', ie, the energy at which the quantum

efficiency approaches unity, increases while the extrapolated optical gap E_{02} decreases even for small amounts of doping. This behaviour may be related to the reduction in C_2 with doping which is evident from Table 8.1 since a reduction in C_2 means an increase in the energy difference ($h\nu - E_{02}$) needed to attain the same level of absorption. It is interesting in this respect that the addition of Ag progressively decreases the slope of the exponential absorption curve[5] which indicates increased random internal electric fields. Therefore, the whole absorption curve in the exponential and square law regions rises more gradually in doped glasses.

8.2.2 DARK CONDUCTIVITY

As expected, the activation energy of the dark conductivity was reduced sharply with the addition of Cu. Measurements were usually started in the temperature range between room temperature and the lowest temperature at which the dark current was measurable. It was soon noticed that at higher temperatures, ie, about 330 - 340 K, measurements of the dark conductivity as well as photoconductivity became difficult because of current fluctuations. Moreover, it was found that the low temperature properties were irreversibly altered after heating to 330 - 340 K. This annealing effect seems to occur in all samples containing Cu, irrespective of preparation or precise composition. After a sample had been annealed above 340 K for a few minutes no further changes were observed. Comparison of the dark conductivities before and after annealing showed that the activation energies either remained unaltered or were slightly reduced. The conductivities at 300 K were reduced by a factor of 2 in two sputtered samples containing 0.51 and 0.90 atomic % Cu, but in a bulk

sample of $As_{40}Se_{60}Cu_{1.0}$ an *increase* by a factor of 7 was observed. An example is shown in Figure 8.2. In view of this and the preliminary nature of the measurements the pre-exponential of the conductivity can only be roughly estimated. Recalling equations 3.9 and 3.13, one can write

$$\sigma = \sigma_o \exp(- E_d/kT) = \sigma_o \exp(\beta/k) \exp(- E_\sigma/kT) \qquad 8.1$$

where β is the linear temperature coefficient of the activation energy. Assume for the moment that the conduction process is electronic and that

$$\beta/\gamma \triangleq E_d/E_{02}(T) \triangleq E_\sigma/E_{02}(0K) \qquad 8.2(a)$$

ie,

$$\beta \triangleq \phi E_\sigma \qquad 8.2(b)$$

where γ is the temperature coefficient of the extrapolated optical gap E_{02}. Using the measured values of E_σ and $\phi = 3.5 \times 10^{-4}\ K^{-1}$, as found in the previous chapter, gives

$$\exp(\beta/k) \triangleq 13 - 26$$

Combining this with the pre-exponential constants, estimated from the conductivity measurements to be $0.5 - 40\ \Omega^{-1}\ cm^{-1}$, gives σ_o in the range $0.02 - 3\ \Omega^{-1}\ cm^{-1}$, which is many orders of magnitude lower than expected for conduction in extended states. Arai et al[6] found that $As_{40}Se_{60}$ doped with silver is *less* conducting than the undoped glass at high temperatures. Calculation similar to that above shows that

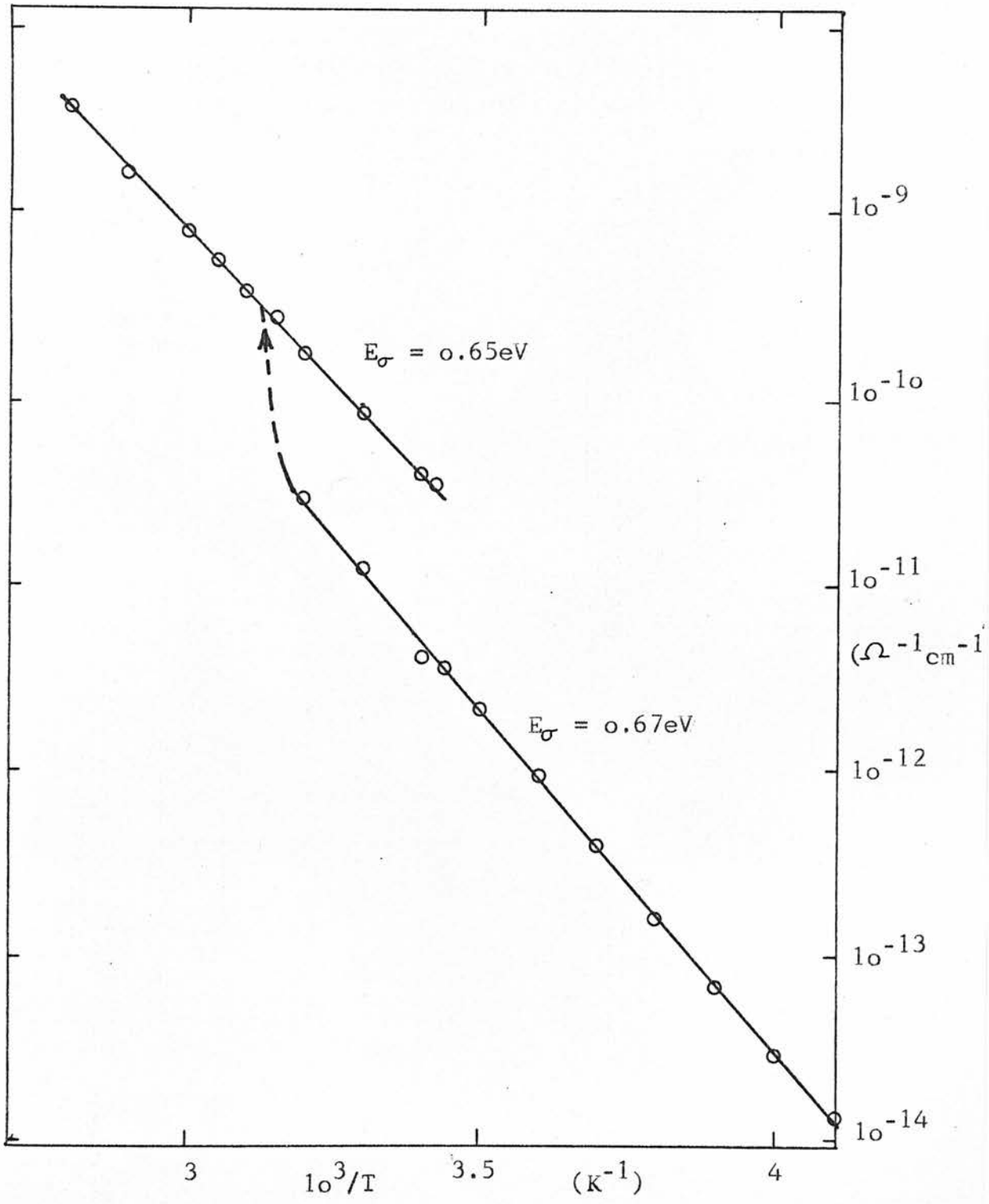

FIGURE 8.2

DC dark conductivity in bulk $As_{4o}Se_{6o}Cu_{1.o}$ with coplanar electrodes. Conductivity pre-exponential = $5\,\Omega^{-1}cm^{-1}$ was used to convert conductance into conductivity. The field was $2 \times 1o^4$ V/cm.

in this case σ_o is reduced by two orders of magnitude with the addition of 1% Ag (atomic). Thus, conduction cannot take place in extended states in glasses doped with ~1% atomic Cu or Ag.

8.2.3 STEADY STATE PHOTOCONDUCTIVITY

Figure 8.3 shows a plot of photoconductivity vs inverse temperature for a bubble containing 1% Cu (atomic). This curve is typical of all the Cu-doped films investigated. The photoconductivity of one film was followed through the annealing region. Some fluctuations were observed but there was hardly any difference in the photoconductivity before and after the annealing. The activation energy in the temperature region 230 - 370 K was found to be 0.26 - 0.28 eV for bulk glasses containing 1% Cu and about 0.30 eV for sputtered films with 0.5 - 0.9% Cu. As this is in the bimolecular region, however, a correction should be made for the temperature dependence of the absorption coefficient and the quantum efficiency (equation 3.48). Referring to the absorption data in Figure 8.1 and using $\gamma \triangleq 7 \times 10^{-4}$ eV/K the correction due to the change in absorption (at $h\nu \triangleq 1.88$ eV) is estimated as $\lesssim 0.02$ eV, ie, the activation energy shown in Figure 8.3 should be increased by that amount to 0.28 eV. This compares with 0.33 eV for pure As_2Se_3 [7]. A thermally activated quantum efficiency on the other hand would tend to decrease the measured activation energy. According to Main[7] the photoconductivity in a-As_2Se_3 is controlled by band-to-localized recombination between the valence band and electron traps situated at E_1, 0.37 eV above E_F, (see Figure 3.10). The temperature dependence of the photoconductivity in region II is controlled by hole traps at E_2 where $E_2-E_v = 0.66$ eV, twice the activation energy of the photocurrent. Since $E_\sigma = 0.92$ eV

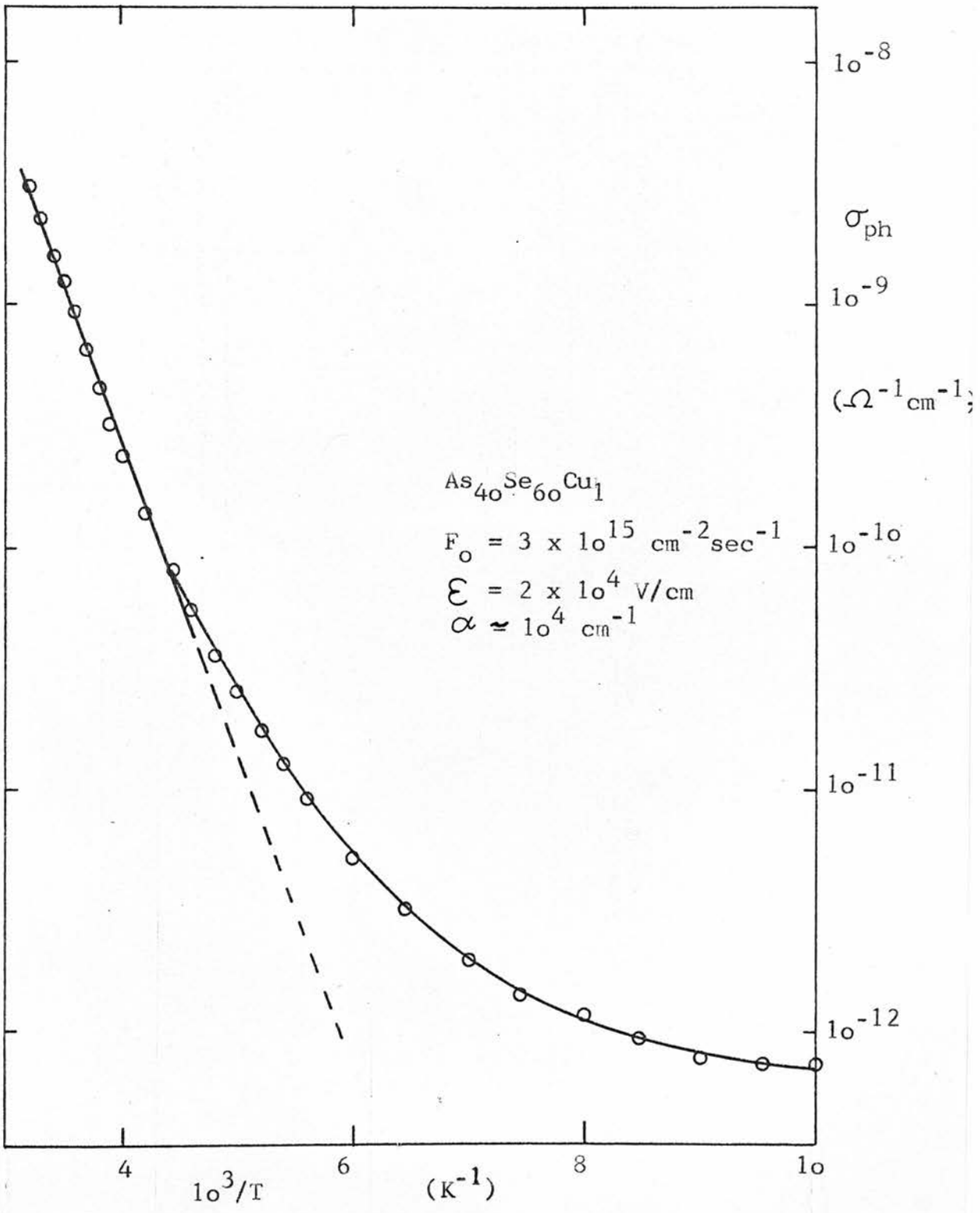

FIGURE 8.3

Photoconductivity vs inverse temperature in a bubble specimen with 1 % Cu. Equation 6.18 was used to obtain σ_{ph}.

in a-As_2Se_3 it follows that $E_F - E_2 = 0.26$ eV [7]. There is not sufficient data available on the Cu-doped glasses to perform similar analysis. It is clear, however, that if the same traps are assumed to control the photoconductivity kinetics in $As_{40}Se_{60}Cu_{1.0}$ as in $As_{40}Se_{60}$ then

$$E_F - E_v \triangleq 2 \times 0.26 \text{ eV} + 0.26 \text{ eV} \triangleq 0.78 \text{ eV} \qquad 8.3$$

which is ~0.15 eV larger than the measured activation energy of the dark conductivity. This is consistent with the previous conclusion that conduction in extended states is not the dominant conduction mechanism in the doped glasses.

8.3 PHOTOMOBILITY

The photocurrent response to a step function illumination of samples doped with Cu showed an approximately linear rise in the first 8 - 10 μsec, followed by a gradual decrease in slope for longer times. This contrasts with pure a-As_2Se_3 which has a linear rise for 50 μsec or more[7]. Measurements in such short time intervals are difficult and it was necessary to use the 'box-car' noise reduction system. The photocurrent rise was converted into 'drift mobilities' by means of equations 6.19 and 6.20. The results are shown in Figure 8.4 for three differently prepared bulk samples of composition $As_{40}Se_{60}Cu_{1.0}$, and in Figure 8.5 for a sputtered sample of composition $As_{42}Se_{58}Cu_{0.5}$. Because of uncertainties in the various parameters used in the conversion of the data, the *absolute* values of the mobilities shown are correct only within a factor of five. The relative error between the two diagrams is less than a factor of two. The effect of annealing

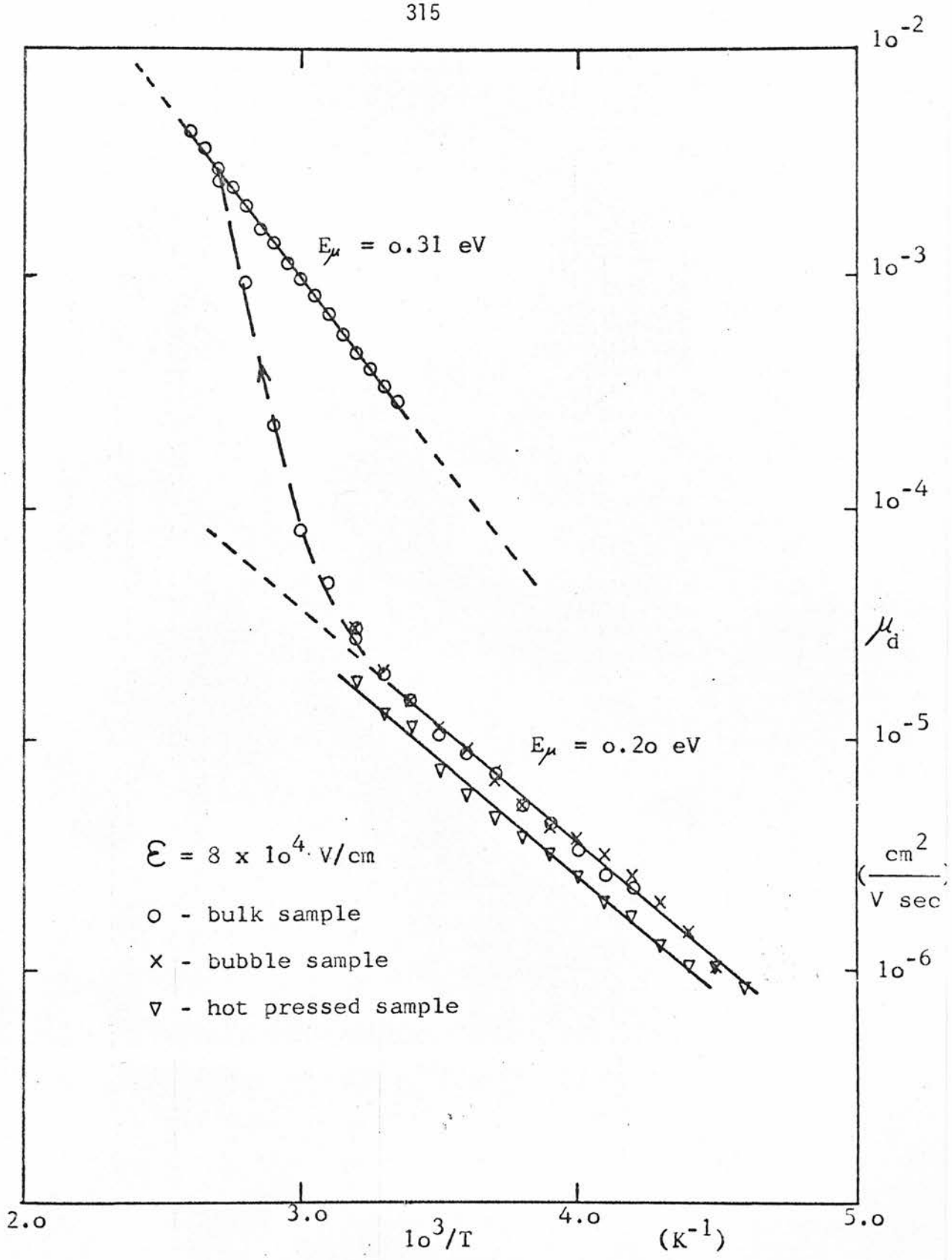

Photoderived drift mobility in $As_{40}Se_{60}Cu_1$,

FIGURE 8.4

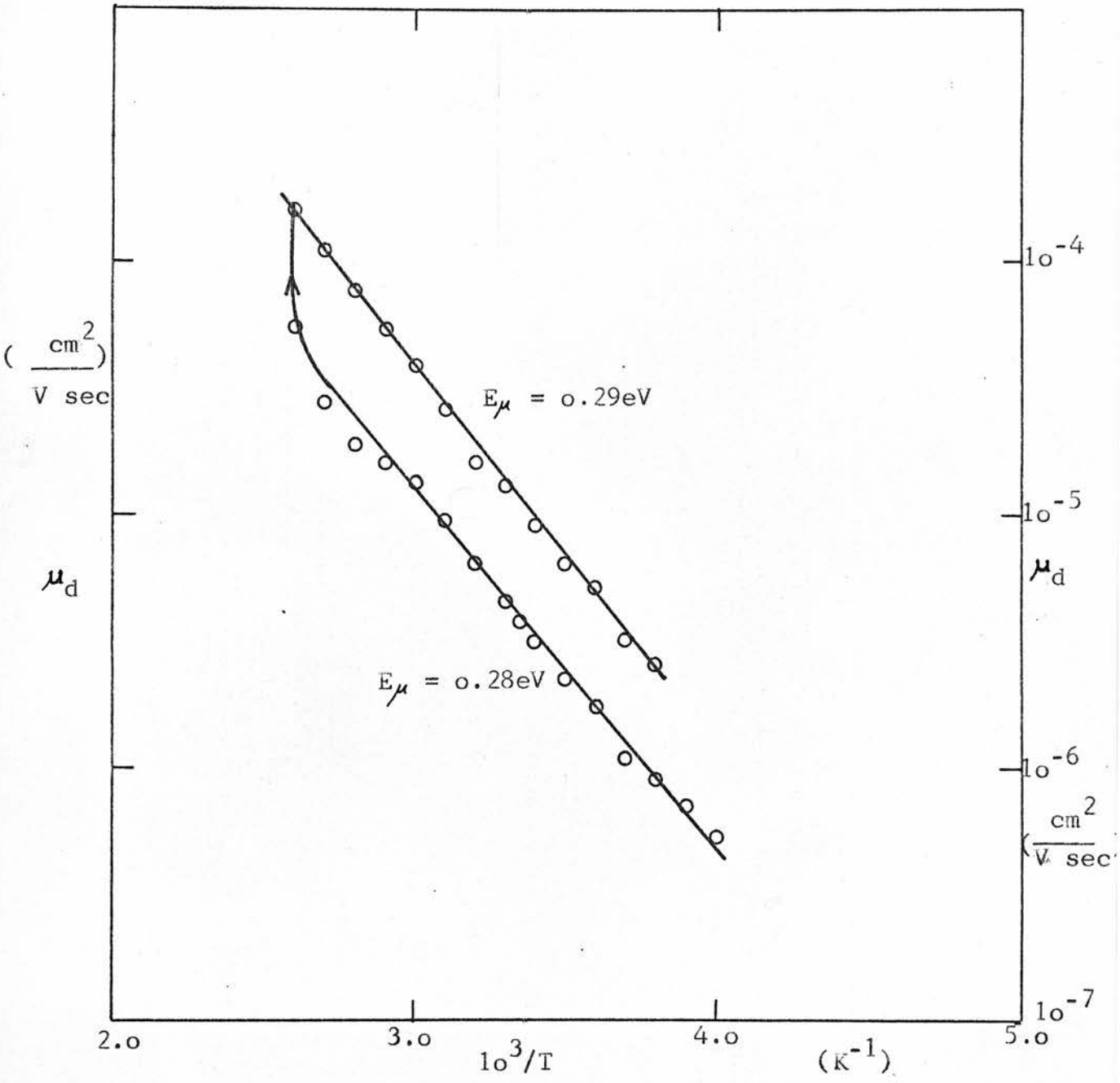

FIGURE 8.5

Photoderived drift mobility in RF sputtered $As_{42}Se_{58}Cu_{o.5}$

Field = 8 x $1o^4$ V/cm.

is to increase the mobility and, in the case of Figure 8.4, the activation energy is also increased by 50%. This increase in E_μ appears to be real although it should be noted that only one sample was investigated after annealing. The mobilities before annealing are 5 - 20 times larger at 300 K than in pure As_2Se_3 [8]. Measurements of photomobility as a function of field indicates that at the field used in obtaining the results shown in Figures 8.4 and 8.5 (8×10^4 volts/cm), the field induced reduction of the activation energies is less than 0.02 eV. The pre-exponential constants are estimated (within a factor of 5) as 0.05 - 50 cm^2/volt-sec (Figure 8.4) and 2 - 10 cm^2/volt-sec (Figure 8.5). This may be compared to ~0.3 cm^2/volt-sec obtained by Marshall and Owen[8] for a-As_2Se_3, corresponding to traps 0.43 eV above the valence band edge. They compared this value with the dark conductivity pre-exponential constant (see equation 3.3 and 3.4) and, assuming that

$$\mu_d = \mu_o(N_v/N_t) \exp(-E_\mu/kT) \qquad 8.4$$

obtained $N_t \sim N_v \sim 10^{19}$ cm^{-3}. Main[7] obtained $N_t \sim 10^{18}$ cm^{-3} from photomobility measurements. In the present case such analysis is not possible as it is concluded that conduction in extended states is not the dominant conduction mechanism in the dark. Nevertheless, taken on their own the mobility results are fully consistent with conduction in extended states limited by traps 0.2 - 0.3 eV above the valence band mobility edge, assuming trap densities similar to those discussed above for a-As_2Se_3 and a reasonable value for the free mobility μ_o. Interpretation in terms of trapping in a tail of localized states, 0.2 - 0.3 eV deep, is also possible. In that case annealing might be expected to *reduce* the activation energy for mobility and thus

increase the drift mobility at room temperature. On the evidence of the present results, however, the activation energy is increased, rather than reduced, by annealing. Interpretation in terms of thermally activated hopping (equation 3.6) also meets with difficulties because the observed pre-exponential constants are larger than 10^{-2} cm^2/volt-sec and creation of hopping centres by annealing would be required to explain the increase in mobilities. The simplest interpretation therefore seems to be in terms of equation 8.4, assuming that annealing reduces N_t and also alters the energy distribution of the localized states.

8.4 THE EFFECT OF ELECTRIC FIELD

Because measurements of photomobility over a sufficiently wide temperature range were only possible at fairly high fields (8×10^4 volts/cm) it was thought necessary to investigate the field dependence of the photomobility. It was found that the results fitted well to an equation similar to equation 4.15 for conductivity, ie,

$$\mu_d(\mathcal{E}) = \mu_d(0) \exp\left(\frac{ae\mathcal{E}}{kT}\right) \qquad 8.5$$

where $\mathcal{E}$ is the electric field. The 'activation length', a, was found to be about 10 Å with no detectable dependence on temperature in the range 250 - 300 K. This is about half the activation distance observed for dark conductivity; 18 - 26 Å . The mobility results for a bulk sample containing 1% Cu (the same one as showed an increase in E_μ upon annealing) gave a = 9.6 Å at 298 K before annealing and a = 22 Å at 384 K; these results are shown in Figure 8.6. The field dependence of σ was only investigated in unannealed samples and

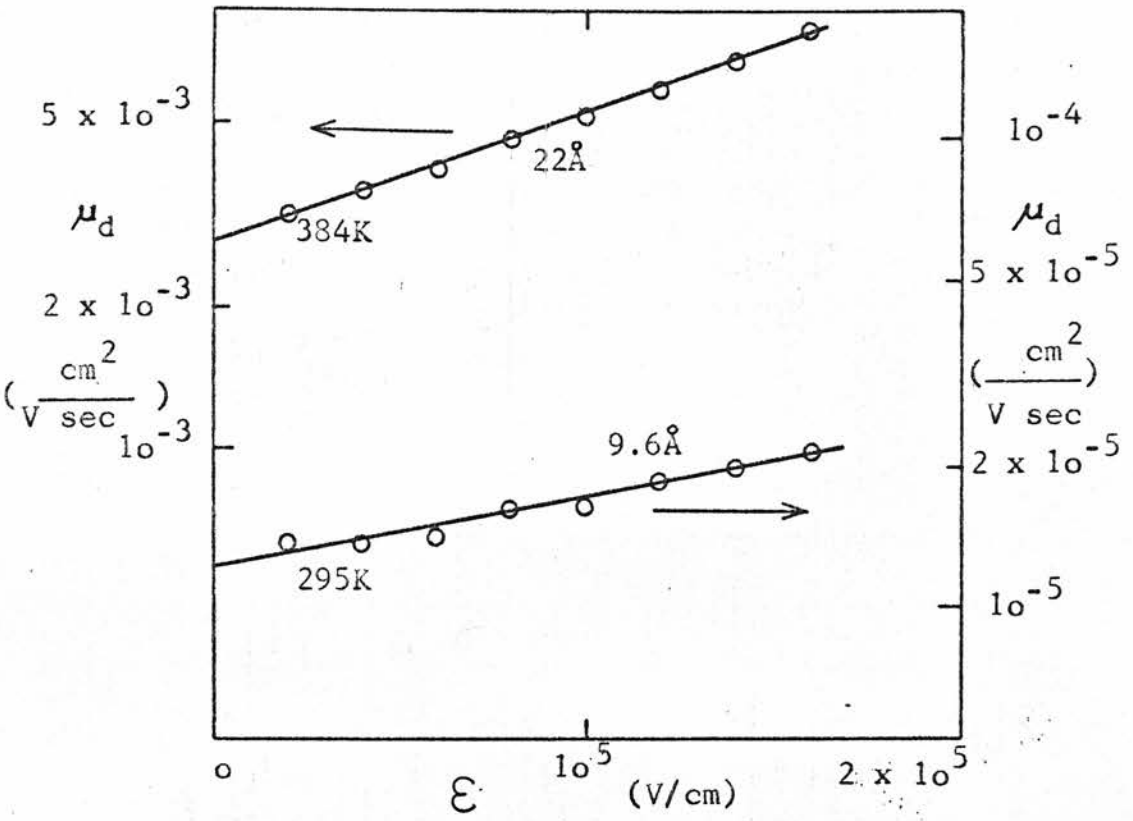

FIGURE 8.6

Log photomobility vs electric field for bulk $As_{40}Se_{60}Cu_1$ before and after annealing.

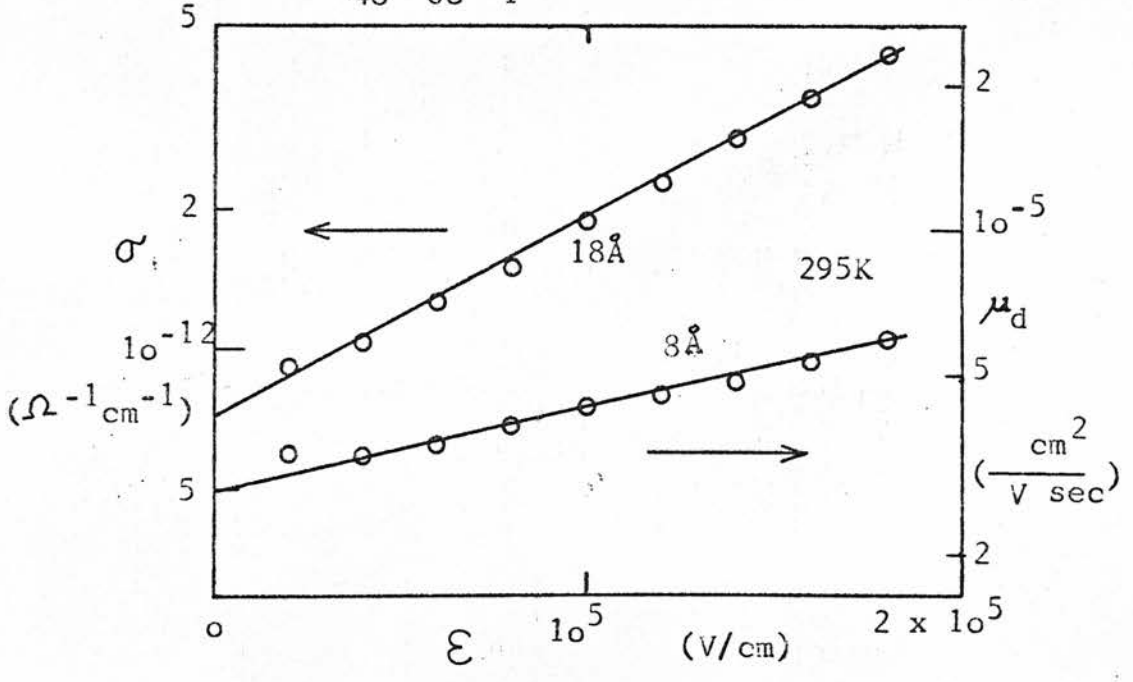

FIGURE 8.7

Electric field dependence of dark conductivity and photomobility for an RF sputtered film of $As_{42}Se_{58}Cu_{0.5}$.

Figure 8.7 shows the field dependence of dark conductivity and photomobility in a sputtered sample of composition $As_{42}Se_{58}Cu_{0.5}$ (the same sample as in Figure 8.5). From Figure 8.7, a = 18 Å for conductivity and 8 Å for photomobility. These results are summarised in Table 8.2.

It is interesting that the field dependence of σ in Cu doped samples is very similar (a $\simeq$ 20 Å) as for undoped As_2Se_3 [9] even though the conduction mechanism is different. This supports the view of Arai et al[6], based on the effect of pressure on conductivity, that the conduction in doped glass involves both electrons and ions in a co-operative mechanism.

the activation length, a, in Cu doped samples

PREPARATION	COMPOSITION	a (from σ)	a (from μ)	T
RF sputtered	$As_{42.5}Se_{57.5}Cu_{0.03}$	26 Å	10 Å	~295 K
RF sputtered	$As_{42}Se_{58}Cu_{0.5}$	18 Å	8 Å	295 K
RF sputtered	$As_{42}Se_{58}Cu_{0.5}$	17 Å	10 Å	295 K
hot pressed	$As_{40}Se_{60}Cu_{1.0}$	26 Å	10 Å	295 K
bubble	$As_{40}Se_{60}Cu_{1.0}$		13 Å	295 K
bulk*	$As_{40}Se_{60}Cu_{1.0}$		9.6 Å	295 K
bulk*	$As_{40}Se_{60}Cu_{1.0}$		22 Å	384 K

* same sample, coplanar electrodes were used

TABLE 8.2

8.5 DISCUSSION

In the model proposed by Arai et al[6,10] to explain the conduction process in As-Se-Ag glasses, the conduction is mostly ionic at low temperatures and pressures but becomes increasingly more electronic as temperature and pressure are increased. The two forms of conduction are not additive, however, as there would then be a change in the activation energy with increased temperature, which is not observed. Arai et al also showed that there is a close relation between the low frequency dielectric loss and the dc conductivity, even when σ increases with pressure, ie, when the conduction is mostly electronic. They therefore envisaged a process in which silver ions and electrons (or holes) co-operate in the transport process. Lebedev et al[11] found that the charge on Ag atoms *during* 'hopping' is positive, but stressed that they had no information about the charge at other times. They also found that the pre-exponential constant of the ionic mobility was 9 cm^2/volt-sec. If the conduction is purely ionic then

$$\sigma = N_{ion}\, e\mu_{ion} \qquad 8.6$$

If all the Cu atoms are available simultaneously for conduction then $N_{ion} = 3.6 \times 10^{20}$ cm^{-3} for $As_{40}Se_{60}Cu_{1.0}$ and the range of pre-exponential constants of the conductivity in the present work (0.5 - 40 Ω^{-1} cm^{-1}) implies (ionic) mobility exponential constants in the range 0.1 - 10 cm^2/volt-sec in reasonable agreement with the value for glasses doped with Ag[11]. The mobilities determined in the present work (photomobilities) are at least six orders of magnitude higher than the silver ion mobilities determined by Lebedev et al[11]. It is of course possible that there is no direct relationship between

the dark conductivity and the photomobility and that the photomobility and the photoconductivity refer to conduction in extended states. On the other hand the results of Arai et al[6], and the phenomenon of photo-doping[12], imply that this is not the case. Another possibility is that the Cu (and Ag) atoms act as hole traps which are mobile when occupied, in that case E_μ would be the activation energy for Cu^+ hopping and

$$E_\sigma - E_\mu = E_F - E_t$$

where E_t is the energy of the hole traps. In this case most of the Cu atoms would be unoccupied and neutral. Liang[12] has shown by means of X-ray photoelectron spectroscopy that this is not the case, indeed most of the Cu atoms are singly charged (Cu^+) at any time.

A more likely explanation is that the Cu^+ ions can only jump to sites containing trapped carriers. It is suggested that these sites are negatively charged electron traps (when occupied) and that the jump is aided by coulombic attraction. If these traps are in a quasi-equilibrium with the conduction band (shallow traps) then their occupation will increase linearly with time in response to a step-function illumination until recombination starts. Therefore, the number of available sites for Cu^+ ions to jump to also increases linearly and the activation energy of 'photomobility' is the average energy required for a jump. The number of occupied traps in the dark is $\propto \exp\left(-\frac{E_e - E_F}{kT}\right)$ where E_e is the electron trap energy, and

$$E_\sigma = E_\mu + (E_e - E_F) \qquad 8.7$$

This suggests that $E_e - E_F \triangleq 0.44$ eV from the results obtained in the present work.

The case of steady state photoconductivity is more difficult to analyse because the trap occupancy will obey bimolecular kinetics at high intensities and (assuming an ionic conductivity enhanced by illumination via an increase in trapped electron density) the average distance between a Cu^+ ion and its occupied electron-trap-neighbours will be inversely proportional to $(f(E_e))^{1/3}$, where $f(E_e)$ is the occupancy of the electron traps.

The above discussion is highly speculative and it is possible to think of various modifications. Its basic appeal is that it can explain, qualitatively at least, diverse experimental observations such as ionic conductivity with some characteristics of electronic conduction and photodoping. The annealing effect must be explained separately as a structural change which affects the trapping and conduction processes. It is interesting to note that the annealing temperature 340 K is approximately 0.7 Tg, suggesting a link with the shoulder at 0.7 Tg in the mechanical damping vs temperature curve observed by Amrhein et al[13].

8.6 REFERENCES

1. Inoue, E et al, 'Non-silver Photographic Processes', (R J Cox, editor), Academic Press, 1975, p 71.

2. Kolomiets, B T, Proc on the 5th International Conference on Amorphous and Liquid Semiconductors, Garmisch-Partenkirchen, Germany (J Stuke and W Brenig, editors), Taylor and Francis, London, 1974, p 189.

3. Kolomiets, B T, et al, J Non-Cryst Sol 5, p 389, 1971.

4. Danilov, A V and El'Mosli, M, Fiz Tverd Tela 5, p 2015, 1963.

5. Kolomiets, B T et al, Soviet Phys Semic 8, p 348, 1974.

6. Arai, K et al, Jap J Appl Phys 11, p 1080, 1972.

7. Main, C, PhD Thesis, University of Edinburgh , 1974.

8. Marshall, J M and Owen, A E, Phil Mag 24, p 1281, 1971.

9. Marshall, J M and Miller, G R, Phil Mag 27, p 1151, 1973.

10. Arai, K et al, J Non-Cryst Sol 13, p 131, 1973.

11. Lebedev, E A et al, Phys Stat Sol (a), 28, p 461, 1975.

12. Liang, K, PhD Thesis, Stanford University, 1973.

13. Amrhein, E M et al, J Non-Cryst Sol 16, p 46, 1974.

APPENDIX TABULATED RESULTS ON OPTICAL INTERBAND ABSORPTION

Average results on As-Se bubbles:

% As	E_{o2}(3ooK)	E_{o2}(oK)	C_2(3ooK)	C_2(12oK)
5o	1.76 eV	1.95 eV	6.1×10^5 $eV^{-1}cm^{-1}$	$7.6 \times 10^5 eV^{-1}cm^{-1}$
45	1.72 -	1.92 -	6.1 -	7.7 -
42.5	1.72 -	1.92 -	6.6 -	8.3 -
4o	1.73 -	1.93 -	6.3 -	7.9 -
37.5	1.77 -	1.97	7.6 -	9.4 -
35	1.78 -	1.98 -	7.5 -	9.1 -
3o	1.81 -	2.o2 -	8.3 -	1o.6 -
25	1.83 -	2.o4 -	8.3 -	11.1 -
2o	1.85 -	2.o6 -	9.o -	12 -
15	1.88 -	2.1o -	1o.2 -	14 -
8	1.91 -	2.13 -	12 -	2o -
5	1.92 -	2.14 -	13 -	21 -
1	1.94 -	2.16 -	15 -	24 -
o.1	1.94 -	2.17 -	15 -	
oo.oo	1.94 -	2.16 -	15 -	

On the following pages the optical absorption of As-Se films is tabulated. α is in units of 10^3 cm^{-1} and x is the wave number in units of $10^3 cm^{-1}$. Thus $h\nu = o.124\ x$, where $h\nu$ is in eV. The tabulated values are from measurements on one or two (typical) samples of each composition. Only a few examples of low temperature results are included here. All the results on the first four pages are from bubble specimens.

	$As_{50}Se_{50}$		$As_{45}Se_{55}$		$As_{42.5}Se_{57.5}$
x	300K	115K	300K	110K	300K
19.0		75		77	
18.8		67		69	
18.6		62		62	110
18.4	75	56		56	100
18.2	68	49		49	93
18.0	62	44	79	43	86
17.8	56	38	71	37	79
17.6	51	33	65	32	72
17.4	45	28	58	28	64
17.2	40	24	53	23	58
17.0	35	20	46	19	52
16.8	31	16	41	15	47
16.6	27	13	36	12	41
16.4	23	11	31	10	36
16.2	20		27	7.0	30
16.0	16		22		26
15.8	13		19		22
15.6	10		15		17
15.4			13		13
15.2			10		10
15.0			8.0		8

x	$As_{40}Se_{60}$ 290K	$As_{40}Se_{60}$ 110K	$As_{37.5}Se_{62.5}$ 295K	$As_{35}Se_{65}$ 300K	$As_{30}Se_{70}$ 295K
20.8		169			
20.6		154			
20.4		144			
20.2	161	135			
20.0	152	128			
19.8	143	120			
19.6	133	111			
19.4	126	104			
19.2	119	96			
19.0	111	87			
18.8	106	80			
18.6	96	74			
18.4	89	67			80
18.2	81	59	83	83	72
18.0	76	54	76	74	65
17.8	70	46	68	68	58
17.6	63	41	63	61	52
17.4	57	35	56	54	46
17.2	52	30	49	48	40
17.0	46	26	44	42	35
16.8	41	23	37	36	30
16.6	36	20	32	31	24
16.4	31	16	28	26	20
16.2	28	12	23	21	16
16.0	23	8	19	18	13
15.8	19		15	15	10
15.6	14		12	12	7.6
15.4	10		10	8	5.6

	$As_{25}Se_{75}$	$As_{2o}Se_{8o}$	$As_{15}Se_{85}$	$As_{8}Se_{92}$	$As_{5}Se_{95}$
x	296K	29oK	295K	295K	29oK
19.2	111			95	
19.o	1o2		95	86	
18.8	95		86	79	97
18.6	87		79	71	86
18.4	8o		71	65	77
18.2	73		63	56	68
18.o	65	56	56	49	59
17.8	58	48	49	43	5o
17.6	44	42	41	36	43
17.4	38	37	37	3o	35
17.2	34	31	3o	24	28
17.o	29	26	24	19	22
16.8	24	21	2o	15	17
16.6	2o	18	15	12	13
16.4	15	14	11	8.o	9.6
16.2	13	11	8.3	63	
16.o	9.4	8.1	6.o	4.5	
15.8	7.o	6.o	4		
2o.4	16o				
2o.2	15o				
2o.o	142				
19.8	135				
19.6	127				
19.4	12o				
19.2	111				

x	As_1Se_{99} 290K	$As_{0.1}Se_{99.9}$ 295K	Se 296K
21.0		170	
20.8		164	
20.6		158	
20.4		152	
20.2		146	
20.0		140	
19.8		134	
19.6		126	108
19.4	116	118	101
19.2	108	112	95
19.0	100	102	88
18.8	91	96	82
18.6	84	88	74
18.4	75	78	67
18.2	66	68	59
18.0	58	60	51
17.8	49	50	44
17.6	41	42	37
17.4	33	34	30
17.2	26	26	24
17.0	21	20	18
16.8	15	14	14
16.6	10	11	10
16.4	7	8	
16.2			
16.0			

Se (evaporated)

x	290K	x	290K
27.5	400	19.5	130
27.0	390	19.0	110
26.5	380	18.5	93
26.0	360	18.0	64
25.5	340	17.8	54
25.0	320	17.6	43
24.5	300	17.4	34
24.0	286	17.2	26
23.5	270	17.0	21
23.0	260	16.8	16
22.5	240	16.6	12
22.0	220	16.4	9
21.5	205	16.2	6
21.0	190		
20.5	170		
20.0	150		

$As_{40}Se_{60}$ (RF sputtered)

x	300K
16.8	32
16.6	28
16.4	24
16.2	20
16.0	16
15.8	13
15.6	10
15.4	7.7
15.2	5.9
15.0	4.3